

PM_{2.5} SOURCE APPORTIONMENT AND MASS CLOSURE STUDY IN DOHA CITY, QATAR

by

LUBNA SALEH AL-SAAD

Submitted to the University of Birmingham in partial fulfilment for the degree of Doctor of
Philosophy

Division of Environmental Health and Risk Management School of Geography, Earth and
Environmental Studies College of Life and Environmental Sciences University of
Birmingham Edgbaston, Birmingham B15 2TT United Kingdom

November 2017

UNIVERSITY OF
BIRMINGHAM

University of Birmingham Research Archive

e-theses repository

This unpublished thesis/dissertation is copyright of the author and/or third parties. The intellectual property rights of the author or third parties in respect of this work are as defined by The Copyright Designs and Patents Act 1988 or as modified by any successor legislation.

Any use made of information contained in this thesis/dissertation must be in accordance with that legislation and must be properly acknowledged. Further distribution or reproduction in any format is prohibited without the permission of the copyright holder.

ABSTRACT

This study aims to identify key sources that contribute to fine particulate matter ($PM_{2.5}$) mass concentrations in Doha city, Qatar. Specifically, to determine the increase in $PM_{2.5}$ mass caused by dust events, by comparing abundance and composition between the dust events season ‘the summer season’ and non-dust event season ‘the winter season’. Knowing $PM_{2.5}$ sources in Doha will help to 1) identify the predominant (natural or anthropogenic) sources responsible for particulate matter (PM) exceedances of the daily and annual air quality standards, 2) ensure an appropriate focus on controlling major anthropogenic sources, and 3) evaluate the current air quality standards and potential improvements to the allowable margin of tolerance for PM limit and the number of allowed exceedances to take appropriate account of natural sources.

Two parallel sampling campaigns at two urban sites in Doha, namely Al-Corniche (AC) and Qatar University (QU) were conducted during the winter of 2014/2015 and the summer of 2015 using low volume samplers. Chemical analysis of minerals, trace metals, soluble inorganic ions, organic and elemental carbon was carried out on $PM_{2.5}$ samples. Subsequently, a mass closure analysis, and a source apportionment by means of positive matrix factorisation (PMF-5) were performed.

The mass closure solution found a good closure between the samples’ gravimetric mass and the reconstructed mass of the chemical constituents determined on those samples. However, mass discrepancies ranged between -5 and +12% were found between reconstructed mass and gravimetric measured mass as a result of using different filters substances (Teflon & Quartz) to collect $PM_{2.5}$ samples with contradictory behaviour in retaining and releasing organic carbon and ammonium nitrate. Then comparing the sum of chemical constituents from both filters to the mass collected on the Teflon filters.

A PMF-5 solution was found with similar factors identified at both sites and seasons primarily crustal components, secondary sulfate, salt/nitrate, traffic, and a construction site. In addition to (Zn & As) factor which was only found at the AC site, in both seasons, and (La & Co) factor which was found in the summer season at both sites.

PM_{2.5} mass showed a seasonal variation in which the mass changed from 34.93 and 33.12 $\mu\text{g}/\text{m}^3$ at the AC and QU sites in the winter season to 73.74 and 99.02 $\mu\text{g}/\text{m}^3$ at the AC and QU sites in the summer season. The changes in PM_{2.5} mass were caused mainly by the increase in mineral oxide and sulfate concentration. The source apportionment solution showed that anthropogenic sources contribution increased from 26.7 and 21.7 $\mu\text{g}/\text{m}^3$ at the AC and QU sites in the winter season to 41.5 and 41.7 $\mu\text{g}/\text{m}^3$ at the AC and QU sites in the summer season. This increase caused by secondary sulfate aerosols and the indirect contribution of dust events to anthropogenic sources such as traffic source by increasing road dust.

On the other hand, the increase in natural sources contribution from 8.12 and 11.4 $\mu\text{g}/\text{m}^3$ at the AC and QU sites in the winter season to 32.08 and 57.25 $\mu\text{g}/\text{m}^3$ at the AC and QU sites in the summer season was mainly due to dust events. These results highlighted the big impact dust events have on PM mass concentrations and the importance of including a margin of tolerance and a number of allowed exceedances to PM limits values to take appropriate account of natural sources.

ACKNOWLEDGEMENTS

A special appreciation goes to my supervisor, Prof Wiliam Bloss for his encouragement, guidance, and support during the last four years.

This study was made possible by the support from ExxonMobil Research Qatar (EMRQ) which provided four samplers for the practical part of the study. Special thanks to Jennifer Dupont and Eric Febbo.

Many thanks to Louisa Kramer and Leigh Crilley for all the constructive comments, suggestions, and advices; Eimear Orgill, Jackie Deans, and Dr. Jianxin Yin for the advice and support in conducting laboratory analysis. Thanks, are also due to Dr. Stephen J. Baker for help in elemental analysis.

Finally, my sincere love and gratitude goes to my mother for her endless love, prayers, and encouragement.

TABLE OF CONTENTS

CHAPTER 1- INTRODUCTION.....	1
1.1 Background.....	1
1.1.1 PM Chemical Composition.....	4
1.1.2 PM Size Properties.....	7
1.2 An Overview of Qatar.....	9
1.3 Particulate Matter Pollution in Doha.....	12
1.4 Sources of Particulate Matter Pollution in Qatar.....	17
1.4.1 Natural Particulate Matter Sources.....	17
1.4.1.1 Sea Salt Aerosols.....	17
1.4.1.2 Dust Storms.....	19
1.4.2 Anthropogenic Particulate Matter Sources within Doha's Boundaries.....	23
1.4.2.1 Construction Activities.....	24
1.4.2.2 Traffic.....	24
1.4.2.3 Doha Harbour.....	27
1.4.2.3 Hamad International Airport.....	29
1.4.3 Industrial Cities in Qatar and Possible Contribution to Doha Pollution.....	29
1.4.3.1 Rass Laffan Industrial City (RLC).....	31
1.4.3.2 Mesaieed Industrial City (MIC).....	32
1.4.3.3 Dukhan and Umm-Bab Industrial Cities.....	33
1.4.3.4 Doha Industrial Area (DIA).....	34
1.5 Source Apportionment and the PMF Model.....	34
1.6 Mass Closure.....	38
1.7 Objectives.....	40
1.8 Thesis Structure.....	41
 CHAPTER 2- METHODOLOGY.....	 42
2.1 Methodology Overview.....	42
2.2 PM-162M Sampler.....	42
2.2.1 Samplers.....	42
2.2.2 Sampler Installation.....	45
2.3 Filters Selection.....	46
2.4 Sampling Locations.....	48
2.4.1 Al-Corniche Site.....	49
2.4.2 Qatar University Site.....	50
2.5 Sampling Campaigns.....	51
2.5.1 Winter Sampling Campaign.....	52
2.5.2 Summer Sampling Campaign.....	52
2.6 Analytical Procedures.....	53
2.6.1 Filter Preparation and Conditioning.....	53
2.6.2 Gravimetric Analysis.....	54
2.6.3 Cleaning Procedure.....	54
2.6.4 Metal extraction.....	54

2.6.5 Ions Extraction	55
2.6.6 Organic and Carbon Analysis	55
2.6.7 Inorganic ions analysis	57
2.6.8 Metals Analysis	58
2.7 Detection Limit	59
2.8 Calculations	61
2.9 Secondary Data.....	61
2.10Data Analysis	62

CHAPTER 3: DESCRIPTIVE DATA, SEASONAL AND SPATIAL VARIATION 63

3.1 Overview of Meteorological Parameters during Both Campaigns	63
3.1.1 Meteorological Parameters' Spatial Variation	64
3.1.2 Meteorological Parameters Seasonal Variation	65
3.2 Descriptive Data for Species Mean, Max, and Min Concentrations in Both Seasons	67
3.3 PM_{2.5} Spatial Variation	70
3.4 PM_{2.5} Seasonal variation	72
3.5 PM_{2.5} Levels and Air Quality Index	77
3.6 Ion Mass Balance and the Changes in Aerosol Acidity through the Seasons	80
3.6.1 Ion Mass Balance during the Winter Season	81
3.6.2 Ion Mass Balance During the Summer Season	82
3.7 Metals Enrichment Factor (EF).....	84
3.8 The Effect of Wind Speed on PM_{2.5} Mass Concentration	86
3.8.1 The Effect of Wind Speed on PM _{2.5} Mass Concentrations in the Winter Season	87
3.8.2 The Effect of Wind Speed on PM _{2.5} Mass Concentrations in the Summer Season	89
3.9 Summary.....	93

CHAPTER 4: MASS CLOSURE 95

4.1 Introduction	95
4.2 Mass Reconstruction Method.....	95
4.2.1 Crustal Matter Estimation.....	96
4.2.2 Trace Metals	100
4.2.3 Organic and Elemental Carbon.....	100
4.2.4 Sea Salt.....	102
4.2.5 Ammonium Sulfate and Nitrate.....	103
4.3 Mass Reconstruction Results.....	103
4.4 Mass Reconstruction Result Evaluation.....	106
4.4.1 Carbonate Compounds	107
4.4.2 Carbonaceous Aerosols Artefact	108
4.4.3 Ammonium Nitrate Artefact.....	110
4.4.4 Sulfate Measurements and Possible Artefact.....	111
4.4.5 Overall Corrections	122
4.5 Seasonal and Spatial Variation in PM_{2.5} Composition	123
4.6 Conclusion.....	125

CHAPTER- 5 SOURCE APPORTIONMENT	128
5.1 Introduction	128
5.2 Estimation of Uncertainty and Data below Detection Limit	129
5.3 Input Data	130
5.4 The Methodology in Selecting Number of Factors	131
5.5 Solution Stability and Rotational Ambiguity	133
5.6 PMF Analysis.....	134
5.7 PMF Results for the Summer and Winter Season.....	136
5.7.1 Traffic Factor	141
5.7.2 Crustal Factor	148
5.7.3 Sea Salt/ Nitrate Factor.....	152
5.7.4 (SS, Ni & V) and (Zn & As) Secondary Sulfate Factor	158
5.7.6 (La & Co) factor	171
5.8 Quantitative Variations between Seasons and Locations	175
5.8.1 Natural Sources Contribution	178
5.8.2 Anthropogenic Sources Contribution	179
5.8.3 Intermittently Sources Contribution	180
5.9 Conclusion.....	180
 CHAPTER 6: POLICY IMPLICATIONS	 182
6.1 Introduction	182
6.2 Accounting for The Exceedances of PM Limit Values from Natural Sources	184
6.3 An Action Plan for Improving Air Quality in Doha.....	188
 CHAPTER 7 – CONCLUSION AND FUTURE WORK.....	 193

LIST OF FIGURES

Figure 1.1 Illustration of particulate matter modes in a typical atmospheric particle size distribution. The dotted line of the accumulation mode penetrates into sizes $<0.1 \mu\text{m}$, as does the PM 10-2.5 mode into the accumulation mode. (Source: Cao et al., 2013).....	8
Figure 1.2 State of Qatar map (Source: Ashour, 2013).....	9
Figure 1.3 Landscape around Dukhan on the west of the peninsula showing limestone rock formations (Source: Catnaps, 2014).....	10
Figure 1.4 Landscape near Al-Wakra on the south-east of the peninsula showing dunes sit on limestone surface (Source: Catnaps, 2014).....	11
Figure 1.5 The MOE air quality stations distribution in Doha (MOE, 2013).....	13
Figure 1.6 Visibility below 5,000 m from 2007 to 2013 showing high frequency during the spring and summer dust event seasons (Source: QCAA, 2014).....	15
Figure 1.7 Numbers of days per year in Doha city when visibility was below 5,000 m (Source: QCAA, 2014) .	16
Figure 1.8 Modelled global distribution of SSA surface number concentration in the winter (December, January, and February) and the summer (June, July, and August) of 2006 (Source: Fan and Toon, 2011).....	18
Figure 1.9 Qatar map showing: 1) salt pans in blue and 2) sand dune in brownish colour (Source: Ashour, 2013).....	19
Figure 1.10 Convective complex on the night of 13 th September 2004 over the UAE domain: (a) Electrically active storm, (b) Significant cloud top heights (18 km), (c) Dust enhancement (haboob appears as a red linear feature), and (d) Frontal advance roughly one-half hour later (Source: Miller et al., 2008).....	22
Figure 1.11 Moderate Resolution Imaging Spectroradiometer (MODIS) on NASA's Terra satellite captured true-color image of dust storm from Iraq on July 31, 2009. (Source: NASA 2009)	22
Figure 1.12 Map Showing Al-Shamal synoptic situation (1200GMT, 9th June 1982) with surface isobars and 850 mb streamlines (broken) of the Arabian Gulf and surrounding Countries. Dotted area represents land over 1,000 m (Source: Pye, 1978).....	23
Figure 1.13 Doha city map showing construction and stockpiles in red areas, Doha harbour, and Hamad international airport.....	24
Figure 1.14 Vessels' density per day in the Arabian Gulf (Sources: Marine vessel traffic, 2013).....	28
Figure 1.15 Industrial areas locations and wind roses in the winter of 2014/2015 and the summer of 2015.....	36
Figure 1.16 Wind direction percentage of occurrences for Doha city (Sources: Weather Online, 2017).....	36
Figure 2.1 PM-162 M Sampler (Source: PM-162M Manual 2011).....	42
Figure 2.2 PM _{2.5} gooseneck inlet head (Source: PM-162M Manual 2011).....	43
Figure 2.3 Diagram of the PM-162 M sampler (Source: PM-162M Manual 2011).....	44
Figure 2.4 Damages to quartz filters due to disc rotations.....	44
Figure 2.5 Two samplers back to back at the top rack in the station.....	45
Figure 2.6 Samplers' goose-neck inlets at the height of 4 m above ground level.....	46
Figure 2.7 Al-Corniche (AC) and Qatar University (QU) Sampling sites in Doha.....	48
Figure 2.8 Al-Corniche Station (AC).....	49
Figure 2.9 The area surrounding AC station.....	49
Figure 2.10 Qatar University Station (QU).....	50
Figure 2.11 The area surrounding QU station.....	50
Figure 2.12 Earth work activity at the QU site during the winter campaign	51
Figure 3.1 Daily pattern of meteorological parameters in the AC and QU in summer.....	64
Figure 3.2 Daily pattern of meteorological parameters in AC and QU in winter.....	65
Figure 3.3 Wind rose of the AC and QU sites during winter and summer campaigns.....	66
Figure 3.4 Time series of PM _{2.5} for both campaigns at the AC and QU sites.....	70

Figure 3.5 Time series of SiO ₂ for both campaigns at the AC and QU sites.....	71
Figure 3.6 Qatar university location showing nearby construction site and sand piles.....	71
Figure 3.7 Pareto chart for the disruption of species total average mass concentration from in descending order and a cumulative line of total percentage in the winter season.....	73
Figure 3.8 Pareto chart for the disruption of species total average mass concentration from in descending order and a cumulative line of total percentage in summer season.....	73
Figure 3.9 Time series of Sulfate at the AC and QU sites in the summer season	75
Figure 3.10 Pollution rose as a function of as a function of relative humidity in the summer season at the AC and QU sites	76
Figure 3.11 Time series of SiO ₂ at the AC and QU sites in the summer season	77
Figure 3.12 Pollution rose of metal oxides by wind direction at the AC and QU sites in the summer season	77
Figure 3.13 Time series of PM _{2.5} daily in the winter and the summer seasons; the red line shows interim target (IT-1= 75 µg/m ³).....	78
Figure 3.14 PM _{2.5} air quality index (AQI) breaking points (Source: AQINC, 2017).....	79
Figure 3.15 PM _{2.5} air quality category in the winter and summer at both sites.....	80
Figure 3.16 Relationship between cations (x-axis) and anions (y-axis) in meq/l in the winter season at the AC site (Unity line in red colour).....	81
Figure 3.17 Relationship between cations (x-axis) and anions (y-axis) in meq/l in the winter season at the QU site (Unity line in red colour).....	82
Figure 3.18 Relationship between cations (x-axis) and anions (y-axis) in meq/l in the summer season at the AC site (Unity line in red colour)	83
Figure 3.19 Relationship between cations (x-axis) and anions (y-axis) in meq/l in the summer season at the QU site (Unity line in red colour)	84
Figure 3.20 EF for PM _{2.5} constituents at both sites and seasons	85
Figure 3.21 Relationship between PM _{2.5} and wind speed at the AC site in the winter season. The points inside the green circle represent the dust storm events. Y and *Y equations represent PM _{2.5} points including dust events and PM _{2.5} excluding dust events respectively.....	87
Figure 3.22 Relationship between PM _{2.5} and wind speed at the QU site in the winter season. The points inside the green circle represent the dust storm events. Y and *Y equations represent PM _{2.5} points including dust events and PM _{2.5} excluding dust events respectively.....	88
Figure 3.23 Back trajectory showing air mass route for A) 11 th of Feb 2015 when wind arrived at high speed and B)- 14th of Feb 2015 when wind arrived at low speed.....	89
Figure 3.24 The Arabian Peninsula showing sand dunes area.....	89
Figure 3.25 Relationship between PM _{2.5} mass against wind speed at the AC and QU sites in the summer season.....	90
Figure 3.26 Scatter plot for PM _{2.5} mass against wind speed colored by RH and sized by the level of AP at the AC and QU sites in the summer season	90
Figure 3.27 Scatter plot for PM _{2.5} mass against wind speed at the AC and QU sites during low atmospheric pressure.....	91
Figure 3.28 Scatter plot for PM _{2.5} mass against wind speed at the AC and QU sites during high AP. The value on the 6 th of June was excluded from the correlation equation	92
Figure 3.29 Back trajectory on the 6 th of June 2015.....	93
Figure 4.1 Surface soil sampling regions shown as green stars on a global map of dust sources as identified from Total Ozone Mapping Spectrometer (TOMS) data (source: Engelbrecht et al., 2016).....	98
Figure 4.2 Relationship between measured mass on X-axis and Constructed mas in Y- axis in winter [A] &[B] and in summer [C] and [D].....	105

Figure 4.3 Relationship between SO_4^{2-} on quartz filters (y-axis) and 3S on Teflon filters (x-axis) in $\mu\text{g}/\text{m}^3$ in winter season [A] AC site and [B] QU site, and in the summer season [C] AC site and [D] QU site. (Red line represents unity line)	112
Figure 4.4 Experimental comparability between sulfate determined by IC on Quartz filter (y-axis) and Teflon filters (X-axis) (Source: Vecchi et al., 2009).....	114
Figure 4.5 Relationship between sulfur measured on Teflon by XRF and sulfate measured on nylon by IC in [A] western site and [B] eastern site (Source: Eldred, 2001)	115
Figure 4.6 Comparison of IC sulfate on nylon [$\text{SO}_4(\text{N})$], IC sulfate on Teflon [$\text{SO}_4(\text{T})$], and PIXE sulfur on Teflon [$\text{S}_3(\text{T})$]. The IC analysis on the Teflon filters was performed after the XRF and PIXE analyses. Only samples with a difference between IC sulfate on nylon and PIXE sulfur on Teflon greater than 15% are included. The samples are differentiated as to whether the IC on Teflon agrees more with the IC on nylon or the PIXE on Teflon. The open squares are 8 samples in which the agreement is best with IC on nylon. For the 10 solid squares, the agreement is better with PIXE on Teflon. The agreement is about equal for the 9 diamonds (Source: Elderred, 2008)	117
Figure 4.7 Relationship between $\text{SO}_4^{2-}/3\text{S}$ ratio with relative humidity at the QU site in summer [A] & [B] and in winter [C] & [D].....	118
Figure 4.8 Illustration for the effect of air flow, type of filters, and liquid particles on the position of the particle on filters.....	120
Figure 4.9 Relationship between constructed mass and measured mass in the summer season using 3S	122
Figure 4.10 Comparison of percentage composition of $\text{PM}_{2.5}$ in the AC and QU in the winter and summer seasons.....	125
Figure 5.1 Factors finger print concentration in percent of individual species contributing to each factor at the AC site in the summer season.....	138
Figure 5.2 Factors finger print concentration in percent of individual species contributing to each factor at the QU site in the summer season.....	138
Figure 5.3 Factors finger print concentration in percent of individual species contributing to each factor at the AC site in the winter season.....	139
Figure 5.4 Factors finger print concentration in percent of individual species contributing to each factor at the QU site in the winter season.....	139
Figure 5.5 Source profile of Traffic factor in the summer and the winter seasons.....	141
Figure 5.6 Scatter plot for traffic factor at the QU and AC sites, coloured by wind direction.....	143
Figure 5.7 Location map of the monitoring sites. Red arrow shows traffic emissions coming from the area in between the QU site and the AC site toward the AC site from north-northwest direction showing a higher traffic contribution at the AC site, and the blue arrow shows emissions coming from the area in between the AC site and the QU site toward QU site from southeast direction, showing a higher traffic contribution at the QU site.....	143
Figure 5.8 Time series of traffic factor in the winter season showing a higher concentration at the AC site.....	144
Figure 5.9 Time series of traffic factor in the winter season showing a higher concentration at the QU site.....	145
Figure 5.10 CPF 90 th percentile rose at the AC site in summer (orange) and winter (blue) showing the direction of traffic source.....	146
Figure 5.11 CPF 90 th percentile rose at the QU site in summer (orange) and winter (blue) showing the direction of traffic source.....	147
Figure 5.12 Source profile of crustal factor in the summer and the winter seasons.....	148
Figure 5.13 EF of crustal components at all sites normalized to aluminium versus EF in the upper continental crust (Mason., 1966, and Taylor & McLennan, 1985).....	149

Figure 5.14 Time series of crustal factor in the summer season at the QU and AC sites.....	149
Figure 5.15 CPF 90 th percentile rose showing the direction of the crustal factor at the AC and QU sites [A&B] in winter, and at the AC and QU sites [C&D] in summer respectively.....	151
Figure 5.16 Source profile of sea salt/ nitrate factor in the summer and the winter seasons.....	153
Figure 5.17 Scatter plot for Cl-/Na+ ratio against the sum of non-sea salt sulfate and nitrate at both sites in summer	154
Figure 5.18 CPF 90 th percentile rose showing the direction of sea salt/nitrate source at the AC and QU sites [A&B] in winter, and at the AC and QU sites [C&D] in summer respectively.....	155
Figure 5.19 Time series of sea salt/nitrate factor in the winter season at both sites. The circle shows the time when the salt factor concentration at the QU site was higher than at the AC site.....	156
Figure 5.20 Time series of nitrate in the winter season at the QU and AC sites. The circle shows the time when nitrate levels increased at the QU site.....	156
Figure 5.21 Scatter plot for Cl-/Na+ ratio against the sum of non-sea salt sulfate and nitrate at the QU and AC sites in the winter season.....	157
Figure 5.22 Source profile of (SS, Ni&V) factor in the summer and the winter seasons.....	158
Figure 5.23 Source profile of (SS, Zn&As) factor in the summer and (Zn&As) in the winter seasons at the AC site.....	159
Figure 5.24 CPF 90 th percentile rose at the AC site in summer (orange) and in winter (blue) showing the direction of (SS, Ni&V) source.....	160
Figure 5.25 CPF 90 th percentile rose at the QU site in summer (orange) and in winter (blue) showing the direction of (SS, Ni&V) source.....	160
Figure 5.26 CPF 90 th percentile rose at the AC site showing the direction of (SS, Zn&As) factor in orange and (Zn &As) factor in blue. Red arch shows Doha port territory.....	161
Figure 5.27 Pollution rose at the AC site showing the direction of (SS, Zn&As) factor as a function of wind speed in the summer season.....	162
Figure 5.28 Pollution rose at the AC site showing the direction of (Zn&As) factor as a function of wind speed in the winter season.....	162
Figure 5.29 Time series of (SS, Zn & As) factor at the AC site and (SS, Ni & V) factor at the QU site in the summer season.....	165
Figure 5.30 Time series of (SS, Ni & V) factor at the AC site and (SS, Ni & V) factor at the QU site in the summer season.....	165
Figure 5.31 Source profile of Lusail factor in the summer and the winter seasons.....	168
Figure 5.32 Time series of Lusail factor in the summer season at both sites. The two circles show high points found at the QU site causing the weak correlation between both sites.....	169
Figure 5.33 CPF 90 th percentile roses for Lusail factor in summer (orange) and winter (blue) at the QU and AC sites intersecting at Lusail city. Yellow and green guide arrows to show the range of wind direction at both sites and their intersection at the Lusail city in the winter and summer seasons.....	170
Figure 5.34 Time series of Lusail factor in the winter season at both sites.....	170
Figure 5.35 Source profile of (La&Co) factor in the summer season.....	171
Figure 5.36 Time series of (La & Co) factor and La element at the AC site in summer. The high value on the May 30 th was considered as an outlier and was omitted from PMF-5 analysis.....	172
Figure 5.37 Time series of (La & Co) factor and La element at the QU site in summer.....	172
Figure 5.38 Time series of La element in summer at both sites.....	173

Figure 5.39 Two high episodic concentrations of La element measured at the AC and QU sites. La concentration is showing a declining behaviour while the wind moves from east to west direction. In the small frame, two potential sources located in the Arabian Gulf namely Halul island and the Al-Shamal north field at 80 Km and 140 km from Doha city respectively. Both sources deal with oil and gas exploration and extraction, and oil storages tanks. Number (1) Represent the episode occurred in the May 30 th , 2015, while (2) represent episode on the July 7 th , 2015.....	174
Figure 5.40 Pollution rose at the QU site showing the direction of (La & Co) factor as a function of wind speed	175
Figure 5.41 Pollution rose at the AC site showing the direction of (La & Co) factor as a function of wind speed	175
Figure 5.42 Factor pie chart for mass concentration distribution among the factors resolved by the PMF-5, at the AC site in the summer season.....	176
Figure 5.43 Factor pie chart for mass concentration distribution among the factors resolved by the PMF-5, at the QU site in the summer season (no correction for multicollinearity was done here).....	176
Figure 5.44 Factor pie chart for mass concentration distribution among the factors resolved by the PMF-5, at the AC site in the winter season.....	177
Figure 5.45 Factor pie chart for mass concentration distribution among the factors resolved by the PMF-5, at the QU site in the winter season.....	177
Figure 6.1 Time series of PM _{2.5} concentration along with sulfate concentration in the winter season for the whole study period, at both sites	181
Figure 6.2 Time series of PM _{2.5} concentration along with silicon oxide concentration in the summer season for the whole study period, at both sites.....	181

LIST OF TABLES

Table 1.1 Annual PM ₁₀ concentrations in µg/m ³ from 2007 to 2013 at Doha monitoring stations (MDPS, 2007 & 2013)	14
Table 1. Annual PM _{2.5} Concentrations in µg/m ³ from 2012 to 2013 from 2012 to 2013 at Doha monitoring stations (MDPS, 2013)	15
Table 1.3 Markers associated with PM sources	38
Table 1.4 Mass reconstruction table.....	39
Table 2.1 An overview of the sampling campaign in Doha	51
Table 2.2 Limit of detections (MDL).....	59
Table 3.1 Overview of meteorological parameters for the winter season (Nov2014-Feb2015) and the summer season (May2015-Aug2015) at the QU and AC sites	63
Table 3.2 Days with dust events in Doha 2014/2015 obtained from Qatar Civil Aviation Authority, Department of Meteorology (QCAA, 2014)	67
Table 3.3 Descriptive data for species mean, max, and min concentrations in the winter season (Nov 2014 - Feb 2015) at the QU and AC sites	68
Table 3.4 Descriptive data for species mean, max, and min concentrations in the summer season (May 2015 - August 2015) at the QU and AC sites.....	69
Table 3.5 Correlation coefficient between same species at both sites	72
Table 4.1 Reconstruction equation from Chow et al., (1996), and a modified equation used in this work.....	96
Table 4.2 Metals ratios results when regression line forced through zero with correlation coefficients and uncertainties.....	97
Table 4.3 Regression result of 3.5Si against the sum of metal oxides in both seasons and sites	100
Table 4.4 Species included in the mass closure, the performed analysis methods, types of filters, and the possible artefact with each filter type.....	104
Table 4.5 Results of linear regression of reconstructed mass (y) upon gravimetric mass (x).....	106
Table 4.6 Results of linear regression of reconstructed mass (y) upon gravimetric mass (x) after carbonate correction	108
Table 4.7 Results of a linear regression of reconstructed mass (y) upon gravimetric mass (x) after organic carbon correction.....	109
Table 4.8 Results of a linear regression of reconstructed mass (y) upon gravimetric mass (x) after ammonium nitrate correction	111
Table 4.9 Results of the linear regression of reconstructed mass (y) upon gravimetric mass (x) after substituting SO ₄ ²⁻ with 3S.....	122
Table 4.10 Results of the linear regression of reconstructed mass (y) upon gravimetric mass (x) after correcting for carbonate mass, ammonium nitrate and organic carbon.....	123
Table 5.1 Summary of the PMF-5 solutions at the AC and QU sites in the summer season.....	140
Table 5.2 Summary of the PMF-5 solutions at the AC and QU sites in the winter season.	140
Table 5.3 Summary of factors mass contributions and correlations between sites.....	163

Table 6.1: Qatar air quality standard for particulate matter with corresponding WHO air quality interim-targets for PM ₁₀ and PM _{2.5} , and WHO air quality guidelines for PM ₁₀ and PM _{2.5}	183
Table 6.2 PM ₁₀ and PM _{2.5} annual concentrations in µg/m ³ from 2007 to 2013 at Doha monitoring stations. Qatar's PM ₁₀ annual AQS is 50 µg/m ³ (MDPS, 2007 & 2013).	184
Table 7.1 Major chemical species percentage and mass concentration found by the mass closure solution.....	194

ABBREVIATIONS

AC	Al-Corniche
AQG	Air quality guideline
AQI	Air quality index
AQMS	Air Quality Management Strategy
AQS	Air quality standards
AZ	Aspire Zone
CAFÉ	Clean Air For Europe
CMB	Chemical mass balance
CPF	Conditional Probability Function
DDW	Distilled deionized water
DIA	Doha Industrial Area
DMS	Dimethyl sulfate
EC	Elemental Carbon
EF	Enrichment factor
EMRQ	ExxonMobil Research Qatar
EPA	Environment Protection Agency
FEM	Federal Equivalent Method
FID	Flame ionization detector
GTL	Gas to liquid
HCl	Hydrochloric acid
HNO ₃	Nitric acid
IAQM	Institute of Air Quality Management
IC	Ion Chromatography
ICP-MS	Inductively coupled plasma mass spectrometry
IMO	International Maritime Organization (IMO)
IMPROVE	Interagency Monitoring of Protected Visual Environments network
IT	Interim target
LNG	Liquefied natural gas
LPG	Liquid petroleum gas
MDL	Method detection limit

MOE	Ministry of Environment
MIC	Mesaieed Industrial City
MW	Molecular weight
OC	Organic carbon
OM	Organic matter
PC	Pyrolytic carbon
PIXE	Particle-induced X-ray emission
PM	Particulate matter
PMF	Positive matrix factorization
POC	Primary organic carbon
QCAA	Qatar Civil Aviation Authority
QU	Qatar University
RLC	Ras Laffan City
ROS	Reactive oxygen species
SA	Source apportionment
SD	Standard deviation
S/N	Signal to noise ratio
SOC	Secondary organic carbons
SSA	Sea-spray aerosol
TSP	Total suspended particles
UCC	Upper continental crust
UF	Ultrafine
WD-XRF	Wavelength Dispersive X-Ray Fluorescence
WHO	World health organization
WMO	World Meteorology Organization

CHAPTER 1- INTRODUCTION

1.1 Background

Urban air quality is a major health concern in cities worldwide. Globally, 3 million deaths were attributed to ambient air pollution in 2012 (WHO, 2016). Particulate matter (PM) is considered one of the most important pollutants found in the ambient air and regardless of pollution control programs, cities across the world often exceed national air quality standards.

PM is defined as a mixture of solid particles and liquid droplets suspended in the air owing to its small gravitational settling rate (NARSTO, 2004). The particle's nature, chemical composition, size, and shape vary according to their origins, formation methods, and the mechanisms of removal and transportation.

Atmospheric PM has an important environmental and health impact including radiation balance of the earth (IPCC, 2001), visibility degradation, long-range transport of toxic materials and pathogenic microorganisms, and its association with excess morbidity and mortality due to respiratory and cardiovascular diseases (Pope, 2009; WHO, 2006; Griffin, 2007; Abdeen et al., 2014).

PM has a direct effect on climate change through scattering and absorbing solar radiation leading to net warming and cooling of the earth, and an indirect effect through the formation of cloud condensation nuclei (IPCC, 2001). For example, sulfate aerosols have a cooling effect because they serve as cloud condensation nuclei, which increase the cloud coverage and cause more reflectivity of solar radiation (Celis et al., 2004; Davidson et al., 2005). However, the black carbon particles have a warming effect, as they reduce the albedo of snow cover when they settle on thereby reducing the fraction of the incident solar radiation that is backscattered to space (IPCC, 2001; Wallace and Hobbs, 2006).

In addition to its impact on the climate, PM is considered one of the key pollutants posing major threats to health (WHO, 2005). Growing epidemiological studies have shown adverse health effects at the acute and chronic exposure to PM resulting in an increase in morbidity and mortality of respiratory and cardiovascular diseases (Donaldson et al., 2005). Long-term exposure to PM can aggravate asthma and respiratory symptoms, as well as decrease lung growth in children, whereas acute exposure to PM can increase hospital admissions and daily mortality due to respiratory and cardiovascular causes shortly after exposure (Kapposa et al., 2004). Studies of short-term exposure to PM₁₀ have reported an increase of 0.5% in mortality per 10 µg/m³ increase in PM₁₀ (WHO, 2005). These findings were tested in multi-city studies conducted in Europe, USA, and Asia with similar results despite the differences in pollutant mixes expected to be found in different locations (WHO, 2005; Harrison and Yin, 2000). Conversely, Shafer et al., (2010) and Valavadinis et al., (2008) found that particle toxicity varies based on particles' chemical composition and that the water-soluble fraction of particles is more harmful because such particles produce reactive oxygen species (ROS) upon their reaction with macrophages and epithelial cells in lung lining leading to oxidative stress which been linked to respiratory infections, cardiopulmonary diseases, and cancer.

The majority of epidemiological studies use PM₁₀ or PM_{2.5} as exposure indicators due to their ability to enter the respiratory tract (Kappos et al., 2004; WHO, 2005; Harrison et al. 2010). Previous epidemiological studies have focused on PM₁₀ size as an exposure indicator due to the particle's capability to penetrate the thoracic region of the respiratory system. However, recent studies have investigated fine particles < 2.5 µm, since this smaller size has far greater efficiency in terms of penetrating the alveolar regions of the respiratory system compared to coarse particles fraction in the 2.5 - 10 µm range (Harrison et al., 2000). According to the WHO (2005), many studies, such as the American Cancer Society Study of Particulate Air

Pollution and Mortality (Abrahamowicz et al., 2003) and the Harvard Six-Cities Study (Laden et al., 2000; Krewski et al., 2003) reported a robust association between long-term exposure to PM_{2.5} and mortality. Long-term exposure to PM_{2.5} is associated with an increase in mortality from cardiovascular disease by 6-13% per 10 µg/m³ increase in PM_{2.5} concentrations. Moreover, the strongest association between mortality and particles size was found for PM_{2.5}, followed by PM₁₀ (Kapposa et al., 2004).

Windblown dust, one of the main sources of PM in arid regions, can cause a damaging effect on human health. A study in Seoul, Korea, Kwon et al., (2002) found a significant correlation between dust storms and mortality due to respiratory and cardiovascular disease. Studies in the Middle East reported that counties impacted with dust storms such as Kuwait and Saudi Arabia have a higher occurrence of asthma compared with European countries (Al-Dawwod, 2000; Abal et al., 2010). Dust induces inflammation and oxidative stress that persists over time in macrophages more pronouncedly than pollen, wood burning, and traffic particles do (Etyemezian, 2014). Dust can also physically scar the alveolar wall, destroy the capillary beds, and cause emphysema (Pye, 1987). Frequent exposure to respirable crystalline silica, which is a major component of the earth's crust, can cause silicosis a non-reversible, disabling, and occasionally deadly lung disease. Silicosis is widely reported among miners and quarry workers (Spellman, 2009), as well as inhabitants of desert regions (Pye, 1987). Dust also can serve as a carrier of pathogenic microorganisms such as *Bacillus anthracis* and influenza viruses causing outbreaks at downwind sites (Griffin, 2007).

According to Kelly and Fussell (2015), Many studies have shown health benefits and a declining in mortality after the reduction of PM pollution levels. A decline of black smoke in Dublin after a ban on coal sales was associated with a decrease in pulmonary and cardiovascular deaths by 15% and 10.3% respectively (Ayres et al., 2006). In Utah Valley

between 1986 and 1987, the closure of a steel mill led to a 50% reduction in PM_{10} concentration, which was associated with a decrease in hospital admissions for children (Molinelli et al., 2002). In the USA, the reduction of $\text{PM}_{2.5}$ mass concentration between 1980 and 2000 was associated with an increase in life expectancy by 2.7 years (Pope et al., 2009). In Switzerland, a declining in PM_{10} mass concentration by $5\text{--}6\ \mu\text{g}/\text{m}^3$ was associated with a reduction in the annual rate of decline of lung function (Downs et al., 2007). According to Kelly and Fussell (2015), the improvement in health can appear directly following any reduction in PM mass concentration which highlights the importance of air quality management and control of PM to reduce pollution levels to protect public health.

1.1.1 PM Chemical Composition

PM is a complex mixture of primary and secondary particles, emitted either from natural sources or by human activities. Primary PM is emitted from sources directly into the atmosphere; it includes windblown dust, sea spray, soot from fuel combustion, fugitive dust from metallurgical processes, and freshly emitted organic compounds condensed on particles. Secondary PM, on the other hand, is formed in the atmosphere by the condensation, oxidation, and reactions of precursor gases such as volatile organic compounds, sulfur oxides, nitrogen oxides, and ammonia (Harrison, 1997).

PM has common major chemical components including secondary sulfate, nitrate and ammonium particles, mineral dust, sea salt, and carbonaceous compounds (Harrison and Yin, 2000). PM composition can be influenced by different types of sources, chemical transformation in the atmosphere, long-range transport and removal process (QUARD, 1996). The breakdown of particulate matter composition in details consists of secondary sulfate particles which are mainly produced by the gas to particle conversion of SO_2 and are typically present in the fine particle fraction as ammonium sulfate. Sulfur from natural sources (e.g.,

volcanoes, and sea spray) enters the atmosphere mostly in a reduced form, such as hydrogen sulfide (H_2S) and dimethyl sulfate (DMS), and then is oxidised in the oxygen-rich atmosphere to SO_2 , whereas anthropogenic sulfur sources include combustion of sulfur-containing coal and petroleum products, biomass burning, and smelting of nonferrous ores (Harrison and Yin, 2004). Nitrate, on the other hand, is formed either in soil through the nitrification process, where ammonia in soil is oxidised by bacteria under oxygen-rich conditions to nitrite and nitrate, or mainly through the oxidation of nitrogen oxide in the atmosphere. Particulate nitrate is expected to be present in the fine particle fraction as ammonium nitrate due to the reaction between ammonia and nitric acid, and in the form of sodium nitrate mainly in coastal areas through the reaction of sea salt particles and gaseous nitric acid (Harrison and Yin, 2004, QUARG, 1996). Nitrogen oxides, an anthropogenic precursor of nitrate, are produced through two formation modes. The first mode of nitrogen oxides formation is the thermal formation which dominates the anthropogenic sources of NO_x and is mainly produced by traffic and power plants. Thermal NO_x is formed when nitrogen (N_2) and oxygen (O_2) in the air of a combustion engine combine because of the high temperature (above 1,000 K). The second formation mode is fuel nitrogen oxide, which is formed through the combustion of nitrogen contained within fuel (Spellman, 2009). Ammonia, a basic nitrogen compound in the atmosphere, is accountable for ammonium formation through the neutralisation of sulfuric and nitric acids. Ammonia is mainly produced by the decomposition of urea excreted from domestic and wild animals and by the biological fixation process (Harrison and Yin, 2004). Mineral dust is transported to the atmosphere by wind and largely found in the coarse particle fraction. Arid and semiarid regions are the main natural sources of mineral particles. In the year 2000, the worldwide direct dust emissions into the atmosphere were around 2000 Tg/year for all particle sizes (Wallace and Hobbs, 2006). Crustal components are also released

to the atmosphere through fugitive emissions from paved/unpaved roads, construction/demolishing activities, storage stockpiles, and by traffic-induced turbulence. Sea salt aerosols are one of the main contributors to atmospheric particles by mass. Salt particles are injected into the atmosphere through bubble bursting and wind-blown spray, and their production from oceans is estimated to be around ~1,000 to 5,000 Tg/year including all sizes of salt particles (Wallace and Hobbs, 2006).

Carbonaceous material contributes a considerable fraction (20% - 80%) to the atmospheric fine PM in an urban environment (Saarikoski et al., 2008). Carbonaceous material is divided into two categories, elemental carbon (EC) and organic carbon (OC). EC enters the atmosphere as primary particles originating from pyrolysis during incomplete combustion of engine fuel, incineration, and biomass burning (Szidat et al., 2009), whereas OC includes primary organic carbon (POC), which originates from fuel combustion processes and primary biogenic emissions, as well as secondary organic carbons (SOC) which is formed through the atmospheric oxidation of organic species (Kroll and Seinfeld, 2008).

The relative abundance of those major chemical components can vary between locations due to differences in pollutants loadings and the effects of the different geographical natures of locations such as arid lands versus agricultural lands (Harrison and Yin, 2000). In the UK, several studies showed that the typical composition of urban fine PM is as follows: carbonaceous material ~ 50%, sulfate, nitrate, and ammonium ~ 42%, minerals ~ 3%, and salt ~ 5% (QUARG, 1993 and 1996). In comparison, in the Middle East, a study in 11 cities including Nablus, east Jerusalem, west Jerusalem, Hebron, Eilat, Tel Aviv, Haifa, Amman, Aqaba, Raham, and Zarqa showed that the composition of urban fine PM is as follows: carbonaceous material ~ 45%, sulfate, nitrate, and ammonium ~29.5%, minerals ~21.5%, and salt ~3% (Abdeen et al., 2014). Also, the average composition of fine particulate matter from

six middle eastern countries namely Qatar, Kuwait, Iraq, Emirates, Djibouti, and Afghanistan that was calculated from (Engelbrecht et al., 2009)'s study showed that PM composition is as follows: carbonaceous material ~ 22.5%, sulfate, nitrate, and ammonium ~ 25%, minerals ~ 50%, and salt ~ 2.5%. Whereas in Saudi Arabia, in Jeddah city, the composition of fine PM apart from nitrate and carbonaceous materials (which was not measured in the samples taken), showed ammonium sulfate ~ 49.4%, minerals ~ 28%, and salt ~3% (Khodeir et al., 2012).

1.1.2 PM Size Properties

The PM size range covers more than five orders of magnitude; it ranges from a few nanometres for freshly formed particles up to several 100s of micrometres (Harrison and Grieken, 1998). Suspended particles are classified according to their size as total suspended particles (TSP), including PM₁₀, PM_{2.5}, and ultrafine (UF) particles. The PM₁₀ fraction comprises a coarse fraction size from 2.5 to 10 µm and a fine fraction below 2.5 µm which includes UF particles with a diameter below 0.1 µm. PM_{2.5} is the mass concentration of particulates passing through a size-selective inlet with a 50% efficiency at an aerodynamic diameter of 2.5 µm (Harrison and Yin, 2000). PM_{2.5} has certain qualities such as their fine size which affect their residence times and their ability to infiltrate indoor environments, which in turn make them potentially more harmful to human health and welfare. Fine particles are important vectors for long-range transport, and more efficient light scatterers hence affecting the visibility. The residence time of aerosol particles is determined by their removal rate, which is a function of particulate size. In the nucleation mode, particles less than 0.01 µm in diameter (Figure 1.1) have a lifetime of hours as they transmute into the next mode by coagulation and condensation (QUARG, 1996). As for the coarse mode, particles with a diameter of more than 10 µm, are deposited by sedimentation and have a lifetime of several hours. On the other hand, fine particles with a diameter between ~0.2 and 2 µm have longer

residence times (e.g., 1-2 weeks) as a result of weak sinks but strong sources from the coagulation of Aitken nuclei (Wallace & Hobbs, 2006).

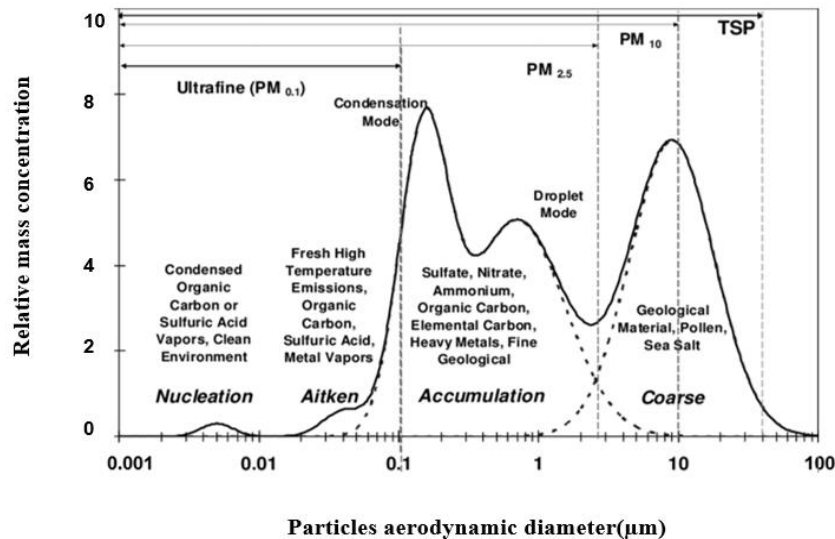


Figure 1.1 Illustration of PM modes in a typical atmospheric particle size distribution. The dotted line of the accumulation mode penetrates into sizes $<0.1 \mu\text{m}$, as does the PM 10-2.5 mode into the accumulation mode. (Source: Cao et al., 2013)

Another issue related to particles size is the efficiency with which fine particles can infiltrate indoor environments. Indoor air quality is of great importance since individuals tend to spend more of their time indoors. According to Thatcher and Layton (1994), buildings provide little filtration of particulate matter. Hence, indoor air quality is influenced by outdoor pollution levels which make personal exposure to air pollutants occurs in both outdoor and indoor environments. Khillare (2004) reported that 60-70% of fine particles penetrate the indoors efficiently and found that the ratio of indoor to outdoor concentration for coarse particles is lower than that of fine particles. This result is consistent with the findings of Thatcher and Layton (1994), which connect the decline in coarse particles' penetration rates to the sudden drop in their velocity at ventilation openings, which enables them to fall-out on windows and doors frames by gravitational settling. Also, Laumbach et al., (2015) reported that staying indoor to reduce exposures to PM is limited when windows are open as the penetration factors

can approach unity and due to relatively little loss particles to surface deposition. For example, in a study to reduce air pollution by using air conditioning, Lin et al., (2013) found an association between high outdoor PM levels and adverse changes in cardiovascular disease markers such as increased plasma CRP when windows are open but no changes with closed windows. Both long residence time and effective penetration to indoor environment properties make fine PM more profoundly harmful to the health and the environment (QUARD, 1996).

1.2 An Overview of Qatar

Qatar Peninsula is located on the north-eastern margin of the Arabian Peninsula (Figure 1.2). It stretches from Saudi Arabia and protrudes into the Arabian Gulf. It is bordered on three sides by Arabian Gulf sea water and connected to the south by Saudi Arabia. The land surface is mainly flat and rocky. Notable surface features include salt pans, which stretch along the coastline (Ashour, 2013), elevated limestone formations along the west coast (Figure 1.3), and vast aeolian sand accumulations of different types, such as thin sheets, sand shadows, and barchan dunes (Figure 1.4), which are found on the south-eastern part of Qatar Peninsula (Embabi and Ashour, 1993).

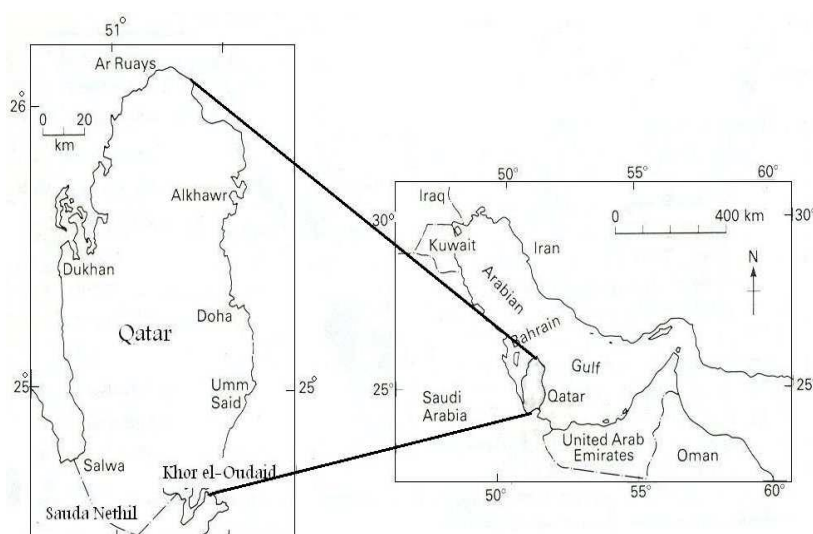


Figure 1.2 State of Qatar map (Source: Ashour, 2013)

Qatar has a desert climate, where the average daily temperature measured in 2012 ranges from 9° to 47°C (MDPS,2013). The summer months start from May through September and are characterised by intense heat (Tsiouri et al., 2015). Temperatures are moderate (~ 15 - 35 °C) from October to April. Annual rainfall is irregular and varies in terms of both time and location; though it is usually concentrated in the winter season with an annual average of 75 mm compared to 885 mm in the UK (Met Office, 2015). The rainfall quantity also differs by location within the peninsula, being heavier in the north and lighter in the south. The prevailing wind locally known as AL-Shamal blows 80% of the time from the north and north-west while about 20% of the winds blow from the opposite direction (Embabi and Ashour, 1993). Dust storms occasionally occur during the summer and spring, reducing visibility and temporarily disrupting transportation. Qatar's location within an arid climate region subjects the country to a substantial amount of crustal components that are generated locally or regionally due to dust storms.



Figure 1.3 Landscape around Dukhan on the west of the peninsula showing limestone rock formations (Source: Catnaps, 2014)



Figure 1.4 Landscape near Al-Wakra on the south-east of the peninsula showing dunes on limestone surface (Source: Catnaps, 2014) nomendatrue

Qatar's economic growth has been almost exclusively based on its natural resources (e.g., oil and gas). Oil was discovered first in Qatar in 1940, in Dukhan Field, in the west of the peninsula; this discovery transformed the state's economy. However, the economy was boosted again in 1991 after the discovery of a large natural gas reservoir off Qatar's north-east coast. Large industrial areas were constructed for the oil and gas industry. The heavy industrial projects in Qatar are based mainly on three locations; Rass Laffan city in the northeast, Misaeed city in the southeast, and Dukhan in the west. Qatar's heavy industries include refineries, liquefied gas plants, an aluminium plant, a fertiliser plant for urea and ammonia, a steel plant, a cement plant, and petrochemical plants. Other small and medium industries are located in the old and new Doha industrial Area at the southwest boundaries of Doha. Those industries, although they increased job opportunities and improved individuals' economic states, they are likely to impose a burden on Doha's air quality.

Doha is Qatar's largest city and the economic center of the country. It is located on the east coast of the peninsula overlooking the Arabian Gulf with a 47.7% of the nation's population residing in it and 27% in its surrounding suburbs (MDPS, 2013). Qatar's population has increased significantly from about 594,000 in 2000 to about 1,800,000 in 2013 (MDPS, 2013).

The increase in population was largely due to workers migrating from other countries to Doha for work opportunities after the country's industrial and economic growth. Accordingly, to contain the population demands, Qatar state improved and integrated its infrastructure over the last decade, which may result in an increase in pollutant emissions from the constructions and demolishing activities. Along with the industrial and infrastructure boost, the increase in population caused a significant increase in traffic volume where the registered vehicles and motorcycles increased from 2010 to 2015 by about 41% (MDPS, 2016). In addition to the increments in vehicles numbers, an increase in the demand for merchandise impacted the export and import trade and increased the number of aircraft by 55% between 2010 and 2015 (MDPS, 2014 & 2015) and the number of seagoing vessels in Doha port resulting possibly in greater levels of emissions.

1.3 Particulate Matter Pollution in Doha

Generally, the Middle East region has elevated concentration of particulate matter (Abdeen et al., 2014; WHO, 2016). Early measurements for PM in the Middle East in 2004, showed that PM₁₀ and PM_{2.5} annual concentration in Beirut city was 84 and 31 $\mu\text{g}/\text{m}^3$ respectively (Kouyoumdjian and Saliba, 2006). In the same year, in Kuwait City, the annual concentration ranged between 66 and 93 $\mu\text{g}/\text{m}^3$ for PM₁₀ across three sites and between 31 and 38 $\mu\text{g}/\text{m}^3$ for PM_{2.5} (Brown et al., 2008). In 2006, a large-scale study for PM in the Middle East region including 15 sampling sites, in which Qatar was one of these sites, showed that mean mass concentration for PM_{2.5} ranged between 35 and 111 $\mu\text{g}/\text{m}^3$ while PM₁₀ concentration ranged between 72 and 303 $\mu\text{g}/\text{m}^3$. Qatar was in the middle of this range with a value of 67 $\mu\text{g}/\text{m}^3$ for PM_{2.5}, and 165 $\mu\text{g}/\text{m}^3$ for PM₁₀ (Engelbrecht et al., 2009).

The WHO (2016) reported that Doha city ranks fifth and second globally for the highest PM_{10} and $PM_{2.5}$ mass concentrations respectively for the measurements in 2011. However, the number of deaths accredits to poor air quality ranks Qatar in the middle range of all listed countries. In Doha, the high PM mass concentrations are generally attributed to natural sources such as dust storms in spring and summer, which can explain the weak correlation between high PM and mortality, as a result of low exposure since people tend to stay indoors during dust storms events.

In Qatar, air quality monitoring started in 2007 after the publishing of Qatar Executive Regulation of the Environmental Protection Law (MOE, 2005). As the ambient air quality standards and gas emissions limits became legally binding, large industrial plants were obligated to monitor their emissions according to the law's standards and limits. Industrial facilities in Qatar maintain ambient air quality monitoring programmes through many fixed stations, providing data on gaseous pollutants to the MOE. Also, the MOE had established a network of fixed and mobile air quality monitoring stations in Doha to monitor ambient air quality. The network consists of three fixed stations and one mobile station. Figure 1.5 shows the fixed station locations including Qatar University (QU), Al-Corniche (AC) and Aspire Zone (AZ).

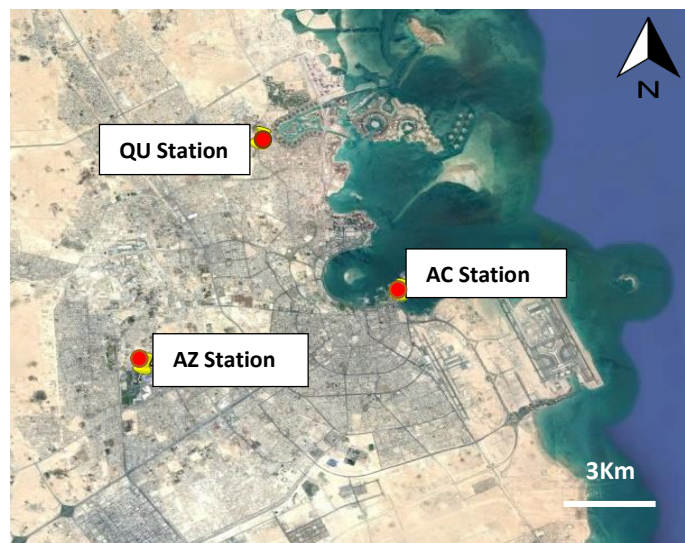


Figure 1.5 The MOE air quality stations distribution in Doha (MOE, 2013)

The air quality stations in Doha have reported repeated exceedances for both PM₁₀ short-term (24-hour standard limit value of 150 µg/m³) and long-term (1-year standard limit value of 50 µg/m³) national standards. The number of exceedances for PM₁₀ ranges from 50 to about 150 exceedances per year from 2010 to 2013 for the short-term standards. As per the annual limits, PM₁₀ continued to exceed the long-term standard from 2007 to 2013 (MDPS, 2013). These exceedances indicate that Qatar is a highly polluted city, at least by this measure in isolation. Table 1.1 shows the annual average from 2007 to 2013. All annual concentrations exceed the 50 µg/m³ annual limit for PM₁₀.

Table 1.1 Annual PM₁₀ concentrations in µg/m³ from 2007 to 2013 at Doha monitoring stations (MDPS, 2007 & 2013).

Stations	2007	2008	2009	2010	2011	2012	2013
Al-Corniche (AC)	129	201	261	155	120	130	147
Qatar University (QU)	197	340	338	269	186	219	122
Aspire Zone (AZ)	149	181	176	—	107	153	69

In 2012 PM_{2.5} and PM₁ monitors were added to all Doha air quality stations. The PM_{2.5} annual readings from the stations were compared against the WHO (2005) air quality guidelines as Qatar's environmental protection law did not regulate PM_{2.5} limit values. The PM_{2.5} interim target-2 (IT-2) value of 25 µg/m³ (WHO, 2005) guideline targets, was chosen for the comparison, because of the similarity between annual PM₁₀ interim target-2 (IT-2) and the Qatar national air quality standard for annual PM₁₀ values of 50 µg/m³. The result showed that annual PM_{2.5} values in 2012 and 2013, in Doha, exceed the annual standards of 25 µg/m³ (Table 1.2).

Table 1.2 Annual PM_{2.5} Concentrations in $\mu\text{g}/\text{m}^3$ from 2012 to 2013 at Doha monitoring stations (MDPS, 2013).

Stations	2012	2013
Al-Corniche (AC)	78	75
Qatar University (QU)	119	64
Aspire Zone (AZ)	92	37

Because of Qatar's desert climate, the increase of PM is thought of as a result of the frequent dust storms that hit Qatar. Figure 1.6 shows monthly dust events' frequencies based on visibility measurements below 5,000 m from 2007 to 2013 (QCAA, 2014). Visibility patterns show two peaks: one in February/March corresponding to spring dust storms and the other one in June/July/August due to summer dust storms which indicates that dust storms have a large influence on the abundance of PM.

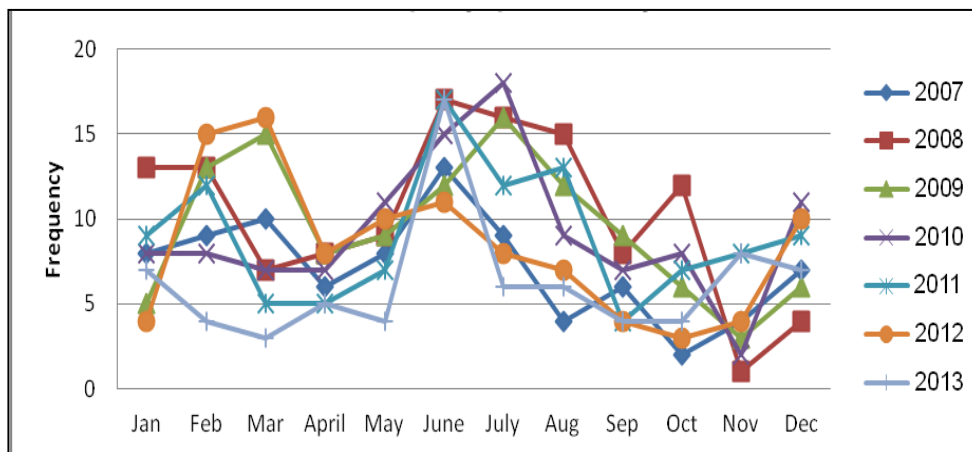


Figure 1.6 Visibility below 5000m frequency from 2007 to 2013 showing high frequency during the spring and summer dust event seasons (Source: QCAA, 2014).

Fine particles in the accumulation size range are likely to be removed from the lower atmosphere by rain in about 10 days whereas the dry deposition alone will take from 100 to

1000 days (QUARD, 1996). In Qatar, due to the scarcity of precipitation, fine particles are likely to be suspended in the air for days after dust events. These suspended particles can degrade visibility, soil buildings, and obscure the blue colour of the sky which according to Malm (2003), can affect people's psychological well-being, increase stress and degrade outdoor activity enjoyment. Figure 1.7 shows the number of days in Doha when visibility was below 5,000 m due to dust events (QCAA, 2014). The fact that Qatar has an arid climate which characterised by high ambient temperatures and dust events; means that people will likely spend more time indoors. Nevertheless, the ability of fine particles to infiltrate indoor environments results in household residents in Qatar being exposed to high levels of indoor fine particles during the event of dust storms and even afterward, as a result of fine particles' long atmospheric residence time. Therefore, the fine particle fraction ($PM_{2.5}$) was chosen for this study as it is a more practical indicator in Qatar to understand both anthropogenic particles sources and natural particles which in Qatar is likely overwhelmed with dust.

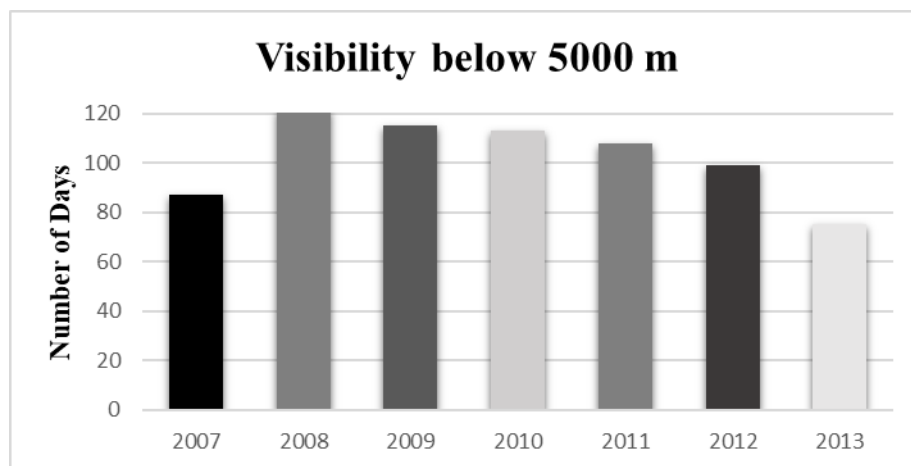


Figure 1.7 Numbers of days per year in Doha when visibility was below 5000 m (Source: QCAA, 2014)

1.4 Sources of Particulate Matter Pollution in Qatar

In Qatar, wind-blown dust and sea salt aerosols are potentially the main primary natural sources. Also, a significant portion of primary and secondary PM is generated from a variety of human (anthropogenic) activities. These activities include transportation, construction and demolition activities, industrial processes, and fossil fuel combustion. Big industries in Qatar are localized in areas outside Doha. However, emissions from industrial areas may contribute to high PM levels in Doha city, through background concentrations. The main natural and anthropogenic sources in Doha are discussed below.

1.4.1 Natural Particulate Matter Sources

1.4.1.1 Sea Salt Aerosols

Sea and ocean surfaces are major sources of atmospheric aerosols. Sea salt aerosol (SSA) is a mixture of inorganic sodium chloride (NaCl), magnesium (Mg^{2+}), and traces of organic sulfate (SO_4^{2-}); which is produced by the oxidation of dimethyl sulfate, released biologically by phytoplankton in the presence of solar radiation (Prijith. et al. 2014). Ocean aerosols global flux ranges from $\sim 1,000$ to $5,000 \text{ Tg yr}^{-1}$ (Wallace and Hobbs, 2006). The main mechanism responsible for ejecting ocean materials into the air is through bubbles bursting from breaking waves. Prijith. et al., (2014) studied SSAs production rate by wind speeds and found that even at low wind speed aerosol production is observed, and the ocean surface wind speed has a linear relationship with production rate for low as well as for high wind speeds. A study of SSA concentration in the Arabian Sea using a coupled climate and sectional microphysical model in 2006 showed that sea salt levels indicated by Na^+ concentrations in aerosol samples have a seasonal variation and that Na^+ was at its highest concentration during summer (Figure 1.8) (Fan and Toon, 2011). The monsoon season in the Arabian Sea region is characterised by strong winds coming from the southeast at high speeds ranging between 15 and 20 m/s during

the summer season. The persistent high wind speeds over the Arabian Sea are accountable for a large amount of SSA production in that region (Vinoj and Satheesh, 2004). Because of the approximate distance between the Arabian Sea and the Qatar peninsula; it is likely that the monsoon season may contribute to SSAs abundant in Qatar. In addition to sea spray aerosols, salt pans are another source of particles in Qatar which may have an impact on salt concentration during strong winds. According to Ashour (2013), salt pans or as they known in Qatar ‘Sabkhas’, are closed depressions with saline surfaces. Sabkhas cover 7% of Qatar’s land surface, and they are classified by their location as coastal sabkhas which are wider and more spread, and land sabkhas. In Qatar, there are 78 inland sabkhas, covering a total area of 205 km², and located away from the shoreline. There are 42 coast sabkhas covering about 590 km² (Ashour, 2013). Figure 1.9 shows sabkhas’ locations in the blue coloured areas.

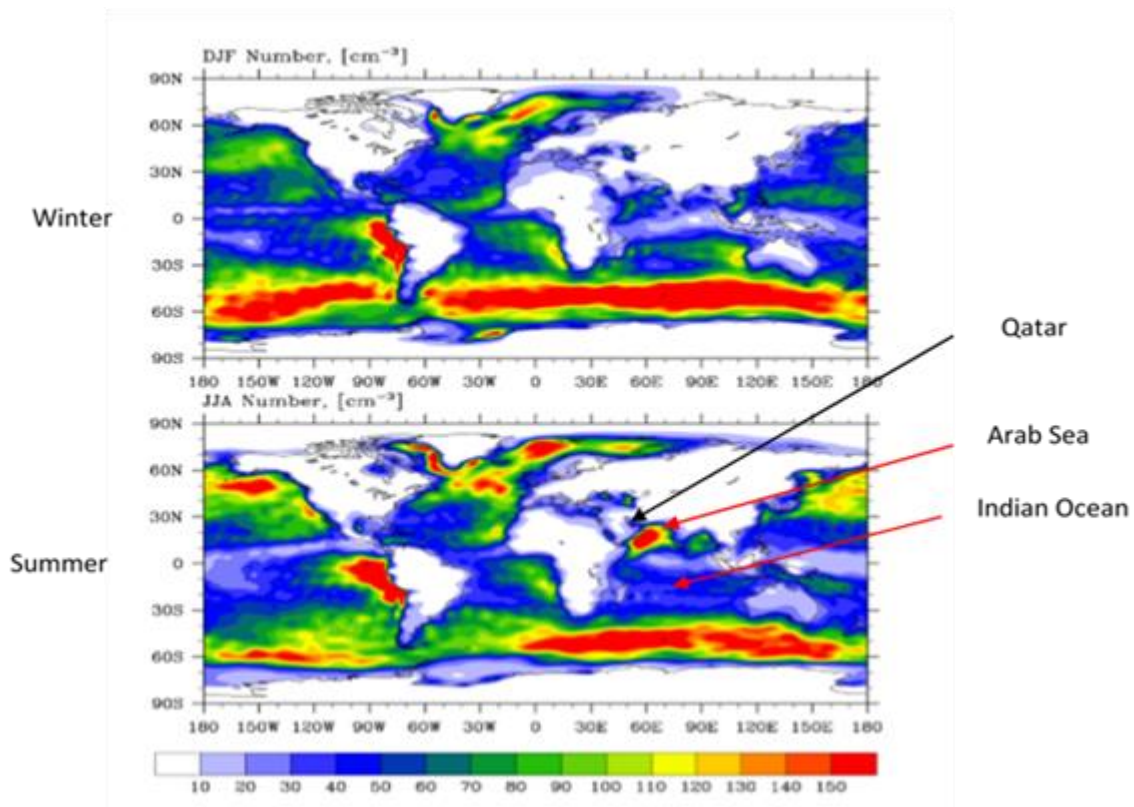


Figure 1.8 Modelled global distribution of SSA surface number concentration in the winter (December, January, and February) and the summer (June, July, and August) of 2006 (Source: Fan and Toon, 2011)

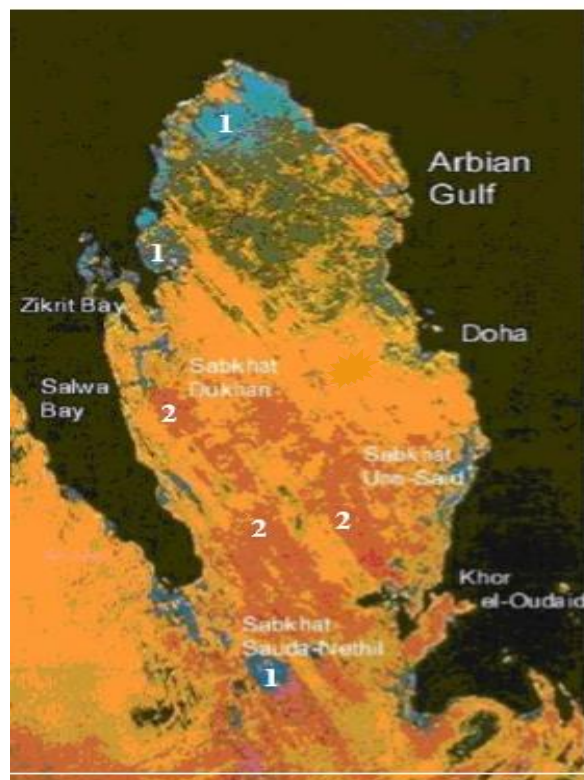


Figure 1.9 Qatar map showing: 1) salt pans in blue and 2) sand dunes in brownish colour. (Source: Ashour, 2013)

NaCl is quantitatively the main contributor to the marine aerosol mass; thus, it is typically used when estimating the natural contribution of marine aerosols to PM levels (Chow et al., 2015). The European Commission (EC, 2011a) recommend using the sum of both Cl^- and Na^+ when calculating the contribution of marine aerosols to PM, because theoretically, Cl^- concentration in the atmosphere can be affected by HCl emitted from anthropogenic sources or by loss through the reaction of NaCl with nitric and sulfuric acid. Na^+ however, has only a limited number of non-sea salt sources, yet its concentration can be affected by local dust re-suspension (EEA, 2012).

1.4.1.2 Dust Storms

Dust storm phenomena occur when strong winds lift fine particles from the land surface into the atmosphere and transport them downwind, affecting regions hundreds to thousands of

kilometers away. For example, Miller et al., (2008) reported that dust/haze episode that occurred in Mali was traced back via a parcel trajectory to a convective system that started 28 hours earlier and 500 km away.

Wind erosion of the surface is caused by the mechanical removal of loose, fine-grained particles in a process known as deflation. The threshold value, which is the critical wind velocity above which deflation of the surface occurs, is highly variable depending on the location, ranging from 5 to 12.5 ms⁻¹ (Miller et al., 2008). The tendency of the wind in eroding surfaces varies spatially, and it depends largely on the size and shape of soil particles, moisture content, and vegetation cover. Soil moisture content and vegetation tend to bind the surface materials reducing its ability for erosion. Therefore, frequent dust storms are mostly seen in arid and semi-arid climatic regions (Miller et al., 2008).

The residence time of particles in the dust column depends on particle size (Wallas and Hobbs, 2006). As the size of particles increase therefore their mass, they fall out due to gravity. Studies have shown that particles in dust-laden winds, with origins in distant sources, are typically found to have volume median diameters of about 5µm, resulting in haze conditions, and they have greater potential impacts on climate and health (Miller et al., 2008). The definition of dust storm agreed on internationally is when visibility goes below 1,000 meters (Middleton, 1986), whereas haze involves a reduction in visibility below 5,000 meters (QCAA, 2014).

Qatar is located on the eastern side of the Arabian Peninsula; the peninsula has a desert topography which extends from Rub' al Kahli 'empty quarter' in the south of the Arabian Peninsula to the south border of Iraq, parallel to the Arabian Gulf coast (Landsberg et al., 1981). According to Pye (1987), dust storms occurrences in this region are the result of strong winds, and times when extreme drought leaves bare surfaces exposed to the wind. The dust

storms in desert climate regions are most usually caused by thunderstorm outflows (downburst), or by strong pressure gradients, which causes an increase in wind velocity over a wide area (WMO, 2012). Haboob and Al-Shamal are two types of dust storms that hit Qatar during the spring and summer.

Haboob is an Arabic term that refers to any violent wind initiating dust storms regardless of its origins (Pye, 1987; Miller et al., 2008). A haboob is generated by a downdraft associated with convective clouds and maintained by the resulting horizontal density gradients (Pye, 1987). When the downdraft of cold air stretches out along the ground and travels forward, it forms a density current that suspends and transport loose dust and sand from the surface. Pye (1978) described haboob dust storms as a solid wall of dust rising to heights ranging from 0.3 to 3 km, blocking out sunlight. Figure 1.10 shows a haboob (dust front) event, appearing as a red line originating in Saudi Arabia and heading toward Qatar. The other type of wind responsible for blowing dust over Qatar is Al-Shamal, an Arabic word meaning north, which describes a strong, persistent north-westerly wind that blows during the summer over the Arabian Gulf (Figure 1.11). During the daytime, surface winds are so strong that they can cause frequent dust storms in Iraq and a dust haze that is carried across the Arabian Gulf to Qatar. The dynamic responsible for producing this type of wind is caused by the intense summer “heat” low over Pakistan and Afghanistan. A low-pressure trough to the lee of the Zagros Mountains is formed creating a steep pressure gradient between the trough and the semi-permanent high-pressure cell located over north-west Saudi Arabia (Figure 1.12) (Pye, 1987).

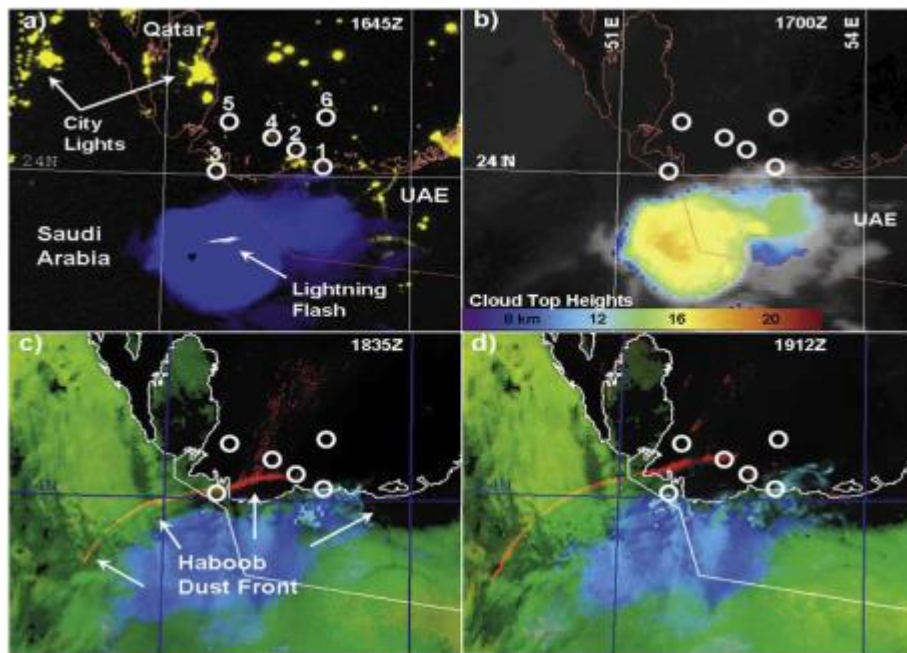


Figure 1.10 Convective complex on the night of September 13, 2004 over the UAE domain: (a) Electrically active storm, (b) significant cloud top heights (18 km), (c) dust enhancement (the haboob appears as a red linear feature), and (d) frontal advance roughly a half an hour later (Source: Miller et al., 2008)

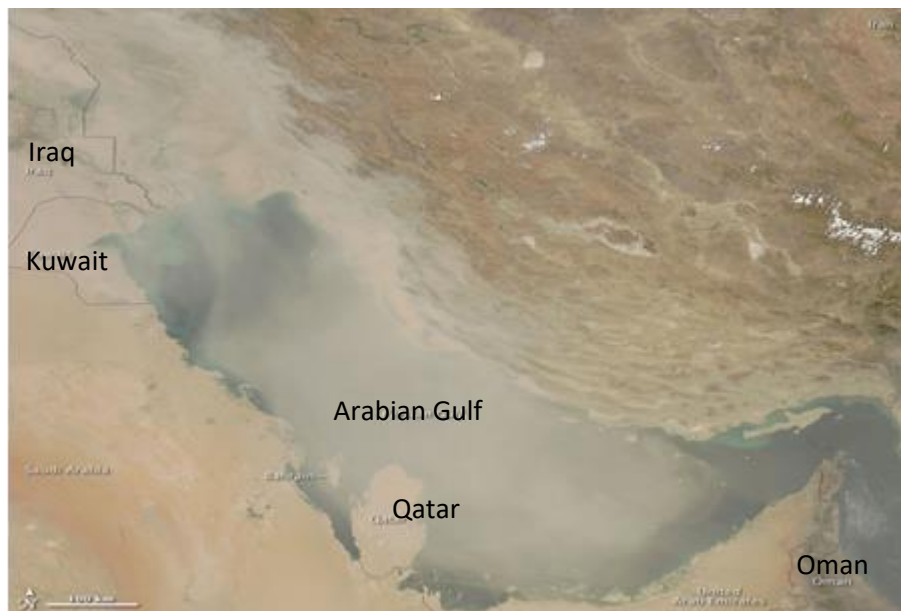


Figure 1.11 Moderate Resolution Imaging Spectroradiometer (MODIS) on NASA's Terra satellite captured a true-colour image of the dust storm from Iraq on July 31, 2009. (Source: NASA 2009).

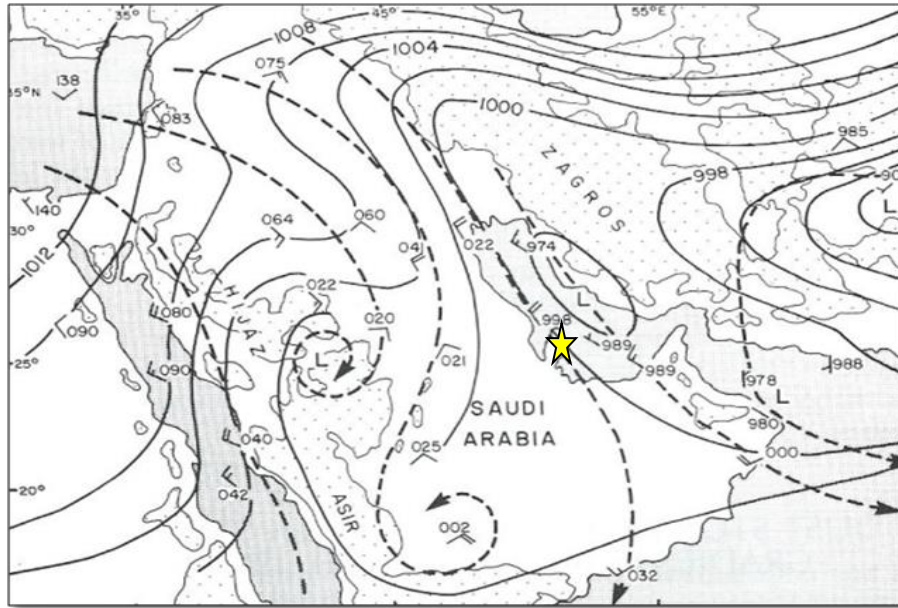


Figure 1.12 Map Showing Al-Shamal synoptic situation (1200 GMT, 9 June 1982) with surface isobars and 850 mb streamlines (broken) of the Arabian Gulf and surrounding countries. The dotted area represents land over 1000m (Source: Pye, 1987). The yellow star mark shows Qatar.

Metals markers which been used previously to identify a crustal source are Al, Si, Fe, Ti, Mn, Ba, Ce and Ca^{2+} (Andrews et al., 2000; Shen, 2009; Aydin et al., 2011; Chow et al., 2007a)

1.4.2 Anthropogenic Particulate Matter Sources within Doha's Boundaries

Main anthropogenic sources within Doha boundaries are transportation and construction activities. Emissions from main roads, Doha harbor, Hamad airport in addition to undergoing construction expansion activities related to infrastructure projects including new cities, stadiums, and the construction of a metro and rail system in Doha, are considered significant sources of primary and secondary PM. Figure 1.13 shows a map of Doha with possible anthropogenic sources of PM and gaseous emissions including Doha Harbour, Hamad airport, the Lusail construction site and several areas designated for sand piles storage.

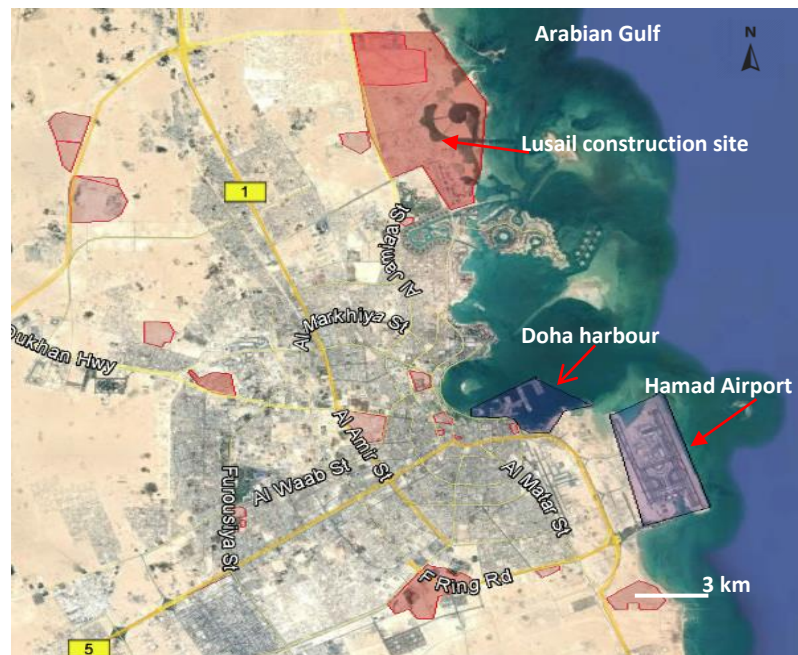


Figure 1.13 Doha city map showing construction and sand stockpiles in red areas, Doha harbor, and Hamad international airport

1.4.2.1 Construction Activities

Construction and demolition activities, earth moving operations and the use of heavy equipment are sources of fugitive dust and engine combustion emissions that could contribute significantly but temporarily to PM increase in ambient air (Dorevitch et al. 2006). Fugitive dust and combustion sources emissions often vary substantially during the day and from day to day, depending on the type of operation, the level of activity, and the meteorological conditions (Giusti et al., 2014). As part of Qatar National Vision 2030, and through a number of programmes and projects, such as the Qatar 2022 FIFA World Cup and developing smart cities, Qatar invested heavily in infrastructure including a new smart city, the revival of old commercial city in the heart of Doha, nine stadiums, roads, highways, and a metro/rail network. Also, hotels were constructed to accommodate the anticipated increase in visitor's numbers expected during the World Cup 2022.

Emissions during construction operations include the following: 1) fugitive dust emissions from earthwork, roadways, sand storage piles, land clearing, ground excavation, and via

trucks inducing turbulence and resuspending dust at construction sites. 2) Further emissions include nitrogen oxides, hydrocarbons, and diesel PM emitted by heavy-duty construction equipment, such as loaders, haul trucks, bulldozers, compressors, and generators which are powered by diesel fuel. For large development projects in Doha, areas near the projects are designated for sand pile storage and for ready-mix plants that are operated by diesel generators for the preparing and mixing of cement and concrete needed for the construction activity.

Emissions from construction areas are expected to have high crustal loading and diesel combustion emissions in addition to elemental markers such as calcium (Ca^{2+}) (Wang et al., 2005), Sulfur (S) (Vecchi et al., 2009), and Strontium (Sr) (Crilley et al., 2017). Ca^{2+} , Sr, and S are used to distinguish construction operations as they are components of cement's composition, and both Ca^{2+} and Sr elements have been used to identify construction source profile in source apportionment studies (Dall'Osto et al., 2013). On the other hand, Wang et al., (2005) used the ratio of Ca^{2+}/Al to investigate the sources of Ca^{2+} in urban aerosols. The Ca^{2+}/Al ratio was found to show a seasonal variation compared to the Ca^{2+}/Al ratio in the upper continental crust of 0.5, found by (Mason, 1966). A low value of 0.76 was observed in the winter season when construction activities decreased, whereas higher values of 1.27 and 2.12 were found in the summer and autumn respectively with increasing construction activities. The change in the ratio is caused by an increased Ca^{2+} contribution from construction activities.

1.4.2.2 Traffic

Air pollutants from transport include nitrogen oxides, particles, and hydrocarbons. All have a damaging impact on human health since they are emitted in the vicinity of human activity (Colville et al., 2001). In areas near busy roads, in London, vehicles are responsible for a

significant proportion of primary PM and NO_x increments (Charron et al., 2007). According to Querol et al., (2004) in European cities, traffic accounts for 40-60% of PM_{2.5} at kerbside from both exhaust and non-exhaust emissions, and that exhaust and non-exhaust sources contribute equally to traffic-related emissions.

Vehicle emissions from the exhaust are composed of burned fuel and lubricating oil, while emissions from non-exhaust sources include the wear and tear of vehicle brakes, tyres and clutches and the re-suspension of road dust. Particles released from the exhaust are in the fine and ultrafine sizes, and they are mainly composed of OC and EC (Fernandes et al., 2002; Brook et al., 2007; Pant 2014). The chemical and physical properties of the emitted particles vary according to the engine age, driving speed, type of fuel and conditions during the combustion (temperature, humidity) (Lighty et al., 2000; Lloyd and Cackett, 2001; Pant, 2014). NO_x, EC, and OC are by-products of high-temperature combustion in vehicles' engines and are often used as markers for road traffic exhaust emissions (Joseph et al., 2012). Non-exhaust emissions contribute to both coarse and fine particle sizes (Pant and Harrison, 2013), and are emitted directly from wear and tear of tyres, brakes, clutches, road surfaces or indirectly through the re-suspension of road dust as a function of vehicle turbulence. Non-exhaust particles in different regions vary in their composition based on the traffic volume and pattern, tyre and brake composition variability based on the manufacturer, and regional geology (Amato et al., 2011a; Amato et al., 2011b; Han et al., 2011). Non-exhaust metals markers include Cu, Sb, Ba, Sn, Fe which are markers of brake wear (Lough et al., 2005; Amato et al., 2011a), Zn which found in tyre materials (Thorpe and Harrison., 2008), and Mn, Fe, As Ca, Si, Al which are markers of the re-suspension of accumulated PM and road wear (Pant and Harrison, 2013). Others used the ratio of Cu to Sb in a typical brake lining material (4.6 ± 2.3) (Sternbeck et al., 2002), as an indicator of traffic emissions which is different

from the ratio existing in the crustal material (Cu/Sb ~ 125). The Cu/Sb ratio in fine particles reported for traffic sources ranges from 2.17 to 10 (Lin et al., 2015; Pey et al., 2010; Pant and Harrison, 2013).

1.4.2.3 Doha Harbour

Trade on a global scale has traditionally been dependent on maritime transport of goods, as it is a more feasible form of transportation per kilogram of material in terms of fuel consumed and fuel emissions (Grewal and Haugstetter, 2007). Marine vessels are accountable globally for 5-8% of SO_x and 15% of NO_x emissions (Corbett et al., 2007). Endresen et al., (2003) estimated that 70% of vessels' emissions are emitted within 400 km of land. Hence, they contribute to air quality degradation in coastal areas.

Marine vessels' diesel engines usually use low-cost fuels which are typically high in sulfur and porphyrins that contain Ni, and V. Emissions from fuel oil combustion exhaust are CO₂, CO, SO₂, SO₃, NO_x, VOC and PM_{2.5} (Agrawal et al., 2008). PM emitted from the engine exhaust, are formed through the agglomeration of small particles of soot, sulfate, partly burned diesel and lubricant. The chemical composition of PM_{2.5} from diesel engines has revealed that sulfate and water bound with sulfate, OC and EC are the main components of PM, in addition, to trace elements such as V, Ni, Al, Zn, Pb, and P (Isakson et al., 2001; Viana et al., 2008). Also, the V/Ni ratio has been used to identify shipping emissions. V/Ni ratio ranging between 2.5 and 4.5 were found in the exhaust of different types of marine engines using different types of fuel and speed modes in the USA (Nigam et al., 2006), as well as in Spain (Pandolfi et al., 2011; Perez et al., 2016)

In addition to shipping emissions, harbor activities, heavy-duty trucks, cargo handling equipment's and harbor crafts loading, were found to contribute substantially to harbor PM

emissions in Europe (Alastuey et al., 2007; Viana et al., 2014). For example, in a study of the Los Angeles Harbor (US), total fine PM emissions were dominated by dust and vehicular sources, and they explained up to 54% of the mass, whereas the contribution from ships was lower than 5% (Minguillon et al., 2008).

Qatar environmental protection law (MOE, 2005) only addresses vessels' oil spill, waste, and ballast water disposal, suggesting that operators follow the International Maritime Organization (IMO) for air emissions limits, which limit sulfur content in fuel oil to not exceed 3.5% m/m (by mass), starting from 2012 (IMO, 2017). However, the IMO through the International Convention for the Prevention of Pollution from Ships (MARPOL) introduced the Emission Control Areas (ECAs), which are sea areas in which firmer controls measurements have been established to minimize vessels emissions. In these areas, the allowable SO_x content in fuel oil should not exceed 1.0% m/m in 2010 and 0.1 % m/m (by mass) starting from 2015. The Arabian Gulf is not designated as an ECA, although emissions produced by the high density of marine vessels (Figure 1.14) in the narrow gulf could be of great significance to air quality in Qatar and the neighboring countries.

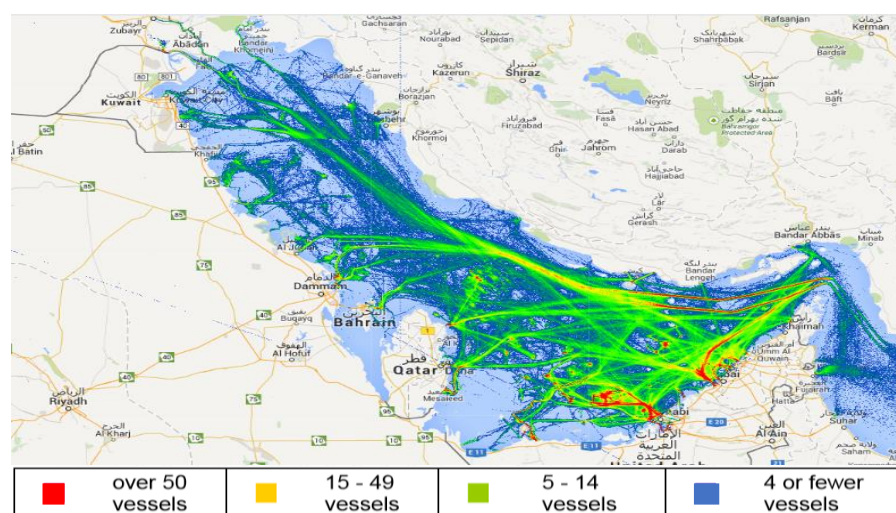


Figure 1.14 Vessels' density per day in the Arabian Gulf (Sources: Marine Vessel Traffic, 2013)

1.4.2.4 Hamad International Airport

Airport emissions include emissions from aircraft operations and surface access. Aircraft emissions are released from a) the exhaust and consists of CO₂, CO, NO_x, SO_x, fine particles, organic compounds, and black carbon (Tesseraux, 2004; Agrawal et al., 2008; Kinsey et al., 2011), and from b) non-exhaust sources and including tyres, brakes and asphalt wear and the re-suspension of particles due to turbulence caused by aircraft movements (Masiol and Harrison, 2014). According to Li et al., (2013) the metal markers for aircrafts profile consist of S, Zn, Br, Zr, and Mo, mostly associated with aircrafts landing. Sulfur and zinc are metal markers for tyre wear and are released as a result of the frictional heat when tyres touch the asphalt surface as aircraft lands (Hopke, 2016). As for zirconium and molybdenum, both elements are used in high-temperature lubricants, which are used to lubricate bearings that undergo major heat stress, and they are released from lubricants when power is placed on bearings (Hopke, 2016). The greatest share of surface access emissions is related to vehicle congestion caused by passengers' daily journeys to and from airports and from operations on the airport site by the service equipment for flights and passengers. The later includes baggage and food carriers, refilling trucks, cleaning, container loader, and tugs for moving aircraft between gates and taxiways, in addition to passenger vehicles and buses. Hence, emissions from surface access source have vehicle markers such as EC, OC, Zn, Cu, Sb, Fe, and Ba.

1.4.3 Industrial Cities in Qatar and Possible Contribution to Doha Pollution

Qatar has four industrial cities namely Rass Laffan, Mesaieed, Dukhan/Umm-Bab and Doha Industrial Area. These cities are located outside Doha city and likely to have a minimum influence on Doha air quality. Figure 1.15 shows industrial areas distance, and location from Doha and the wind rose during the summer and winter seasons to point out which of the industrial cities can contribute to air quality in Doha.

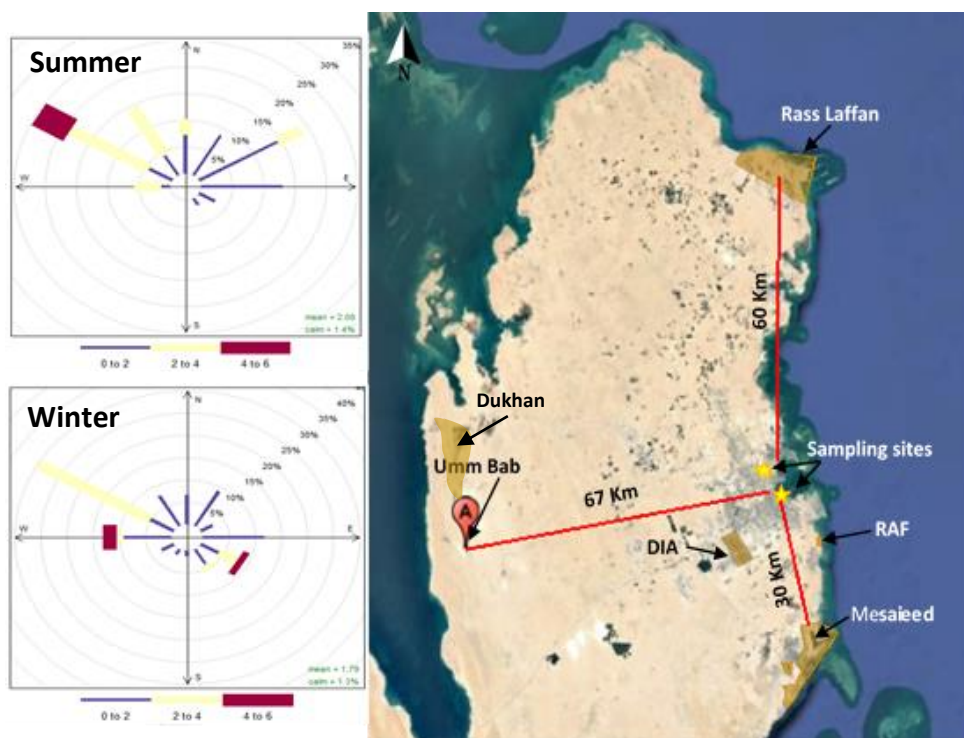


Figure 1.15 Industrial areas locations and wind roses in the winter of 2014/2015 and the summer of 2015

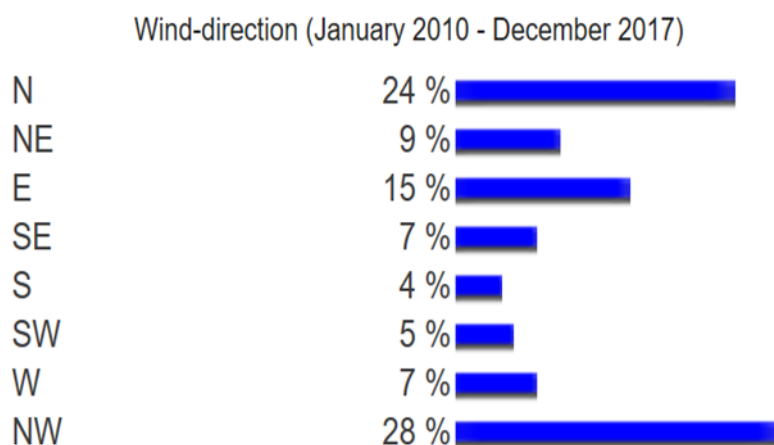


Figure 1.16 Wind direction percentage of occurrence in Doha (Sources: Weather Online, 2017)

Figure 1.16 shows percentages of wind arriving from a specific direction. The prevailing wind in Qatar is from the northwest and north directions, with 28% and 24% respectively. When the wind comes from north-west direction; emissions from all industrial areas are directed away

from Doha. However, when the wind comes from the north; Rass Laffan (60 km away from Doha) may contribute to Doha particulate concentration, yet all other industrial cities are located downwind of Doha and do not influence the air quality in Doha under these conditions. South and southwest winds have the lowest percentage of occurrence. Therefore, a low contribution of particles is suspected from Umm Bab and Mesaieed. Doha Industrial Area (DIA) is located southwest Doha city border. In Doha, 5% of wind is coming from southwest direction, and although the percentage of occurrence is low (Figure 1.16) and the wind from SW sector arrive at low wind speeds (Figure 1.15), because of the short distance between the sampling sites and the DIA (~12 km), it is expected that the DIA will have an influence on Doha air quality.

1.4.3.1 Rass Laffan Industrial City (RLC)

Ras Laffan Industrial City (RLC) is located along the north-east coast of Qatar overlooking the Arabian Gulf, approximately 60 km from Doha. RLC was built to provide infrastructure and services to facilitate the establishment and functioning of the industrial entity to exploit Qatar's gas reserves in the North Field. The port at this location is primarily designated to service the industries situated within RLC. It has been designed as the export facility for liquefied natural gas, liquid petroleum gas, condensates, petroleum products and sulfur, derived from the processing of gas in the North Field reservoir (QP, 2014).

The area of RLC is home to a broad industrial complex, mainly for the oil and gas industry. Emissions from RLC industry and port are expected to include sulfur dioxide, nitrogen oxides, hydrocarbon emissions, and trace metals markers in oil and gas such as Ni, V, and Cr (Querol et al., 2007; Figueroa et al., 2006).

1.4.3.2 Mesaieed Industrial City (MIC)

Mesaieed Industrial City (MIC) is located along the south-east of Qatar coast approximately 35 km south Doha. MIC is considered as the core of Qatar's industry, and it hosts many industrial activities including refineries, lubricants, fertilisers, fuel additives, petrochemicals, steel, vinyl, waste management, and recycling facility, power, and MIC Port. Because of its location downwind to Doha for most of the prevailing wind in Qatar; it is not expected to have a huge impact on the air quality in Doha.

A mix of industrial metal markers such as Ni, Cd, Zn, Mn, Cu, Cr and V (Pant and Harrison, 2012) is used to identify industrial emissions sources including SO_x and NO_x from power generation. Emissions from the iron and steel industry include sulfur oxides, nitrogen dioxide, carbon monoxide, as well as soot and dust containing iron oxides. The Iron and steel industry can contribute to elevated episode of air pollution associated with the emission of OC, and EC as well as an increase in trace metal concentrations such as Fe, Al, Si, S, Mn, Cr, and Zn, at areas close to blast furnace and basic oxygen furnace steelmaking (Querol et al., 2007; Taiwo, 2013).

In petrochemical manufacturing and petroleum refining, a fluidised-bed catalytic cracking process is used to convert the high-molecular-weight hydrocarbon fractions of crude oils to more valuable low-molecular-weight products. In this process, a zeolite catalyst enriched with rare earth elements (La, Ce, Nd, Sm, Eu, Gd, Pr, and Lu) is used. During cracking operations, some of these elements may escape to the atmosphere (Kulkarni 2005). According to Kulkarni (2005), the rare earth elements La, Ce, Pr, and Nd in fine particles are a signature for petrochemical and oil operation and can be used as markers.

Domestic solid waste is treated in the Mesiaeed Waste Management Centre. Burning refuse reduces the volume of waste effectively, though heavy metals concentrated in the fly ash could escape into the atmosphere (Chang et al., 2000). Metals markers from refuse burning include Cd, Cu, Pb, and Zn (Pacyna, 1984; Chang et al.; 2000; Pant and Harrison, 2012), as well as Cr and Ni from slag burning (Morselli, 1993).

The Ras Abu Fontas water and power plant is responsible for generating electricity and desalinating water. Emissions from this sector are related to fuel burning for power generation. Emissions include NO₂ and SO₂ along with heavy metals, such as Cd, V, and Ni in oil fly ash (Strauss and Mainwaring, 1984; Pant and Harrison, 2012).

1.4.3.3 Dukhan and Umm-Bab Industrial Cities

Both of these sites are in the western part of Qatar peninsula. They are approximately 70 km from Doha. Contribution from this sector to Doha air quality could be negligible due to the distance between these industrial cities and Doha and the low wind percentage coming from this sector. Emissions in Dukhan are associated with crude oil production from Dukhan onshore oil field such as SO₂, NO_x, Ni, V, and Cr (Huggins et al., 2000). In Umm-Bab, however, emissions are likely related to cement production and fugitive dust such as silica (SiO₂), lime (CaCO₃), gypsum (CaSO₄), and dolomite CaMg(CO₃)₂, from quarries that supply the cement plants with the raw materials. Ca²⁺ has been used as a marker for cement dust emanating from the cement manufacturing process (Callén et al., 2012), however, using Ca²⁺ to identify construction sources could be problematic in Doha because Ca²⁺ can be enriched in the samples due to the presence of high limestone concentration in the crust.

1.4.3.4 Doha Industrial Area (DIA)

Doha Industrial Area is located in south-west Doha. It covers an area of approximately 25 km², and it consists of small and medium-sized industries among them are carpentry, metal works, dyes, bricks, glass manufacturing, garages, and warehouses (MDPS, 2014). A complex of organic and inorganic compounds, heavy metals, and gaseous mixtures is likely to be emitted from this area to Doha. The DIA is expected to have an impact on Doha air quality due to the close distance, although the wind blows only 4 - 8% from the DIA direction.

1.5 Source Apportionment and the PMF Model

Source apportionment (SA) is an approach used to quantify the contribution of different pollution sources to the total particulate mass from atmospheric measurements (Belis, 2013). PM is considered as the most complex of air pollutants and one of the most difficult to control because of the multiplicity of PM sources and the factors influencing its behaviour (QUARG, 1996). Understanding PM sources accurately and how much each of the sources contributes to PM concentration in ambient air is essential prior to designing and implementing air quality control strategies and will help policymakers to suggest appropriate control strategies to target major sources of primary and secondary emissions. Hence, SA is required to 1) give information on pollution sources' contributions and 2) measure the effectiveness of abatement implementations on pollution sources.

Several methods are used to quantify the impacts of air pollution sources on air quality, including emissions inventories, dispersion models, and receptor models. Emission inventories are detailed collations of emissions within a specific year produced from all source categories in a certain geographical area or industry, and they use emission factors and activity levels to calculate them (Belis, 2013). Dispersion models, on the other hand, are used

to estimate a specific source's impact on air quality in an area using emission rates, meteorology, and local topography. Receptor models are used to estimate the contribution of different sources to ambient PM concentrations on a specific area based on measurements and subsequent chemical analysis (Belis, 2013; Pant, 2014).

Receptor models are used in air quality management to quantify the contribution of different sources in ambient particulate samples collected at a specified receptor site by measuring the concentration of chemical species in these samples (Watson et al. 2002). The relationship between sources and receptors in these models is based on the principle of mass conservation and the use of mass balance analysis. The principle assumes that the total concentration of the particulate constituents measured at a particular location can be thought of as the sum of contributions from independent source types (Hopke, 1990). Thus, the equation of mass balance can be written as follows:

$$X_{ij} = \sum_{k=1}^p f_{ik} g_{kj} \quad (1)$$

where, X_{ij} is the i^{th} element concentration measured in the j^{th} sample, f_{ik} is the concentration in $\mu\text{g}/\text{m}^3$ of the i^{th} element from source k^{th} , and g_{kj} is the airborne mass concentration in $\mu\text{g}/\text{m}^3$ of material from the k^{th} source contributing to the j^{th} sample.

There are two statistical chemical methods that have been successfully used to solve the mass balance equation. Chemical mass balance (CMB) is one method that uses information on an ambient sample's chemical species and source compositions in a multiple linear regression to obtain the mass contribution from different sources to that sample (Hopke, 1990). However, because local source profiles are not always available, positive matrix factorization (PMF) based on multivariate data analysis is used to extract information from ambient data alone (Hopke, 1990).

The multivariate method only needs general knowledge on the characteristics of source emissions to identify potential sources (Pant and Harrison, 2012). Multivariate data analysis identifies the interrelationship between chemical species in ambient samples, based on the fact that chemical species emitted from the same source will have the same temporal pattern, and they will correlate perfectly. These methods are able to group chemical species with a unique temporal profile characteristic of a source in chemical profiles called factors (Pant and Harrison, 2012).

Functioning as a factor technique, the PMF decomposes the matrix of chemical species in a number of samples into factor contributions and factor profiles matrices (EPA, 2008). The PMF equation can be written as follows:

$$X_{ij} = \sum_{k=1}^p f_{ik} g_{kj} + e_{ij} \quad (2)$$

where e_{ij} is the residual matrix of the difference between the measurement X_{ij} and the model $Y_{ij} = f_{ik} \cdot g_{kj}$, as a function of f_{ik} and g_{kj} (Vecchi et al., 2008).

The limitations of the PMF model include the requirement for a large data set (at least 50 samples) (Pallavi and Harrison, 2012), and multicollinearity, which can occur when two or more sources have similar emission profiles and can affect the model estimates or when the wind direction affects two sources located in a collinear position (Gordon, 1988; Pant, 2014). Thurston and Liou, (1987) recommended multivariate models followed by CMB to be used in analysis for chemical speciation data for source identification and quantification, and the PMF model has been used extensively for source apportionment of PM mass (Kim et al., 2003a; Zhou et al., 2004; Ogulei et al., 2006; Reff et al., 2007; Kasumba et al., 2009; Friend et al., 2011a; Perrone et al., 2012; Green et al., 2013).

In terms of source apportionment studies in the Middle East region, the PMF model has been used recently in few studies for the PM₁₀, PM_{2.5}, and nanoparticles (Dabbous and Kumar, 2015; Tsiouri et al., 2015; Khodeir et al., 2012). According to Tsiouri et al., (2015), crustal dust, oil combustion, traffic, marine aerosols, and re-suspended soil are the key contributing factors for PM in the Middle East. In Kuwait, using data from 2005, the PMF model found five major sources contributing to PM_{2.5} including sandstorms (54%), oil combustion from power plants (18%), petrochemical industries (12%), road traffic (11%), and regional background (5%) (Alolayan et al., 2013). In another study in Kuwait, in 2013, the PMF identified six sources in PM size below 1 µm. The six sources include fresh traffic emissions (46%), aged traffic emissions (27%), Industrial emissions (9%), regional background (9%), miscellaneous sources (6%), and dust (3%) (Dabbous and Kumar, 2015).

In Jeddah in 2011, a source apportionment study found four and five sources for PM₁₀ and PM_{2.5} size fraction respectively (Khodeir et al., 2012). The study showed that heavy oil combustion (66.5%), re-suspended soil (21%), industrial mix 1 (8.2%), industrial mix 2 (1.1%), and traffic (3.2%) are the key sources in PM_{2.5}. Whereas crustal component (66%), heavy oil combustion (16.7%), industrial mix (9.3%), and marine aerosol (8%) were the key contributor to PM₁₀ size fraction.

In Ahvaz city, Iran, a source apportionment study for TSP using the PMF model for data from 2010 showed seven sources including crustal dust (56%), road dust (7%), traffic (8%), marine aerosols (9%), secondary aerosols (7%), metallurgical plants (4.5%), and fossil fuel combustion (8.5%) (Sowlat et al., 2012).

A range of source metal markers is used in receptor modeling studies to identify sources (Table 1.3).

Table 1.3 Markers associated with PM sources

Source	Markers	References
Mineral dust	Si, Al, Fe, Ca ²⁺ , Ti, Mg ²⁺	Harrison et al., (1996); Chow et al., (2007a); Pey et al. (2010)
Sea salt	Na ⁺ , Cl ⁻ , Mg ²⁺	Harrison et al. (1996); Pey et al. (2010)
Traffic	Fe, Ba, Zn, EC, Cu, Sb, Pb, Sn	Schauer et al., (1996); Grieshop et al., (2006); Pey et al., (2010); Lin et al., (2015); Pant and Harrison (2013)
Ship emissions/fuel oil combustion	Ni, V	Harrison et al. (1996); Pey et al. (2010); Querol et al., (2007)
Secondary inorganic aerosol	NH ₄ ⁺ , SO ₄ ²⁻ , NO ₃ ⁻	Harrison et al., (1996); Belis et al., (2013); Pant (2014)
Construction	Al, Ca ²⁺ , Sr	Wang et al., (2005); Dall'Osto et al., (2013); Vecchi et al., (2009)
Airport emissions	EC, OC, S, Zn, Br, Zr, and Mo	Dong et al., (2011); Li et al., (2013); Hopke (2016)
Municipal waste incineration	Cd, Cu, Pb, Zn	Chang et al., (2000); Pant and Harrison (2012)
Iron and steel production	OC, EC, Fe, Al, Si, S, Mn, Cr, Zn	Querol et al., (2007); Taiwo (2013)
Petrochemical	La, Ce, Nd	Kulkarni et al., (2003); Kulkarni et al., (2006); Chellam et al., (2005)

1.6 Mass Closure

The mass closure method attempts to reach an agreement between the gravimetric mass of PM samples and the sum of reconstructed major aerosol constituents in those samples (Joseph et al., 2012; Rees et al., 2004) with the assumption of accounting for unmeasured components, such as hydrogen and oxygen, associated with geological minerals, organic carbon, and water (Chow et al., 2015). The mass closure approach is used for data validation

by identifying potential measurements errors and correcting them, understanding chemical species' temporal and spatial variation, and estimating sources contributions to PM (Chow et al., 2015).

In order to reconstruct the major aerosol constituents, a small number of chemical components are measured in the samples. Then, an estimated correction factor, based on the ratio of the molecular weight of the elements associated with each of the assumed major aerosol constituents, is multiplied by the measured chemical components. For example, to account for oxygen mass associated with SiO₂, Si is multiplied by 2.14, which is calculated based on the molecular weights of SiO₂ and Si as follows:

$$\text{Unaccounted Oxygen} = \text{MW of SiO}_2 (28 + (2 \times 16)) / \text{MW of Si} (28) = 2.14$$

Typically, six chemical components are used in PM mass construction including geological minerals (Al, Si, Fe, and Ca²⁺), sea salt aerosols (Cl⁻ and Na⁺), inorganic ions (SO₄²⁻, NH₄⁺, and NO₃⁻), organic matter(OC), elemental carbon(EC), and trace metals (Harrison et al., 2003; Sillanpää et al., 2006; Joseph et al., 2012; Chow et al., 2015). Commonly used reconstructed mass equation include sum up the following components shown in Table 1.4:

Table 1.4 Mass reconstruction table

Inorganic ions	Organic mass	Elemental carbon	Geological minerals	Sea salt	Trace metals
SO ₄ ²⁻ + NO ₃ ⁻ + NH ₄ ⁺	OC * factor multiplier range from 1.2 to 2	yes	Metal oxides of (Al, Ca, Fe, Si)	Na ⁺ + Cl ⁻	Summing all species measured by XRF excluding the ones accounted for in the other fractions

Usually, with a mass reconstruction solution, a mass discrepancy between the reconstructed mass of constituents and the gravimetric mass is found, and no perfect closure can be attained because in principle a gap is expected since not all possible species can be measured, and the

reconstructed mass depends on various assumptions of the constituents' chemical compositions and the factors multiplier being used (Turpin and Lim, 2001). Mass discrepancy could also be caused by uncertainty in the measurements of chemical composition (Rees et al., 2004), the presence of unaccounted for strongly bound water (Harrison et al., 2003), an incorrect OC multiplier to estimate organic matter (OM), and inaccurate estimates of the crustal components (Rees et al., 2004). Hence, Chow et al., (2015) specify a percent mass of $100 \pm 20\%$ as good criteria for a mass closure solution.

Chemical composition is a strong indicator for particles sources (Yin and Harrison 2008). Although each of the previous components could be contributed to by many sources, they are often dominated by few sources (Chow et al., 2015). Consequently, the importance of the mass closure approach comes from the ability of a simple method to provide a general knowledge of the major component composition of PM in the atmosphere and the contributions of individual categories to particle concentrations (Harrison et al., 2003).

1.7 Objectives

The aim of this thesis is to identify and quantify the main sources that contribute to fine particulate matter (PM_{2.5}) concentrations in ambient air in Doha, Qatar. This aim has been addressed through:

- conducting a parallel sampling of PM_{2.5} in two locations in Doha city using Teflon and quartz filters,
- analysing existing measurement and monitoring data to assess the air pollution climatology in Doha,
- identifying the chemical composition of particulate matter, following the chemical analysis of the samples,
- understanding the key components that constitute the chemical composition of PM_{2.5} using the mass closure model,

- inferring the likely pollution source using the PMF receptor model,
- and identifying those sources (areas/industries) that might most effectively be addressed in future air quality legislation.

1.8 Thesis Structure

The following chapters are organized as follows:

- Chapter 2 describes the general methods and procedures used during the winter and summer sampling campaigns including the instrumentation and chemical analysis methods.
- Chapter 3 presents a statistical analysis of meteorology and PM_{2.5} mass and composition in both campaigns to assess the impact of spatial and seasonal variation on PM mass and composition.
- Chapter 4 presents mass closure results to identify the major chemical composition of PM_{2.5}, and to assess the accuracy of assumptions made regarding the abundance of unmeasured species.
- Chapter 5 presents results of a source apportionment using the EPA PMF-5 model to identify and quantify the key natural and anthropogenic sources contributing to PM_{2.5} in Doha.
- Chapter 6 describes the policy implications of the results obtained, and the need for a new PM metric and/or an allowable number of exceedances to account for natural sources of PM in Doha.
- Chapter 7 describes the conclusions from the current study and provides recommendations for future work.

CHAPTER 2- METHODOLOGY

2.1 Methodology Overview

For the purpose of this study, four low volume samplers were purchased and installed inside two air quality stations (Al-Corniche and Qatar University) in Doha city. Sampling campaigns in Doha city were conducted in the winter of 2014-2015 and the summer of 2015. Inorganic ions, metals, organic and elemental carbon chemical analysis were all performed at the University of Birmingham (UOB). Excel software, OpenAir, and the PMF-5 receptor model were used for the data analysis. This chapter presents detailed information about the sampling campaigns and the laboratory analytical procedures are in the following sections.

2.2 PM-162M Sampler

2.2.1 Samplers

ExxonMobil Research Qatar (EMRQ) funded the study with four automatic sequential ambient air particulate samplers (Model – PM-162M) associated with a PM_{2.5} inlet head (US EPA 1m³/h). The samplers were purchased from a French company (Environnement S.A), and they meet the requirements of AFNOR × 43-021 standards, EN 12341 standards and CEN standard project about PM_{2.5} (Environnement S.A., 2012).



Figure 2.1 PM-162 M Sampler (Source: PM-162M Manual, 2011)

Ambient PM_{2.5} size particles were collected using a selective cyclonic inlet head with a constant flow rate onto 47mm diameter filters. The sampling head is a PM_{2.5} cyclonic inlet with a gooseneck adapter made of aluminium. The desired cut-off curve for airborne size particles close to 2.5 µm is determined by the design of the cyclonic inlet head and the flow rate. Once the dust-laden air enters the inlet head, it is forced to rotate taking the path of the cyclone geometry which causes the large particles to settle down due to a combination of inertia and aerodynamic drag forces, whereas the smaller particles will continue their movement to the filter (Dirigo and Leith, 1985).

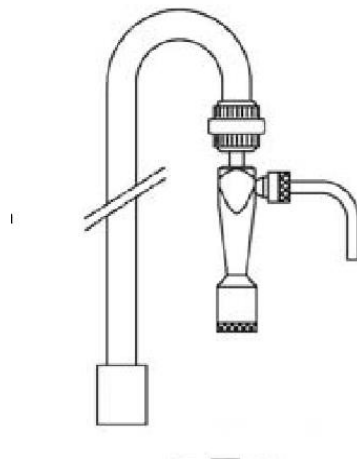


Figure 2.2 PM_{2.5} gooseneck inlet head (Source: PM-162M Manual 2011)

The collection mechanism is illustrated in Figure 2.3. The sampler has an external pump that draws ambient air with a constant flow rate of 16.7L/min through a PM_{2.5} size-selective inlet. The particulate – laden air is then directed through a preweighed 47mm diameter filter media, where the particulate material deposits on the filter surface.

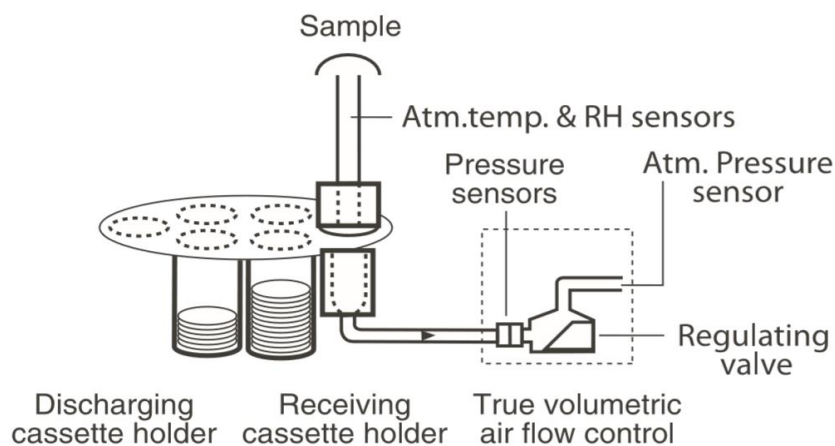


Figure 2.3 Diagram of the PM-162M sampler (Source: Environment S.A., 2011)

The sampler is equipped with temperature, humidity, and atmospheric pressure sensors to regulate the sampling performance at a constant flow rate with compensation of pressure losses due to any changes in the atmosphere or the filter efficiency. The sampler is fitted with a standard orifice system and a powered valve downstream of the filter, to control the pressure at the sampling head level, ensuring an accurate separation of particles through the sampling head and to maintain a true calculation of the sampled volume at different atmospheric conditions. PM-162M has an automated filter exchange mechanism device and it can hold up to 22 filters at a time, but the system was found to be unreliable, as the filters cassette often jammed inside the rotation disk causing a failure of the rotation mechanism and change to the filters see Figure 2.4.



Figure 2.4 Damages to quartz filters during disc rotation

2.2.2 Sampler Installation

One of the installation requirements for the PM-162M sampler is to be in an environment where the ambient temperature does not exceed 40 °C in order to operate efficiently. Therefore samplers were installed inside air-conditioned air-quality stations, as the temperature in Doha city usually exceeds 40 °C in the summer season. It also provided protection for the samplers from severe dust storms and allow us to benefit from the gaseous concentrations, meteorological data, and PM mass concentrations that are also measured at these stations.

Another requirement of the source apportionment study was the need to collect samples on two different types of filters (Quartz and Teflon) to allow for all types of analysis that are needed, thus two samplers were installed back to back inside each of the air quality stations. Figure 2.5 shows the samplers' position inside the station on the top rack. Figure 2.6 shows the samplers' goose-neck inlets at the height of 4 m above ground level.



Figure 2.5 Two samplers back to back at the top rack in the station



Figure 2.6 Samplers' goose-neck inlets at the height of 4 m above ground level

2.3 Filters Selection

Particulate matter sampling can be achieved by filtering air through a wide range of collecting media. Choosing the proper type of filters depends on the purpose which it is used for. In case of determining mass concentration, European legislation recommends quartz filters for PM₁₀ measurements while Teflon, quartz and glass fibre can be used for PM_{2.5} (EN 14907, 2005). However, if the filters are being used to identify particles' chemical components; other criteria should be looked at such as blank levels, and physical and chemical stability.

In general, quartz fibre filters can stand high temperature and therefore they are suitable for organic and elemental carbon analysis, which has to be carried out at high temperature. They also have high loading capacity and are less likely to clog hence they are used in high volume samplers. Teflon filters have lower blank levels and are more suitable for ions and elements analysis (Chow and Watson, 1998). Teflon filters are more favourable for gravimetric analysis since they are less likely to absorb ambient water vapour. They also have high flow resistances and low loading capacity. Therefore, they are often used in low volume samplers.

Filter performance is affected by artefact formation which depends on ambient temperature and relative humidity. Quartz filters show high retention of organic vapour and lower release of ammonium and nitrate salts causing a positive artefact (Vecchi et al., 2009) while Teflon filters adsorb little or no gas phase organic carbons. Another cause of artefact is PM-adsorbed water. The hydrophilic nature of quartz filters encourages the transfer of water molecules from particles to filter fibres; from which they evaporate to the atmosphere, whereas the hydrophobic characteristic of Teflon filters prevents water molecules transferring and they remain attached to particles causing a positive artefact (Perrino et al., 2013; Zdziennicka, et al., 2009). This artefact formation can lead to a gap in mass closure when the mass concentration determined on a Teflon filter is compared to the sum of the chemical components determined on both quartz and Teflon (Sillanapaa et al., 2006).

Another important factor in selecting filters is the pore size. Smaller pore sizes increase the collection efficiency and the flow resistance, but it does not affect the size of particles collected on filters beyond a certain limit (NIOSH, 2014). Particles collected by filters includes all size of aerosol particles even those smaller than the pore size, because small particles $\leq 0.1 \mu\text{m}$ are captured on filters by diffusion mechanism, which occurs due to Brownian motion of gas molecules; in which gas molecules collide with small particles causing them to deflect randomly in a zig-zag motion hitting the filter's fibres and depositing on them (Lindsley., 2016)

Typically, Teflon filters are used to determine metals, inorganic ions, and gravimetric mass determination and quartz filter for the carbonaceous species and inorganic ions as well (Harrison et al., 2003; Vecchi et al., 2008; Mooibroek et al., 2011; Pant., 2014)

Whatman membrane filters PTFE $1\mu\text{m}$ pore size with 47 mm diameter were used in this study for the determination of particle mass loading since they are not prone to absorption of

ambient water vapour hence their mass is more stable through weighing process. The same filters were also used for the determination of crustal minerals and trace metals due to the low blank levels and their resistance for XRF measurements (Chow and Watson 1998; Vecchi et al., 2008). Whatman quartz filters 47 mm diameter was used to determine inorganic ions and carbonaceous species.

2.4 Sampling Locations

The sampling sites were located in Doha city capital of Qatar. Doha is an urban city in the middle of the east coast of Qatar peninsula. It is influenced by several PM sources, among which Doha port, Doha airport, traffic emissions from busy roads and highways, small and medium Doha industrial Area (DIA) in addition to natural sources (dust storms and sea salts).

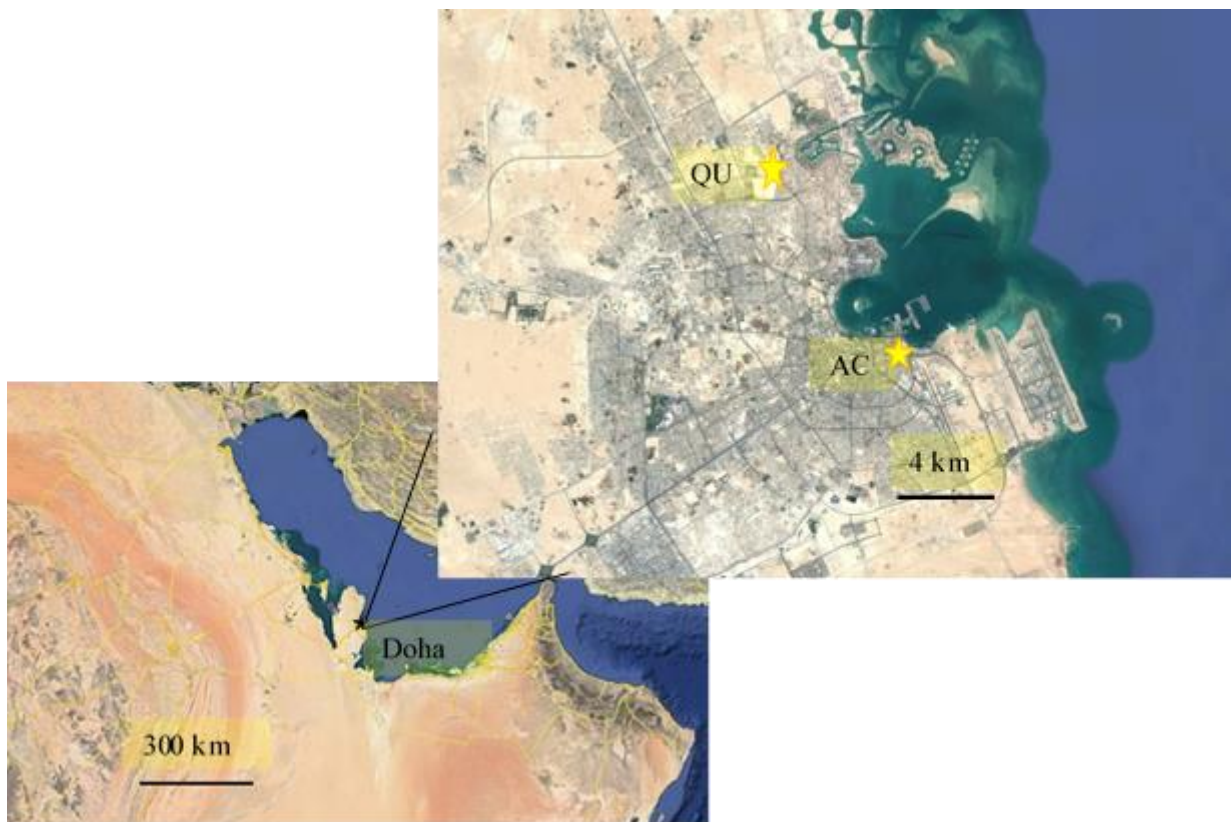


Figure 2.7 Al-Corniche (AC) and Qatar University (QU) Sampling sites.

2.4.1 Al-Corniche Site

Al-Corniche monitoring (AC) station is placed in a small park near a heavily trafficked road. Doha Port is about 300 m from the north, whereas Hamad International Airport is 4 km away to the east. Also, the station is surrounded from the south by a car park, governmental buildings, and small hotels, and by a construction work area for a new museum about 300 m to the east-southern direction of the station see Figure 2.9.



Figure 2.8 Al-Corniche Station (AC)



Figure 2.9 The area surrounding the AC station

2.4.2 Qatar University Site

Qatar University (QU) station (Figure 2.10) is located near the southern gate in QU campus, surrounded by a vacant unpaved area from all directions and by two main busy roads, Jelaiah street; 35 m from the south, Al-Jamiaa streets, 160 m away from the east and by QU inner street 500 m from the west (Figure 2.11). During the sampling period (November 2014 to February 2015) there were earthworks involving excavating material, haulage, and stockpiling close to the station (Figure 2.12)



Figure 2.10 Qatar University Station (QU)



Figure 2.11 The area surrounding the QU station



Figure 2.12 Earthwork activity at the QU site during the winter campaign

2.5 Sampling Campaigns

The study involved two sampling campaigns (winter and summer). Samples were collected from two locations in Doha city (Qatar University and Al-Corniche). Parallel PM_{2.5} sampling was collected using PM-162M samplers on Teflon and quartz filters to allow for gravimetric determination and metals, ions and carbon analysis.

Table 2.1 An overview of the sampling campaign in Doha

Campaign	Locations	Samplers	Sampling time	Size Fraction	Filters type	Chemical analysis
Winter	Qatar University	PM162 M	24 hours starting from 11 AM local time	PM _{2.5}	Quartz	EC/OC - Ions
Nov2014- Feb 2015 Summer May-Aug 2015					Teflon	Minerals & Trace Metals
	Al-Corniche					

2.5.1 Winter Sampling Campaign

The first sampling campaign started on November 13th, 2014 and ended on February 14th, 2015. Parallel PM_{2.5} samples were collected on 47-mm diameter (Quartz and Teflon) filters with 1µm pore size. 24 hours (11:00am to 11:00am, local time) PM_{2.5} samples were obtained using a low volume flow rate 16.7 L/min.

A total of 76 pairs of filters was collected from Qatar University and 74 pairs from Al-Corniche. The exposed filters were stored in a freezer at – 18 °C, to minimize the evaporation of volatile compounds until the shipping date. At the end of the sampling campaign, filters were shipped by air to Birmingham, and it took 4 days to arrive. After samples arrival, they were placed in a cold room until the day of analysis.

The ambient temperature during the sampling periods ranged from 14 to 25 °C with a few showers in November and minor dust storms on the 10th, 11th, 13th, and 14th of February. The main issue with winter sampling campaign was the leakage of rainwater from the station ceiling into the samplers every time it rained causing electrical malfunction and stopping the sampling for days for the maintenance, which happened in late November early December.

2.5.2 Summer Sampling Campaign

The same procedures, instruments, and type of filters were used in the same locations for the second campaign. The sampling started on May 12th, 2015 and ended on August 23rd, 2015.

65 pairs of samples were collected from Qatar university location whereas 76 pairs collected from Al-Corniche. After the sampling; all filters were kept in the freezer to minimize organic compounds loss. The samples shipping from Doha to the UK were done in two stages. The first two boxes contain samples from May to mid of July took 3 days to arrive in the UK, whereas the other shipment contains samples collected from mid of July until August took 6

days and the boxes arrived slightly damaged from the outside. However, the samples were sound.

The weather during the second campaign was very hot and humid. The average temperature was around 40 °C, and the sky was hazy most of the summer season due to dust suspension and lack of precipitation. Nonetheless, there were no major dust storms during the sampling time. The main issue with sampling this season was the high temperature and humidity. Because of the temperature differences outside and inside the station, which is a conditioned cool area, water vapour started to condense on the cold ceiling and penetrate through weak points of the sampling line to the samplers. To solve these issue plastic wrapping sheets were used to cover the sampling line tube and direct the condensed water away from the sampler.

2.6 Analytical Procedures

Mass measurements and chemical analysis for both campaigns were conducted at the University of Birmingham facilities. Soluble ions (SO_4^{2-} , NH_4^+ , NO_3^- , Cl^- , Na^+ , Ca^{2+} , PO_4^{3-} , K^+ , Mg^{2+}), crustal metals (Fe, Al, Si, S), trace metals (Zn, Ba, Pb, Cd, Cr, Co, Ni, V, As, Ti, Mn, La, Ce) and organic and elemental carbons were analysed for all samples.

2.6.1 Filter Preparation and Conditioning

Quartz filters were heated overnight in an oven at 450 °C to remove carbon impurity whereas no cleaning procedure was done for Teflon filters. Teflon filters were conditioned in a controlled environment room with 35-45% RH and 20 °C for 48 hours prior to weighing. After the pre-sampling weighing, all filters were stored in Petri-slides and kept in plastic bags until sampling.

2.6.2 Gravimetric Analysis

Sampled mass was calculated as the difference between filter mass before and after sampling. In order to obtain the sampled mass, Teflon filters were left to equilibrate in a windowless room with controlled temp and humidity for 48 hours. Then they were exposed to an α particle source (210Po) to neutralize the static electricity on the filter before weighing them using a Sartorius Model MC5 microbalance (sensitivity- 1 μ g). Filters were weighed three times before and after the sampling, and the average weights were used for the calculation.

2.6.3 Cleaning Procedure

New clean plastic wares were used for all the extraction procedures. No further cleaning was required for those used for IC extraction, but for the metal extraction, 4 ml Nalgene polypropylene vials and 15 ml polypropylene tubes were soaked in 2% Aristar Grade HNO₃ for 48 hours then rinsed thoroughly using 18.2 M Ω distilled deionized water (DDW). All clean vials were then placed in polypropylene containers and left to dry. After the drying of vials, caps were placed on the tubes which were then kept in sealed containers to minimize contamination.

2.6.4 Metal extraction

In order to determine trace metal concentrations on the filter samples using Inductively Coupled Plasma Mass Spectrometry (ICP-MS), metals should be in an aqueous solution. The metals digestion of the filters was carried out using aqua regia solution (Allen et al., 2001) in closed vials with an energy source provided by a hot water bath and mild ultrasonic bath. After completing Wavelength Dispersive X-Ray Fluorescence (WD-XRF) analysis on Teflon filters, they were placed inside 4ml Nalgene polypropylene vials using pre-cleaned forceps and then 2 ml aqua regia solution was added to the filters using a Gilson pipette. Reverse

aqua regia solution was prepared using Aristar grade hydrochloric acid (HCl) and Nitric acid (HNO₃). 3.3 ml HCl and 9.45 ml HNO₃ were pipetted into a 50 ml volumetric glass then the final volume was completed with distilled deionized water (DDW).

Tightly screwed vials were placed in a small polypropylene container half filled with DDW and placed in a water bath (Grant) operating at 100 °C for 30 minutes, followed by 30 minutes ultrasonic water bath (Decon) operating at 30 °C. The process was repeated once, and the resulting solutions were transferred to 15 ml polypropylene tubes. The total aqueous solution volume was then made up to 11 ml using DDW. Extracted samples were then placed in zip-lock bags and stored in the cold room at 4 °C until analysis.

2.6.5 Ions Extraction

Quartz filters were used for ion extraction. Three 1cm² punches of each quartz filter were removed using a punch cutter and saved in the Petri-slides for future organic and elemental carbon analysis, while the rest of the quartz filters were placed in 50ml tubes. The tubes were filled up to 12 ml with DDW and loaded onto a mechanical shaker. The samples mixtures were shaken for 50 minutes, then samples were filtered using 0.45 µm Acrodisc syringe filters into 15ml tubes and stored in zip-lock bags in the refrigerator at 4 °C until analysis.

2.6.6 Organic and Carbon Analysis

Organic (OC) and Elemental carbon (EC) concentrations were determined on quartz filters using a Sunset Laboratory Thermo-Optical OC-EC Aerosol Analyser, using the EUSAAR2 (European Supersites for Atmospheric Aerosol Research) protocol (Cavalli et al., 2010). The instrument was checked with an external multipoint sucrose (C₆H₁₂O₆) solution calibration with standards ranging from 4.2 µg/cm² to 42 µg/cm². Then the precision was checked

throughout the analysis by running one-point standard after every 10 samples. Blank filters were analyzed with every batch, and the reported samples were blank corrected.

A 1cm² punch was removed from the quartz filter and loaded into the analyzer. In the first, the sample was heated in a stepwise increasing temperature (200, 300, and 450 to 650 °C) under inert Helium mode. Carbon evolved from this step was oxidized to CO₂ gas in the MnO₂ oven, then reduced to methane in the methanator oven for subsequent detection with flame ionization detector (FID).

After cooling the sample oven to 500 °C for 30 seconds; the second oxidizing phase (Oxygen/Helium mode) started with four increasing temperature steps (500, 550, 700 and 850 °C). In this phase, the original elemental carbon EC in addition to pyrolytic carbon PC produced in the first phase was oxidized to CO₂, and then they were converted to methane and detected by FID. At the end of each sample analysis, an internal calibration was performed using a known concentration of methane gas hence each sample was calibrated to a known quantity of carbon. One main complication during the first phase “helium mode” of the analysis is that a fraction of the OC undergoes charring and forms pyrolytic carbon (PC) which is then detected as EC in the oxidizing phase. To account for the pyrolysis, the transmission of the filters is continuously monitored throughout all stages of the analysis and used to split the total carbon into OC and EC. The split is defined as the point where the transmittance level returns to its initial maximum level (Cheng et al., 2011). Different carbon fractions resemble carbon evolves at each of temperature ramps OC1 (200 °C), OC2 (300 °C), OC3 (450 °C), OC4 (650 °C), EC1 (580 °C), EC2 (500 °C), EC3 (550 °C) and EC4 (850 °C). Organic carbon is calculated as the sum of OC1 to OC4, and PC, whereas Elemental carbon is calculated as the sum of EC1 to EC4 minus PC.

2.6.7 Inorganic ions analysis

After the Ion extraction of quartz filter; samples were analyzed for anions using ion chromatography using Dionex ICS1200 and cations via Dionex DX500. 1000 mg/L anions and cation stock solutions were prepared using ACS reagent-grade chemicals (salt form) and 18.2M Ω -cm deionized water. Five-point calibration standards ranging from 0.2 to 10 ppm were prepared from each stock. Filter blanks were analyzed with the sample batches, and the samples were blank corrected.

Aqueous samples are loaded into the autosampler using either 0.5 or 5 ml vials. Then they are injected into the eluent stream and transported to the separator column by a pumping system. Within the ion-exchange column, each ion is identified by its retention time. When the eluent ions exit the separator column, they are neutralized in the following suppressor column, and sample ions are transformed to their corresponding strong acidic and basic form for quantitative detection (Chow and Watson, 1998). In both campaigns methanesulfonic acid was used as eluent for cations analysis whereas for anions; potassium hydroxide (KOH) was used in the winter campaign, while sodium carbonate and sodium bicarbonate (Na_2CO_3 and NaHCO_3) for the summer campaign. The difference in eluents type was caused by using two different instruments between seasons, as the instrument used in the first campaign failed to produce good results at the time of the second campaign (peaks for different species were overlapping). At the first campaign, pre-used and cleaned 5ml vials were used to load the samples into the analyzer. The vials showed high-level blanks for NO_3^- (0.5 ppm) and Cl^- (0.3 ppm) which was equal to 17% and 60% of their average concentration respectively therefore in the second campaign they were replaced by new 0.5ml vials which showed a better result for the blank.

2.6.8 Metals Analysis

Metals were analyzed in two stages. In the first stage; S, Al, Fe, and Si were analyzed on Teflon filters using a Wavelength Dispersive X-Ray Fluorescence (WD-XRF) instrument (Tiger Bruker S8). The XRF is not a destructive method. Therefore, the same samples' filters were used to determine trace metals using ICP-MS. The XRF instrument was calibrated using thin film metal standards by the responsible technician prior the analysis. However, after the mass balance calculations, a big discrepancy was found between the gravimetric mass and the reconstructed mass. The reconstructed mass was ~27% higher than gravimetric mass. After checking thin film standards against XRF previous calibration, Si and Al elements' results showed a big difference between the standards values and the calibration curve. All Si and Al values were then scaled to the resultant regression equation which solved the mass discrepancy issue. Also, two control samples from each of the sampling campaigns were reanalysed again to check that the instrument calibration did not degrade in-between both campaigns. All four samples gave the same previous results indicating that the calibration error was prior to the first campaign analysis, and that the instrument precision is good however the accuracy was not.

Trace metals on Teflon filters were chemically extracted and the following trace metal (Cu, Zn, Ba, Ti, Sb, Ni, Mn, V, Co, Cr, As, La, Ce, Sn, Zn, and Pb) were determined in the aqueous solution using Inductively Coupled Plasma Mass Spectrometry (Agilent 7500ce ICP-MS) for the first campaign and a Perkin Elmer NexION 300X ICP-MS for the second campaign. For ICP-MS optimization, a mixture of Sc (45), Y (89), Ge (72), In (115), Tb (159) and Bi (209) were used as an internal standard along with multi-point calibration standard ranges between 1 and 200 µg/l, which were prepared from VWR or Agilent stock solutions in the same acid mixture as the samples. Both instruments were operated in the helium collision

mode for Ti, V, Cr, Mn, Co, Ni, Cu, Zn and As (to eliminate interference from polyatomic species) and in standard mode for Cd, Sb, Ba, La, Ce, and Pb.

2.7 Detection Limit

Ten blank filters were analyzed at the end of each analytical technique to calculate the standard deviation (SD) and the limit of detection (MDL). MDL was calculated as (3×SD).

Table 2.2 Limit of detection (MDL)

Compound	MDL (µg/filter)
Ions using pre-used and washed 5-ml vials	
Cl ⁻	0.185
NO ₃ ⁻	0.529
SO ₄ ²⁻	0.0198
NH ₄ ⁺	0.087
Na ⁺	0.846
K ⁺	0.189
Mg ²⁺	0.093
Ca ²⁺	0.583
PO ⁻³	0.343
Ions using new 0.5 ml vials	
Cl ⁻	0.0647
NO ₃ ⁻	0.178
SO ₄ ²⁻	0.007
NH ₄ ⁺	0.039
Na ⁺	0.331
K ⁺	0.112
Mg ²⁺	0.035
Ca ²⁺	0.224
PO ⁻³	0.239

Metals using XRF	
Si	0.078
Al	0.174
Fe	0.078
S	0.028
Trace metals using ICP-MS	
Ti	0.00045
V	0.00264
Cr	0.01839
Mn	0.00124
Co	0.00003
Ni	0.01140
Cu	0.00039
Zn	0.00683
As	0.00025
Cd	0.00009
Sb	0.00002
La	0.00001
Ce	0.00004
Ba	0.00219
Sn	0.00220
Organic and elemental Carbon	
OC	1.400
EC	0.005

2.8 Calculations

The concentration of the elements in ambient air is given by two equations. The first one is for elements obtained from ICP-MS and IC techniques

$$\text{Element concentration in air } (\mu\text{g}/\text{m}^3) = (M (\mu\text{g}/\text{ml}) \times V (\text{ml})) / v t (\text{m}^3)$$

Where: M is the concentration of elements in $\mu\text{g}/\text{ml}$

V is final volume of the sample extract (ml)

vt is sampling time (h) \times sampler flow rate (m^3/h)

Whereas the following equation is for elements determined by XRF and OC/EC techniques

$$\text{Element concentration in air } \mu\text{g}/\text{m}^3 = (M (\mu\text{g}/\text{cm}^2) \times A (\text{cm}^2)) / v t (\text{m}^3)$$

Where: M is the concentration of elements in $\mu\text{g}/\text{cm}^2$

A is total filter area in (cm^2)

vt is sampling time (h) \times sampler flow rate (m^3/h)

2.9 Secondary Data

Hourly data for both campaigns durations were obtained from Al-Corniche and Qatar University stations for NO_x , NO, and NO_2 in addition to meteorological parameters. NO_x , NO, and NO_2 were measured using automatic chemiluminescence method. A weekly zero point and span check for two points and quarterly multipoint calibrations were done for the monitoring device with certified primary calibration gas cylinders, also a data validation was done by removing error readings (MOE, 2013).

The daily averages for the parameters were calculated from 11am to 11am local time using a data acquisition system to line-up with the readings from the sampling campaign.

2.10 Data Analysis

Excel software was used for data analysis. The source apportionment study was performed using US-EPA PMF 5 Model see chapter 5 for more details. Polar and pollution rose plots were performed using Open Air (0.9-0) software; which is a statistical package based on R computer programming language. A detailed manual of Open Air tools for analyzing air - pollution data is given in Carslaw (2013).

CHAPTER 3: DESCRIPTIVE DATA, SEASONAL AND SPATIAL VARIATION

3.1 Overview of Meteorological Parameters during Both Campaigns

Daily meteorological data for the QU and the AC sites were obtained from air quality stations owned by the Ministry of Municipality and Environment (MME, 2016). The data covers the study period for the winter season (November 2014 – February 2015) and the summer season (May 2015-August 2015). Because of Qatar's location in the Northern Hemisphere desert, it's arid desert climate is characterised by short winters and long summers that last from May to September. The summer season is characterised by scarcity in rainfall, high evaporation rates, very hot weather where the hourly temperature can easily exceed 40 °C, and by the Al-Shamal prevailing wind, which is a hot, dust-laden wind that blows from a north-westerly direction and may cause dust storms (Abu Sukar et al., 2007). In contrast, the winter season is cool with occasional rainfall. Overview of meteorological data are shown in Table 3.1.

Table 3.1 Overview of meteorological parameters for the winter season (Nov 2014-Feb 2015) and the summer season (May 2015-Aug 2015) at the QU and AC sites

Meteorological parameters	Summer Season					
	AC			QU		
	Mean	Min	Max	Mean	Min	Max
Temp °C	35.3	30.9	39.3	35.9	31.9	39.3
RH %	44.9	15.2	78.3	35.0	13.2	61.3
AT. Press mb	1015.8	1008.5	1029.7	1022.78	1014.1	1035.4
WS m/s	1.8	0.5	4.8	2.1	0.5	5.3
Meteorological Parameters	Winter Season					
	AC			QU		
	Mean	Min	Max	Mean	Min	Max
Temp °C	20.8	14.3	25.6	20.4	13.8	26
RH%	66.1	49.1	82.1	58.3	45.2	72
AT. Press mb	1038.2	1033.4	1042.8	1044.1	1039.2	1049.3
WS m/s	1.3	0.1	3	1.8	0.2	4.9

3.1.1 Meteorological Parameters' Spatial Variation

In both seasons, significant correlations were observed for meteorological parameters between locations $r \geq 0.94$. Although meteorological patterns were similar at both sites, a noticeable difference in their values was observed, namely for relative humidity, atmospheric pressure, and wind speeds as shown in Figures 3.1 and 3.2. Higher relative humidity was found at the Al-Corniche site (AC) in both seasons relative to the QU site. The reason for the increase in relative humidity is changing water vapour content (Ahrens, 2000). The AC site is nearer to the sea coast; hence, the contribution of water vapour from air masses coming from the sea can cause such a difference. The high relative humidity occurred with a depression in atmospheric pressure because of the displacement of oxygen and nitrogen molecules with water molecules. Wind speed, on the other hand, showed higher speeds at the QU site because the station is located in an open area where there are no obstacles to reduce wind velocity, while the AC site station is surrounded from the north-west and south-west by tall buildings, which may affect wind velocity.

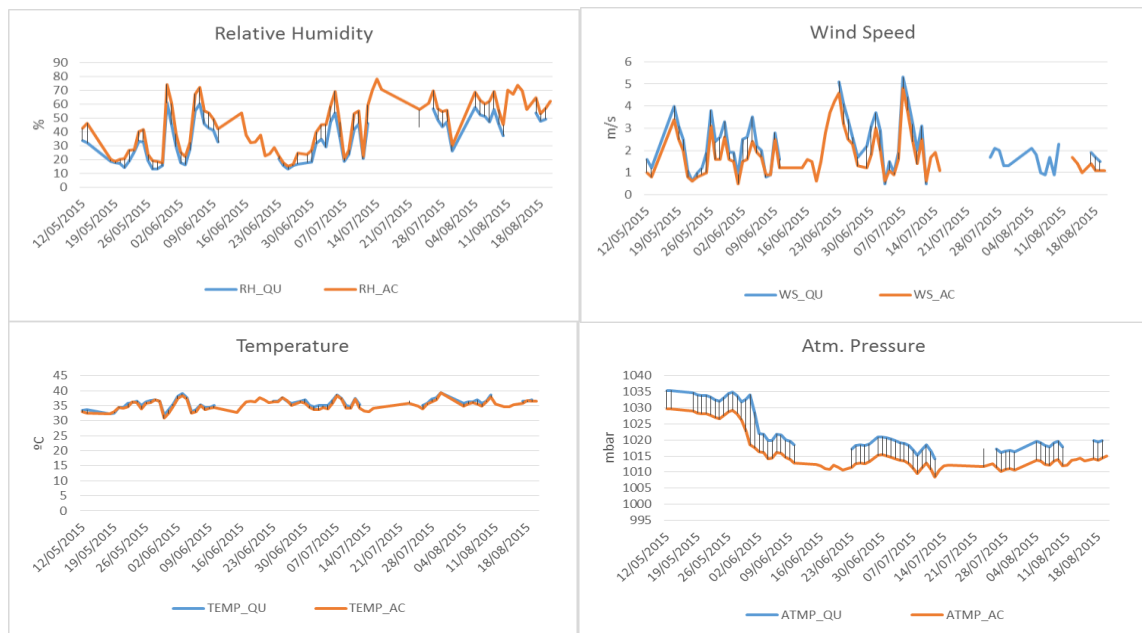


Figure 3.1 Daily pattern of meteorological parameters at the AC and QU sites in summer

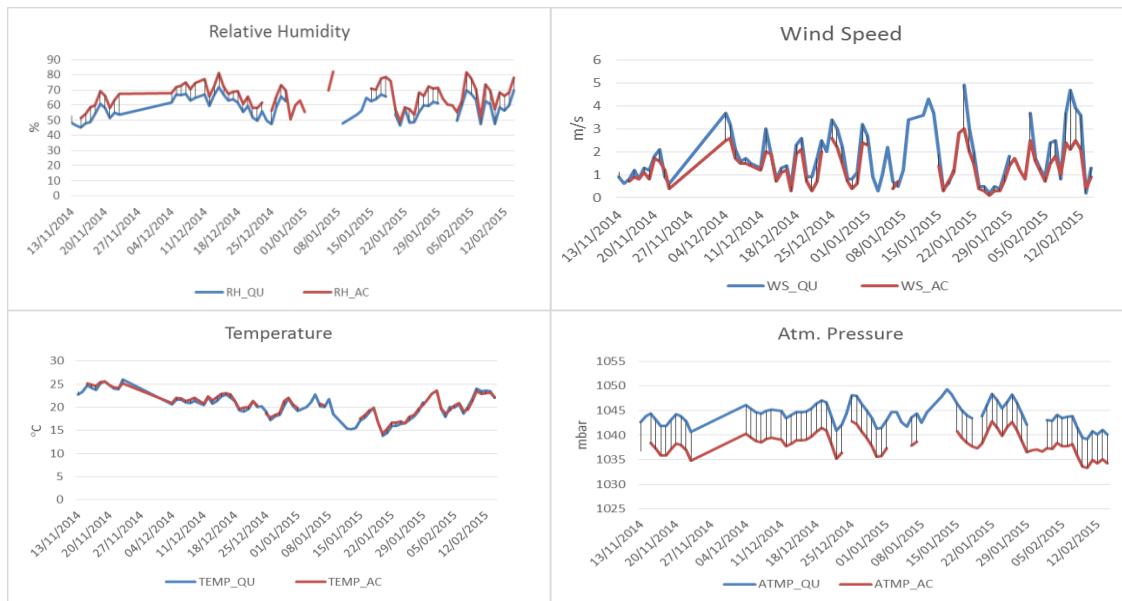


Figure 3.2 Daily pattern of meteorological parameters at the AC and QU sites in winter

3.1.2 Meteorological Parameters Seasonal Variation

The seasonal variation between the summer and winter seasons was characterised by changes in wind direction and an increase in the frequency of dust events in the summer season. The winter season was characterised by few occasions of precipitation, as well as an increase in relative humidity and atmospheric pressure.

The prevailing wind during the summer season blew mostly from the north and north-west directions and occasionally from the north-east, while in the winter, the wind blew from the north-west and south-east (Figure 3.3). Average relative humidity was 44.9% at the AC site and 35% at the QU site in the summer season and was 66.1% at the AC site and 58.3% at the QU site in the winter season. In winter, an average of 21% rise in relative humidity was observed relative to the summer season. Relative humidity is the ratio of water vapour content compared to the amount of water vapour required for an air parcel to be saturated at a particular temperature (Ahrens, 2000). Relative humidity changes based on the extra amount of vapour added to the air parcel or by changes in ambient temperature. In the summer season, as the air temperature increase, the capacity to hold water vapour increases due to water

vapour pressure changes with temperature. Therefore, the air becomes less saturated compared to the winter. The seasonal variation of atmospheric pressure is also caused by the differences in ambient temperature. In the summer, with increasing temperature, the earth's surface is heated, and the air above it gets warm and expands, resulting in less dense air and hence lower pressure.

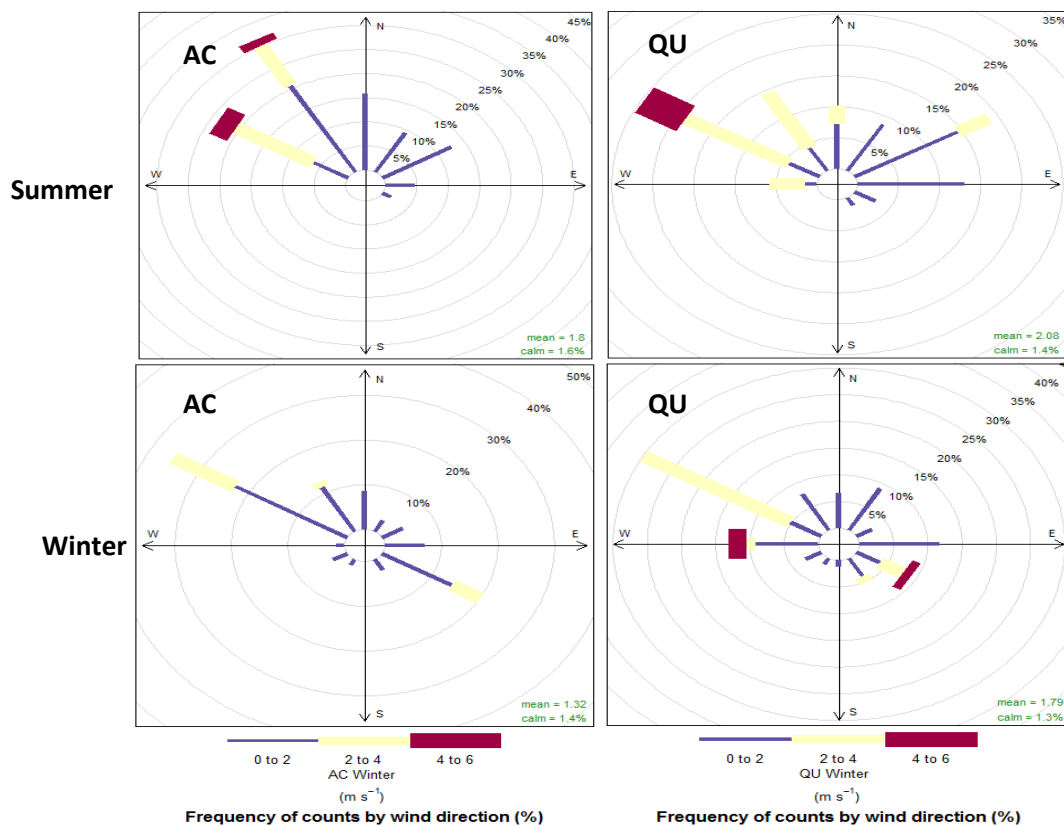


Figure 3.3 Windrose at the AC and QU sites during the winter and summer campaigns

A dust storm is a natural phenomenon, which reflect strong dust-transporting wind occurrences; and times when dry conditions leave bare surfaces exposed to wind (Pye, 1987). Qatar atmosphere is under occasional dust storms (visibility < 1000 m) and more frequent dust haze events (visibility between 1000 and 5000 m), whereas rainfall is scarce (QCAA, 2014). Dust storms usually occur in the spring starting from mid of February to April, and then again in the summer from June to August. During the sampling period, there were no

major dust storms, but there were many dust haze events (Table 3.1). Trace amounts of precipitation occurred in the winter season from November 2014 to January 2015 with the exception of three days, which witnessed a measurable amount of precipitation of 0.4, 4.6, and 8.4 mm on November 23 and 30, and January 18, respectively. There is a time gap between the precipitation and dust events data provided by the meteorology department in Table 3.2 and campaigns' data. Campaigns data were sampled for 24h, starting from 12 PM, and were allocated to the following day when the sampling ended, whereas dust events and precipitation represent the same day of occurrence.

Table 3.2 Days with dust events in Doha 2014/2015 obtained from Qatar Civil Aviation Authority, Department of Meteorology (QCAA, 2014)

Month	Date	Minimum Visibility (m) (5000m or less)	Month	Date	Minimum Visibility (m) (5000m or less)
January 2015	10/01/2015	1500	July 2015	08/07/2015	5000
February 2015	06/02/2015	5000		11/07/2015	5000
	09/02/2015	1500		12/07/2015	2000
	11/02/2015	4500		13/07/2015	4000
	12/02/2015	5000		15/07/2015	4000
June 2015	04/06/2015	5000		23/07/2015	3500
	05/06/2015	2000		26/07/2015	4000
	11/06/2015	5000		28/07/2015	5000
	21/06/2015	2500	August 2015	01/08/2015	4000
	23/06/2015	5000		02/08/2015	3400
	27/06/2015	5000		03/08/2015	4200
July 2015	01/07/2015	4500		04/08/2015	3500
	02/07/2015	3000		05/08/2015	4000
	04/07/2015	5000		06/08/2015	5000
	05/07/2015	4000		07/08/2015	3500
	06/07/2015	2000		08/08/2015	3200
	07/07/2015	3000			

3.2 Descriptive Data for Species Mean, Max, and Min Concentrations in Both Seasons

Tables 3.3 and 3.4 present descriptive data of the mean, minimum, maximum and standard deviation (SD) for PM_{2.5} concentration and its chemical constituents at each site during the winter and summer campaigns. The data are based on 74 samples collected at Al-Corniche,

and 76 at Qatar University in the period between November 2014 and February 2015, as well as 76 samples collected at Al-Corniche and 65 at Qatar University between May and August 2015.

Table 3.3 Descriptive data for species mean, max, and min concentrations in the winter season (Nov 2014 - Feb 2015) at the QU and AC sites

Species	Al-Corniche Site (AC) Winter				Qatar University Site (QU) Winter			
	Mean $\mu\text{g}/\text{m}^3$	Min $\mu\text{g}/\text{m}^3$	Max $\mu\text{g}/\text{m}^3$	SD $\mu\text{g}/\text{m}^3$	Mean $\mu\text{g}/\text{m}^3$	Min $\mu\text{g}/\text{m}^3$	Max $\mu\text{g}/\text{m}^3$	SD $\mu\text{g}/\text{m}^3$
PM _{2.5}	38.55	14.70	93.95	10.89	37.46	18.17	95.20	9.55
Al	0.46	0.10	3.62	0.24	0.58	0.09	5.28	0.63
Al ₂ O ₃	1.39	0.31	10.86	0.45	1.73	0.26	15.85	1.19
Fe	0.49	0.14	2.69	0.18	0.63	0.12	5.14	0.58
Fe ₂ O ₃	0.57	0.21	3.85	0.26	0.90	0.18	7.34	0.83
Si	1.99	0.41	14.90	2.10	2.48	0.38	22.23	2.60
SiO ₂	4.26	0.88	31.90	4.5	5.31	0.82	47.57	5.56
S	4.89	1.16	8.94	1.58	4.47	1.83	8.39	1.57
SO ₄ ²⁻	15.36	0.77	37.86	7.64	11.83	2.92	22.60	5.04
NH ₄ ⁺	6.29	1.02	15.06	3.01	4.55	0.26	9.39	2.09
Cl ⁻	0.10	0.00	2.04	0.17	0.13	0.01	1.25	0.24
NO ₃ ⁻	2.05	0.09	7.33	1.84	2.74	0.02	7.91	1.93
Na ⁺	0.65	0.01	1.57	0.39	0.77	0.02	2.38	0.45
Ca ²⁺	0.44	0.01	3.38	0.55	1.29	0.01	6.67	1.07
CaO	0.62	0.02	4.73	0.77	1.80	0.01	9.34	1.50
K ⁺	0.64	0.05	5.11	1.19	0.29	0.00	2.42	0.48
Mg ²⁺	0.10	0.01	0.42	0.05	0.16	0.04	0.35	0.07
OC	5.86	2.29	16.47	2.29	4.47	2.87	11.03	1.62
EC	4.18	1.78	10.16	1.64	3.61	0.00	8.34	1.83
Ti	0.0089	0.0025	0.0490	0.0076	0.0105	0.0015	0.0750	0.0092
V	0.0113	0.0032	0.0287	0.0047	0.0096	0.0044	0.0238	0.0030
Cr	0.0153	0.0017	0.1021	0.0160	0.0169	0.0015	0.1029	0.0170
Mn	0.0124	0.0034	0.0368	0.0067	0.0103	0.0037	0.0584	0.0065
Co	0.0003	0.0001	0.0016	0.0003	0.0005	0.0001	0.0097	0.0012
Ni	0.0086	0.0021	0.0447	0.0071	0.0091	0.0020	0.0445	0.0076
Cu	0.0112	0.0020	0.0676	0.0087	0.0152	0.0016	0.0493	0.0114
Zn	0.0557	0.0105	0.1922	0.0372	0.0389	0.0111	0.2270	0.0353
As	0.0007	0.0001	0.0025	0.0005	0.0006	0.0001	0.0019	0.0004
Cd	0.0002	0.0001	0.0004	0.0001	0.0002	0.0001	0.0004	0.0001
Sb	0.0016	0.0006	0.0051	0.0008	0.0023	0.0005	0.0064	0.0015
Sn	0.0024	0.0008	0.0066	0.0010	0.0026	0.0004	0.0067	0.0016
Ce	0.0003	0.0001	0.0022	0.0004	0.0003	0.0001	0.0046	0.0005
Ba	0.0140	0.0050	0.0858	0.0129	0.0182	0.0027	0.0589	0.0127
Pb	0.0097	0.0034	0.0260	0.0042	0.0090	0.0039	0.0193	0.0039

Table 3.4 Descriptive data for species mean, max, and min concentrations in the summer season (May 2015 - August 2015) at the QU and AC sites

Species	Al-Corniche Site (AC) Summer				Qatar University Site (QU) summer			
	Mean µg/m ³	Min µg/m ³	Max µg/m ³	SD µg/m ³	Mean µg/m ³	Min µg/m ³	Max µg/m ³	SD µg/m ³
PM _{2.5}	73.67	30.25	202.21	32.29	100.90	35.45	383.33	52.11
Al	2.12	0.58	6.81	1.31	2.72	0.65	8.30	1.64
Al ₂ O ₃	4.01	1.09	12.86	2.47	5.13	1.23	15.67	3.09
Fe	1.88	0.48	7.73	1.29	2.53	0.50	12.29	1.85
Fe ₂ O ₃	2.69	0.69	11.06	1.86	3.62	0.71	17.57	2.65
Si	8.89	2.33	31.01	6.01	11.78	2.83	40.63	7.94
SiO ₂	19.02	4.98	66.35	12.85	25.20	6.05	86.94	16.99
S	6.58	1.79	19.08	3.56	6.85	2.59	17.10	3.64
SO ₄ ²⁻	25.42	4.82	93.79	17.44	23.32	4.53	93.54	20.78
NH ₄ ⁺	5.50	0.68	15.35	3.27	5.27	0.49	15.19	3.82
Cl ⁻	0.39	0.04	2.24	0.33	0.55	0.10	4.62	0.65
NO ₃ ⁻	1.91	0.47	7.22	1.25	2.67	0.77	18.48	2.34
Na ⁺	1.11	0.54	2.70	3.27	1.19	0.51	4.69	0.63
Ca ²⁺	3.61	1.17	10.60	2.16	5.40	1.71	20.93	3.18
CaO	5.05	1.64	14.84	3.03	7.56	2.40	29.30	4.45
K ⁺	73.67	30.25	202.21	32.29	100.90	35.45	383.33	52.11
Mg ²⁺	2.12	0.58	6.81	1.31	2.72	0.65	8.30	1.64
OC	4.01	1.09	12.86	2.47	5.13	1.23	15.67	3.09
EC	1.88	0.48	7.73	1.29	2.53	0.50	12.29	1.85
Ti	0.0325	0.0090	0.1406	0.0213	0.0509	0.0135	0.2543	0.0342
V	0.0235	0.0055	0.0551	0.0128	0.0188	0.0063	0.0447	0.0079
Cr	0.0110	0.0026	0.0691	0.0115	0.0115	0.0032	0.0496	0.0083
Mn	0.0309	0.0088	0.0919	0.0184	0.0443	0.0115	0.2091	0.0308
Co	0.0016	0.0004	0.0226	0.0027	0.0018	0.0004	0.0161	0.0021
Ni	0.0135	0.0033	0.0287	0.0059	0.0134	0.0037	0.0421	0.0069
Cu	0.0107	0.0043	0.0374	0.0050	0.0140	0.0052	0.0395	0.0072
Zn	0.0389	0.0116	0.1491	0.0306	0.0420	0.0159	0.2115	0.0354
As	0.0008	0.0002	0.0024	0.0005	0.0011	0.0003	0.0721	0.0006
Cd	0.0001	0.0000	0.0002	0.0000	0.0001	0.0000	0.0003	0.0000
Sb	0.0015	0.0007	0.0004	0.0008	0.0023	0.0007	0.0241	0.0029
La	0.0037	0.0055	0.1317	0.0149	0.0021	0.0006	0.0099	0.0015
Ce	0.0013	0.0004	0.0077	0.0011	0.0019	0.0004	0.0091	0.0014
Ba	0.0254	0.0090	0.1827	0.0229	0.0354	0.0124	0.1237	0.0199
Pb	0.0074	0.0029	0.0187	0.0034	0.0083	0.0030	0.0311	0.0049

3.3 PM_{2.5} Spatial Variation

Mean PM_{2.5} mass concentrations of 38.55 µg/m³ at the AC site and 37.46 µg/m³ at the QU site were similar in the winter season with a 2.8% mass difference. However, in the summer season, there was a 27% mass difference between PM_{2.5} masses of 73.67 µg/m³ at the AC site and 100.9 µg/m³ at the QU site. Figure 3.4 shows that PM_{2.5} mass concentration at both sites tracks each other closely, suggesting relatively similar background loading. However, in summer, the period from 23 to 30 June showed a higher mass concentration at the QU site. An increase in the crustal components at the QU site caused the changes in PM_{2.5} mass between sites in late June based on the SiO₂ time series which showed a similar behaviour (Figure 3.5). The increase in the crustal components at the QU site at that time was probably caused by the effect of dust-laden wind in increasing the number of fine particles ejected from unpaved surroundings and sand stockpiles from a construction site located in proximity to the sampling site and in the same direction as the north-westerly winds (Figure 3.6). The passage of air loaded with dust over erodible surfaces containing fine materials can cause a higher number of particles leaving the surface. According to Pye, (1987), abrasion by impacting particles has been observed to be important in breaking-up sediments aggregates and releasing particles into the air-stream

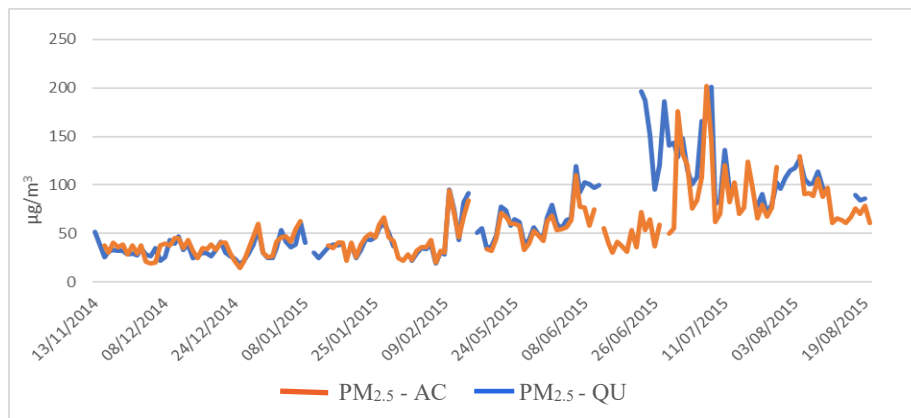


Figure 3.4 Time series of PM_{2.5} for both campaigns at the AC and QU sites

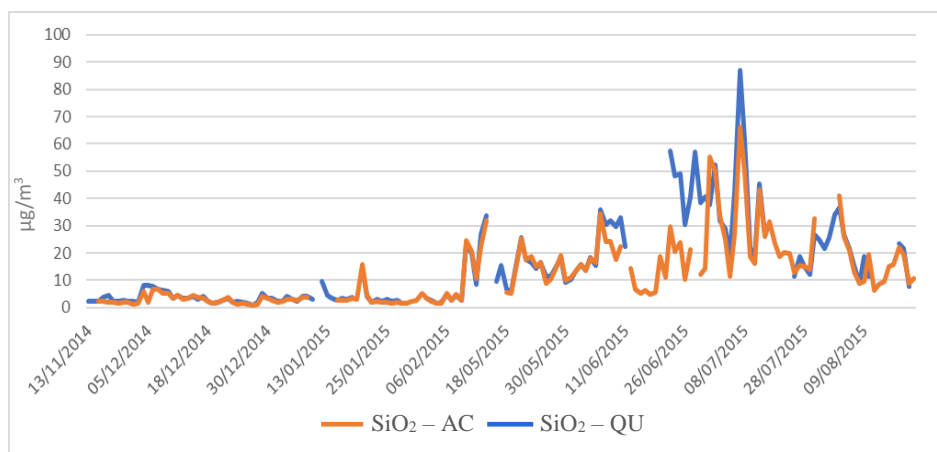


Figure 3.5 Time series of SiO₂ for both campaigns at the AC and QU sites

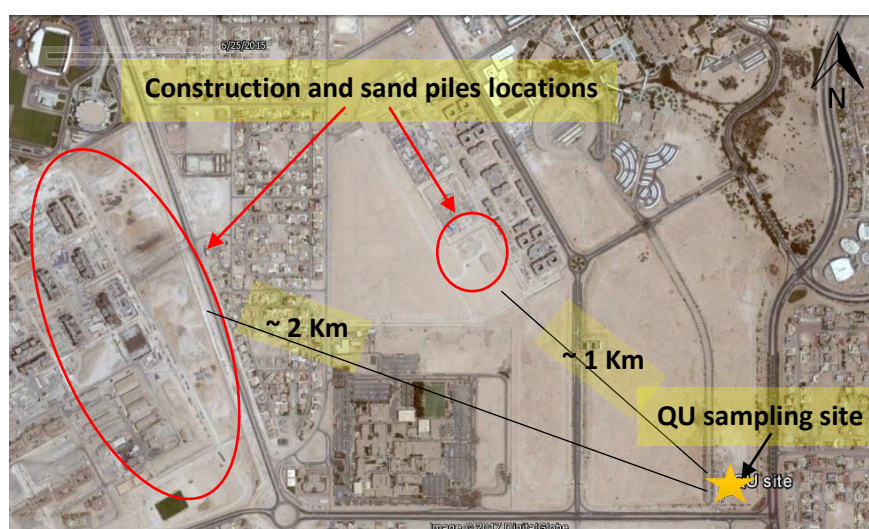


Figure 3.6 Qatar university location showing nearby construction site and sand piles

Overall, similar average mass concentrations were found for individual constituents between the AC and QU sites within the winter and summer seasons (Tables 3.3 and 3.4). On average, crustal elements, such as Si, Al, Fe, Ca, and Ti showed a higher mass concentration at the QU site, whereas sulfate and ammonium were slightly higher at the AC site. A Pearson correlation analysis was performed to investigate the relationship between individual species at the QU and AC sites (Table 3.5). Significant correlations were observed between the species at the 0.01 significance level except for potassium which showed a weak correlation at the 0.08 significance level. Major contributors to PM_{2.5} such as crustal species, sulfate and ammonium

showed a strong correlation between the sites. Salt elements (Na^+ , Cl^- , Mg^{2+}), and trace metals namely As, Cd, Pb, Ce, and Co also showed a good correlation indicating that the same sources impact both sites. OC, EC, NO_2 , Zn, Ba, Sb, Cu, and Sn elements which are primary products of traffic tailpipe emissions, brake and tyre wear, (Gillies et al. 2001; Sternbeck et al., 2002; Thorpe and Harrison., 2008; Pant and Harrison., 2013), showed moderate correlations indicating that both sites are influenced by both local and background traffic emissions.

Table 3.5 Correlation coefficient between same species at both sites

Species	Coeff. of correlation	Species	Coeff. of correlation	Species	Coeff. of correlation	Species	Coeff. of correlation
$\text{PM}_{2.5}$	0.80	NO_3^-	0.47	Ce	0.71	Ba	0.54
Al	0.91	Na^+	0.81	Zn	0.54	As	0.87
Fe	0.88	K^+	0.23	Ti	0.91	Cd	0.79
Si	0.91	Mg^{2+}	0.87	V	0.82	Sb	0.32
SO_4^{2-}	0.88	PO_4^{3-}	0.86	Cr	0.39	Sn	0.15
NH_4^+	0.77	OC	0.45	Mn	0.83	Ni	0.42
Cl^-	0.78	EC	0.67	Co	0.76	NO_2	0.51
Ca^{2+}	0.82	Cu	0.34	Pb	0.74	O_3	0.81

3.4 $\text{PM}_{2.5}$ Seasonal variation

Measurements of $\text{PM}_{2.5}$ for the two seasons were compared to see the extent of variation caused by dust events to fine particles levels and the constituents' percentage contribution. The average concentrations of individual species from both locations were in each season were plotted in figure 3.7 and 3.8 in descending order to observe the overall effect of seasonality on $\text{PM}_{2.5}$ in Doha city. In winter, sulfate concentration of $13.59 \mu\text{g}/\text{m}^3$ was the major contributor to $\text{PM}_{2.5}$ followed by ammonium $5.42 \mu\text{g}/\text{m}^3$, organic carbon $5.16 \mu\text{g}/\text{m}^3$, elemental carbon $3.95 \mu\text{g}/\text{m}^3$, and silicon oxide $3.63 \mu\text{g}/\text{m}^3$. This descending order indicates

that sulfate is the major contributor to $PM_{2.5}$ in winter followed by traffic emissions as it is the main source of organic and elemental carbon whereas crustal components come last. In the summer season, the concentration and percentage contribution changed due to the increase in dust events and the big increase in sulfate concentration at the end of July and early August. In the summer, sulfate is still the main contributor with $24 \mu\text{g}/\text{m}^3$ followed by SiO_2 with $22 \mu\text{g}/\text{m}^3$. However, the sum of all mineral metal oxides makes the crustal components the main contributor in the summer season, followed by secondary sulfate and organic and elemental carbon.

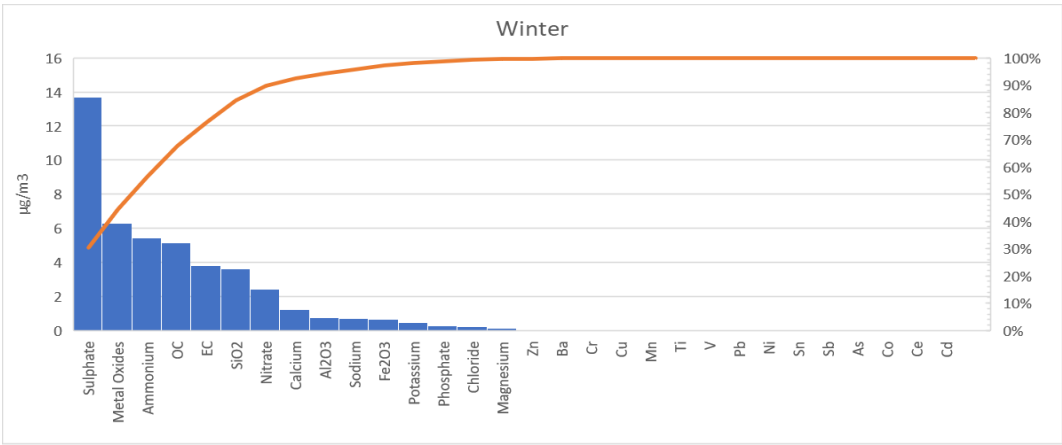


Figure 3.7 Pareto chart for the distribution of species total average mass concentration in descending order and a cumulative line of total percentage in the winter season

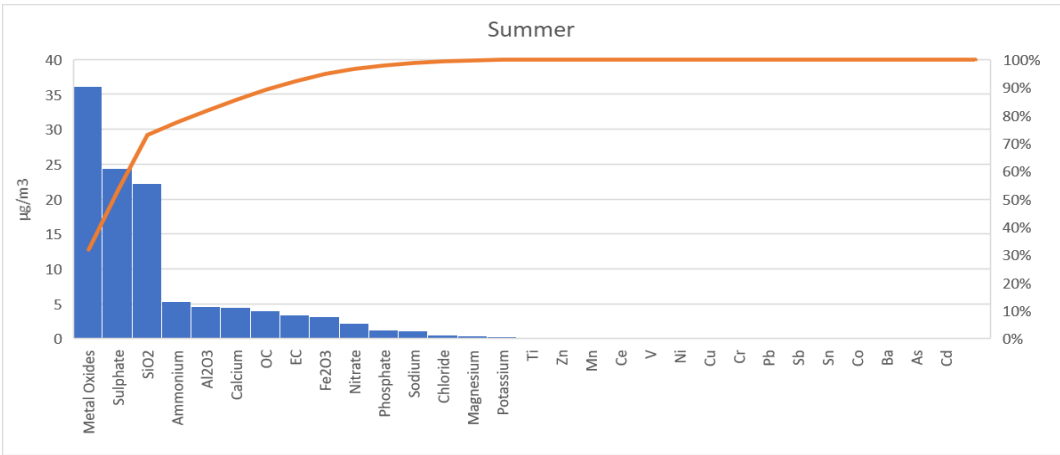


Figure 3.8 Pareto chart for the distribution of species total average mass concentration in descending order and a cumulative line of total percentage in the summer season

PM_{2.5} concentrations ranged between 14.7 and 67 µg/m³ in the winter season with mean values of 36.26 and 34.77 µg/m³ for the AC and the QU sites and between 30.25 to 383.33 µg/m³ in the summer season with mean values of 73.67 and 100.9 µg/m³ for the AC and QU sites, respectively. PM_{2.5} mass concentration increased more than twice at the AC site, and tripled at the QU site, from the winter to the summer.

The seasonality effect on PM_{2.5} mass concentration in Doha city is different than what been found in European cities. PM_{2.5} in Doha, in the summer season showed higher mass concentration in contrast to a 28 European cities study in 1993/94 (Marcazzan et al., 2001), which showed higher PM₁₀ concentration in the winter season. In Europe, the high PM₁₀ values are caused by the frequent occurrences of thermal inversion which tend to concentrate the pollutants in the lower layer of the atmosphere. While in summer, higher wind speeds and deeper mixing layer increase pollutants dispersion and decrease PM concentration. However, in Qatar, the significant factor causing PM increase in the summertime is dust events, which in addition to their direct effect on PM increase on the day of occurrences, also contributes to the high dust background levels after dust storms as it takes days to a week for PM_{2.5} to be removed from the atmosphere by dry deposition. (Wallace and Hobbs 2006).

The most significant changes in the concentration of individuals' constituents between winter and summer are the metal oxides and sulfate, which showed a large mass concentration increase. The sum of mean metal oxides (SiO₂, Al₂O₃, Fe₂O₃, CaO) concentrations increased from 6.84 µg/m³ in wintertime "excluding dust events days" to 30.77 µg/m³ in the summer season at the AC site and from 9.739 to 41.51 µg/m³ at the QU site. Sulfate, on the other hand, increased from 15.36 µg/m³ in the winter season to 25.42 µg/m³ in summer at the AC site, and from 11.8 to 23.32 µg/m³ at QU site. The sulfate increase started in late July and early August

(Figure 3.9). During this period, the prevailing wind changed its direction from north-west direction to north and north-east coming from Arabian Gulf. The high sulfate was also associated with high relative humidity. Figure 3.10 shows the frequency of counts by wind direction for sulfate conditioned by relative humidity. High sulfate concentration occurrences were more frequent at both sites when wind originated from north-east, coming from the Arabian Gulf, and it was associated with maritime air masses hence it showed an increase in relative humidity. High sulfate is likely caused by burning sulfur containing fuel from seagoing vessels and flaring activities for oil and gas extraction operations in the Arabia Gulf Sea.

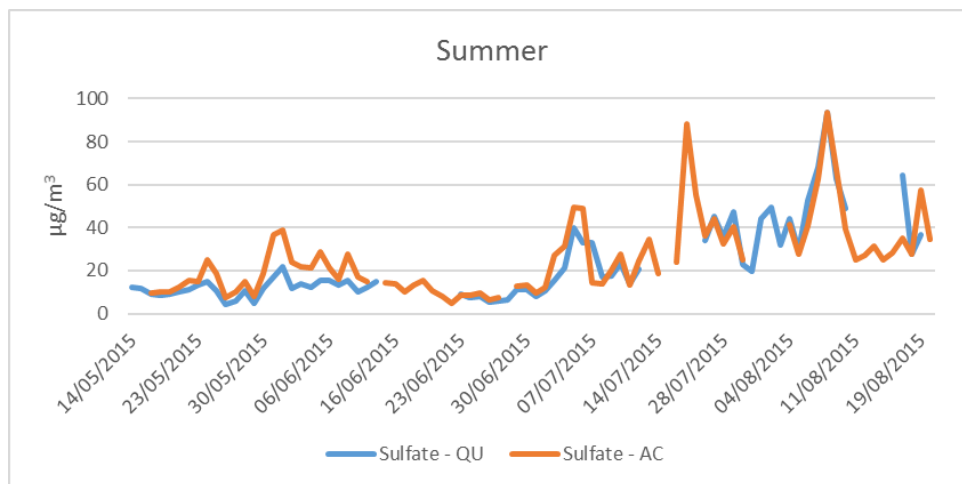


Figure 3.9 Time series of Sulfate at the AC and QU sites in the summer season

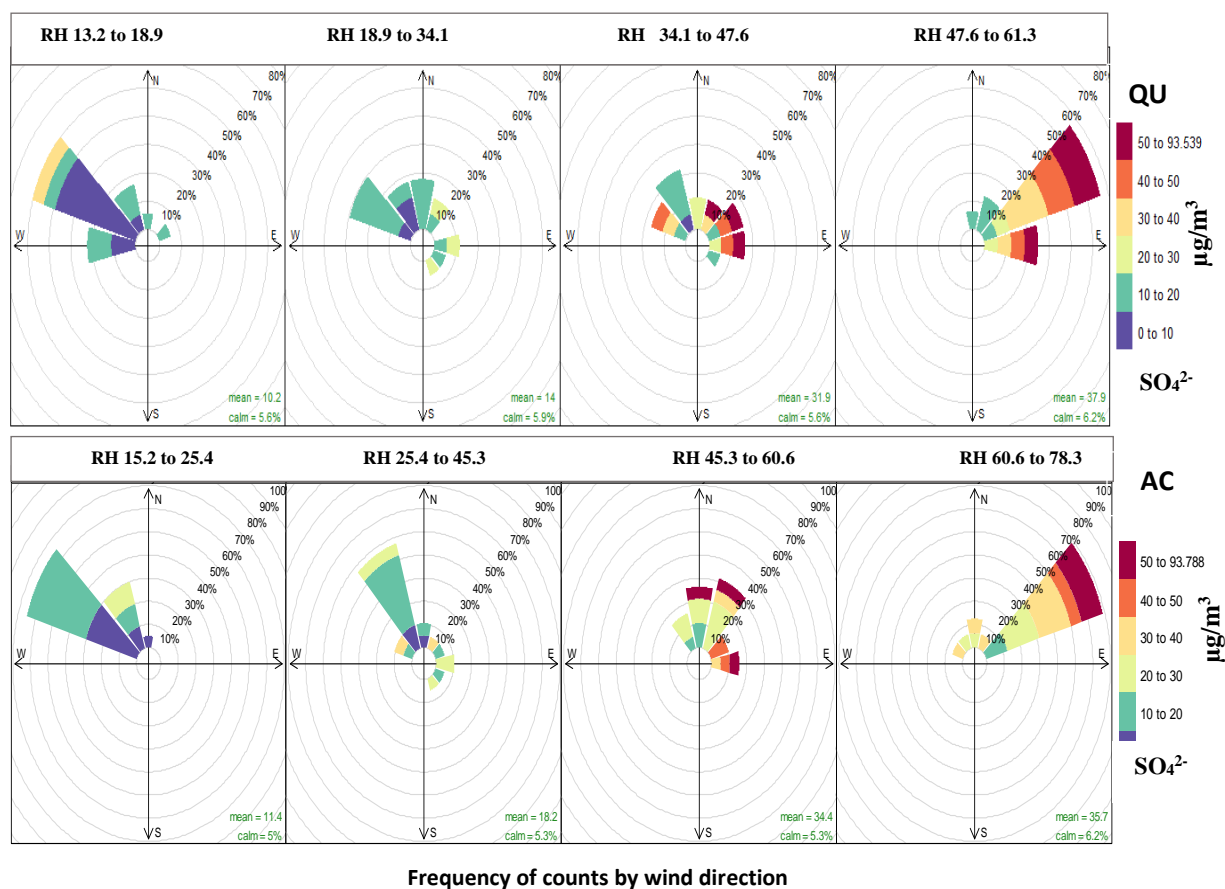


Figure 3.10 Pollution rose as a function of relative humidity in the summer season at the AC and QU sites

The increase in the crustal elements in the summer season came from the frequent occurrences of dust events. In summer, crustal mass (sum of SiO_2 , Al_2O_3 , Fe_2O_3 , CaO) increased by more than four folds compared to the winter season. On average, the QU site had a higher crustal contribution due to the contribution from the unpaved surrounding local to the site. Figure 3.11 shows silicon oxide peaking in late June and July, while the pollution rose indicates that the high metal oxides occurs when the wind is coming from the NW (figure 3.12), which is the prevailing wind direction in Qatar due to the Al-Shamal dust storm in the summer season.

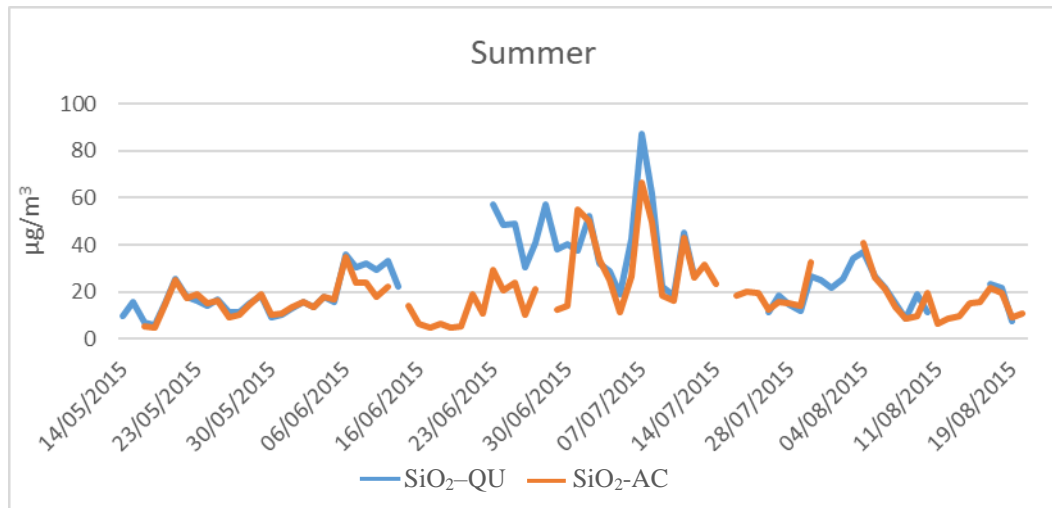


Figure 3.11 Time series of SiO₂ at the AC and QU sites in the summer season

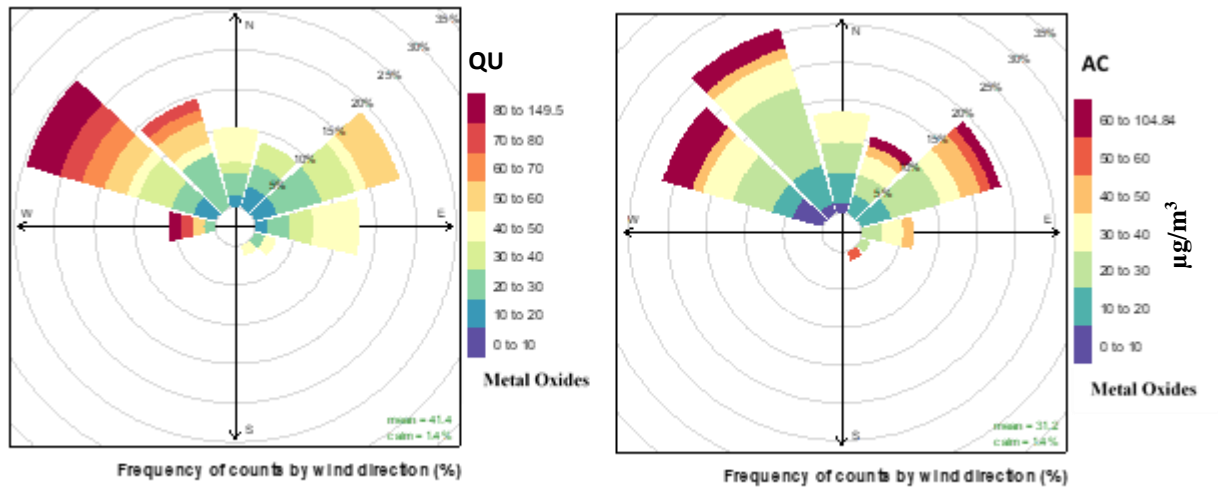


Figure 3.12 Pollution rose of metal oxides by wind direction at the AC and QU sites in the summer season

3.5PM_{2.5} Levels and Air Quality Index

The WHO air quality guideline (AQG) for PM_{2.5} daily concentration is 25 µg/m³. Besides the guideline value, three interim targets (IT) are defined for PM_{2.5} daily mean namely IT-1=75 µg/m³, IT-2=50 µg/m³, and IT-3=27.5 µg/m³. Based on published risk coefficients from multicentre studies and meta-analyses (WHO 2005), PM_{2.5} at the interim levels is responsible

for 5%, 2.5% and 1.2% increases in short-term mortality over the AQGs value respectively. These interim targets were established to be used by countries to progressively achieve the WHO target of $25 \mu\text{g}/\text{m}^3$ with successor abatement measures. According to the WHO (2005), PM_{10} guideline values are based on studies that use $\text{PM}_{2.5}$ as an indicator. Then, PM_{10} corresponding values are calculated by applying a $\text{PM}_{2.5}/\text{PM}_{10}$ ratio of 0.5 which is a typical ratio for $\text{PM}_{2.5}/\text{PM}_{10}$ for urban cities in developing countries and is at the bottom of the range found in urban cities in developed countries (0.5–0.8)(WHO, 2005). Because Qatar's environmental law only legislates PM_{10} , a $\text{PM}_{2.5}$ standard was calculated using the 0.5 ratio, giving a $\text{PM}_{2.5}$ value of $75 \mu\text{g}/\text{m}^3$ for the corresponding value of $150 \mu\text{g}/\text{m}^3$ for Qatar guideline daily PM_{10} . Hence it was used for the comparison. Figure 3.13 shows the time series of $\text{PM}_{2.5}$ concentration in the winter and the summer seasons with the daily $\text{PM}_{2.5}$ guideline of $75 \mu\text{g}/\text{m}^3$ included as a line. In the winter season, all the daily values complied with $\text{PM}_{2.5}$ daily standard except on the last few days of sampling on 10th, 11th, 13th, and 14th of February, when the spring dust events started in Qatar. In the summer season however, with the rising number of dust events, a 68% of the QU values and 34% of the AC values in July and August were above the $75 \mu\text{g}/\text{m}^3$ target, which emphasises the role of natural sources in exceeding particulate matter guidelines.

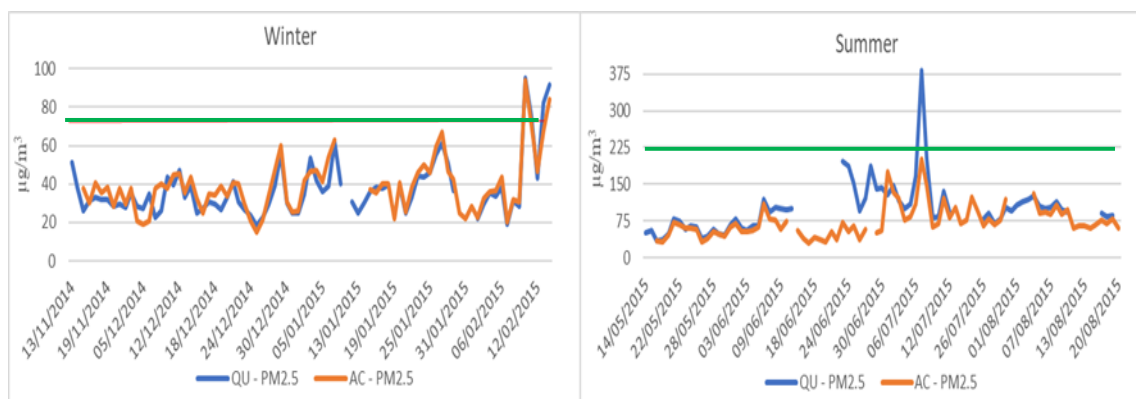


Figure 3.13 Time series of $\text{PM}_{2.5}$ daily in the winter and the summer seasons; the green line shows interim target (IT-1= $75 \mu\text{g}/\text{m}^3$)

Air quality index (AQI) scores were also used to assess the seasonal changes in Doha air quality. The AQI is a rating scale for reporting the ambient air pollution recorded at monitoring sites on a particular timescale. The higher the AQI value is, the greater the level of air pollution and the dangers to human health. The main objectives of AQI are to advise the public about the exposure risk to daily pollution levels and to impose required regulatory actions for immediate local impact (Stieb et al., 2005; Gurjar et al., 2008). The EPA's (2013) AQI was used to calculate daily AQI in both seasons. The index involves seven categories from good to hazardous. Daily PM_{2.5} data were scaled using the breakpoints shown in Figure 3.14 and the number of days in each of the category is presented in Figure 3.15 for the winter and summer seasons. In winter, the air quality for most of the days was in the moderate and unhealthy for sensitive groups categories. Few days were found in the unhealthy category. However, these points were associated with four dust events that occurred at the end of the sampling campaign. In the summer, most of the days were in the unhealthy category, which caused by the elevated crustal components from the frequent dust events and the increase in sulfate concentrations in August.

AQI Category	Index Values	Revised Breakpoints ($\mu\text{g}/\text{m}^3$, 24-hour average)
Good	0 - 50	0.0 – 12.0
Moderate	51 - 100	12.1 – 35.4
Unhealthy for Sensitive Groups	101 - 150	35.5 – 55.4
Unhealthy	151 - 200	55.5 – 150.4
Very Unhealthy	201 - 300	150.5 – 250.4
Hazardous	301 - 400	250.5 – 350.4
Hazardous	401 - 500	350.5 – 500

Figure 3.14 PM_{2.5} air quality index (AQI) breaking points (Source: AQICN, 2017)

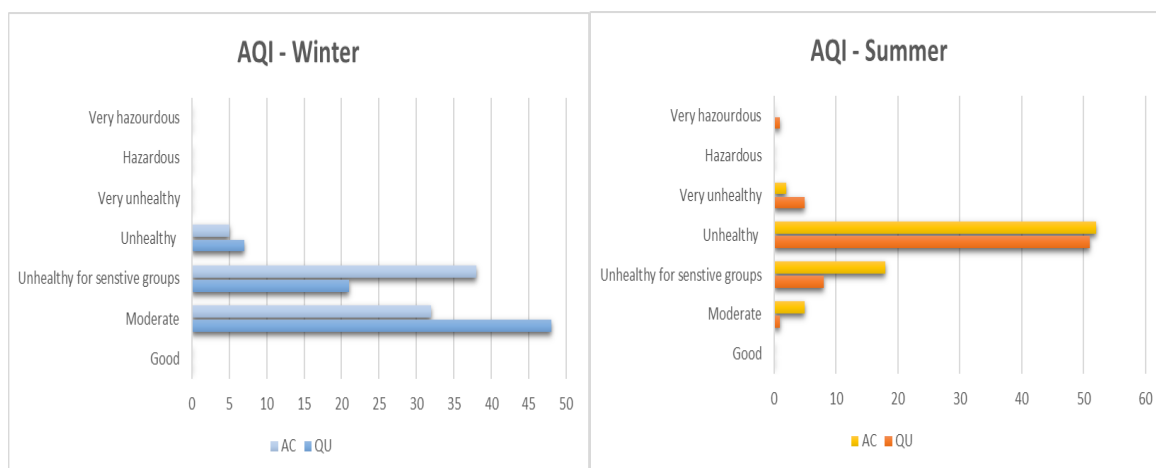


Figure 3.15 PM_{2.5} air quality category in the winter and summer at both sites

As for trace metals levels, the European Union has developed a 1-year air quality limit value of 0.5 µg/m³ for Pb in 2004 and 6, 5, and 20 ng/m³ for arsenic, cadmium, and nickel in 2008 respectively (Guerreiro et al., 2014). The four-month averages for the metals mentioned above in both seasons were compared to these annual limit values, and none of them exceeds the annual limit value in Doha.

3.6 Ion Mass Balance and the Changes in Aerosol Acidity through the Seasons

Ion mass balance calculations are commonly used to evaluate the acid–base balance of aerosol particles (Z. Shen et al., 2009). Ions mass concentration were converted to molar-equivalents by dividing their mass by (the molecular weight/ oxidation number). The cations and anions were calculated as follows:

- Cation molar-equivalent (C) = $\text{NH}_4^+/18 + \text{Ca}^{2+}/20 + \text{Mg}^{2+}/12 + \text{Na}^+/23 + \text{K}^+/39$
- Anion molar-equivalent (A) = $\text{SO}_4^{2-}/48 + \text{NO}_3^-/62 + \text{PO}_4^{3-}/31.6 + \text{Cl}^-/35.5$

Anion and cations include species that are soluble in water such as salts, acidic and alkaline compounds. A perfect balance means analysing all the ionic species found in the samples, but this is not achievable for H⁺, OH⁻, CO₃²⁻ and HCO₃⁻ owing to practical analytical limitations.

The comparison result between anions and cations will be either acidic PM_{2.5} if there are more anions than cations, hence the cation loss may be attributed to H⁺ absence, or alkaline PM_{2.5} if there is a lower concentration of anions than cations owing to CO₃²⁻ and HCO₃⁻ absence.

3.6.1 Ion Mass Balance during the Winter Season

At the AC site, PM_{2.5} ion masses were in the following order SO₄²⁻ > NH₄⁺ > NO₃⁻ > Na⁺ > K⁺ > Ca²⁺ > Cl⁻ > Mg²⁺ > PO₄³⁻. The average anion-cation ratio (A/C) was 0.84, and the position of regression line below the unity line (Figure 3.16) indicates that PM_{2.5} is alkaline. The fact that the samples show more cation to anion fraction indicates that the ratio difference is caused by the absence of CO₃²⁻ and OH⁻ measurements.

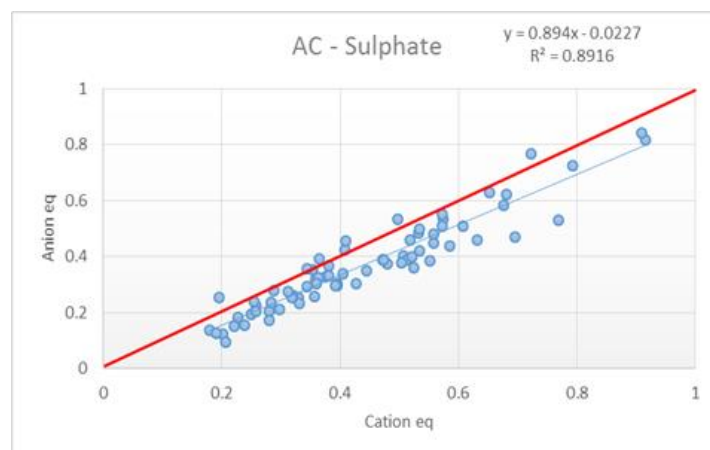


Figure 3.16 Relationship between cations (x-axis) and anions (y-axis) in meq/l in the winter season at the AC site (Unity line in red colour)

The ratio of 0.84 at AC site is within the range of 0.8 for storm days, and 0.9 for normal days that was found in China for PM_{2.5} (Shen et al., 2009). The lower A/C ratio during dust storms according to (Zhang et al., 2002; Shen et al., 2009) is caused by the buffering action of mineral dust on acidic samples.

At the QU site, PM_{2.5} ion masses were in the following order $\text{SO}_4^{2-} > \text{NH}_4^+ > \text{NO}_3^- > \text{Ca}^{2+} > \text{Na}^+ > \text{K}^+ > \text{Mg}^{2+} > \text{Cl}^- > \text{PO}_4^{3-}$. The ions order was different at the QU site for Ca^{2+} , as it showed a higher ranking than at the AC site because of the contribution of CaCO_3 and CaSO_4 from the QU site surrounding areas, as both compounds are common in Qatar crust. The A/C ratio at the QU was 0.8, indicating that PM_{2.5} is more basic at the QU site than at the AC site.

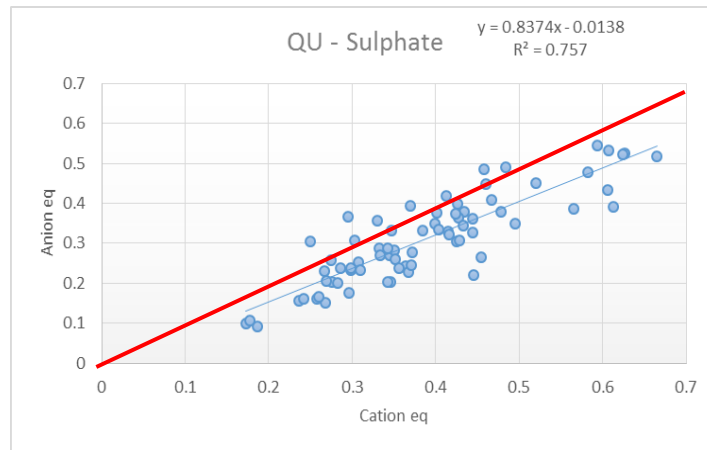


Figure 3.17 Relationship between cations (x-axis) and anions (y-axis) in meq/l in the winter season at the QU site respectively (Unity line in red colour)

3.6.2 Ion Mass Balance During the Summer Season

In summer, PM_{2.5} ion mass concentrations were in the following order $\text{SO}_4^{2-} > \text{NH}_4^+ > \text{Ca}^{2+} > \text{NO}_3^- > \text{Na}^+ > \text{K}^+ > \text{Cl}^- > \text{Mg}^{2+} > \text{PO}_4^{3-}$ at AC site and in the order $\text{SO}_4^{2-} > \text{Ca}^{2+} > \text{NH}_4^+ > \text{NO}_3^- > \text{Na}^+ > \text{Cl}^- > \text{Mg}^{2+} > \text{K}^+ > \text{PO}_4^{3-}$ at QU site. Frequent dust storm in the summer season are expected to increase mineral species including calcium concentrations which could change the order of the ions between seasons especially at the QU site due to calcium contribution from local surroundings. The A/C average ratios were 0.87 at the AC site and 0.86 at the QU site.

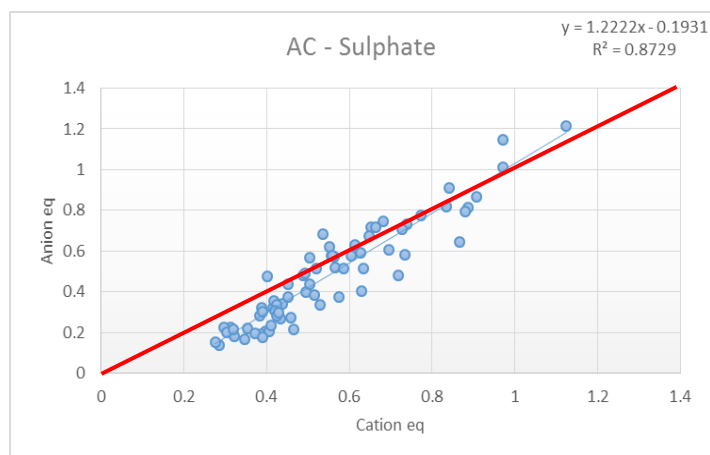


Figure 3.18 Relationship between cations (x-axis) and anions (y-axis) in meq/l in the summer season at the AC site respectively (Unity line in red)

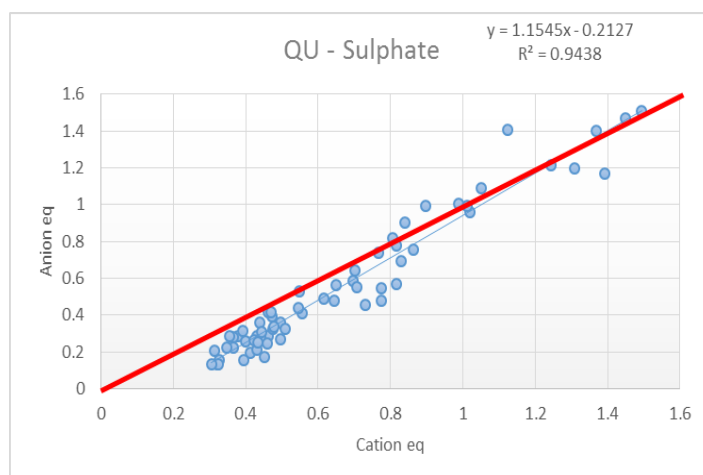


Figure 3.19 Relationship between cations (x-axis) and anions (y-axis) in meq/l in the summer season at the QU site respectively (Unity line in red)

Figures 3.18 and 3.19 show that some of the points lie on the unity line, indicating neutral $PM_{2.5}$, whereas the other points below the unity line indicate alkaline $PM_{2.5}$ samples. Similar behaviour was found in China for $PM_{2.5}$ where some of the points lie above the unity line and some beneath it (Shen et al., 2009). This behaviour was attributed to different types of pollution episodes related to dust storm days and normal days for low (A/C) ratio, and to biomass burning and haze from anthropogenic sources for neutral (A/C) ratio. The ion balance behaviour in summer was also caused by different type of pollution episodes. Neutral $PM_{2.5}$ at

the high end of the regression line is caused by the big increase in sulfate concentration in late July and August (Figure 3.7). Sulfate increase from that period are probably in sulfuric acid form because if the sulfate was in salt form, such as $(\text{NH}_4)_2\text{SO}_4$ or CaSO_4 , then the points should be below the unity line since SO_4^{2-} , NH_4^+ , and Ca^{2+} are all included in the comparison, however the carbonate is not included. Therefore, the neutral points were probably caused by a combination of unmeasured cation H^+ and anion CO_3^{2-} species. $\text{PM}_{2.5}$ aerosols were more basic in the winter season, and the regression lines at both locations were below the unity line, which indicates a deficiency in the anion fraction. The anion deficiency in the winter is likely related to the absence of carbonate analysis since CaCO_3 is a component of Qatar's crust. In the summer season, most of the points were on the unity line or below the line. The average anion fraction was still lower than cation fraction, which indicates carbonate deficiency.

3.7 Metals Enrichment Factor (EF)

An enrichment factor (EF) approach was used to estimate metal enrichment in airborne particles by comparing metals to a reference metal concentration for the upper continental crust (Taylor and McLennan, 1995, Mason 1966). EF is calculated using the following equation:

$$\text{Enrichment Factor (X)} = \left(\frac{\frac{\text{Concentration (x)Sample}}{\text{Concentration (Reference)Sample}}}{\frac{\text{Concentration (x)Crustal}}{\text{Concentration (Reference)Crustal}}} \right) \quad (3)$$

where (X) is the concentration of species in the sample/earth's crust concentration; and (Reference) is Al concentration in the sample/earth's crust. Due to the insignificance of the input of Al from anthropogenic sources, it is usually used as a reference-normalising crustal

element to calculate enrichment factor. Elements with EF values close to 1 are consistent with strong crustal component (Furuta et al., 2005) while elements with EF values equal to or higher than 10 are strongly suggesting a contribution of anthropogenic sources (Chester et al., 1999).

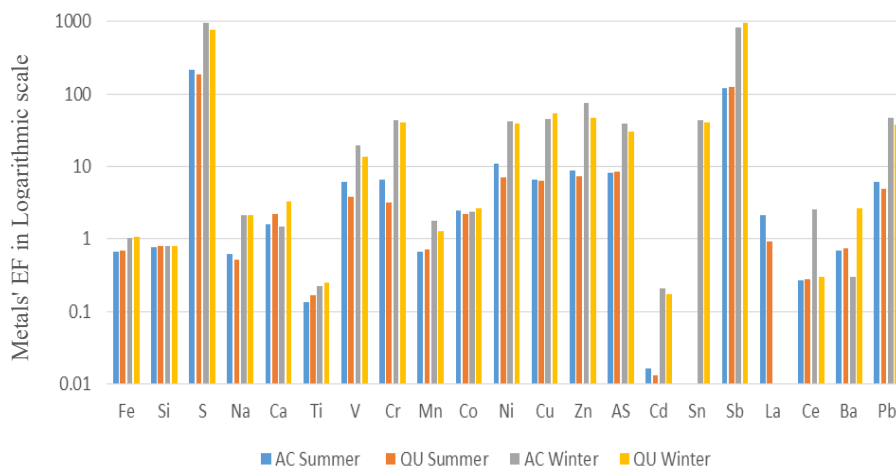


Figure 3.20 EF for PM_{2.5} constituents at both sites and seasons.

The EFs of metals in Doha have a seasonal variation, with trace metal EFs higher in the winter season (Figure 3.20). According to Chester et al., (1999) when sufficient crustal material is present in the air, the enriched elements can display EF values of non-enriched elements. This phenomenon is clear in Qatar. During the summer, the frequency of dust storms and dust haze events increases causing an increase in crustal metal concentrations in the atmosphere. Thus, comparing the concentration of trace metals contributed by anthropogenic sources to a crustal reference element which is enriched by dust events will cause an underestimation of the EF.

The elements S, V, Ni, Cr, Cu, Zn, As, Sn, Sb, and Pb have EF values above 10 in the winter season indicating a contribution from anthropogenic sources. The highest EFs observed were for S and Sb (~1000). Enriched elements ≥ 10 were separated into three groups based on the

correlation between their mass concentrations. In the first group, sulfur was strongly correlated with NH_4^+ ($r=0.7$, $p<0.01$) at the AC site and ($r=0.84$, $p<0.01$) at the QU site for the whole data set, indicating secondary sulfate aerosols which are likely associated with the combustion of fossil fuel containing sulfur. In the second group, Sb was correlated mainly with EC ($r= 0.50$, $p<0.01$), OC ($r=0.47$, $p<0.01$); Cu ($r=0.62$, $p<0.01$); and Sn ($r= 0.40$, $p<0.01$) at the AC site and with EC ($r= 0.52$, $p<0.01$), OC ($r=0.43$, $p<0.01$); Sn ($r=0.72$, $p<0.01$); Cu($r=0.45$); Zn ($r= 0.39$, $p<0.01$) at the QU site indicating contribution from traffic source related to exhaust emissions, brake dust, and tyre wear (Furuta et al. 2005; Pant, 2014). The third group includes Ni, V, and Cr. The Ni and V elements are inorganic markers for gasoline engine exhaust (Song et al. 2001), whereas Cr and Ni are related to heavy fuel oil combustion (Huggins et al. 2000). The element Ni was moderately associated with V ($r=0.46$, $p<0.01$) and Cr ($r=0.62$, $p<0.01$) at the AC site and with V ($r=0.36$, $p<0.01$) and Cr ($r = 0.76$, $p<0.01$) at the QU site. The contribution from heavy fuel oil in Doha city is likely to be emitted from vessels emissions in Doha port and from onshore and offshore flaring activities.

3.8 The Effect of Wind Speed on $\text{PM}_{2.5}$ Mass Concentration

Wind speed exerts an important control over PM concentrations (Harrison et al. 2001). Fine particles largely arise from high-temperature combustion sources and through the gas to particles conversion process, and they are mainly composed of ammonium sulfate and nitrate salts in addition to organic and elemental carbon (Harrison et al. 2001). On the other hand, the coarse fraction of PM arises from erosion, and mechanical disruption thus is essentially composed of street dust, dust haze/storms and fugitive dust from construction sites and unpaved areas. According to Harrison et al. (2001), the resultant curve from plotting fine particle abundance with average wind speed shows a dilution process, in which the $\text{PM}_{2.5}$ concentration decreases with the increasing wind speed. Whereas the coarse component of

PM shows a U-shaped relationship which indicates that it has two components, one decreases in abundance with wind speed, while the other one increases in abundance due to wind resuspension and erosion of soil. To investigate the impact of seasonality on the relationship between wind speed and particles abundance; the PM_{2.5} relation with wind speed was separated by season.

3.8.1 The Effect of Wind Speed on PM_{2.5} Mass Concentrations in the Winter Season

Generally, windy conditions are highly associated with dilution effects (Pateraki et al., 2012). Figures 3.21 and 3.22 show the variation of PM_{2.5} with wind speed in the winter season, conditioned by relative humidity and atmospheric pressure. PM_{2.5} concentration showed a significant ($p < 0.01$) decline with increasing wind speed at both sites after removing four dust storm events.

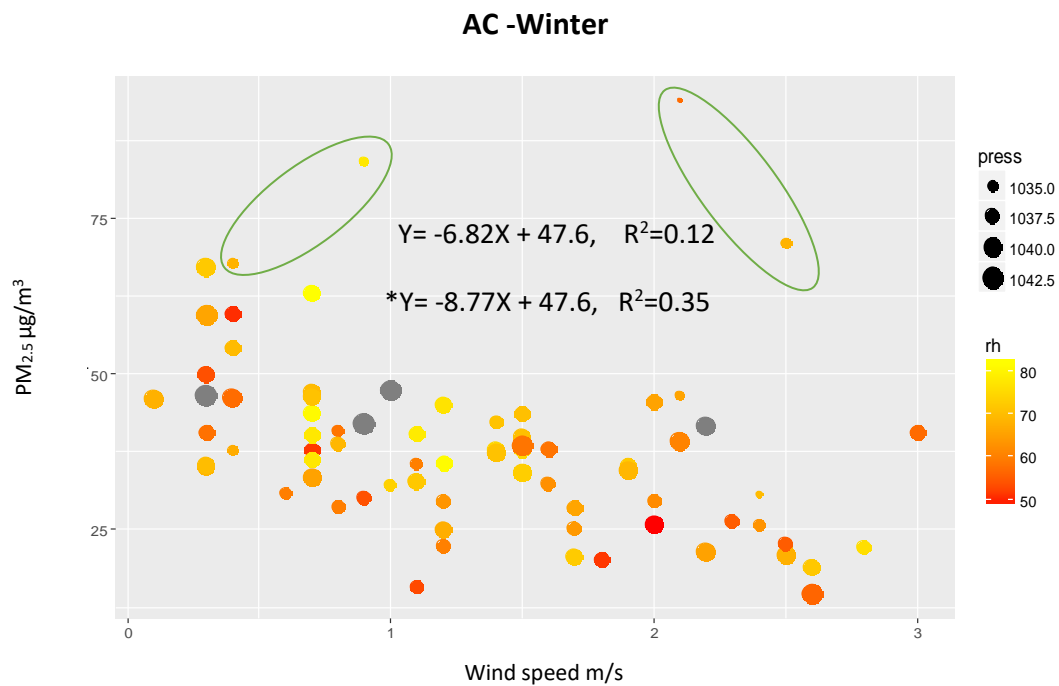


Figure 3.21 Relationship between PM_{2.5} and wind speed at the AC site in the winter season. The points inside the green circle represent the dust storm events. Y and *Y equations represent PM_{2.5} points including dust events and PM_{2.5} excluding dust events respectively.

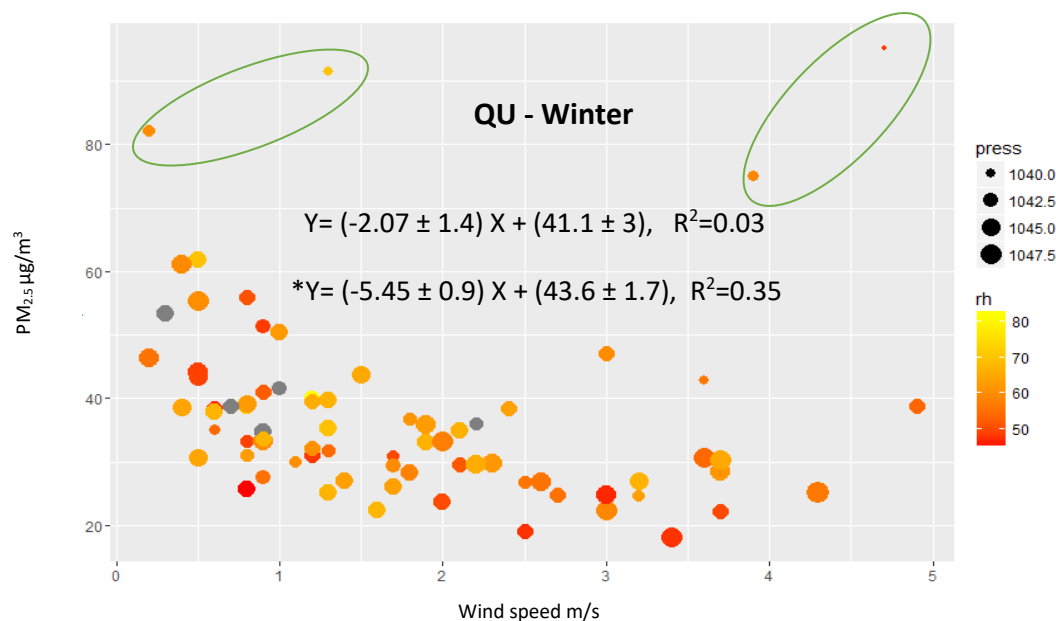


Figure 3.22 Relationship between PM_{2.5} and wind speed at the QU site in the winter season. The points inside the green circle represent the dust storm events. Y and *Y equations represent PM_{2.5} points including dust events and PM_{2.5} excluding dust events respectively.

In the winter season, four consecutive days of dust events which are presented in the green circles in figures 3.21 and 3.22, which occurred at the end of the sampling campaign; in which two of the dust events days occurred at low wind speeds and the other two at high wind speed.

To investigate the origins of the dust events and why they occurred at different wind speeds, a back trajectory analysis was performed. The results in Figure 3.23 show that for all four days, the wind came from the Arabian Sea direction, and it passed over a region of sand dunes just before entering Qatar (Figure 3.24), which could cause the wind to drag, lift, and transport particles from this region to Qatar. Figure 3.23 shows that on all four days, wind arrived from the south-east. The decline in wind velocity for the last two dust events may have been due to the wind coming from a reduced height of 1,000 m to 500 m (Figure 3.23) above ground level, which increased the wind friction.

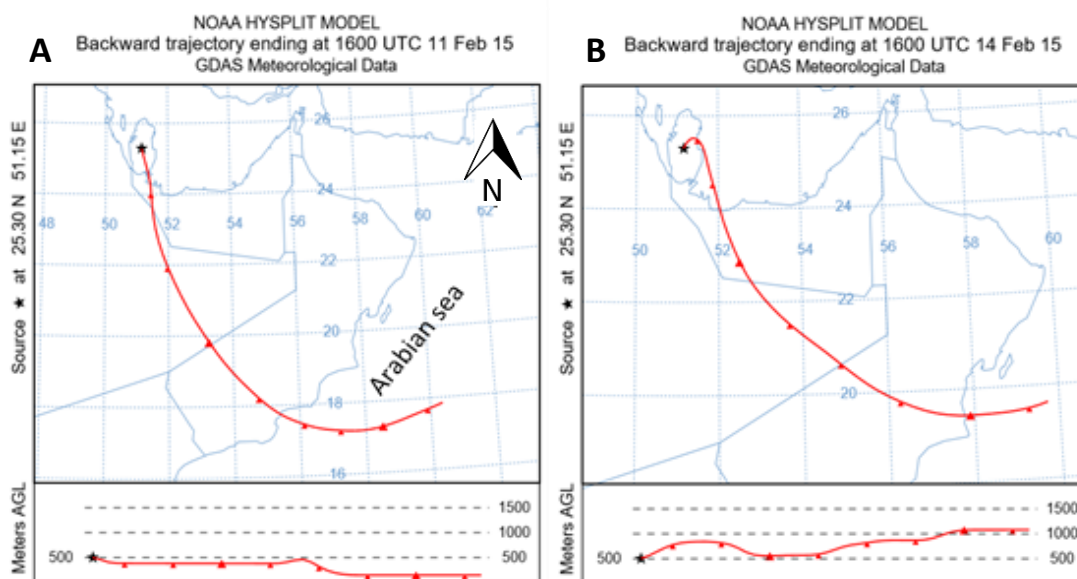


Figure 3.23 Back trajectory showing air mass route for A) 11th of Feb 2015 when wind arrived at high speed and B)- 14th of Feb 2015 when wind arrived at low speed.



Figure 3.24 The Arabian Peninsula showing sand dunes area

3.8.2 The Effect of Wind Speed on PM_{2.5} Mass Concentrations in the Summer Season

In the summer season, no linear relationship between PM_{2.5} abundance and wind speed was found (statistically insignificant, $p > 0.1$) and the form of the relationship was complicated.

Figure 3.25 shows a scattered distribution of PM levels with windspeed.

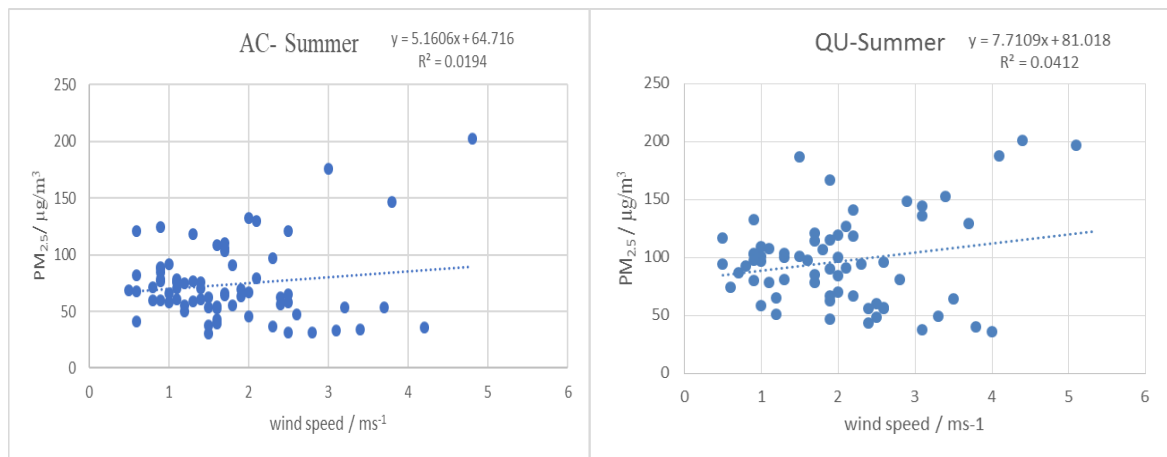


Figure 3.25 The relationship between PM_{2.5} mass concentration against wind speed at the AC and QU sites in the summer season.

To investigate potential the effect of meteorology on particles abundance, a scatter plot using ggplot2 package has performed for both sites. The ggplot2 is a statistical package for graphics and visualization of statistical data which breaks up graphs into semantic components such as scales and layers (Wickham, 2017). Figure 3.26 shows the variation of PM_{2.5} mass concentration with wind speed conditioned by relative humidity (RH) and by atmospheric pressure (AP).

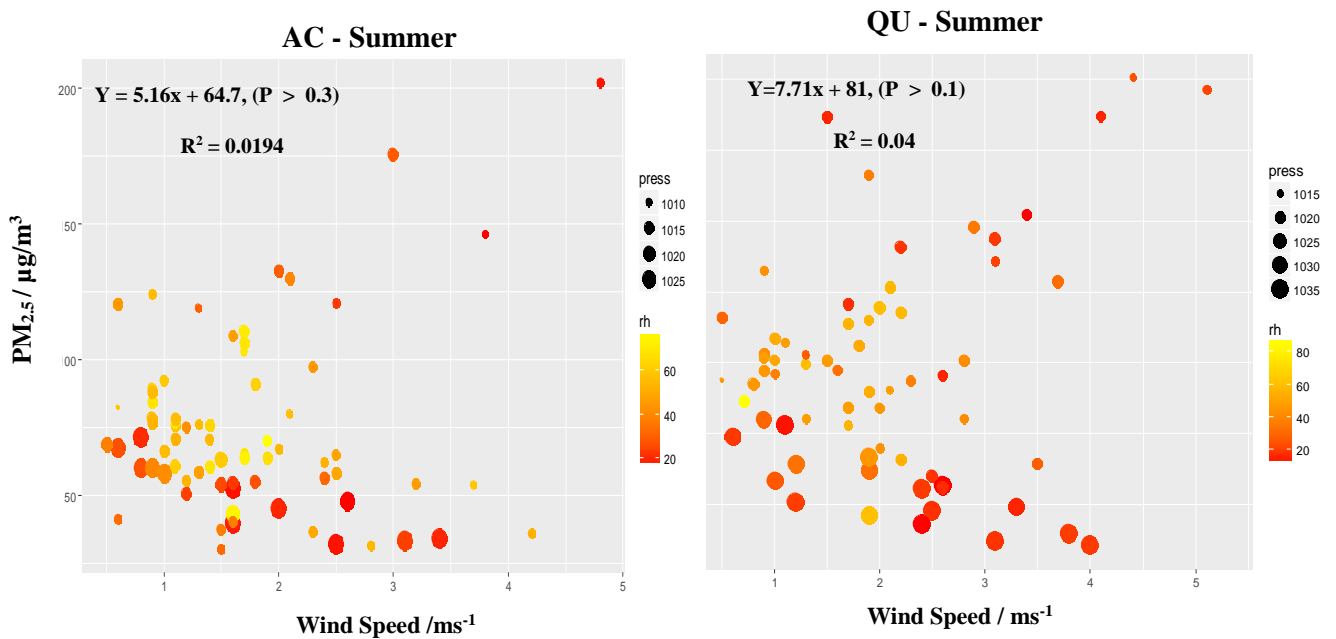


Figure 3.26 Scatter plot for PM_{2.5} mass against wind speed colored by RH and sized by the level of AP at the AC and QU sites in the summer season.

Trends at both sites showed a declining effect for points with high AP (large dots). However, points with low AP (small dots) showed both low and high PM_{2.5} values with increasing wind velocity. In the summer season, the AP showed a declining trend from May toward August which seems to have an impact on the relationship between PM_{2.5} abundance and wind speed with time. Therefore, the data was divided into two periods 1) high AP from May to late June, and 2) low AP from late June to August. Figure 3.27 present PM_{2.5} abundance at low AP showing a significant increase with wind speed at both sites.

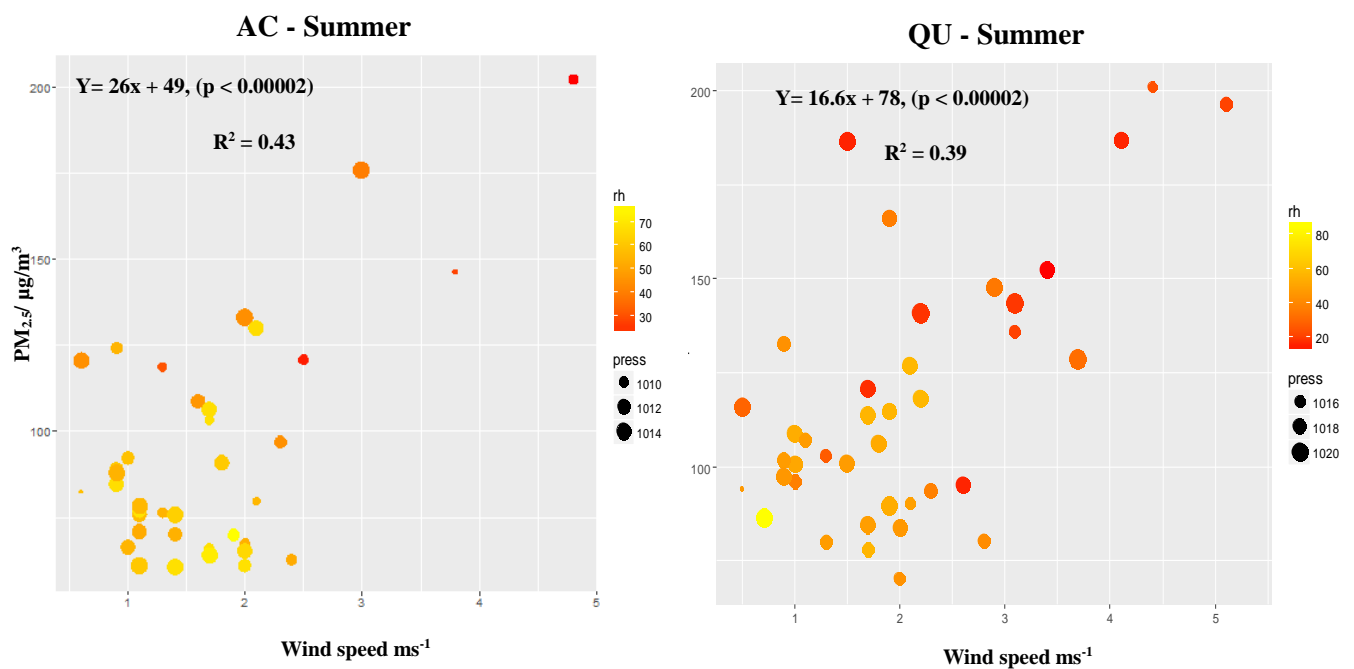


Figure 3.27 Scatter plot for PM_{2.5} mass against wind speed at the AC and QU sites at low atmospheric pressure.

In the summer season with increasing ambient temperature, the warm air which heated by contact with the surface in daytime ascends leading to low pressure at the surface (Met-office, 2017). In drylands, dust haze can occur when dust particles are raised by wind from the ground surface (NCMS, 2011) or by transport of dust through pressure gradients. According to Pye (1987) in the Middle East region in the summer season, the north-westerly wind

namely Al-Shamal sweeps dust from prevailing high-pressure areas in Iraq and Kuwait to low-pressure areas across the Arabian Gulf and over Qatar.

The effect of relative humidity appears in figure 3.27, as PM abundance shows higher abundance with low RH. These points represent days when wind arrived from north-west indicating that the air masses spent more time above terrain as they arrived from a far side of the coast. Thus they are low in RH, carry more dust burden from moving over arid areas, and they have more force in eroding crustal components through ballistic impactation. According to (Pye, 1987) abrasion by impacting particles is important in breaking up soil aggregates and releasing fine particles into the airstream. As a result, particle concentration increased with increasing wind speeds under low RH conditions. Conversely, at high AP, PM2.5 abundance systematically decreased with increasing wind velocity (Figure 3.28) apart from one dust storm episode on the 6th of June arriving from southeast direction (Figure 3.29). At high AP, dust supply arriving to Qatar by pressure gradient differences stopped therefore wind speed had a dispersion effect on the suspended particles.

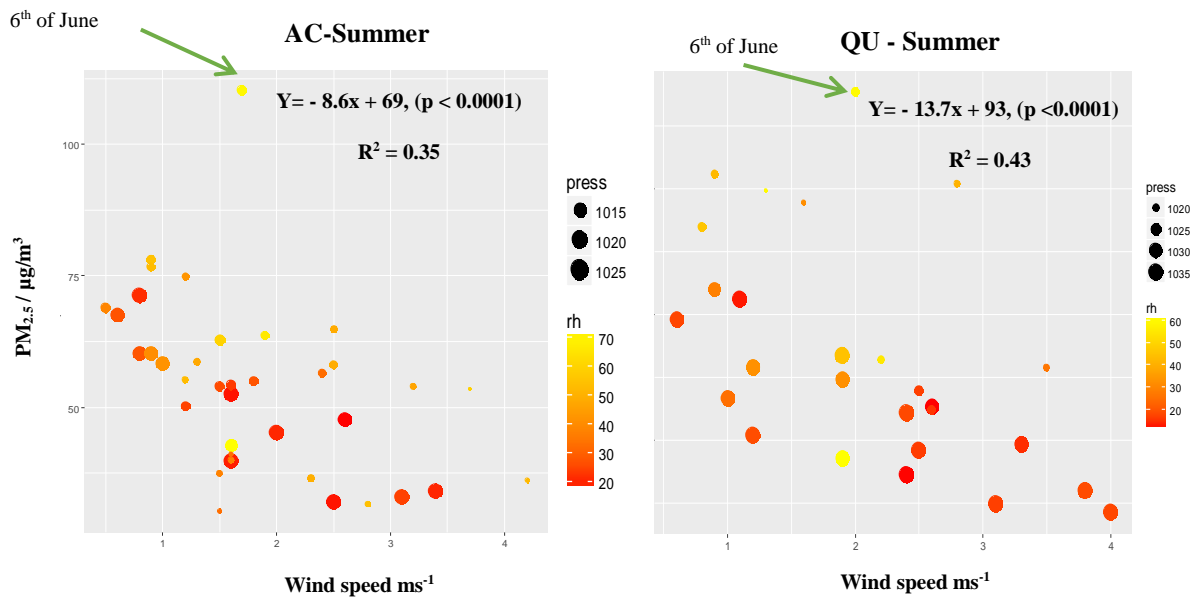


Figure 3.28 Scatter plot for PM_{2.5} mass against wind speed at the AC and QU sites during high AP. The value on the 6th of June was excluded from the correlation equation.

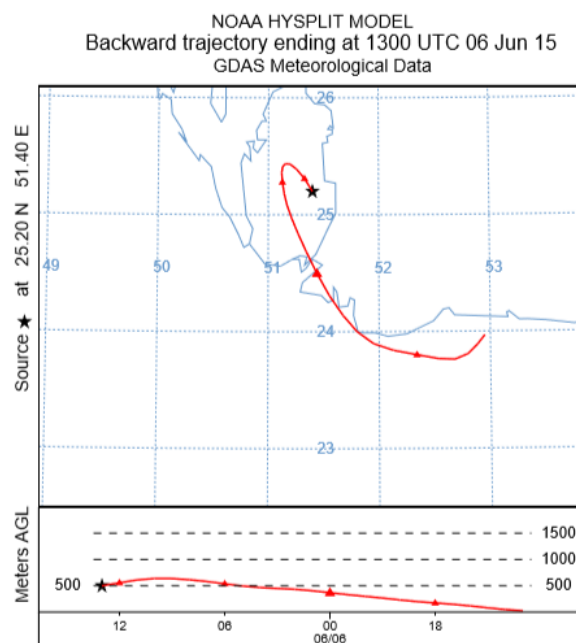


Figure 3.29 Back trajectory on the 6th of June 2015

3.9 Summary

PM_{2.5} levels were similar at both sites except for a short period during dust events in the summer season when the QU site showed a higher mass concentration as a result of dust-laden wind action in eroding loose particles from the unpaved backgrounds and sand stockpiles at a construction site in proximity to the QU sampling site. The spatial similarity between PM_{2.5} levels is caused by the regional similarity of major contributors such as secondary sulfate in the winter season and crustal materials and secondary sulfate in the summer season as they showed significant correlations at both sites. Conversely, constituents related to traffic emissions such as OC, EC, Cu, Sb, and Zn showed moderate correlations between sites, suggesting that each location is affected by contrasting local traffic emissions.

The seasonal variation appeared as a big increase in crustal materials caused by frequent dust events in the summer season in addition to sulfate increments from late July onwards, most likely caused by sulfate contributions from vessels emissions in the Arabian Gulf when the prevailing wind changed its direction from the north-west to the north-east. High PM_{2.5} levels

in the summer season impact air quality in Doha and the number of unhealthy days increased from 4 days in winter, also caused by dust events, to more than 50 days in the summer season.

Air masses origins and meteorological parameters have an important control over PM_{2.5} concentration. Low atmospheric pressure is the main factor of Al-Shamal dust events in Qatar in the summer season (Pye, 1987). Air masses moving from high to low atmospheric pressure areas, the speed of moving, and origins are what determine the air masses' burden of particles and water vapour content and their influence in suspending or dispersing atmospheric particles.

CHAPTER 4: MASS CLOSURE

4.1 Introduction

Chemical mass closure is a useful tool to validate and address uncertainty among gravimetric mass and chemical measurements (Chow et al., 2015). It also gives a comprehensive picture of how much each of the chemical components is contributing to particles' mass. The mass closure is a simple mass balance model that attempts to reach closure between the total gravimetric mass, and the particulate reconstructed mass obtained from the sum of measured major components (Chow et al., 2015). The reconstructed mass is obtained by summing up a small number of individual chemical components which are measured in the samples, and corrected by a conversion factor based on the ratio of molecular weight of elements associated with each of the assumed constituents, in order to estimate the unmeasured species such as the oxygen and hydrogen molecules (Joseph et al., 2012, Chow et al., 2015). Major particulate matter components that are typically used to explain gravimetric mass include (1) minerals (e.g., Fe, Al, and Si); (2) inorganic ions (e.g., SO_4^{2-} , Cl^- , NO_3^- , Na^+ , Ca^{2+} , and NH_4^+); and (3) organic and elemental carbon.

4.2 Mass Reconstruction Method

The reconstruction method used in this work was based on the study of Chow et al. (1996). In this method; Chow et al., (1996) summed six chemical components, including inorganic ions (SO_4^{2-} , NO_3^- , and NH_4^+) + sea salt (Na^+ and Cl^-) + elemental carbon (EC) + organic carbon (1.4OC) + geological minerals (1.89Al, 2.14Si, 1.4 Ca^{2+} , and 1.43Fe) + trace elements. The same approach was used in this study with some modifications (Table 4.1). The modifications in the reconstructed mass components method used in this study and the assumptions behind the conversion factors are described in the following subsections.

Table 4.1 Reconstruction equation from Chow et al., (1996), and a modified equation used in this work

NO.	Method	Inorganic Ions	Organic carbons	Elemental carbon	Geological minerals	Salt	Trace metals
1	Chow et al., (1996)	$\text{SO}_4^{2-} + \text{NO}_3^- + \text{NH}_4^+$	1.4OC	yes	$(1.89\text{Al} + 1.43\text{Fe} + 2.14\text{Si} + 1.4\text{Ca}^{2+})$	$\text{Na}^+ + \text{Cl}^- + \text{Mg}^{2+}$	Sum all species measured by XRF excluding all elements accounted for in the other fractions
2	The modified approach	$\text{SO}_4^{2-} + \text{NO}_3^- + \text{NH}_4^+$	1.3*OC	yes	$(1.89\text{Al} + 1.43\text{Fe} + 2.14\text{Si} + 1.4\text{Ca}^{2+})$	$\text{Na}^+ + \text{Cl}^- + \text{Mg}^{2+}$	Not considered

4.2.1 Crustal Matter Estimation

The crustal matter is a significant component of particulate matter in Qatar because of the frequent dust storms and haze events in addition to traffic-induced resuspension and fugitive dust from construction/demolition activities. Silicon, aluminium, and iron are usually selected as tracers for crustal components. In this study, all three elements were determined on Teflon filters using the XRF technique. Very strong correlations were found between all the elements for the entire duration of the two sampling campaigns (Table 4.2)

Table 4.2 Metals ratios result when the regression line forced through zero with the correlation coefficients and uncertainties

winter AC site	winter QU site	Summer AC site	Summer QU site
[Fe]=0.86*[Al]; $R^2 = 0.84 \pm 0.1$	[Fe]=0.93*[Al]; $R^2 = 0.89 \pm 0.21$	[Fe]=0.92*[Al]; $R^2 = 0.94 \pm 0.29$	[Fe]=0.98*[Al]; $R^2 = 0.88 \pm 0.4$
[Fe]= 0.19*[Si]; $R^2 = 0.85 \pm 0.13$	[Fe]=0.19*[Si]; $R^2 = 0.87 \pm 0.2$	[Fe]=0.21*[Si]; $R^2 = 0.97 \pm 0.21$	[Fe]=0.22*[Si] $R^2 = 0.94 \pm 0.23$
[Al]=0.22*[Si]; $R^2 = 0.98 \pm 0.08$	[Al]=0.2*[Si]; $R^2 = 0.93 \pm 0.092$	[Al]=0.23*[Si]; $R^2 = 0.97 \pm 0.18$	[Al]=0.22*[Si]; $R^2 = 0.97 \pm 0.53$

Although the strong correlations between metals, the metals ratios in Doha showed different values than what has been found in other locations. The Fe/Al mass ratio average of 0.92 in Doha is higher than the ratios of 0.67, 0.64, and 0.66 reported for Saharan dust by Sciare et al., (2005); Guieu et al. (2002); Tuncel et al., (1997) respectively; and also, higher than the ratio of 0.68 calculated from metal concentrations in crust by Mason (1966). However, the ratio of 0.2 for Fe/ Si in Doha does agree with the value of 0.2 for a typical crust of Mason (1966). The differences between ratios are probably due to the differences in the percentage of metals in the crustal material in Doha. The Fe/Al ratio of ~0.92 is within the range of ratios found in most of the Middle Eastern countries. A recent worldwide mineralogical study (Engelbrecht et al., 2016) with 165 samples collected from 22 countries (Figure 4.1), four of which are in the Middle East namely (Iraq, Kuwait, Qatar, and United Arab Emirates), showed an average Fe/Al ratio of 0.76 with a strong correlation ($R^2 = 0.8$) for 122 samples out of the complete set of 165 samples. The study found that the Fe/Al ratio ranged from 0.41 to 3.78 for $PM_{2.5}$. This range includes all Fe/Al ratios for $PM_{2.5}$ which have been found in the Middle East in previous studies. Those findings include ratios between (1) 0.74 and 1.10

found in the Middle East (Engelbrecht et al., 2009b), (2) 0.95–1.85 found during dust events in Beirut, Lebanon (Jaafar et al., 2014), (3) and 0.64–0.81 for suspended particle dust in Iran (Najafi et al., 2014). In addition, a study using 15 sampling sites in the Middle East conducted in 2009 found that Fe/Al ratio in PM_{2.5} in Qatar is about 0.9 (Engelbrecht et al., 2009), which is equal to what been found in this study.

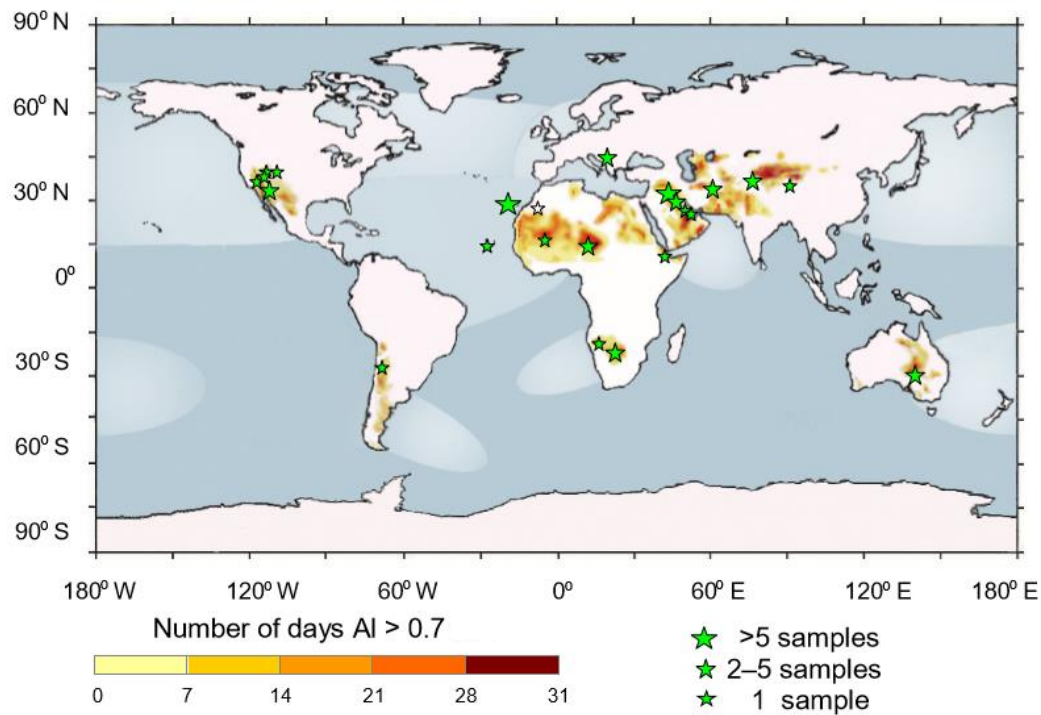


Figure 4.1 Surface soil sampling regions shown as green stars on a global map of dust sources as identified from Total Ozone Mapping Spectrometer (TOMS) data (source: Engelbrecht et al., 2016)

In mass closure studies, the dust fraction contribution to PM mass is either calculated by summing up metals oxides (Al_2O_3 , SiO_2 , Fe_2O_3 , CaO) (Chow, 2015) or based on a single crustal element (Countess et al., 1980).

In the single crustal element, the crustal components mass fraction is approximated by multiplying one of the crustal elements by a factor equal to its percentage in the crust. A

single crustal element approach has been used whenever there is a lack of measurements for one of the crustal elements or due to uncertainty in quantifying one or more of them (Chow, 2015). The Si and Al elements have both been used previously in reconstructing dust fraction using single element approach. Countess et al., (1980) used 3.5Si assuming 28.5% as the global average of Si mass fraction of crustal matter. On the other hand, 12.5Al, 13.77Al, and 14Al were used by Hsu et al., (2008); Ho et al., (2006) and Guieu et al., (2002) respectively.

In this study, the crustal mass was calculated using summing up metals oxides methods as follow:

Crustal mass fraction = $1.89\text{Al} + 2.14\text{Si} + 1.43\text{Fe} + 1.4 \text{Ca}^{2+}$, where the coefficients conversion factors are accounting for oxygen atoms, assuming a composition of: Al_2O_3 , SiO_2 , Fe_2O_3 , and CaO . The conversion factors were calculated based on the molecular weight (MW) of metal oxides to metal, for example:

$$\text{CaO} = (\text{calcium MW} + \text{oxygen MW}) / \text{calcium MW} = (40 + 16)/40 = 1.4.$$

However, a single element method was also explored, Al element needed different conversion factors, which ranged between 13.5 and 15.5, to estimate the crustal components fraction mass through different seasons and during dust events days and non-dust days.

On the other hand, 3.5Si was found to be the most suitable conversion factor to calculate dust fraction (defined as the sum of 1.89Al , 2.14Si , 1.43Fe , and 1.4Ca^{2+}) through different seasons and locations (Table 4.3), except for the QU site which showed a large intercept in the summer season. The large intercept probably caused by the changes in crustal chemical composition which caused by the contribution of particles from sand and cement stockpiles near the QU site.

Table 4.3 Regression result of 3.5Si against the sum of metal oxides in both seasons and sites

Campaign	Relationship between 3.5Si against sum of metal oxides (1.89Al, 2.14Si, 1.4Ca²⁺, 1.43Fe)	R²
AC summer	3.5Si = (1.0402 ± 0.371) x - (0.819 ± 0.01)	0.99
QU summer	3.5Si = (1.0553 ± 0.022) x - (2.447 ± 1.06)	0.97
AC winter	3.5Si = (1.0058 ± 0.011) x + (0.018 ± 0.13)	0.99
QU winter	3.5Si = (0.9954 ± 0.013) x - (0.7755 ± 0.21)	0.98

4.2.2 Trace Metals

In previous mass closure studies, trace metals were used in the reconstruction equation by Solomon et al., (1989); Chow et al., (1994b); Malm et al., (1994); and Andrews et al., (2000), while others excluded them from the reconstruction method, such as DeBell et al., (2006), Hand et al. (2011), and Simon et al. (2011). Trace metals are more noticeable in coarse fraction and in areas close to industrial facilities, but still only accounted for a small fraction of PM_{2.5} mass in literature studies (0.5-1.6%) Chow et al. (2015). In this work, the sum of trace metals (Ti, Ce, La, Cd, Zn, Mn, As, Ce, Ni, V, Co, Sn, Pb) contributed between 0.25 and 0.35% of the total PM_{2.5} mass, a minimal contribution, therefore in this study trace metals were not included.

4.2.3 Organic and Elemental Carbon

The carbonaceous fraction of PM_{2.5} consist mainly of elemental carbon (EC), organic carbon (OC), and a smaller amount of carbonates primarily in the form of CaCO₃ (Na et al., 2003). EC is produced through the combustion of carbon-containing fuel sources such as road traffic, marine traffic, and power plants. EC is a form of graphite carbon, and therefore its mass is used in mass construction equations without modification (Harrison et al., 2003).

However, for organic carbon (OC) which is a mixture of hydrocarbons and oxygenates, a conversion factor (F) is needed to account for unmeasured O, H, and N associated with organic compounds when constructing PM mass. The factor ranges between 1.2 to 2.2 (Turpin and Lim 2001) with near universal use of 1.4 factor to estimate organic molecular weight from carbon weight (Solomon et al., 1989; Chow et al., 1994b; Malm et al., 1994; Andrews et al., 2000).

The factor is chosen based on the level of oxygenation of organic compounds; meaning that more oxygen equals more organic molecular weight to carbon weight, thus a higher factor is needed in the construction method. In urban areas, where fresh primary anthropogenic organic particles are emitted; a factor between 1.2 and 1.4 is used (Andrews et al., 2000). In nonurban areas, the average organic aerosols molecular weight per carbon weight is greater than for organic aerosols in urban areas. Because primary organic aerosols from vegetations contain more oxygen, hydrogen, and nitrogen to carbon atoms, therefore a higher factor is used (Turpin and Lim., 2001; Sciare et al., 2005). European studies typically use a factor of 1.4 factor (Sillsnpaa et al., 2006). Qatar as an arid climate country is not affected by biogenic emissions such as vegetative detritus and biomass combustion. Also, Doha is an urban city with a high contribution from anthropogenic sources. Therefore, a conversion factor between 1.2 and 1.4 is likely to be more suitable. However, this could not be the case due to the warm sunny climate which likely can increase secondary organic aerosols formation (Monod and Liu, 2011). Nevertheless, a conversion factor of 1.3 was used in this study to estimate organic matter mass fraction in Qatar, because the reconstructed mass overestimated the measured mass hence a lower conversion factor is applicable to find agreement between both reconstructed and measured mass. A 1.3 conversion factor for Doha samples was calculated to cause 7.69% less organic particles than a 1.4 factor would have given.

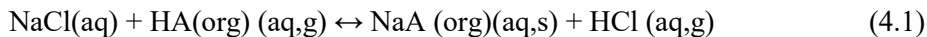
4.2.4 Sea Salt

Doha is a coastal city hence it is expected to have a large contribution of sea salt to $PM_{2.5}$. Dust events also contribute to a substantial amount of NaCl. In the winter season, the difference in Na^+ and Cl^- concentration during normal days (days without dust events) and dust events days was large in both sampling locations. The average concentrations of Na^+ and Cl^- elements at the AC site were 0.68 and 0.068 $\mu g/m^3$ for normal days and 1.57 and 0.57 $\mu g/m^3$ for dust events days respectively, while at the QU site, Na^+ and Cl^- concentrations were 0.77 and 0.15 $\mu g/m^3$ in normal days, and 2.12 and 1.45 $\mu g/m^3$ for dust events days. Six ions (Na^+ , Mg^{2+} , Ca^{2+} , K^+ , Cl^- , and SO_4^{2-}) contribute more than 99% of the mass of salt dissolved in seawater (Sciare et al. 2005). Sea salt sulfate [ss- SO_4^{2-}] and sea salt calcium [ss- Ca^{2+}] were calculated based on their molar ratio to Na^+ in sea water, as total [Na^+] times 0.252 and 0.038 respectively (Chow et al., 2015). The calculation showed that their contribution to the sea salt component was insignificant, and therefore they were excluded from sea salt fraction equation.

A number of different approaches have been used to calculate the sea-salt component. Some used the sum of Na^+ and Cl^- (Chow et al., 1996; Kozłowska et al., 2012), others used multiplier factors based on the ratio of sea-salt to Na^+ or Cl^- . Ohta and Okita (1994) used $3.27Na^+$, Yan et al., (2012) used $2.5 Na^+$, Harrison et al., (2003) used $1.65 Cl^-$, and Simon et al., (2011) used $1.8 Cl^-$.

Using a multiplier to calculate the salt fraction is not suitable for this study because $PM_{2.5}$ showed Cl^- depletion. The ratio of Cl^-/Na^+ in fresh sea salt aerosols is 1.8 (Okada, 1978), whereas, in Doha, the Cl^-/Na^+ ratio is 0.14 and 0.28 in the AC and QU sites in the winter season and 0.34 and 0.44 in the AC and QU sites in the summer season, which indicates Cl^- loss. The chloride depletion can be caused by the release of hydrochloric acid gas (HCl) when

sea salt particles react with organic acid and nitric acid, driven by HCl high volatility (Wang and Laskin, 2014):



As a result, using a Na^+ multiplier to calculate sea salt fraction will result in an overestimation for chlorine mass on filters while using Cl^- multiplier will underestimate the Na^+ element. For this reason, sea-salt mass fraction was calculated as follows:

$$[\text{Sea salt}] = [\text{Na}^+] + [\text{Cl}^-] + [\text{Mg}^{2+}].$$

4.2.5 Ammonium Sulfate and Nitrate

Ammonium sulfate and ammonium nitrate are secondary inorganic aerosols that form in the atmosphere through oxidation from their precursor gases (SO_2 , NH_3 , and NO_3^-) and gas to particle conversion. Secondary aerosols are considered one of the most abundant components in $\text{PM}_{2.5}$ (Sillanpaa et al., 2006). Doha results showed that SO_4^{2-} was the dominant anion in both sites and seasons. To estimate secondary aerosol mass fractions, the contribution of SO_4^{2-} , NH_4^+ , and NO_3^- were summed up without weighting factors, which do not account for H^+ associated with sulfuric acid when sulfate is not neutralized completely by ammonium (Chow et al., 2015).

4.3 Mass Reconstruction Results

The mass closure analysis was performed for the four sets of data collected from the two sites for winter 2014 and summer 2015. The sites are 12 km away from each other, and they have different surroundings. The AC site is located near the coastline and is influenced by emissions from Doha port and traffic. The area around the sampling site is covered by

pavement and grass, so there are no extra crustal components coming from the immediate vicinity of the site. On the other hand, the QU site is located in a vacant area and is subject to dust from the loose soil which induced by winds and traffic turbulence. The mass closure analysis was performed using method 2 in Table 4.1. Table 4.4 summarizes the species used in the reconstruction method, including the type of filters each component was collected on and the possible artefacts associated with each of the filters.

Table 4.4 Species included in the mass closure, the performed analysis methods, types of filters, and the possible artefact with each filter type.

PM Mass	Species	Analysis technique	Filters	Filters artefact
Constructed mass	OC, EC	Thermo-Optical OC-EC Aerosol Analyzer	Quartz	Quartz filters show high retention of organic vapour and lower release of ammonium nitrate causing a mass gap when compared with mass collected on other types of filters (Vecchi et al., 2009)
	Na ⁺ , Mg ²⁺ , Ca ²⁺ , NH ₄ ⁺ , NO ₃ ⁻ Cl ⁻ , and SO ₄ ²⁻	Ion chromatography		
	Al, Si, Fe, S	Dispersive X-Ray Fluorescence (WD-XRF)	Teflon	Teflon filters adsorb little or no gas phase organic carbons (Vecchi et al., 2008) and show a nitrate underestimation larger than quartz filters especially during summer. (Ashbaugh and Eldred, 2004). Which can underestimate PM mass collected on Teflon filter
Gravimetric measured mass	sample mass in µg/m ³	Sartorius Model MC5 microbalance (sensitivity- 1 µg)		

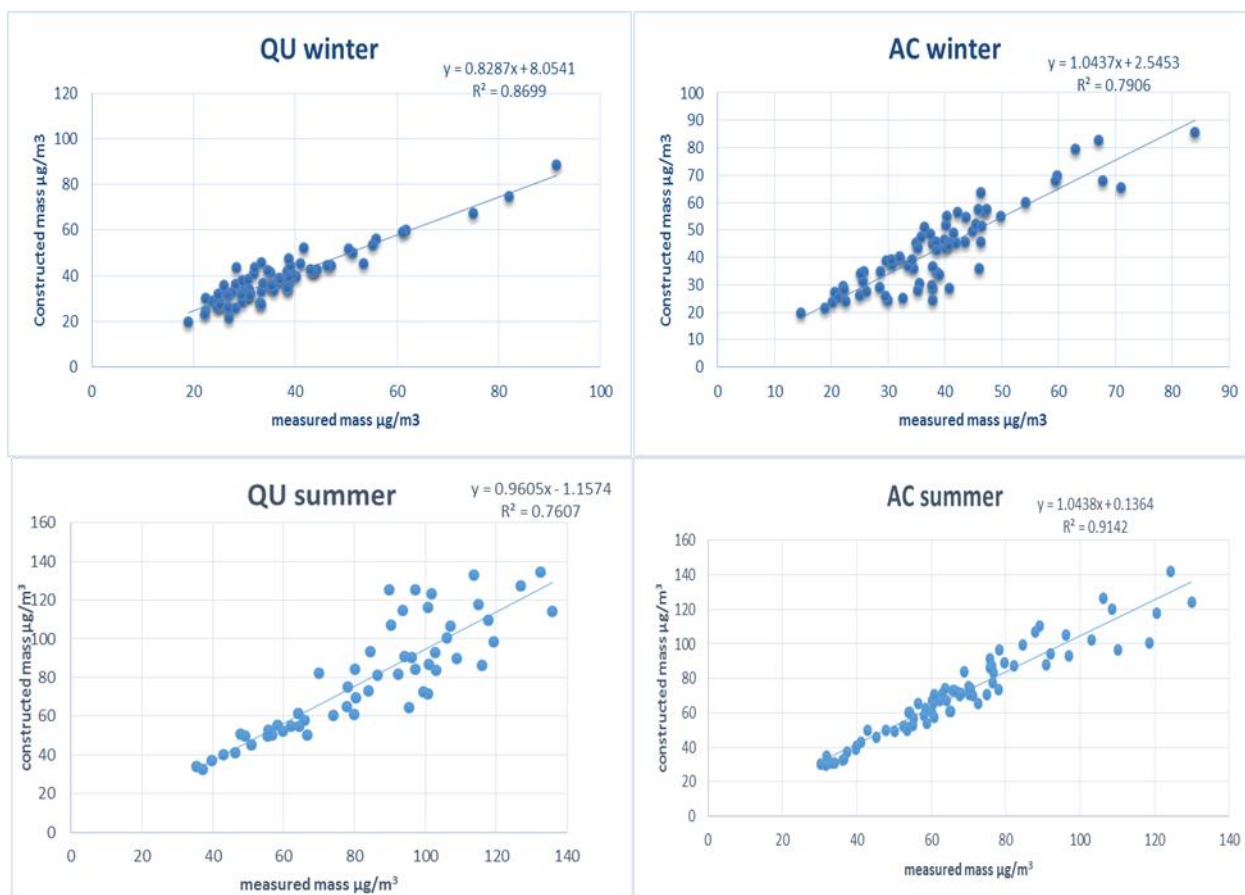


Figure 4.2 Relationship between measured mass on X-axis and reconstructed mas in Y-axis in winter [A]&[B] and in summer [C] and [D]

The least squares regression method was used to assess the correlation between measured mass and reconstructed mass, assuming that the independent variable (measured gravimetric mass) is more precise than the dependent variable. In the reconstruction method, samples with missing values were excluded from the equations. Also, in the summer season, four samples were excluded from the reconstruction method at both sites as they largely affected the regression line. The four samples occurred on dust events days, and they showed about 40 % low reconstructed mass. According to Andrews et al., (2000) underestimation of PM mass could be caused by using only a few metals to estimate the dust fraction, and also not all metals are in the oxide form. It is unlikely that the mass underestimation in this study caused by an error in the measurements as these days showed the same behavior at both sites even

though they were analyzed in different batches, hence the underestimation is likely caused by unmeasured or unaccounted for species. Figure 4.2 shows the regression line between measured mass and constructed mass in the winter and in summer seasons. Table 4.5 shows the mass closure regression results:

Table 4.5 Results of the linear regression of reconstructed mass (y) upon gravimetric mass (x)

Campaign	Regression	R²	% of the average constructed mass / measured mass
AC winter	$y = (1.0437 \pm 0.064) x + (2.5453 \pm 2.6)$	0.7906	+12
QU winter	$y = (0.8287 \pm 0.038) x + (8.0541 \pm 1.48)$	0.8699	+4.7
AC summer	$y = (1.0438 \pm 0.038) x + (0.1364 \pm 2.75)$	0.9142	+4
QU summer	$y = (0.9605 \pm 0.073) x - (1.1574 \pm 6.47)$	0.7607	-5.3

4.4 Mass Reconstruction Result Evaluation

A good fit is characterised by three factors: a gradient close to 1, a small intercept, and a high R² value (Yin and Harrison 2008). Also, Chow et al., (2015) suggested $100 \pm 20\%$ as a good practical criterion for mass construction over measured mass. Overall, a good closure has been found at all locations (Figure 4.2 and Table 4.5) except for the QU site in the winter season, which showed a low gradient and high intercept. The percentage difference of the average mass construction over average gravimetric mass for AC and QU sites were +12% and +4.7% in winter and +4% and -5.33% in summer respectively. Although the constructed mass percentage is within Chow et al., (2015) suggested percentage, the negative discrepancy (reconstructed mass overestimates the measured mass) is in contrast with most mass closure study results that usually shows a positive discrepancy due to unmeasured species. In many literature studies, parallel sampling was carried out using Teflon and quartz filters, where both

metals and ions were measured on Teflon filters while OC and EC were measured on quartz filters. Then the sum of all chemical constituents was compared with the gravimetric mass of the Teflon filters. A positive discrepancy in those studies was credited to water mass on Teflon filters (Harrison et al., 2003; Sillanpaa et al., 2006). The evaluation below discusses the discrepancy between measured mass and constructed mass based on the absence of key species measurements and inorganic artefacts.

4.4.1 Carbonate Compounds

The absence of carbonate measurements could be the cause of the weak regression line at the QU site. As mentioned in Chapter 2, during the winter season sampling campaign there was an excavation work at the QU site that produced dust particles which are likely to contain calcium carbonate (CaCO_3) as its one of Qatar's crustal components (Embabi and Ashour, 1993). However, during the summer season, the QU regression equation does not seem to be affected by the absences of carbonate concentration measurements, probably because the summer samples have more calcium oxide contributed by dust events.

To overcome the absences of carbonate measurements, a few studies have used a 1.95 conversion factor to account for both CaO and CaCO_3 assuming an equal contribution from both species (Terzi et al., 2010; Remoundaki et al., 2013).

The 1.95 factor is an average of 1.4 and 2.5 factors which is the ratio of CaO, and CaCO_3 compounds molecular weight to Ca^{2+} elemental weight.

Based on a previous study of $\text{PM}_{2.5}$ composition in Qatar, 46% of Ca^{2+} was in CaCO_3 form, whereas 54% in CaO form (Engelbrecht et al., 2009).

Hence the conversion factor for Qatar was calculated as follow:

$$= (0.46 * \text{CaCO}_3 \text{ ratio to Ca}^{2+} \text{ of } 2.5) + (0.54 * \text{CaO ratio to Ca}^{2+} \text{ of } 1.4)$$

$$= (0.46 * 1.4) + (0.54 * 2.5) = 1.91$$

Therefore, the reconstructed mass in Doha was recalculated for all sites using a 1.91 conversion and are presented in Table 4.6.

Table 4.6 Results of the linear regression of reconstructed mass (y) upon gravimetric mass (x) after carbonate correction

Campaign	Regression	R ²	Ca convertor factor	%
QU winter	y = (0.869±0.038) x + (7.27±1.51)	0.876	1.91	+ 6.6
QU summer	y = (0.9898±0.08) x – (2.845±7.04)	0.754		-2.3
AC winter	y = (1.0678±0.062) x + (1.9638± 1.57)	0.802		+11.8
AC summer	y = (1.069± 0.034) x – (1.659± 2.21)	0.924		+ 9.2

4.4.2 Carbonaceous Aerosols Artefact

Carbonaceous aerosols are a major contributor to PM_{2.5} mass (Malm et al., 1994; Turpin et al., 2000). In this study, carbonaceous aerosols average concentration was 8.4 and 10.1 µg/m³ in the summer and winter seasons respectively. Two factors associated with organic matter can lead to overestimation of the constructed mass over the measured mass: (1) Positive artefact on quartz filters; (2) using the wrong conversion factor. Organic carbon was collected on quartz filters for the purpose of thermal evolution analysis since quartz filters can withstand high temperatures (1000 °C). However, quartz filters fibers are prone to adsorption of organic carbon gases which can lead to overestimation of OC concentration. Subrmanian et al., (2004), found in a long study period throughout the year that sampling OC on a bare quartz filter for 24 h at 16.7 L/min caused a constant positive artefact of 0.5 µg-C/m³. This value would cause on average a 6% increase in OC mass for Doha samples. Also, Vecchi et

al., (2009) found that the positive artefact percentage of OC given as the ratio between the OC measured on a bare quartz filter and on the backup quartz filter for a Teflon filter in a parallel sampling setup accounted for $23 \pm 9 \%$ in the winter and $39 \pm 8 \%$ in the summer which corresponded to an absolute OC artefact concentration of $3.8 \mu\text{g}/\text{m}^3$ and $2.4 \mu\text{g}/\text{m}^3$ in the winter and summer respectively. The mass closure results in both seasons were tested using 23% and 39% for the winter and summer respectively. The artefact effect was removed by multiplying the organic mass ($1.3 \times \text{OC}$) concentrations by 0.77 and 0.61 for the winter and summer, and the new data were used in the reconstructed mass instead of ($1.3 \times \text{OC}$) concentrations. Table 4.7 shows the mass closure regression equation after removing the organic artefact. Overall an average of 4 % and 2% were removed from the constructed mass in the winter and summer samples respectively.

Table 4.7 Results of a linear regression of reconstructed mass (y) upon gravimetric mass (x) after organic carbon correction

Campaign	Regression	R ²	% of the average constructed mass / measured mass
AC winter	$y = (1.0153 \pm 0.0623)x + (1.8883 \pm 2.53)$	0.79	+ 6.4
QU winter	$y = (0.8136 \pm 0.038)x + (7.1814 \pm 1.5)$	0.87	+0.82
AC summer	$y = (1.0388 \pm 0.038)x - (1.2787 \pm 2.75)$	0.91	+2
QU summer	$y = (0.9573 \pm 0.074)x - (2.6966 \pm 6.46)$	0.75	-7.48

As for the conversion factor, White and Robert (1977) suggested that 1.2 to 1.4 factor is a universal estimation for particulate organic molecular weight per carbon weight. Turpin and Lim, (2011) suggest that a 1.4 factor is the lowest reasonable estimation. Therefore, using the 1.3 factor will be within the conversion factors limits for organic carbon, and it should not cause the mass discrepancy. Even if a lower conversion factor is used such as 1.2, it would

only reduce the total particulate organic matter mass by 7.7%, which equates to 0.35% and 1.1% reduction “a minimal effect” of the average total constructed mass in the summer and in winter seasons respectively.

4.4.3 Ammonium Nitrate Artefact

The most abundant inorganic ions in Doha samples are sulfate, followed by ammonium then nitrate. Nitrate average concentrations are slightly lower in the summer compared to the winter season. In the summer season, NO_3^- accounted for 1.82 and 2.43 $\mu\text{g}/\text{m}^3$ at the QU and AC sites, while it accounted for 2.83 and 2.27 $\mu\text{g}/\text{m}^3$ in the QU and AC sites in the winter season respectively. In a study for six urban sites in Europe, Sillanpaa et al., (2006) stated that NO_3^- concentrations are high (7.5-18 $\mu\text{g}/\text{m}^3$) in the cold weather when temperature ranged from -2 to 9 °C, but moderate to low (1.1-6.8 $\mu\text{g}/\text{m}^3$) at higher temperatures (15 to 29 °C). Ammonium nitrate is thermally unstable, and in dynamic equilibrium with ammonia and nitric acid (CENR, 1999) thus it is subject to volatilization and loss from filters during and after sampling. Doha average temperature was 20 °C in the winter and 35 °C in the summer seasons, which explains the low ammonium nitrate levels in Doha samples. The average percentage of ammonium nitrate in Doha's samples was for 3.4% of $\text{PM}_{2.5}$ mass in the summer season and 8.7% of $\text{PM}_{2.5}$ mass in the winter season. According to Perrino et al., (2013), Teflon filters release more ammonium salts than quartz filters. Vecchi et al., (2009) also found that Teflon filters underestimate nitrate mass more than quartz filters, particularly in the summer season. In the Vecchi et al., (2009) study for the performance of Teflon and quartz filters in collecting ammonium nitrate in Italy, they found that the average nitrate volatilization was about 51% on Teflon filters and 22% on quartz filters in the summer which means that quartz filters collected 29% more ammonium nitrate than Teflon filters did. In the winter season, however, with a temperature between 4 and 22 °C, ammonium nitrate loss was

negligible. Moreover, their data suggests a tendency toward nitrate volatilization with increasing temperature due to the dissociation of ammonium nitrate with increasing temperature and remaining constant at a given temperature below the deliquescence RH. To correct for the nitrate artefact in Doha samples, the difference of 29% between nitrate volatilization percent in Teflon and quartz from (Vecchi et al., 2009) study was used to calculate the extra mass ammonium nitrate on quartz filters and subtracted from the constructed mass. First, the nitrate element was multiplied by the conversion factor 1.29 to account for ammonium nitrate mass fraction then it was multiplied by 0.29 to calculate the extra mass of ammonium nitrate on quartz filters. Finally, the values were subtracted from the constructed mass. The same correction was used for both seasons due to the relatively high temperature in the winter season in Doha. Table 4.8 shows the regression equation after removing the ammonium nitrate artefact. The correction reduced the total constructed mass percentage by an average of 2% and 1% in the winter and summer seasons respectively.

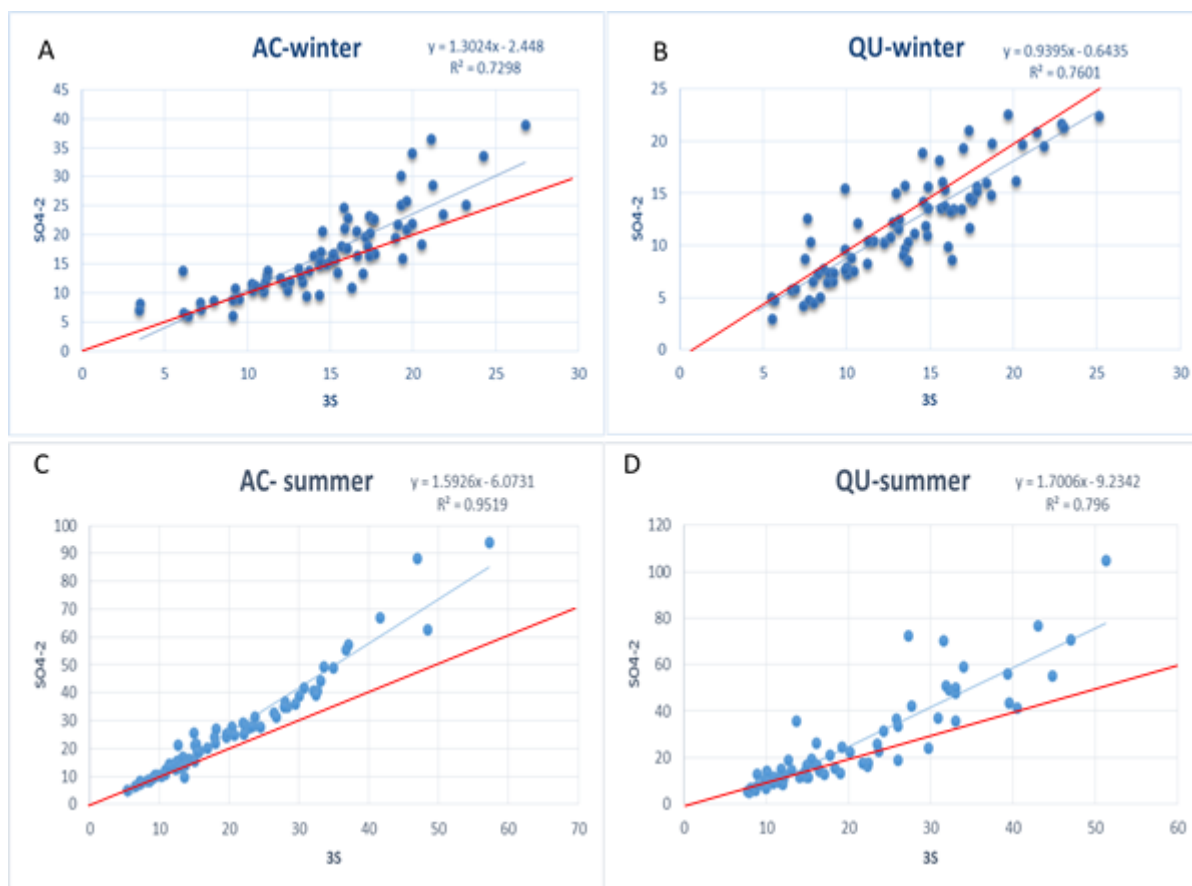
Table 4.8 Results of a linear regression of reconstructed mass (y) upon gravimetric mass (x) after ammonium nitrate correction

Campaign	Regression	R²	%
AC winter	$y = (1.0358 \pm 0.063)x + (2.0624 \pm 2.56)$	0.794	+8.9
QU winter	$y = (0.816 \pm 0.038)x + (7.461 \pm 1.48)$	0.865	+1.8
AC summer	$y = (1.035 \pm 0.039)x - (0.059 \pm 2.8)$	0.908	+3.59
QU summer	$y = (0.956 \pm 0.0724)x - (1.679 \pm 6.3)$	0.76	-6.4

4.4.4 Sulfate Measurements and Possible Artefact

Two analytical approaches to measuring SO_4^{2-} were possible. Sulfate (SO_4^{2-}) was determined on quartz filters by the IC technique, and sulfur (S) was measured on Teflon filters by the

XRF technique. Sulfur (S) mass concentration was multiplied by three, for an equivalent mass of sulfate (SO_4^{2-}). The correlation between SO_4^{2-} and 3S was good. However, the SO_4^{2-} concentration on quartz filters was higher than the 3S concentration on Teflon filters



especially in the summer season (Figure 4.3).

Figure 4.3 Relationship between SO_4^{2-} on quartz filters (y-axis) and 3S on Teflon filters (x-axis) in $\mu\text{g}/\text{m}^3$ in the winter season [A&B] for the AC and QU sites respectively, and in the summer season [C&D] for the AC and QU sites respectively (Red line represents unity line).

The AC site showed a higher relative humidity and higher sulfate concentration compared to the QU site, due to the proximity to the coastline and sulfur emission sources such as the combustion of fuel containing sulfur in vessels from Doha port. In the winter season, sulfate concentration at the AC site ranged from 0.77 to 37.8 $\mu\text{g}/\text{m}^3$ on quartz and from 3.48 to 26.7

$\mu\text{g}/\text{m}^3$ on Teflon; and the mean relative humidity was 66%. At the QU site, on the other hand, sulfate ranged from 2.9 to 22.6 $\mu\text{g}/\text{m}^3$ on quartz and from 5.5 to 25 $\mu\text{g}/\text{m}^3$ on Teflon with mean relative humidity of 58%. Figures 4.3A and 4.3B, show the relationship between 3S and sulfate (SO_4^{2-}) at the AC and QU sites. At the AC site, SO_4^{2-} determined on Quartz filters was higher than 3S on Teflon filters; in contrast, SO_4^{2-} was slightly lower than 3S at QU site.

In the summer season, the difference between SO_4^{2-} and 3S was greater at both locations than in the winter. Average sulfate mass concentration at the AC site ranged from 5.37 to 57.25 $\mu\text{g}/\text{m}^3$ and 4.8 to 93.7 $\mu\text{g}/\text{m}^3$ for 3S and SO_4^{2-} . Similarly, in the QU site, sulfate ranged from 7.76 to 51.28 $\mu\text{g}/\text{m}^3$ and from 4.5 to 93.54 $\mu\text{g}/\text{m}^3$ for 3S and SO_4^{2-} respectively, with mean relative humidity of 44.9% and 35% at the AC and QU sites respectively. Figures 4.3C and 4.3D, show that the SO_4^{2-} and 3S mass difference start to increase gradually above 10, and 20 $\mu\text{g}/\text{m}^3$ at the AC and QU sites with a stronger correlation $R^2=0.95$ at the AC site.

Typically, sulfate (3S) determined by XRF, is either equal to or higher than SO_4^{2-} determined by ion chromatography. This is because S can be associated with insoluble compounds that can't be detected by IC such as methyl mercaptans (CH_4S), Pyrite (FeS_2), and S contained in SO_2 adsorbed on particles (soot) (Chow et al., 2015).

The reason for the discrepancy between sulfates measurements is then possibly due to (1) analytical error or, (2) due to the difference in filters performance in collecting sulfate. Two papers have discussed the performance of different types of filters on sulfate sampling; (1) the experimental work done by Vecchi et al., (2009) to estimate organic and inorganic artefacts on filters and (2) the review of IMPROVE network (The Interagency Monitoring of Protected Visual Environments) in the USA by Eldred (2001).

Vecchi et al., (2009), found no difference between measurements of sulfate on quartz and sulfate on Teflon filters (Figure 4.4). Notice here that sulfate in both measurements was detected using one analytical technique (Ion chromatography) and sulfate concentration did not exceed $15 \mu\text{g}/\text{m}^3$.

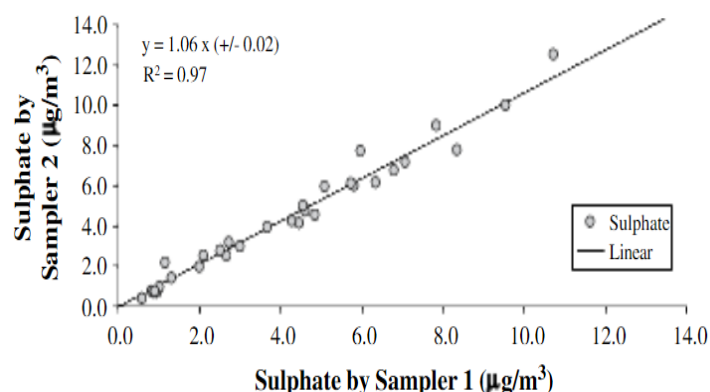


Figure 4.4 Experimental comparability between sulfate determined by IC on Quartz filter (y-axis) and Teflon filters (X-axis) (source : Vecchi et al., 2009)

In the course of the Interagency Monitoring of Protected Visual Environments network (IMPROVE) which cover the national parks in the USA, the same phenomenon (3S lower than SO_4^{2-}) appeared between 1992-1994. 3S measured on Teflon filters by the XRF technique was lower than the sulfate determined on nylon filters by the IC technique for samples collected in the summer season in Eastern sites (Figure 4.5).

According to Eldred (2001), the mechanism of sulfate loss from Teflon filters is not clear but it most likely produced by a combination of high relative humidity, acidic sulfate particles, and high sampling face velocity. In 1995, when the sampling face velocity at Eastern sites for the IMPROVE network was reduced from 170 cm/s to 110 cm/s by increasing the collection

area, the discrepancy between filters disappeared except for one day in three nearby sites in August 1995.

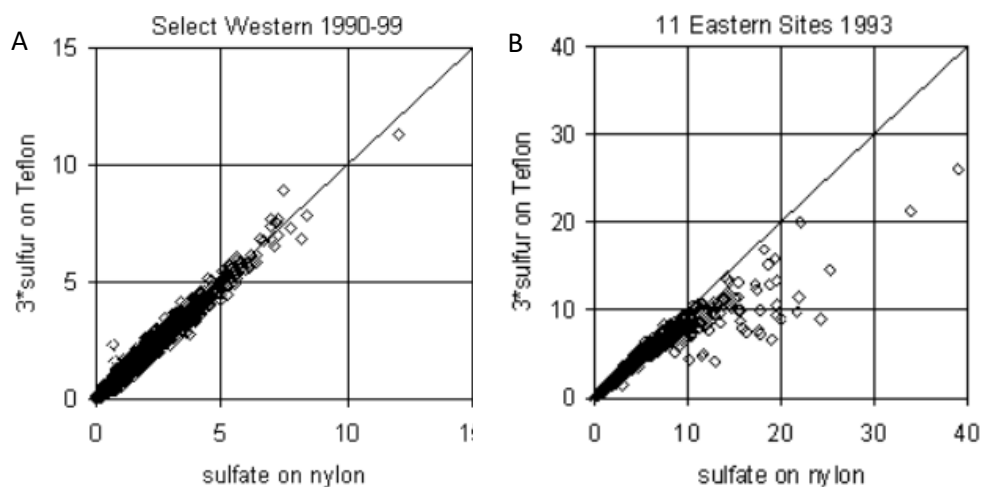


Figure 4.5 Relationship between sulfur measured on Teflon by XRF and sulfate measured on nylon by IC in [A] western site and [B] eastern site (Source: Eldred, 2001)

Also, high relative humidity was mentioned as a cause for the low sulfate concentration on Teflon filters; however according to Eldered (2001), the mechanism was not clear. A special study was conducted for 4h, and 12h measurements using Teflon and nylon filters at the Great Smoky Mountains in summer 1994, to study the possible causes of sulfate losses from Teflon filters (Eldered, 2001). All sampling units had a denuder except for the 12h Teflon. Sulfate concentrations on 4h Teflon agreed with the 4h nylon and 12h nylon determination, but the 12h Teflon measurements sometimes gave lower sulfate concentrations. Since relative humidity, sulfate acidity, and filter face velocity was the same for 4h and 12h Teflon filters, it was proposed that sulfate loss was happening in 12h Teflon because acidic sulfate takes several hours for migration, or that the carbonate denuder moderated RH at the filter for the 4h Teflon.

Elderred (2001) pointed out that the discrepancy between both sulfate measurements occurred in the summer season (June and August) and was never observed in the winter season. Also, Figure 4.5 shows a higher sulfate concentration at the eastern sites compared to the western sites, where the phenomenon occurred. It is hypothesized that high face velocity, acidic sulfate, and high relative humidity cause the sulfate to either migrate away from the center of the filter or perhaps even be lost from the filter. In ion chromatography analysis, the whole filter can be prepared and used in the analysis while in the XRF and PIXE technique the area analyzed by the instrument is smaller than the sampled area of the filter, and the instrument only focuses on the center of the filter. Therefore, if there is non-uniformity of PM distribution on the filter surface, the IC results will not be affected, whereas the XRF will obtain biased results (Caballero et al., 2017). To check if the sulfate discrepancy is an actual sulfate loss, or it remains on the filter but not detected by the XRF technique, Elderred (2001) selected samples where the difference between sulfate concentration measured on Teflon and on nylon filters was above 15% and determined the sulfate concentration again on Teflon filters using the IC after the previous analysis with the XRF. The results of (1) sulfate on Teflon using the IC, (2) sulfate on Teflon using the XRF and (3) sulfate on nylon using the IC were compared. Figure 4.6 shows sulfate correlation on different filters and analytical techniques. Figure 4.6A shows sulfate determined by the XRF on Teflon and by the IC techniques on nylon. Figure 4.6B and 4.6C determine if the sulfur loss is real or if it is still on the filters. In Figure 4.6B, the open squares cases, where sulfate was measured using the IC on Teflon and on nylon, showed better agreement indicating that the sulfate remained on Teflon filters but simply migrated outside the view of the PIXE, hence wasn't detected by the instrument. In Figure 4.6C, the solid squares where the IC on Teflon filters agreed with the PIXE on Teflon indicate that the sulfate discrepancy between Teflon and nylon filters in

Figure 4.6A is because sulfur was removed from the Teflon filters. Finally, the diamond cases which showed the IC values on Teflon are halfway between the PIXE on Teflon and the IC on nylon indicate that some of the sulfates left the Teflon filter while some migrate outside the PIXE view. The Teflon filters were also scanned using a focused PIXE beam which showed that on some of the Teflon filters, sulfate was found on the outer portion of the filters (Elderred, 2001).

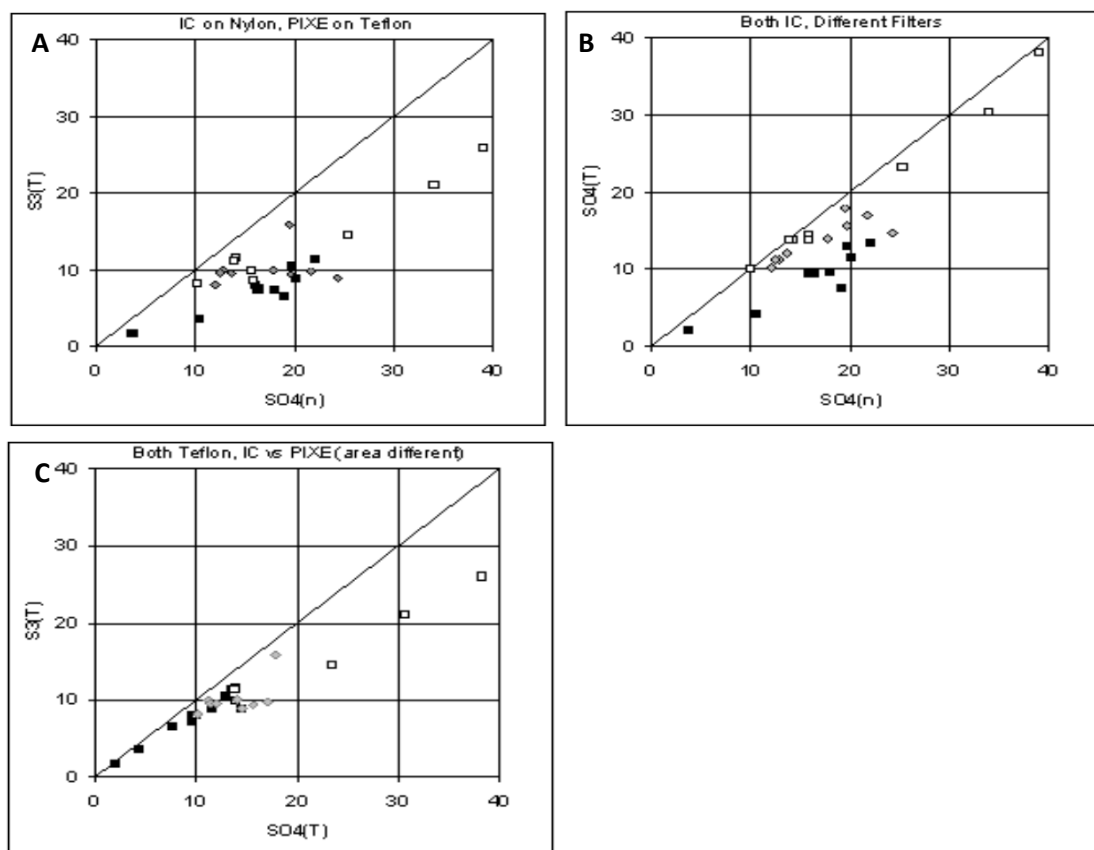


Figure 4.6 Comparison of IC sulfate on nylon [$SO_4(N)$], IC sulfate on Teflon [$SO_4(T)$], and PIXE sulfur on Teflon [$S3(T)$]. The IC analysis on the Teflon filters was performed after the XRF and PIXE analyses. Only samples with a difference between IC sulfate on nylon and PIXE sulfur on Teflon greater than 15% are included. The samples are differentiated as to whether the IC on Teflon agrees more with the IC on nylon or the PIXE on Teflon. The open squares are 8 samples in which the agreement is best with IC on nylon. For the 10 solid squares, the agreement is better with PIXE on Teflon. The agreement is about equal for the 9 diamonds (Source: Elderred, 2001).

In comparison to the IMPROVE network outcomes, the sulfate discrepancy in Doha samples was larger with high sulfate concentration and was clearer in the summer season (Figure 4.3). To examine the effect of high relative humidity on SO_4^{2-} and 3S, a scatter plot was produced for the relationship between the $\text{SO}_4^{2-}/3\text{S}$ ratio against the relative humidity (Figure 4.7). However, the relationship between $\text{SO}_4^{2-}/3\text{S}$ ratio and relative humidity was not statistically significant to build any conclusion.

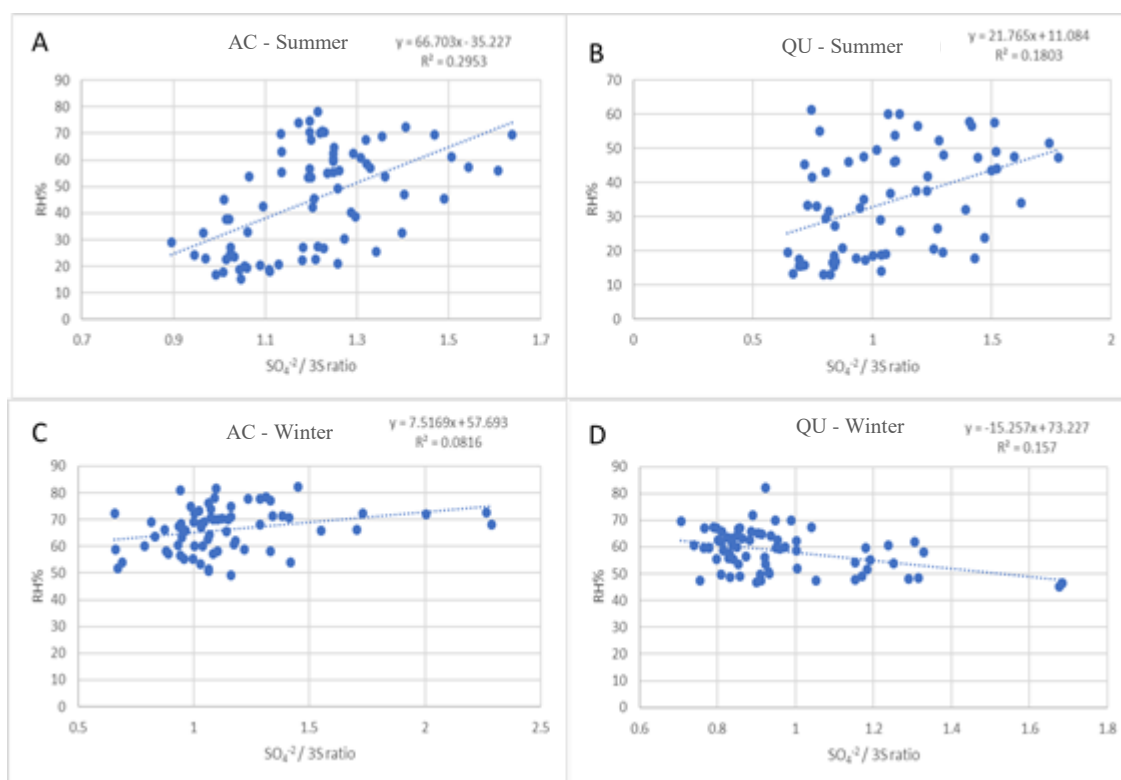


Figure 4.7 Relationship between $\text{SO}_4^{2-}/3\text{S}$ ratio with relative humidity at the QU site in summer [A] & [B] and in winter [C] & [D]

The gap between sulfate on quartz and sulfur from Teflon filters in Doha city is probably caused by a combination of factors including the collection performance of different types of filters, the analytical technique and the different sulfate compounds found on each site.

Perrino et al., (2013) explained the different behavior of Teflon and quartz filters due to their different response to atmospheric water. Quartz filters have a hydrophilic nature hence; they can absorb water molecular from particles in which they evaporated during the sampling period. On the other hand, the hydrophobic nature of Teflon filters prevents the transfer of water from particles leading to more clogging during fog events. In Doha, Teflon filters at both campaigns did not show a pressure drop during the sampling periods which excluded filter clogging that may affect filter performance. However, the explanation of sulfate migration from Teflon filters due to increased relative humidity can be explained by the work of Agranovski (1995) where the performance of hydrophilic and hydrophobic filters in collecting liquid particles was assessed. The results showed that when hydrophilic filters such as quartz filters were placed in a vertical position through the filtration of liquid particles, it collected the majority of the particles on their surface. As the number of liquid particles increases on top of quartz filter's surface, droplets start to join forming a cluster that moves toward the bottom of the filters under gravitational force wetting other fibers as it does so. In the case of hydrophobic filters, such as Teflon filters, the captured liquid particles remain attached to the filter and are not absorbed due to the high droplet surface tension, then once the gravitational forces prevail, the cluster of droplets falls from the filter.

If sulfuric acid exists in a liquid form due to high relative humidity or if the particles are coated with a liquid layer which according to Hsiao (2009) will likely behave in a similar way to liquid droplets, then collecting sulfuric acid dissolved in liquid droplets will differ using Teflon and quartz filters. The quartz filters will absorb liquid droplet into its fibers. However, droplets will either evaporate, pushed away from the center, or fall off the Teflon filters due to the force of air flow face velocity. Schematic diagram illustrates the effect of air flow on liquid droplets.

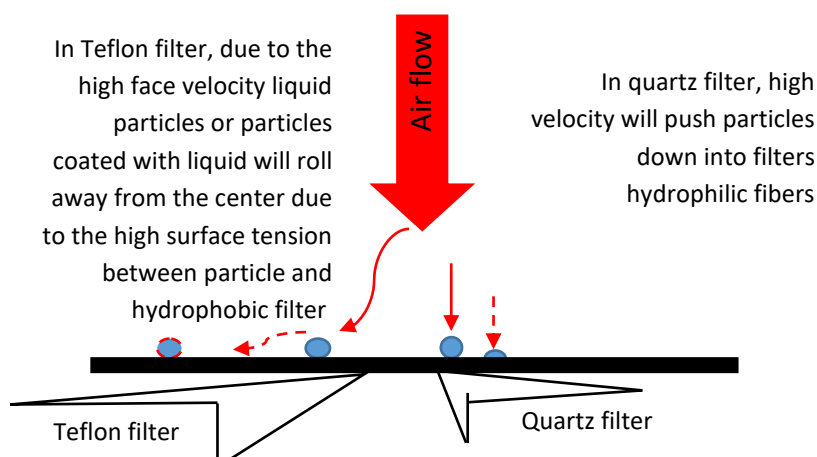


Figure 4.8 Illustration for the effect of air flow, type of filters, and liquid particles on the position of the particle on the filter

The two main sources of sulfur in Doha are (1) crust in the form of gypsum CaSO_4 , and (2) anthropogenic sources in the form of SO_2 which oxidises in the atmosphere to sulfuric acid and reacts with ammonia to form ammonium sulfate and ammonium bisulfate. As stated in chapter 2, the QU site in the winter season was exposed to earthworks and the presence of trucks which likely produced more CaSO_4 compared to the AC site and to other seasons. Gypsum is in a solid form hence it will not be subjected to migration from Teflon filters. It is a semi-soluble compound (Chow et al. 2015), and its concentration is entirely measured by the XRF technique, and so but is underestimated by the IC analysis. Therefore, sulfate using the XRF at the QU in the winter season showed a higher concentration compared to sulfate determined by the IC.

To examine the impact of sulfate migration from the center of a Teflon filter or entirely leaving the filter, sulfate by the XRF was used in the mass reconstruction instead of sulfate by the IC. To avoid uncertainties caused by using ammonium from quartz filters, sulfate (3S) and NO_3^- were multiplied by 1.38 and 1.29 respectively for an equivalent mass of ammonium

sulfate and ammonium nitrate assuming that all the sulfate and nitrate was in the form of ammonium salts, and they were used to calculate the mass closure (Table 4.5).

The mass closure result, when compared to the reference reconstruction method (Table 4.5), showed some improvement for R^2 values at the expense of gradient and intercept (Table 4.9). The R^2 improvement is anticipated since the comparison between S concentration, and gravimetric mass was done using the same Teflon filters.

Table 4.9 Results of the linear regression of reconstructed mass (y) upon gravimetric mass (x) after substituting SO_4^{2-} with 3S

Campaign	Regression	R^2	%
AC winter	$y = (0.9205 + 0.042)x + (7.85 + 1.74)$	0.868	+9
QU winter	$y = (0.8598 + 0.035)x + (9.9421 + 1.4)$	0.8881	+12
AC summer	$y = (0.9242 + 0.024)x + (6.6133 + 1.76)$	0.9524	+2.15
QU summer	$y = (0.8118 + 0.046)x + (12.421 + 4.8)$	0.8495	-3.99

The reference construction method in Figure 4.2, showed a higher ratio of constructed mass over measured mass for points at the high-end of the curve for the summer season (i.e., when reconstructed PM was greater than measured mass). In Figure 4.9 when sulfate by the IC was substituted with sulfate by the XRF the same high points showed a constructed mass lower than the measured mass. If some sulfates entirely evaporated from Teflon filters, then this should also affect $\text{PM}_{2.5}$ gravimetric mass. Hence no discrepancy should be found due to sulfur loss. However, the result obtained when the XRF sulfate was substituted for the IC sulfate (Figure 4.9) agree with the hypothesis of some of the sulfate migrating from the Teflon center to the corner and some left the filter. Thus the XRF analysis underestimated sulfate concentration, and the resulting constructed mass was lower than the measured mass.

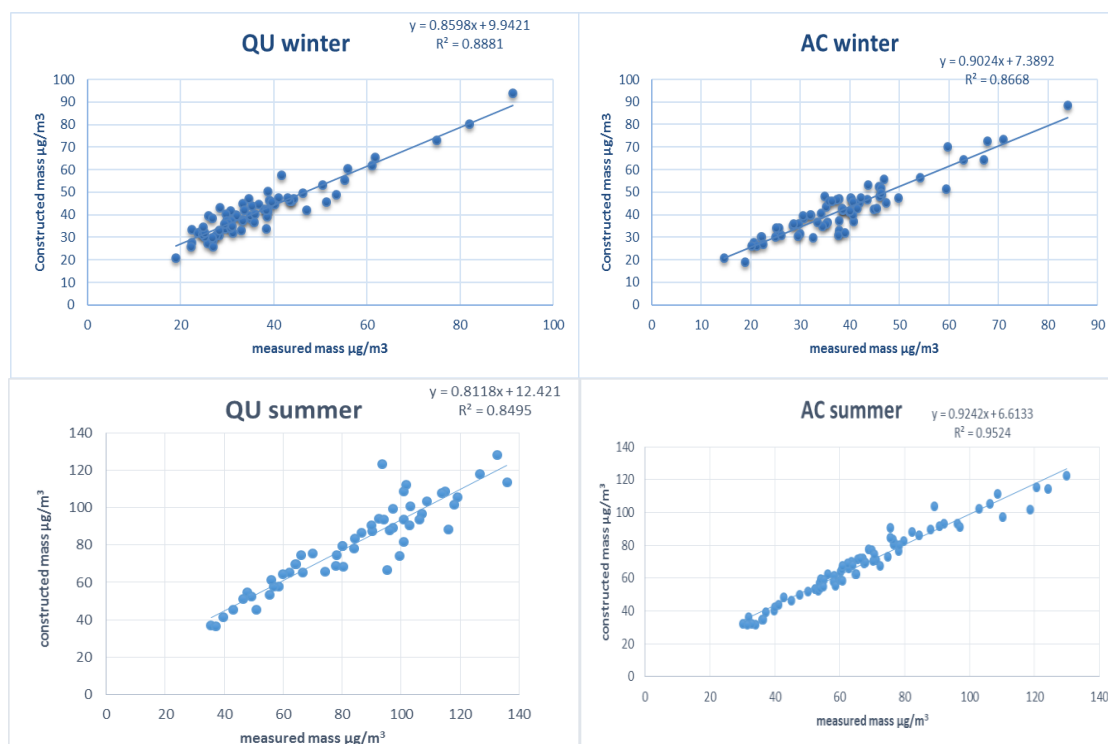


Figure 4.9 Relationship between reconstructed mass and measured mass in the summer season using 3S.

4.4.5 Overall Corrections

The constructed mass equation was adjusted for carbonate, ammonium nitrate and organic carbon. The sulfur correction was not included in the reconstructed method due to the uncertainty around sulfur concentration biased measurements by the XRF and the amount of sulfur that left the Teflon filters. Table 4.9 presents the reference regression equations and the results after the corrections described in this chapter. The percentage difference between the average constructed mass after correction, and the average measured mass was lower in the winter season but did not significantly change for the summer season. The R^2 value also did not show a significant improvement. Overall only a small improvement was observed for the gradient and intercept when all the corrections were completed.

Table 4.10 Results of the linear regression of reconstructed mass (y) against gravimetric mass (x) after correcting for carbonate mass, ammonium nitrate and organic carbon

After and before correction	Campaign	Regression	R ²	%
After correction for carbonate, ammonium nitrate and organic carbon artefact	QU winter	$y = (0.841 \pm 0.379)x + (5.82 \pm 1.489)$	0.8700	-0.1
	QU summer	$y = (0.9852 \pm 0.076)x - (3.3675 \pm 6.6)$	0.7569	-5.5
	AC winter	$y = (1.0314 \pm 0.06)x + (0.8239 \pm 2.46)$	0.8051	+4.2
	AC summer	$y = (1.0606 \pm 0.037)x - (1.7362 \pm 2.68)$	0.9189	+3.5
Before correction	QU winter	$y = (0.8287 \pm 0.038)x + (8.0541 \pm 1.48)$	0.8699	+4.7
	QU summer	$y = (0.9605 \pm 0.073)x - (1.1574 \pm 6.47)$	0.7607	-5.33
	AC winter	$y = (1.0437 \pm 0.064)x + (2.5453 \pm 2.6)$	0.7906	+12
	AC summer	$y = (1.0438 \pm 0.038)x + (0.1364 \pm 2.75)$	0.9142	+4

4.5 Seasonal and Spatial Variation in PM_{2.5} Composition

The chemical mass closure results obtained at both sites and seasons are shown in Figure 4.10. In the winter, crustal components explained 15% ($5.2 \mu\text{g}/\text{m}^3$) and 25% ($8.3 \mu\text{g}/\text{m}^3$) of PM_{2.5} mass at the AC and QU sites, while in the summer, their contribution increased, mainly due to frequent dust events, to 38% ($28 \mu\text{g}/\text{m}^3$) and 43% ($42.6 \mu\text{g}/\text{m}^3$) at the AC and QU sites respectively. The QU site showed a higher percentage of crustal components in both seasons. The increase is attributed to a mixture of windblown dust and particles suspension due to vehicle-induced turbulence from the unpaved surroundings of the QU site. The percentage of the crustal components in Doha city is higher than that found in other European cities as anticipated due to the frequent dust events. For example, in Birmingham city center, the percentage contribution of dust in addition to calcium salts was approximately 8.4% of the total PM_{2.5} mass of $15.8 \pm 3.2 \mu\text{g}/\text{m}^3$, which accounted for $1.33 \pm 0.27 \mu\text{g}/\text{m}^3$ (Yin and Harrison, 2008).

Ammonium sulfate explained 47% ($16.4 \mu\text{g}/\text{m}^3$) and 42% ($14 \mu\text{g}/\text{m}^3$) of $\text{PM}_{2.5}$ mass at the AC site and 41% ($30.2 \mu\text{g}/\text{m}^3$) and 38% ($37.6 \mu\text{g}/\text{m}^3$) at the QU site in the winter and summer respectively. Ammonium sulfate is the dominant fraction in the winter season and the second dominant in the summer which is also as expected due to the high SO_2 emissions from oil refining and gas flaring industry, which is the main industry in Qatar. Ammonium nitrate, however, only accounted for 5% ($1.7 \mu\text{g}/\text{m}^3$) and 3% ($2.3 \mu\text{g}/\text{m}^3$) of $\text{PM}_{2.5}$ mass at the AC site and 7% ($2.3 \mu\text{g}/\text{m}^3$) and 3% ($2.2 \mu\text{g}/\text{m}^3$) at the QU site in the winter and in summer respectively. Ammonium nitrates low abundance in Doha samples is most likely caused by the evaporation of ammonium nitrate from filters due to high ambient temperatures and the equilibrium in atmosphere (Vecchi et al., 2009).

Organic matter and elemental carbon explained 26% ($9 \mu\text{g}/\text{m}^3$) and 23% ($7.6 \mu\text{g}/\text{m}^3$) of $\text{PM}_{2.5}$ mass at the AC and QU sites in the winter season, and 13% ($9.6 \mu\text{g}/\text{m}^3$) and 8% ($8 \mu\text{g}/\text{m}^3$) at the AC and QU sites respectively in the summer season. The high organic particles loading in the winter season according to Vecchi et al., (2008) was likely due to low temperature, which favoured the aerosol particles phase of organic compounds, and to the low mixing layer which allowed the build-up of gaseous precursors and accelerates the formation of secondary organic particles. Organic matter and elemental carbon concentrations in Qatar do not vary by much from the concentration of $5.89 \mu\text{g}/\text{m}^3$ found in $\text{PM}_{2.5}$ in Birmingham city (Yin and Harrison, 2008), or to the levels found in Tianhu city in China which ranged between 7.2 and $12.2 \mu\text{g}/\text{m}^3$ of $\text{PM}_{2.5}$ (Lia et al., 2016). Salt concentrations ranged between 2 and 3% (0.9 to $2 \mu\text{g}/\text{m}^3$) in all seasons; however, the summer season showed a higher salt concentration than the winter probably due to contributions from dust event or the Monsoon phenomenon.

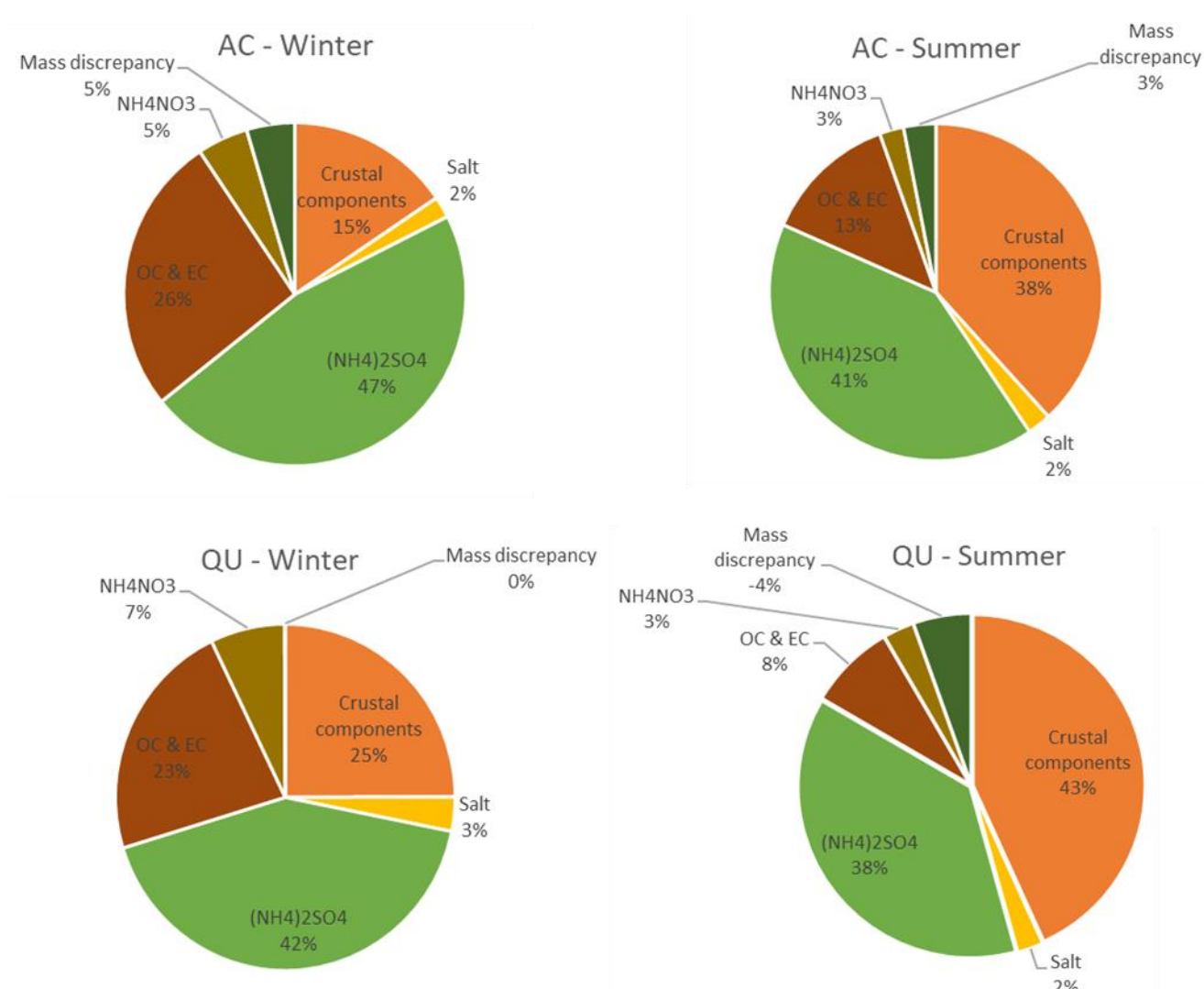


Figure 4.10 Comparison of the percentage composition of PM_{2.5} at the AC and QU sites in the winter and summer seasons

4.6 Conclusion

The result of the mass closure study showed a negative discrepancy (reconstructed mass overestimates the measured mass) in both seasons excluding the QU site in the winter season. The percentage discrepancy for the AC and QU sites were + 12% and + 4.7% in the winter season and + 4% and - 5.33% in the summer season respectively.

In this study, inorganic ions, EC, and OC percentage contribution to PM_{2.5} mass ranged from 45% to 53% in the winter season and from 73% to 78% in the summer season. The inorganic ions, OC and EC species were determined on quartz filters whereas PM_{2.5} gravimetric mass measurements performed using Teflon filters. According to Vecchi et al. (2009), Teflon and quartz filters perform differently toward retaining organic carbon and releasing ammonium nitrate, which is a reason for the mass discrepancy in parallel sampling studies (Vecchi et al., 2009). However, correcting for organic carbon and ammonium nitrate did not show a big improvement in the final solution.

As for the ammonium sulfate, this study showed a large discrepancy between SO₄²⁻ and 3S determined on quartz and Teflon filters respectively. 3S mass concentration determined on Teflon filters using XRF technique were lower than SO₄²⁻ determined on quartz filters using the ion chromatography. The sulfate discrepancy was caused by a combination of filters performance and the analytical technique.

Correcting for sulfate by using 3S instead of SO₄²⁻ in the reconstructing equation did improve R² however it affected both the gradient and the intercept. The improvement in R² was because the gravimetric mass measurements and 3S analysis were done using the same filter. However, the changes in the gradient and intercept were likely caused by the uncertainty in the estimation of the associated ammonium mass concentration and the underestimation of 3S by the XRF technique which was caused by the undetectable amount of 3S that migrate to the corners of the filters.

To avoid large discrepancies for future studies in Qatar, mass measurements and inorganic ions analyses should be performed using the same filter. Sulfate determined by IC on Teflon filters will provide more accurate results and will prevent the issue of biased measurements of

sulfate due to the migration from the filter center. Moreover, limestone (CaCO_3) is one of the common rocks in Qatar hence carbonate measurements should be included in future work.

CHAPTER- 5 SOURCE APPORTIONMENT

5.1 Introduction

Receptor models use ambient species concentration measurements to identify sources and apportion the observed species concentrations from samples to sources by looking at the changes in species correlation with time and finding the optimum solution that explains all observed constituents. The problem is solved by decomposing the species data matrix (species measured in each sample) into two matrices; source profile and source contribution, for each of the assumed sources. This needs to be interpreted subsequently by an analyst using previous knowledge on source profiles, element ratios, wind direction and temporal variation to identify source types and locate their positions from the sampling point (Hopke, 1991).

Positive matrix factorization (PMF) is a multivariate factor analysis tool based on a weighted least squares fit approach (Paatero and Tapper, 1994). In the PMF model, the user chooses the number of factors or “sources”, then the model identifies the species profile of each factor, and the amount of mass contributed by each factor to each sample using the following equation:

$$x_{ij} = \sum_{k=1}^p g_{ik} f_{jk} + e_{ij} \quad (4)$$

where x_{ij} matrix is the concentration of species j in samples i . P is the number of factors contributing to the samples, g_{ik} is the contribution of factor k to sample i , f_{jk} is the concentration of species j in factor profile k , while e_{ij} , the error of PMF model, is the difference between x_{ij} matrix and the modeled matrices g_{ik} and f_{jk} .

The goal of the model is to reproduce x_{ij} matrix by finding values for g_{ik} and f_{jk} matrices for a given P . The values of g_{ik} and f_{jk} matrices are adjusted until a minimum Q “the loss function” for a given P is found (Paatero et al., 2002).

PMF solves the receptor modeling problem by minimizing the loss function Q based on the uncertainty of each observation (Paatero, 1997). The function is given by the following equation:

$$Q = \sum_{i=1}^n \sum_{j=1}^m \left[\frac{e_{ij}}{\sigma_{ij}} \right]^2 \quad (5)$$

where σ_{ij} is an estimate of the uncertainty for the j th species in the i sample, n is the number of samples and m is the number of species. In order to minimize Q , the model solves the problem iteratively using weighted least square method with respect to the G and F matrixes and with the non-negative constraint (Paatero and Tapper, 1994). To have a physically meaningful solution, PMF factor elements are constrained so that no sample can have significantly negative source contributions hence the name “positive”. In addition, PMF uses realistic error estimates to weight each individual point. Therefore values below the detection limit are not rejected and can be engaged in the model with their uncertainty values adjusted, so they have only a minor impact on the solution (Song, 2001; EPA, 2008).

5.2 Estimation of Uncertainty and Data below Detection Limit

A matrix of uncertainty file corresponding to each measurement matrix, is needed as input data which the model uses when minimizing Q value (Reff et al., 2007). Uncertainty files for the model were calculated using the following equation (EPA PMF 5 User Guide, 2014).

$$Unc = \sqrt{(Error_fraction * Concentration)^2 + (0.5 * MDL)^2} \quad (6)$$

- Error fraction was calculated from the check standards that been analysed with the analytical techniques:

$$\text{Error fraction} = (\text{Actual value} - \text{Measured value}) / (\text{Actual value}) \quad (7)$$

- Method detection limit (MDL) was calculated using the formula 3*standard deviation of 10 blanks filter concentrations.

Data below MDL have been adjusted in different ways in many studies. Hung et al., (1999) treated values below MDL as a missing value and replaced them with the mean value. Pollissar et al., (1998) used $(5/6) \times \text{MDL}$ to calculate the uncertainty for values below MDL and in another study, Pollissar et al., (2001) replaced below detection limit data with half detection limit values and missing data with mean concentration. Others would eliminate the species if 50% of the data were below detection limits (Amato, 2016).

5.3 Input Data

Because PMF is a weighted least-squares method, two files are needed for a PMF model; (1) a concentration file and (2) an individual estimate of the uncertainty for each data value. The chemical species that can be included in the PMF solution are determined by the percentage of values below the detection limit; where the species is rejected if 50% of its values are below the detection limit, and the signal to noise ratio (S/N), which determines if a species has a significant signal or its dominated by noise (Paatero and Hopke, 2003). Two calculations are performed by the model to determine S/N: 1) for concentrations equal to or below the calculated uncertainty, the difference between signal and noise is defined as zero, and 2) for concentrations above the uncertainty, the difference between the concentration (x_i) and uncertainty (s_i) is used as the signal. The PMF model calculates the (S/N) ratios based on the following equations:

$$d_{ij} = \left(\frac{x_{ij} - s_{ij}}{s_{ij}} \right) \quad \text{if } X_{ij} > S_{ij} \quad (8)$$

$$\text{and, } d_{ij} = 0 \quad \text{if } X_{ij} \leq S_{ij} \quad (9)$$

$$\left(\frac{S}{N} \right) = \frac{1}{n} \sum_{i=1}^n d_{ij} \quad (10)$$

where d_{ij} is the difference between a species concentrations x_{ij} and associated uncertainties s_{ij} , while n is the number of samples.

When species' concentrations are below their uncertainty; they will have an S/N ratio of 0, whereas species with concentrations more than twice their uncertainty value will have an S/N ratio > 1 . When the model calculates S/N ratios, the user should label species according to their S/N values as “bad” species for an S/N ratio below 0.5, “weak” species for an S/N value between 0.5 and 1, and “strong” species for an S/N ratio above 1.

5.4 The Methodology in Selecting Number of Factors

The total number of factors to extract is a compromise: Choosing too many factors can split a real source profile into two sources; whereas selecting too few factors will combine sources into one factor (Mooibroek et al., 2011). The number of factors that best explains the case under study should show realistic and reasonable source profiles and contributions. For example, a traffic factor should show a weakly profile as anticipated and give reasonable correlations with external tracers, such as NO_2 (Crilley et al., 2017). The chosen number of factors must also be supported by quantitative indicators (Reff et al., 2007). The indicators that have been examined throughout the different attempts to find the optimal number of factors are Q/Q-theoretical, scaled residual distribution, and R^2 for the measured and the modelled $\text{PM}_{2.5}$ mass concentrations.

The Q value is an assessment of how well the model fits the input data. The difference between the modelled Q value and the theoretical Q value gives a good indication of the suitability of the chosen number of factors. As mentioned before the objective function of the model is to minimize the Q value (the residual of each sample/species). Therefore the change in Q value should be monitored when an additional factor is added until the difference between both modelled and theoretical Q values is very small. The theoretical Q value is equal to the total number of good data points in the input array minus the total number of fitted factor elements, and it can be approximated as $nm - p(n+m)$, where n is the number of species, m is the number of samples and p the number of factors fitted by the model (Belis et al., 2013)

The modelled Q value is examined through the process of increasing the number of factors and comparing it with theoretical Q value. However, if the model reaches the appropriate number of factors, any additional factor will not significantly lower the Q value except by additional factor elements. Accordingly, the number of factors in this work was chosen after the difference between the Q value and Q theoretical value decreased significantly, while the stability and rational tests gave the optimum solution. Detailed explanation on stability tests in section 5.5.

The scaled residual is the ratio of residuals to input uncertainties. If species are well modelled then the scaled residual should be distributed symmetrically between +3 and -3 (+3 to -3 scales represent 3 times the residual standard deviation). Otherwise, the residual analysis can indicate that (1) the uncertainty is too small if the scaled residual is outside the range (2) uncertainties are large or that the variable is explained by one unique factor if the scaled residuals are close to zero, and (3) the model fit is not correct if there is a large skewness in the scaled residual distribution. Hence other solutions should be pursued.

The suitability of the selected solution can also be assessed by the correlation between reconstructed mass and observed mass (R^2 value), which should improve when reaching the best solution.

5.5 Solution Stability and Rotational Ambiguity

A number of analyses were performed to evaluate the stability of the final solution and the rotational ambiguity, which is the existence of a vast number of solutions comparable in many ways to the solution produced by PMF and generated by a simple rotation for pairs of matrices with only non-negativity constraint (EPA PMF 5 User Guide, 2014). These analyses include bootstrap analysis, displacement analysis, and FPEAK analysis.

Bootstrap analysis (BS) is used to evaluate the disproportionate influence of a small set of observations on the solution and to assess rotational ambiguity. A bootstrap data set is constructed by sampling blocks of observations from the original data set in random order until reaching the size of the original input data. Then the newly constructed BS data set is processed in the PMF. The BS modelled factors are then compared to the base run factors by mapping the BS factors to the base factor with which the BS factor contribution has the highest correlation (Reff et al., 2007). When no BS factor correlates with a base factor, that factor is considered “unmapped”. Differences in mapping are expected with the absence of few critical observations, but it should not be below 80% for a particular base factor. In case of finding a lower mapping percentage, an additional assessment of the base model results should be performed with the DISP error estimation methods.

Displacement (DISP) is an analysis method that examines the rotational ambiguity for the final solution by assessing source profile values without a noticeable increase in the Q-value. The PMF model adjusts each value in the factor profile for the chosen solution by (dQmax)

values of 4, 8, 15, and 25. The (dQ_{max}) value is the maximum allowable differences between the Q-value in the base run and the adjusted run. Then the model generates new solutions for each dQ_{max} value while achieving the Q-minimum. Assessing the drop in the Q value during DISP and the number of swaps for each dQ_{max} value gives an indication of the stability of the chosen solution. If the drop in Q value was greater than 1% or the swaps occurred for dQ_{max} 4; then it indicates that there is a significant rotational ambiguity and another solution should be looked for.

FPEAK is a parameter used to examine the effect of rotation on the final solution and to assess the rotation ambiguity. Typically values between -1 and +1 are selected by the user, then the model will force rows and columns of G and F matrices to be added or subtracted from each other based on the sign of FPEAK value. The suitability of solution produced by negative and positive rotation is assessed by the Q value, the improvement in the sources profile, source contribution, and subsequent bootstrap. Usually, FPEAK = 0 is the optimum solution with the lowest Q value, and it should be used unless other FPEAK values significantly improve the profiles (Paatero et al., 2005; Reff et al., 2007).

5.6 PMF Analysis

The PMF analysis was performed separately for the different seasons and sites. The results for a different number of factors and multiple values of FPEAK were systematically explored to determine the most reasonable solution. For each case, similar conditions were used for each of the four PMF analysis, including a total of 28 species including weak species, 60 to 70 samples, and an extra 10% to 12% modelling uncertainty in summer and winter respectively to account for errors that are not considered as measurement errors (Mooibroek et al., 2011). One of the study objectives is to understand the influence of dust events in increasing PM concentration in Doha city. Dust events usually peak in the summer season (June to August)

and in the spring season (mid of February to mid-April). The summer campaign covered the period from mid of May to August where dust events occur hence it represents “dust event season”. The winter campaign covered the period from November to mid of February. The months of November, December, and January did not experience dust events however in February four days were affected by dust events at the end of the sampling campaign, hence for the comparison between dust season and non-dust season; the dust events days in the winter campaign were removed from the data for the “non-dust season”.

In addition to the PMF analysis, the openair package in R was used to plot pollution roses to identify source direction (Carslaw, 2013). The polar plot using conditional probability function (CPF) analysis was used to calculate pollutant concentrations larger than the 90th percentile as a function of wind direction and wind speed. Most of the source apportionment studies use polar plots with CPF analysis to identify sources. However, with the Doha samples, the uncertainty results were very high when using polar plots due to the small number of samples therefore only percentile rose plots were used for identifying factors sources.

The CPF percentile plots give the probability that high concentrations of a pollutant came from a particular wind direction using defined wind sectors, which help in identifying unknown new sources in a specific direction (Carslaw, 2013). The CPF percentile rose calculate the number of events with a concentration greater than the 90th percentile and plots them by wind direction as follows:

$CPF = m_y/n_y$, where m_y is the number of samples in the wind sector y with a concentration greater than the 90th percentile, and n_y is the total number of samples in the same wind sector (Carslaw, 2013).

The pollution rose with wind speed function from openair was used also to show how pollutant concentrations depended upon wind speed, which is used here to differentiate local sources where pollutants come at low wind speed, from remote sources where pollutants arrive at high wind speed.

5.7 PMF Results for the Summer and Winter Season

The number of factors in the AC and QU sites were chosen after Q/Q expected decreased significantly while keeping the best stability. In the summer, with seven factors solution at the AC and six factors at the QU sites, most of the scaled residuals were between ± 3.0 and normally distributed, as suggested by Paatero and Hopke (2003). In addition, the predicted concentrations of $PM_{2.5}$ strongly correlated with observed values at both sites with $R^2 > 0.9$. Over 90% of the factors were mapped using bootstrap, which indicates that the factor numbers are most likely to be appropriate. Also, the DISP analysis showed no significant drop in Q value and no swaps on dQmax 4, 8, and 16 levels. Multiple FPEAK values were tested, but they did not appear to improve the source profiles. Therefore base model results for the FPEAK = 0 are presented in this chapter.

The winter PMF solution found 6 factors at the AC site and 5 at the QU site. The number of factors was achieved after finding the lowest Q/Q expected. The bootstrap analysis mapped more than 80% of each BS factors to the base factors. The DISP analysis shows no swaps for dQmax at 4, 8, and 16 values. The correlation between observed and predicted $PM_{2.5}$ was $R^2 = 0.75$ at the AC and $R^2 = 0.68$ at the QU. The final solution found the same factors as in the summer with the exception of a La, Co factor because La element was not within the analysis list of metals in the winter season.

Figures 5.1 to 5.4 display factors fingerprint concentration in percent of individual species contributing to each factor as a stacked bar chart. Factors fingerprints plots (5.1 to 5.4) with the source profile graphs (5.5, 5.12, 5.16, 5.22, 5.23, 5.31, and 5.35) were used to verify unique factor names. The main factors found at all sites and seasons identified as traffic, crustal, secondary sulfate (SS, Ni&V), Lusail city (wide earthwork activity involving the use of non-road mobile machinery), and salt/nitrate. The (Zn & As) source was found only at the AC site at both seasons, whereas (La & Co) appeared in the summer season at the AC and QU sites. The significant change in the mass contribution was due to the influence of frequent dust events in increasing crustal components which affected PM_{2.5} mass concentration and altered sources percentage contribution between both seasons.

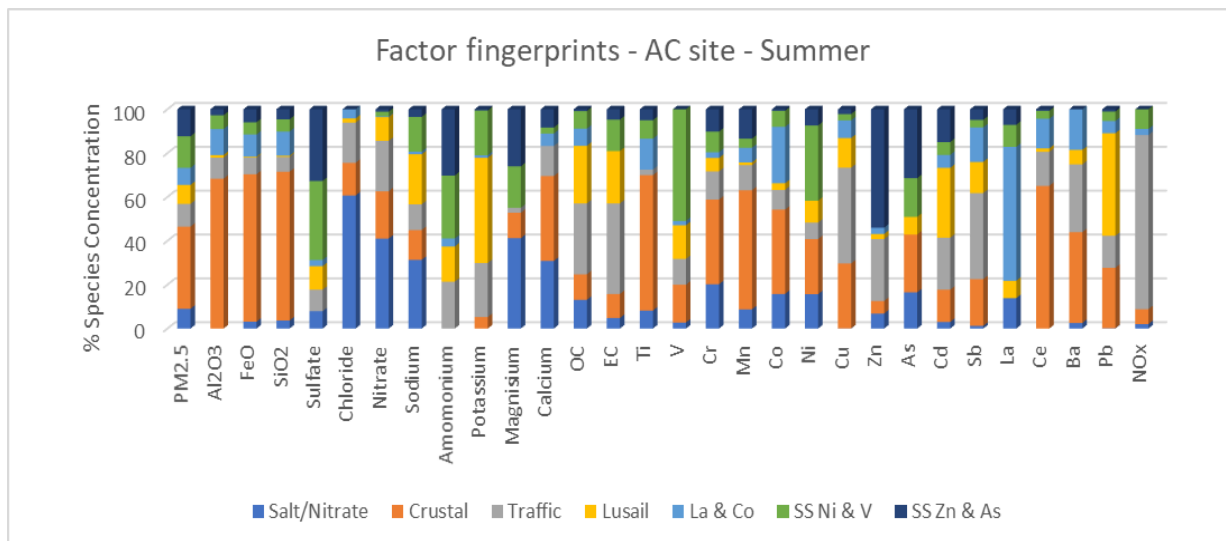


Figure 5.1 Factors finger print concentration in percent of individual species contributing to each factor at the AC site in the summer season.

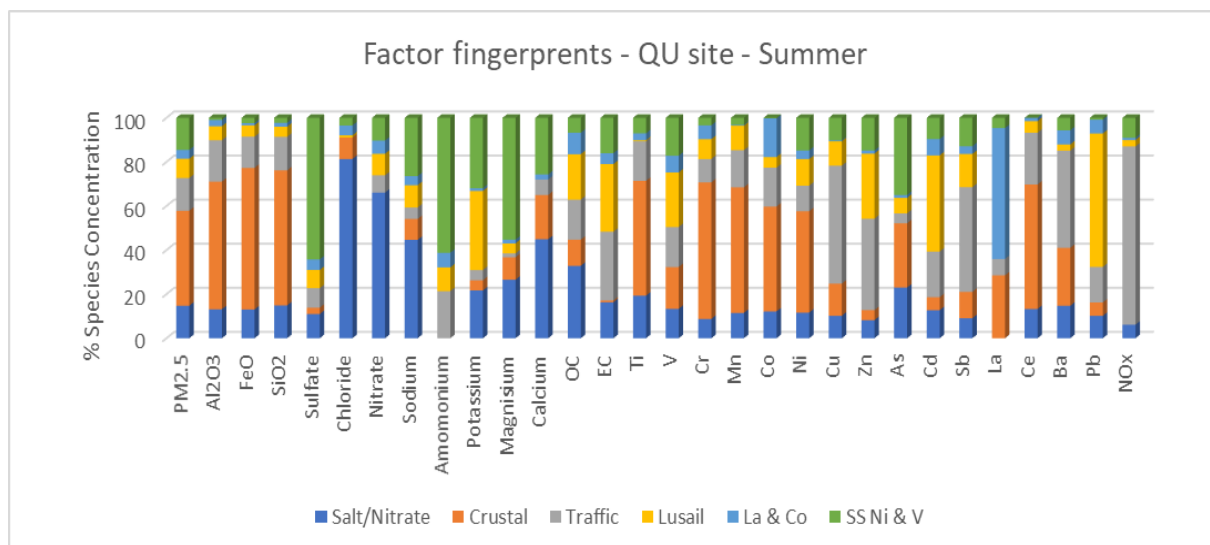


Figure 5.2 Factors finger print concentration in percent of individual species contributing to each factor at the QU site in the summer season.

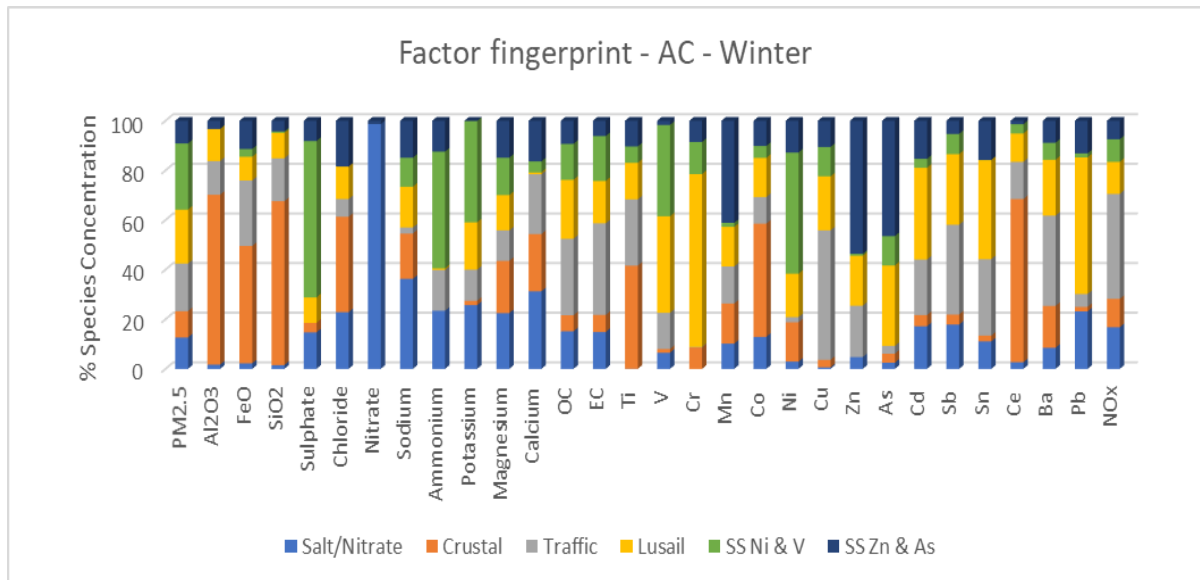


Figure 5.3 Factors finger print concentration in percent of individual species contributing to each factor at the AC site in the winter season.

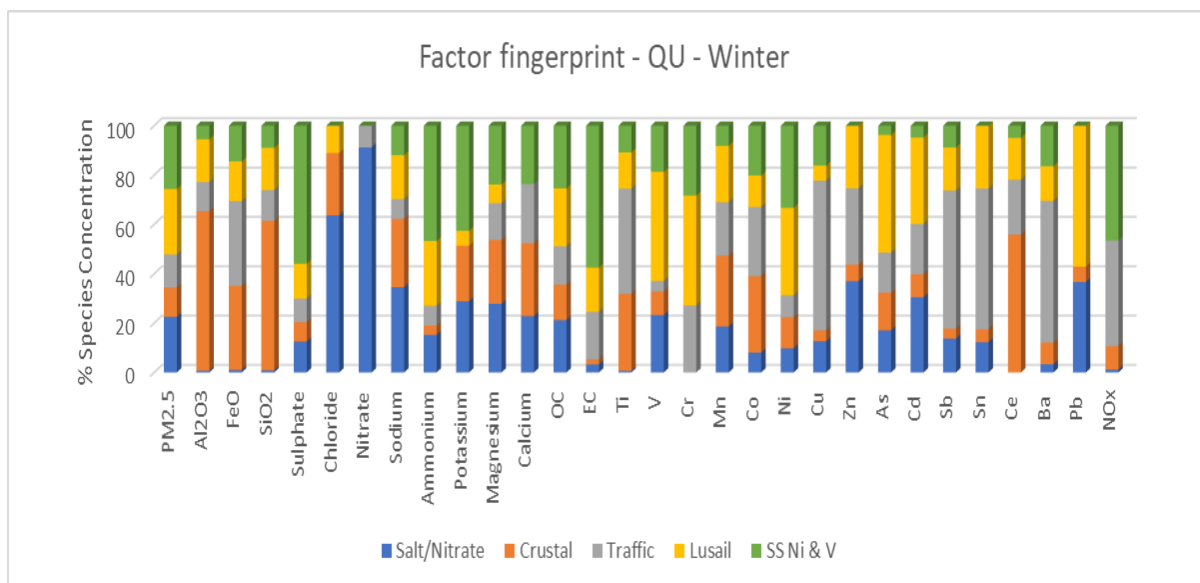


Figure 5.4 Factors finger print concentration in percent of individual species contributing to each factor at the QU site in the winter season.

Tables 5.1 and 5.2 summarise the PMF solutions for the AC and QU sites in the winter and summer seasons.

Table 5.1 Summary of the PMF solutions at the AC and QU sites in the summer season.

Factors NO.	Results of the summer season					
	The AC Site			The QU Site		
	Sources	%	µg/m ³	Sources	%	µg/m ³
1	Traffic	13.5	9.98	Traffic	14.9	14.7
2	Crustal	34.8	25.65	Crustal	43.1	42.66
3	SS(Ni&V)	21.43	15.8	SS(Ni&V)	14.5	14.39
4	Lusail	9.4	6.89	Lusail	8.7	8.65
5	Salt/ Nitrate	8.7	6.43	Salt/Nitrate	14.7	14.59
6	Zn&As***	5	3.7			
7	La&Co	7	5.17	La&Co	4	4
PM _{2.5}	73.74 µg/m ³			99.02 µg/m ³		

Table 5.2 Summary of the PMF solutions at the AC and QU sites in the winter season.

Factors NO.	Results of the winter season					
	The AC Site			The QU Site		
	Sources	%	µg/m ³	Sources	%	µg/m ³
1	Traffic	19.2	6.69	Traffic	13.4	4.43
2	Crustal	10.6	3.7	Crustal	11.9	3.94
3	SS(Ni&V)*	26.7	9.3	SS(Ni&V)	25.6	8.48
4	Lusail**	21.7	7.59	Lusail	26.6	8.79
5	Salt/ Nitrate	12.7	4.42	Salt/Nitrate	22.5	7.46
6	Zn&As	9.2	3.19			
PM _{2.5}	34.93 µg/m ³			33.12 µg/m ³		

*SS refers to secondary sulfate aerosols

**Lusail factor named by Lusail city because the emissions at both sites pointed at Lusail city which witnesses earthwork activities involving the use of non-road mobile machinery.

*** The value presented was adjusted (see 5.7.4 for more details)

5.7.1 Traffic Factor

The traffic factor appears for both sites with the same profile. High NO_x, OC, EC, Cu, Sb, Ba, and Zn characterize the factor in addition to elevated concentrations of Fe and Sn in the winter season (Figure 5.5). Nitrogen oxide, elemental carbon, and organic carbon are emissions of vehicles exhaust (Pant and Harrison, 2013). NO_x is formed through the combustion of fuel containing nitrogen and through high-temperature regions via the Zeldovitch mechanism; as (N₂) and oxygen (O₂) molecules in the combustion air disassociate into their atomic states, they start a series of reactions producing thermal NO_x, whereas OC and EC are produced during combustion of fuel in low oxygen conditions (O'Donoghue., 2010).

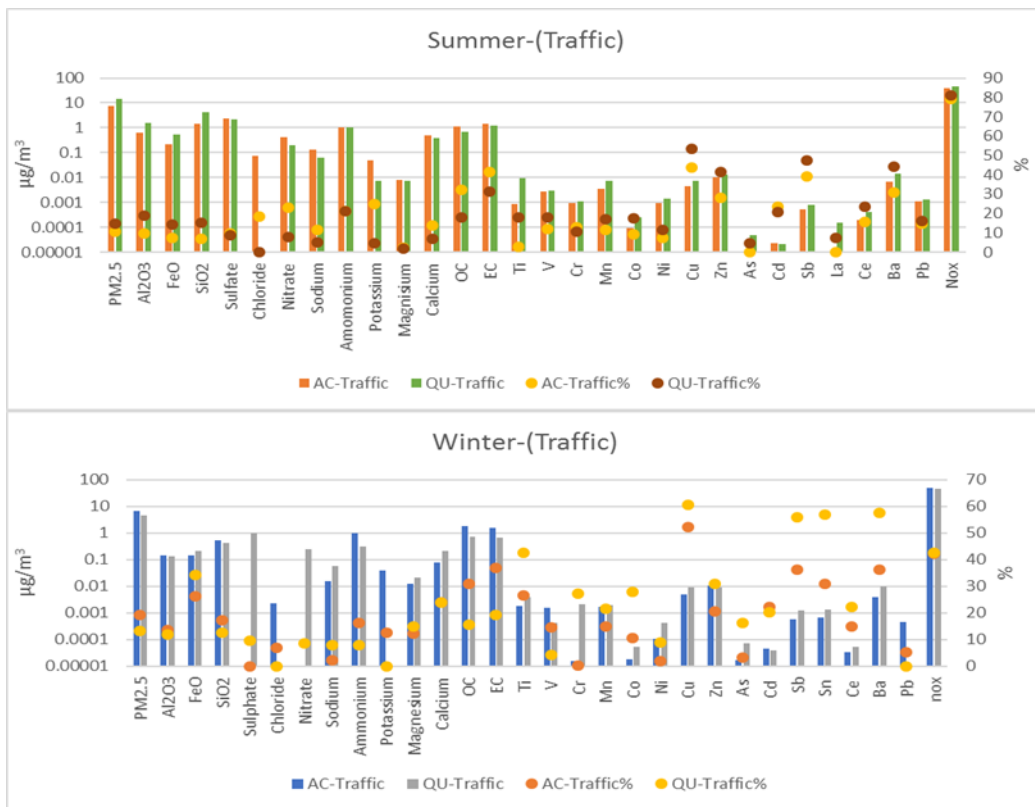


Figure 5.5 Source profile of Traffic factor in the summer and the winter seasons.

The factor also includes notable contributions from elements associated with brake wear particles, e.g., Sb, Cu, Fe, Zn, Fe and Ba (Thorpe and Harrison, 2008). The Cu/Sb ratios of 7.85 and 8.9 at the AC and QU sites at the summer time and 8.7 at and 7.17 at the AC and QU sites in the winter are comparable to the range of brake wear ratios of 8.5 to 8.9 in Europe (Amato et al., 2009). In addition to the high Zn concentration which is a marker for tire wear (Pant and Harrison, 2013), Fe element was reported as the most abundant metal in brake wear (Adachi and Tainosho, 2004). This metal is clearly appearing in the winter, but its concentration cannot be distinguished from other crustal components in the summer season, probably due to the load of crustal components from dust events. According to Chester et al., (1999), when sufficient crustal material is present in the air; the enriched elements can appear as non-enriched elements.

In the summer, traffic factors at the AC and QU sites were significantly correlated ($R^2 = 0.764$, $p < 0.01$), whereas in the winter they were weakly correlated $R^2=0.08$. In the winter season, the traffic factor at the AC site was plotted against the traffic factor at the QU site and coloured by wind direction (Figure 5.6). The regression plot showed two relationships: 1) days where traffic at the AC site has a higher mass contribution as the wind comes from north north-west versus 2) days when the QU site has a higher mass as the wind arrives from south-east direction.

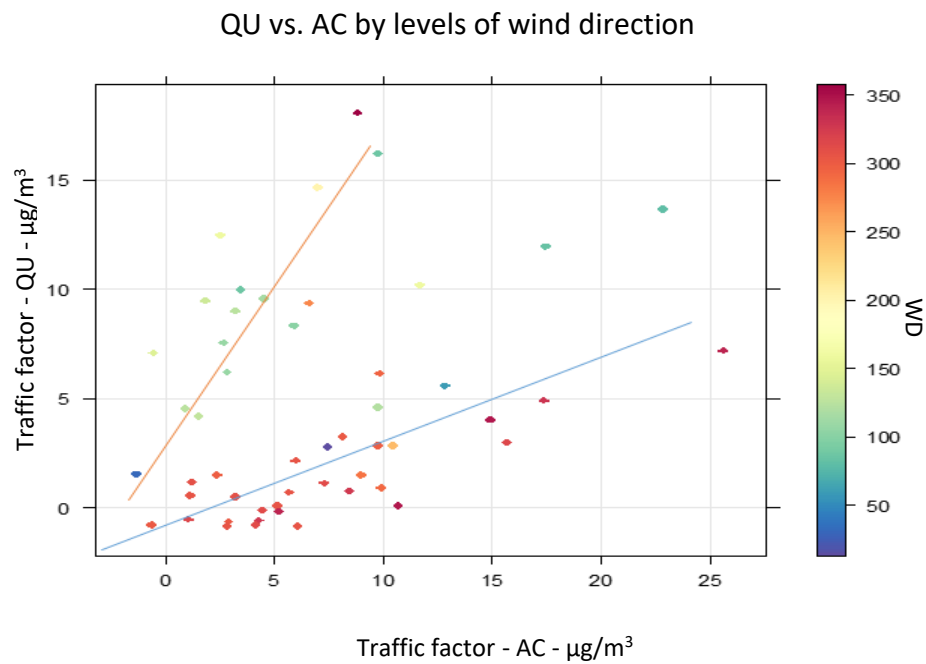


Figure 5.6 Scatter plot for traffic factor at the QU and AC sites, coloured by wind direction



Figure 5.7 Location map of the monitoring sites. Red arrow shows traffic emissions coming from the area in between the QU site and the AC site toward the AC site from north-northwest direction showing a higher traffic contribution at the AC site, and the blue arrow shows emissions coming from the area in between the AC site and the QU site toward QU site from southeast direction, showing a higher traffic contribution at the QU site

When the wind at the AC site blows from a north north-west direction, arriving from the area in between the QU and AC sites as shown by the red line in Figure 5.7, the traffic source showed a higher traffic mass concentration at the AC site as result of the accumulation of background emissions along the distance from the QU site to the AC site. However, when the wind reverses its direction, the situation reversed as well, showing a higher concentration at the QU site. The data were divided based on their concentration to days when the particle concentrations of the traffic sources were highest in the AC site, and the days at which the QU site had the highest concentrations (Figure 5.8 & 5.9). The majority of points showed a higher concentration at the AC site over the QU site. The correlation between both sites was strong after dividing the data showing ($R^2=0.62$, $p<0.01$) for days where AC has higher traffic contribution and ($R^2=0.7$, $p<0.01$) for days where QU has higher traffic contribution.

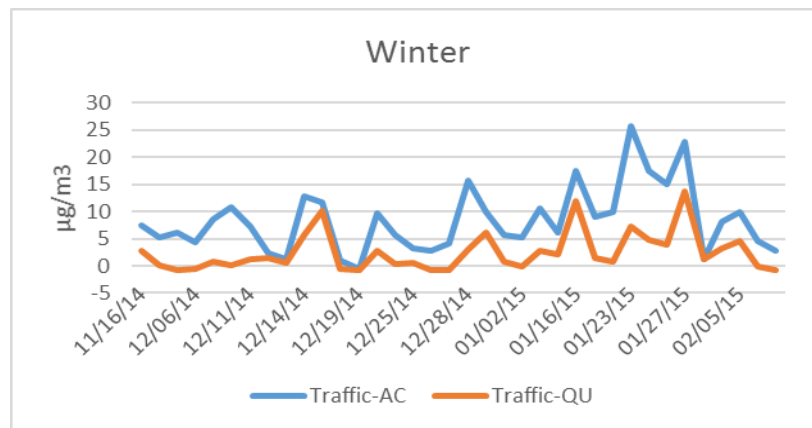


Figure 5.8 Time series of traffic factor in the winter season showing a higher concentration at the AC site

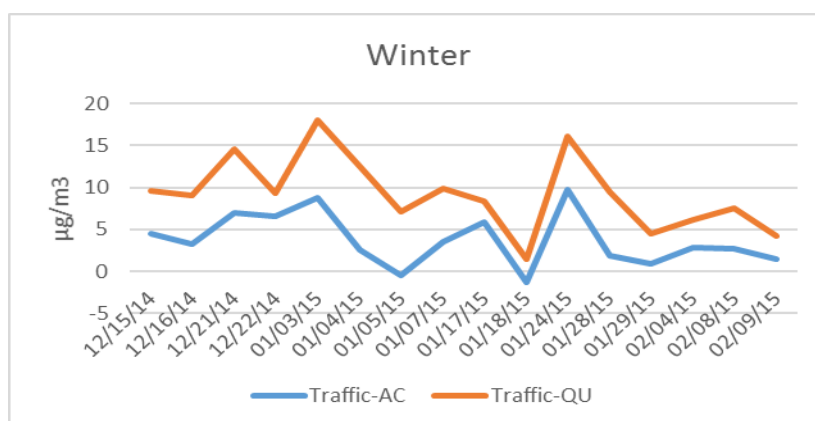


Figure 5.9 Time series of traffic factor in the winter season showing a higher concentration at the QU site

The CPF 90th percentile rose analysis shown in Figure 5.10 illustrates two combined roses; the orange coloured rose represents the summer season while the blue rose represents the winter season. At the AC site, the roses pointed at the area from northwest west to southeast covering Al-Corniche Street, which is one of the busiest roads in Doha city.

At the QU site, different seasons showed different directions for traffic emissions (Figure 5.11). Jelaiah Street south and Al-Jamaa Street east of the sampling site are the busiest roads at the QU site. Therefore, it is expected to contribute to the traffic factor. In the winter season with the wind coming from every direction (Figure 3.3), Jelaiah and Al-Jamaa streets were the highest contributors. However, in the summer season, the prevailing wind in Qatar is from the north-west direction (Figure 3.3), and there is almost no contribution from south and south-west, which explains the absence of traffic emissions from Jelaiah Street.

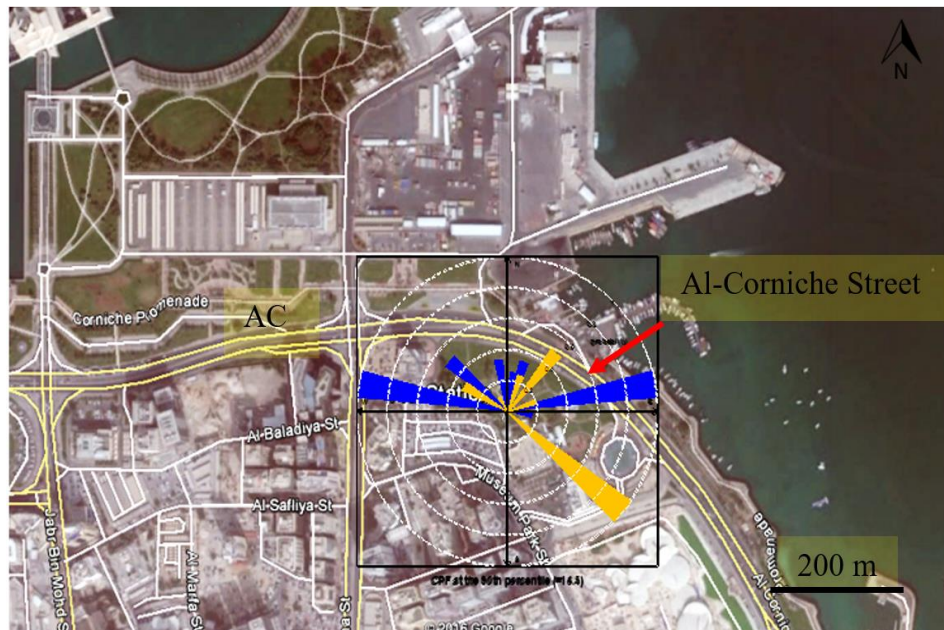


Figure 5.10 CPF 90th percentile rose at the AC site in summer (orange) and winter (blue) showing the direction of traffic source

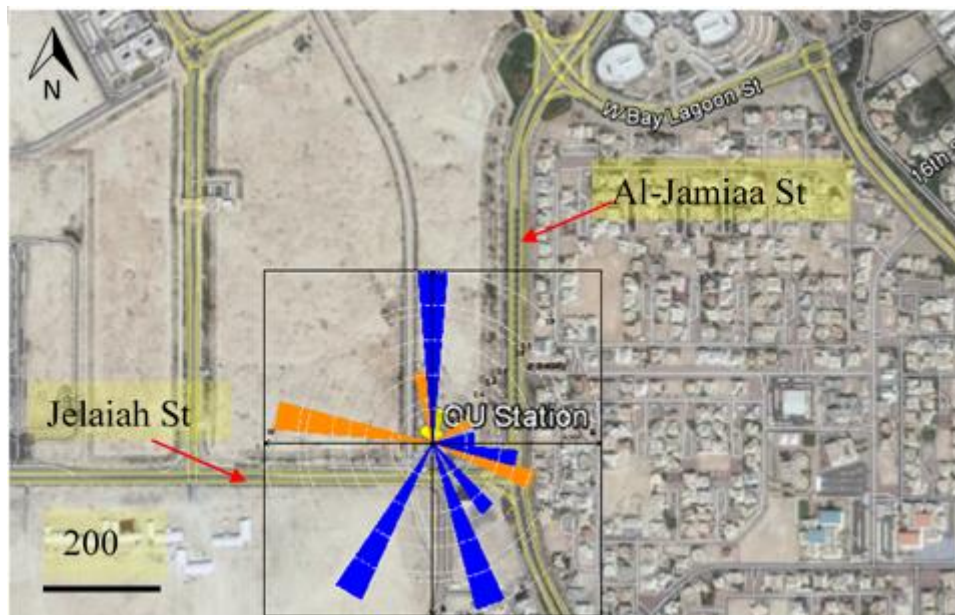


Figure 5.11 CPF 90th percentile rose at the QU site in summer (orange) and winter (blue) showing the direction of traffic source

In the summer season, the AC traffic factor accounted for $9.98 \mu\text{g}/\text{m}^3$ (13.5 %) whereas the QU traffic factor accounted for $14.7 \mu\text{g}/\text{m}^3$ (14.9%). Traffic source profile at the QU site in the summer season, showed higher crustal components (Figure 5.5) than the AC site. As described in chapter (2), the QU site is a vacant unpaved area thus during the summer time with high temperature and scarcity of precipitation; soil becomes dry, light and easy to be suspended by wind and vehicles turbulence (Pye, 1987). However, at the AC site, the surrounding area are either paved or planted, therefore, no significant contribution is expected from crustal components due to vehicles turbulence. In the winter season, the traffic factor contributed $6.7 \mu\text{g}/\text{m}^3$ (19.2%) at the AC site and $4.43 \mu\text{g}/\text{m}^3$ (13.4%) at the QU site. The influence of precipitation and low temperature in wintertime preserved surface crust moisture and reduced the effect of crustal suspension by wind and vehicles turbulence hence with the absence of crustal components contribution, the AC site showed higher traffic contribution as anticipated.

5.7.2 Crustal Factor

A factor was attributed to crustal components at the AC and QU sites based on the factor profile which was characterised by high fractions from typical crustal elements such as Al, Si, Fe, Ti, Mn, Ba, Ce and Ca^{2+} (Andrews et al., 2000), (Figures 5.12).

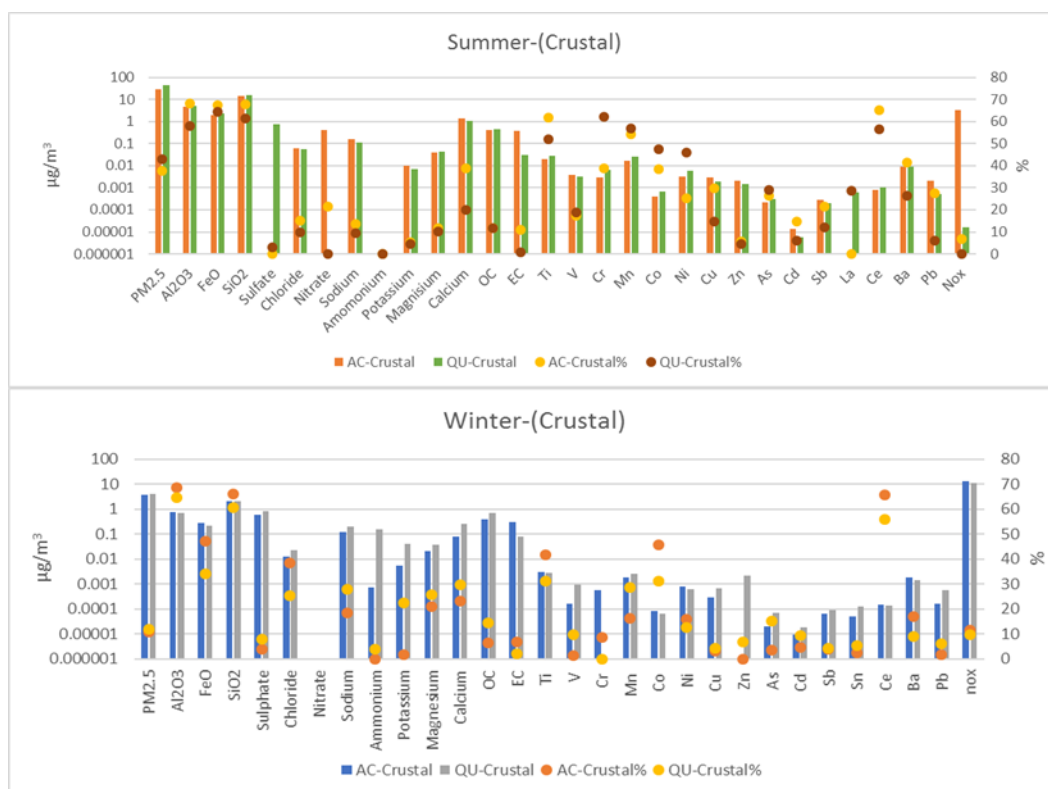


Figure 5.12 Source profile of crustal factor in the summer and the winter seasons.

Crustal factor's elements enrichment factors were compared to the enrichment factors of the upper continental crust (UCC) values to ensure that the factor is related to continental crust and not enriched by anthropogenic sources. The EF gives the degree of enrichment of trace elements in atmospheric aerosols by comparing the ratio of elements concentration in aerosols to the same ratio in crustal or marine samples (Brimblecombe, 1986). An enrichment factor

below 10 indicates that elements are not enriched. Figure 5.13 showed that crustal factor elements are below 10 and they have a typical ratio of an average upper continental crust (Mason, 1966 and Taylor & McLennan, 1985).

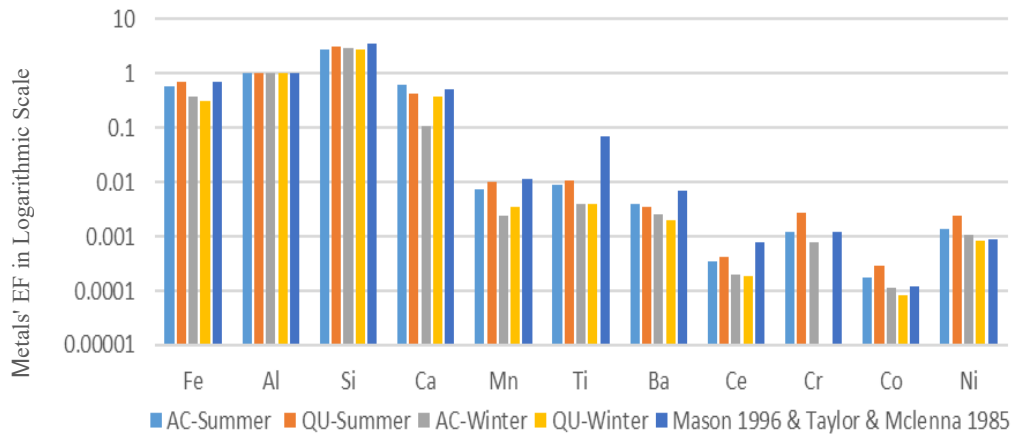


Figure 5.13 EF of crustal components at all sites normalized to aluminium versus EF in the upper continental crust (Mason., 1966, and Taylor & McLennan, 1985)

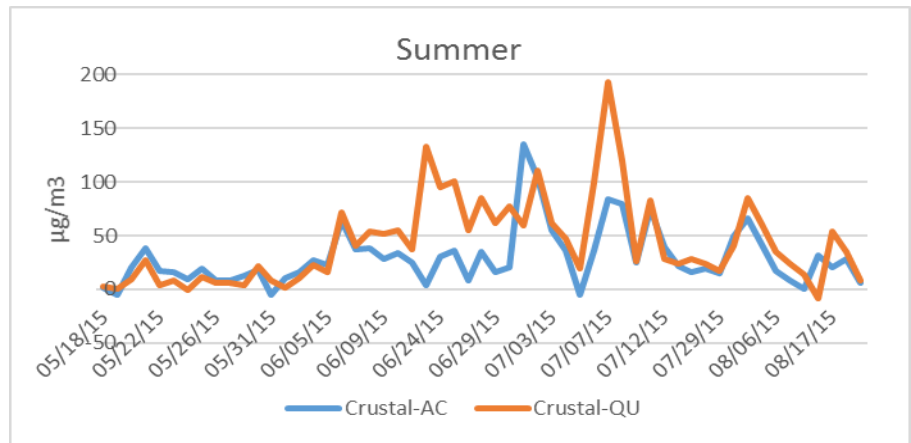


Figure 5.14 Time series of crustal factor in the summer season at the QU and AC sites

In the summer season, crustal factors at both sites were correlated ($R^2 = 0.44$, $p < 0.01$). Both sites showed a similar trend apart from June and July (the months when the frequency of dust events increases) (Figure 5.14). The QU results showed a higher crustal concentration during

June and July compared to the AC site, which represents the effect of strong laden-dust wind in suspending and introducing crustal particles from the unpaved surrounding of the QU site to the crustal factor, accordingly causing a weaker correlation between sites.

At the AC site, the crustal factor accounted for 37% of $PM_{2.5}$ mass while in the QU site accounted for 43%. The high crustal components at the QU are contributed by the loose soil from the unpaved surrounding area. The percentile rose analysis for the AC and QU sites (Figure 5.15) shows that the contribution at both sites was from north-west which is the prevailing wind in Qatar and the direction of Al-Shamal dust storms, and more significantly the factor peaked during the Al-Shamal dust storms season in June and July. The CPF 90th percentile plot for the AC site (Figure 5.15c) shows a contribution from the north-east east direction at 70°, which occurred on the 6th of June 2015 at both locations. However, this occasion did not appear in the QU site (Figure 5.15d). The dust event on the 6th of June contributed 63 and 72 $\mu g/m^3$ to the crustal factor at the AC and QU sites respectively. At the QU site, there were more days when the crustal concentration was above 72 $\mu g/m^3$. Hence the 6th of June dust event mass concentration was not within the 90th percentile at the QU site.

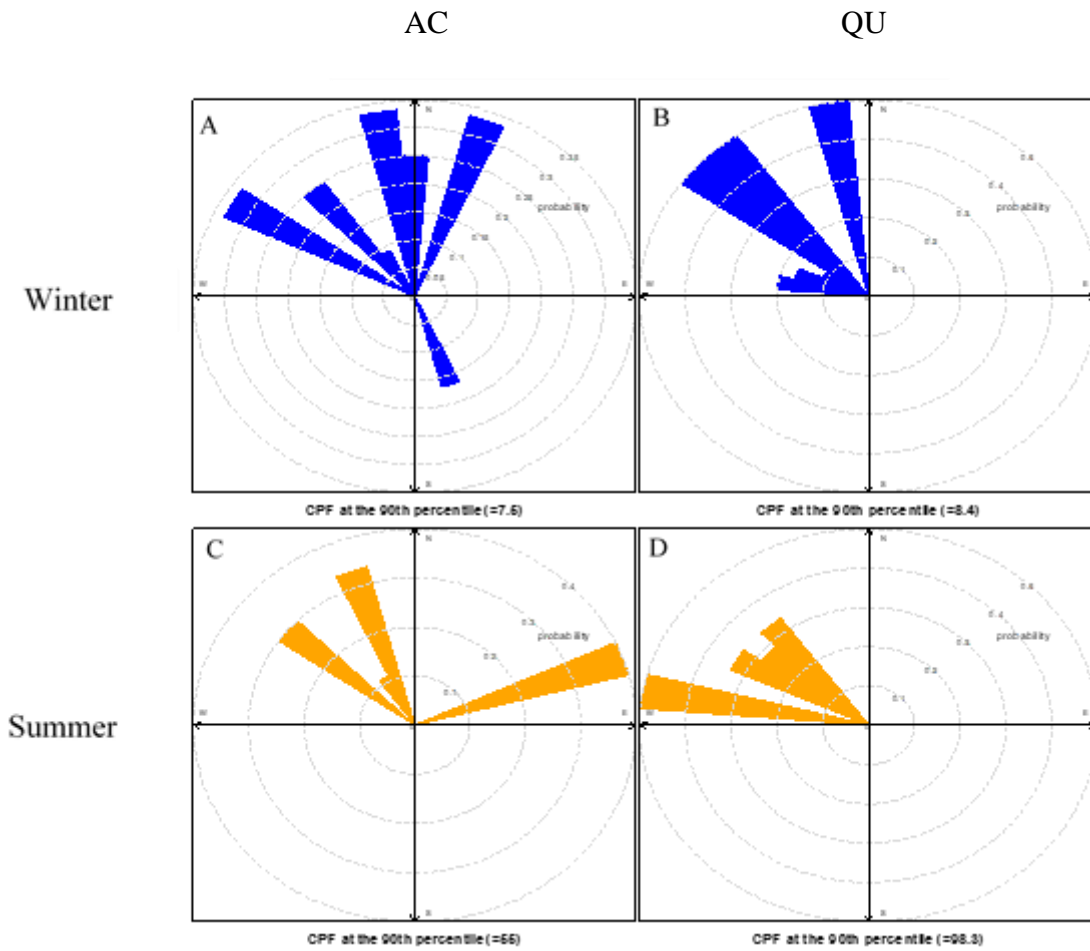


Figure 5.15 CPF 90th percentile rose showing the direction of the crustal factor at the AC and QU sites [A&B] in winter, and at the AC and QU sites [C&D] in summer respectively.

In the winter, the correlation between crustal factors at the AC and QU was $R^2 = 0.61$, $p < 0.01$.

In contrast to the summer findings, there was no big difference between the crustal factors contribution at QU (11.9%) and AC (10.6%) due to the low ambient temperature and occasional rainfall role on preserving crust moisture which kept the crust at the QU surrounding from suspension, in addition to the absence of laden-dust wind which had a huge impact on crustal material resuspension at the QU site in the summer season.

The crustal contribution differs greatly for both season; in the summer, crustal fraction accounted for 42.6 and 25.65 $\mu\text{g}/\text{m}^3$ at the QU and AC sites (Figures 5.42 & 5.43), while in the winter, it accounted for 3.9 and 3.2 $\mu\text{g}/\text{m}^3$ at the QU and AC sites (Figures 5.44 & 5.45).

Several points can be understood from the spatial and seasonal variation in crustal factor mass contribution:

- i) The difference of $22.5 \mu\text{g}/\text{m}^3$ between the AC crustal factors' mass contribution between the winter and the summer represents the dust event contribution to the $\text{PM}_{2.5}$ increase.
- ii) The difference between the crustal factors' values at the AC and QU sites in the winter season represent the extra addition of $0.6 \mu\text{g}/\text{m}^3$ contributed from the unpaved area around QU site.
- iii) However, the difference between the QU and AC values in the summer season, which accounted for $17 \mu\text{g}/\text{m}^3$, explains the effect of dust event on the re-suspension of loose surface crusts in the dry, warm weather.

5.7.3 Sea Salt/ Nitrate Factor

In the summer season, sea salt/ nitrate factors were characterised by notable contributions from typical salt elements Na, Mg^{2+} , Cl^- and nitrate (Figure 5.16). The factors at both sites were significantly correlated ($R^2 = 0.65$, $p < 0.01$). In the summer season, Na^+ and Cl^- concentrations were 0.35 and $0.24 \mu\text{g}/\text{m}^3$ at the AC site and 0.53 and $0.43 \mu\text{g}/\text{m}^3$ at the QU site respectively. The Cl^-/Na^+ ratio in the sea salt factor of 0.67 and 0.81 at the AC and QU sites respectively were lower than the expected ratio of fresh seawater of 1.8 , indicating an ageing of the marine source particles and a loss of chloride.

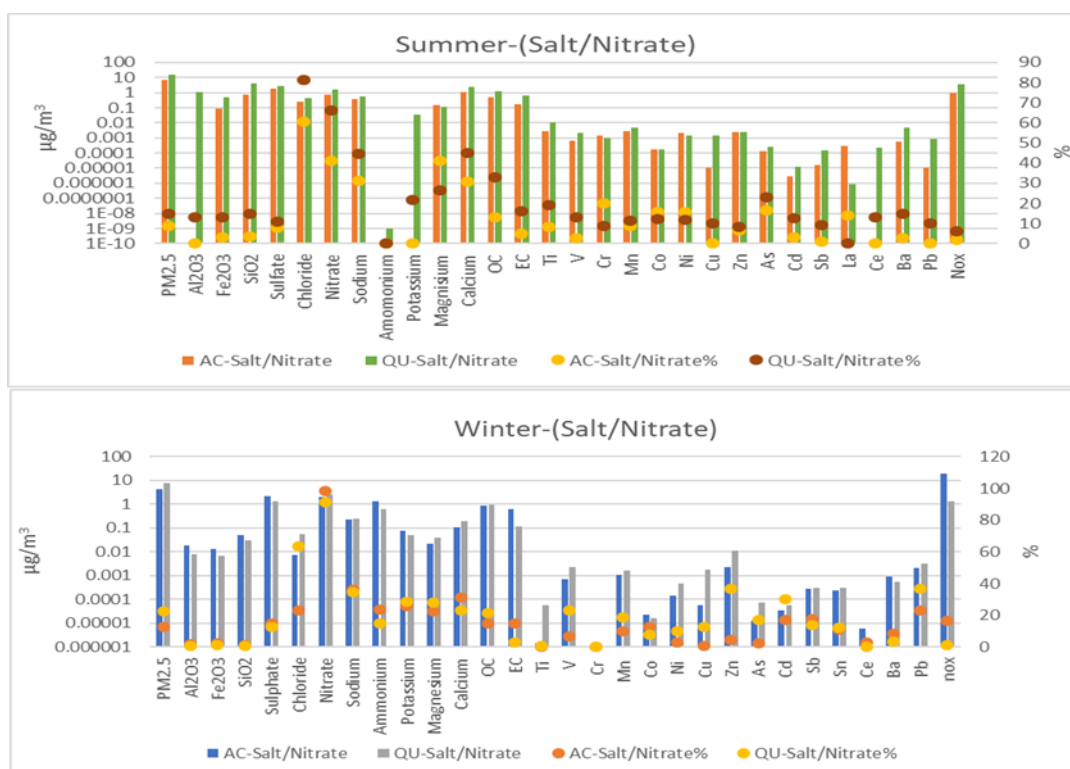


Figure 5.16 Source profile of sea salt/ nitrate factor in the summer and the winter seasons.

The ratios found in sea salt/nitrate factor are comparable to the ratio of 0.67 found in the coast of Owase city in Japan (Okada, 1978), and to the ratio of 0.77 and 0.66 found at an urban site and urban background site respectively in Italy (Cesare et al., 2016). According to Okada (1978), the low ratio is either due to the depletion of Cl^- or due to the introduction of Na^+ from crustal sources. Okada (1978) calculated the Na^+ contribution from crustal sources, based on Ca^{2+} concentrations in the aerosols and the ratio of $\text{Na}^+/\text{Ca}^{2+}$ in crustal rock from Mason (1958), to be 15% of the total Na^+ , which only increased Cl^-/Na^+ ratio from 0.67 to 0.78, and which still does not explain the low ratio. In this study, a Cl^-/Na^+ ratio of 0.67 and 0.81 at the AC and QU sites respectively were calculated in the sea salt factor. Hence the effect from crustal Na^+ should be negligible since Na^+ from crustal components should be assigned to crustal factor and should not influence the Cl^-/Na^+ ratio at the sea salt factor.

Chloride depletion is caused by the reaction of sea salt with HNO_3 and H_2SO_4 (Okada, 1978; Cesare et al., 2016). To investigate Cl^- uptake by nitric and sulfuric acids, the Cl^-/Na^+ ratio was calculated using Cl^- and Na^+ daily concentrations in the original dataset and compared with the sum of non-sea salt sulfate and nitrate concentration. The non-sea salt sulfate (nssSO_4^{2-}) was calculated based on the initial $\text{SO}_4^{2-}/\text{Na}^+$ ratio of 0.25 for sea salt particles as follow:

$$\text{nssSO}_4^{2-} = \text{SO}_4^{2-} - (0.25 * \text{Na})$$

Figure 5.17 shows a declining relationship between the Cl^-/Na^+ ratio with increasing the sum of non-sea salt sulfate and nitrate, indicating chloride depletion. Also, a high value of nitrate and sulfate was found in the salt factor which prove the formation of nitrate and sulfate salt, as well as chloride ion volatilization which is caused by the reaction between sea-salt aerosols and anthropogenic emissions such as NO_2 , nitric acid and sulfuric acid (Peters and Ewing, 1996; ChunXiang, 2010). A high nitrate percentage in the sea salt factor has also been found in other studies, e.g., London summer 2012 (Crilley et al., 2017), and in the coastal area in Korea (Choi et al., 2013), and has been attributed to anthropogenic contributions.

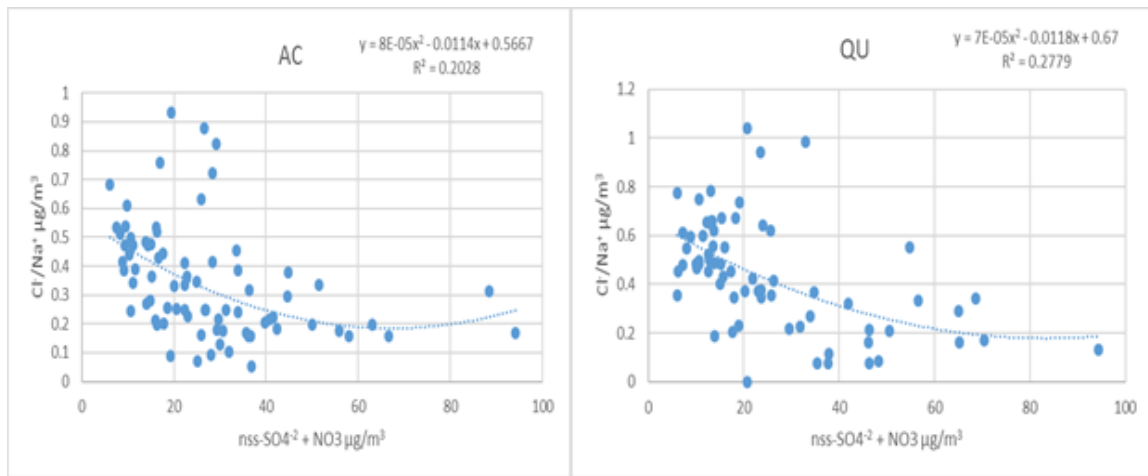


Figure 5.17 Scatter plot for Cl^-/Na^+ ratio against the sum of non-sea salt sulfate and nitrate at both sites in summer

In the summer season, at the AC and QU sites, the application of the CPF analysis showed that apart from the 30th of July, the source contribution of sea salt/nitrate factor came from two main directions (Figures 5.18). Sea salt/nitrate factor came from the north-east direction pointing at Gulf Sea, whereas the highest concentration was from the north-west. According to Fan and Toon (2010) wind speed is the main factor that controls sea salt aerosols (SSA) fluxes, and that sea salt lifting, like desert dust lifting, depends on wind power. The prevailing wind during the summer campaign was from the north-west direction and is likely the cause of high sea salt contribution, though the closest coastline to Doha is to the east.

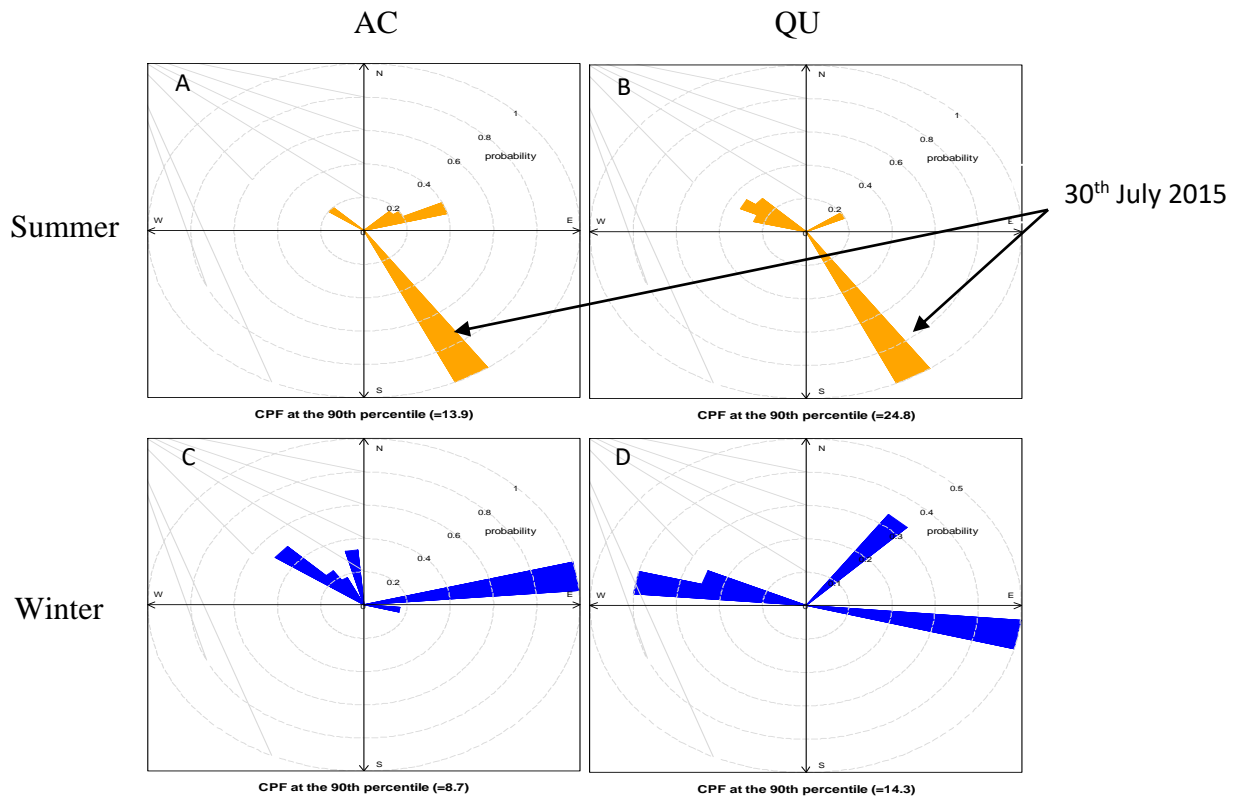


Figure 5.18 CPF 90th percentile rose showing the direction of sea salt/nitrate source at the AC and QU sites [A&B] in winter, and at the AC and QU sites [C&D] in summer respectively

As for the 30th July 2015 occasion, the air mass arrived from the south-east, the direction of the Arabian Sea. The air mass is likely to be affected by the summer monsoon season over the Arabian Sea. Therefore it is loaded with salt particles. When it passes over the Arabian

Peninsula land, it lifted dust and transported to Qatar, which caused an increase in salt and crustal factors.

In the winter season, salt factors at both sites were characterised by a high percentage of salt minerals such as Na^+ , Mg^{2+} , Cl^- , K^+ , and Ca^{2+} in addition to NO_3^- , NH_4^+ , OC, and EC. The factors were weakly correlated ($R^2 = 0.29$, $p < 0.01$). Figure 5.19 shows the time series of the salt factor at the AC and QU sites. The period from 18-24/12/2013 showed an increase in the QU salt factor, as a result of high nitrate concentrations (Figure 5.20). Removing the effect of those days; increase the correlation between the sea salt factors at both sites to ($R^2 = 0.58$, $p < 0.01$).

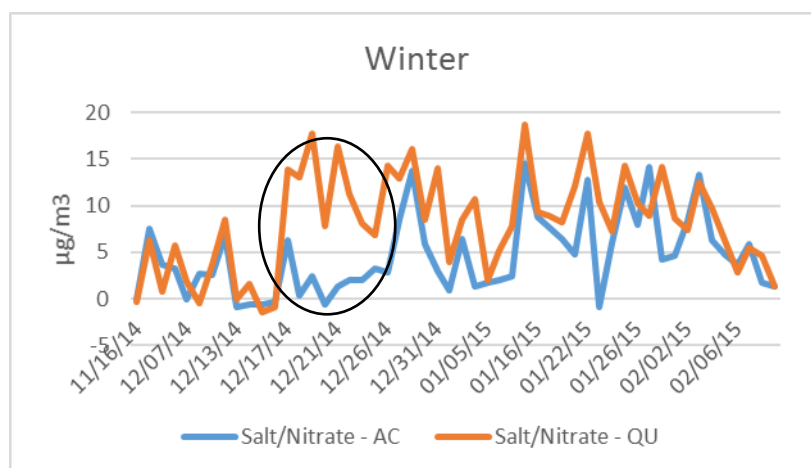


Figure 5.19 Time series of sea salt/nitrate factor in the winter season at both sites. The circle shows the time when the salt factor concentration at the QU site was higher than at the AC site

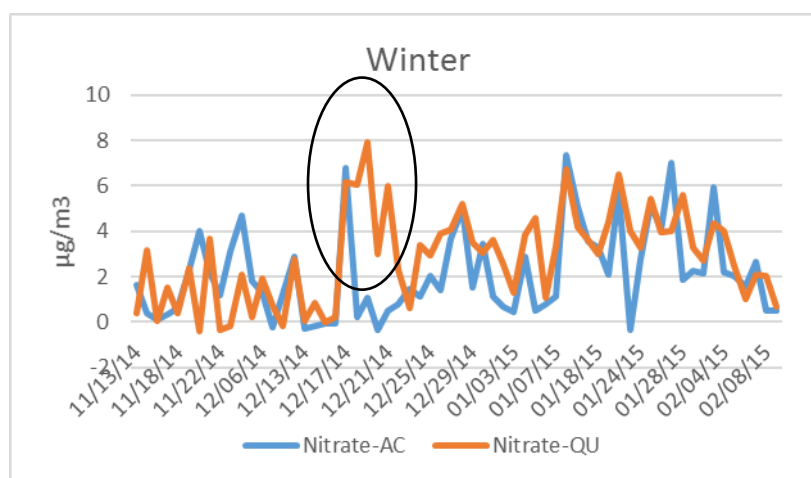


Figure 5.20 Time series of nitrate in the winter season at the QU and AC sites. The circle shows the time when nitrate levels increased at the QU site

In winter time, Na^+ and Cl^- concentrations were 0.23 and $0.007 \mu\text{g}/\text{m}^3$ at the AC site and 0.24 and $0.057 \mu\text{g}/\text{m}^3$ at the QU site respectively. The salt factor showed a depletion of Cl^- ions by one order magnitude compared with the concentration of Na^+ ions. The Cl^-/Na^+ ratio was much lower in winter time (0.03 and 0.23 at QU and AC sites respectively) than in the summer measurements. The decline of Cl^-/Na^+ with sulfate and nitrate behavior was not clear. In the winter season, the chloride concentration was very low hence no relationship was found between Cl^-/Na^+ ratio with sulfate and nitrate (Figure 5.21).

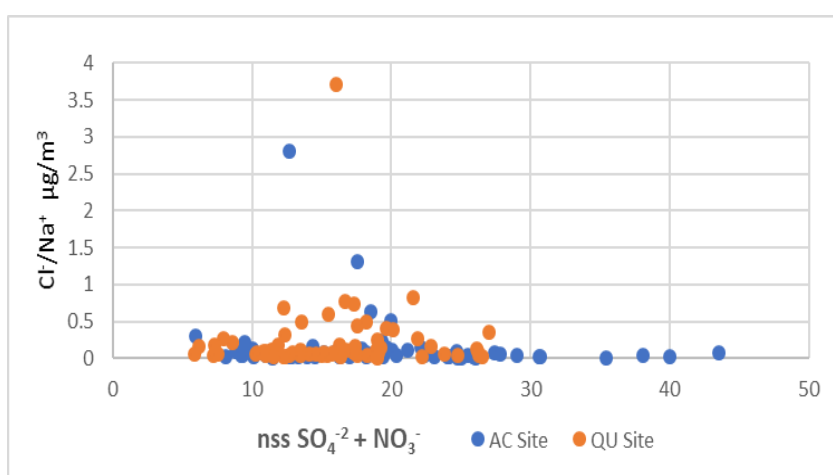


Figure 5.21 Scatter plot for Cl^-/Na^+ ratio against the sum of non-sea salt sulfate and nitrate at the QU and AC sites in the winter season.

The presence of nitrate, OC, and EC in the salt source profile (Figure 5.16), support the suggestion of anthropogenic emissions mixing with sea salt or condensation of these compounds on salt particles (e.g. marine combustion sources). Although the nearest coast is to the east, CPF 90th percentile rose (Figure 5.18), shows more frequent salt contribution from the north-west direction associated with strong north-westerly wind. The contribution of salt from NW direction gives more time for sea salt coming from the remote north-west coast to interact with polluted air masses from land, which could explain the depletion of chloride. This source is a mixture of aged salt with anthropogenic contributions.

5.7.4 (SS, Ni & V) and (Zn & As) Secondary Sulfate Factor

In the summer, there were two factors characterised by high loadings of SO_4^{2-} and NH_4^+ at the AC site. Both factors were assigned to secondary sulfate aerosol (SS). One of the factors labeled (SS, Ni & V) has a large contribution from Ni and V (Figure 5.22). The other factor labelled (SS, Zn & As) is characterised by a high percentage of Zn, As, Mg^{2+} , Cr, and Ni (Figure 5.23). The CPF 90th percentile rose analysis showed that the (SS, Ni & V) factor comes from the north-east direction, while the (SS, Zn & As) factor comes from the east (Figures 5.24 & 5.26). The (SS, Ni & V) and (SS, Zn & As) factors were weakly and insignificantly correlated ($R^2 = 0.017$) with each other. However, the source contribution showed that both of them started to increase from late July towards the end of the sampling campaign (Figure 5.29).

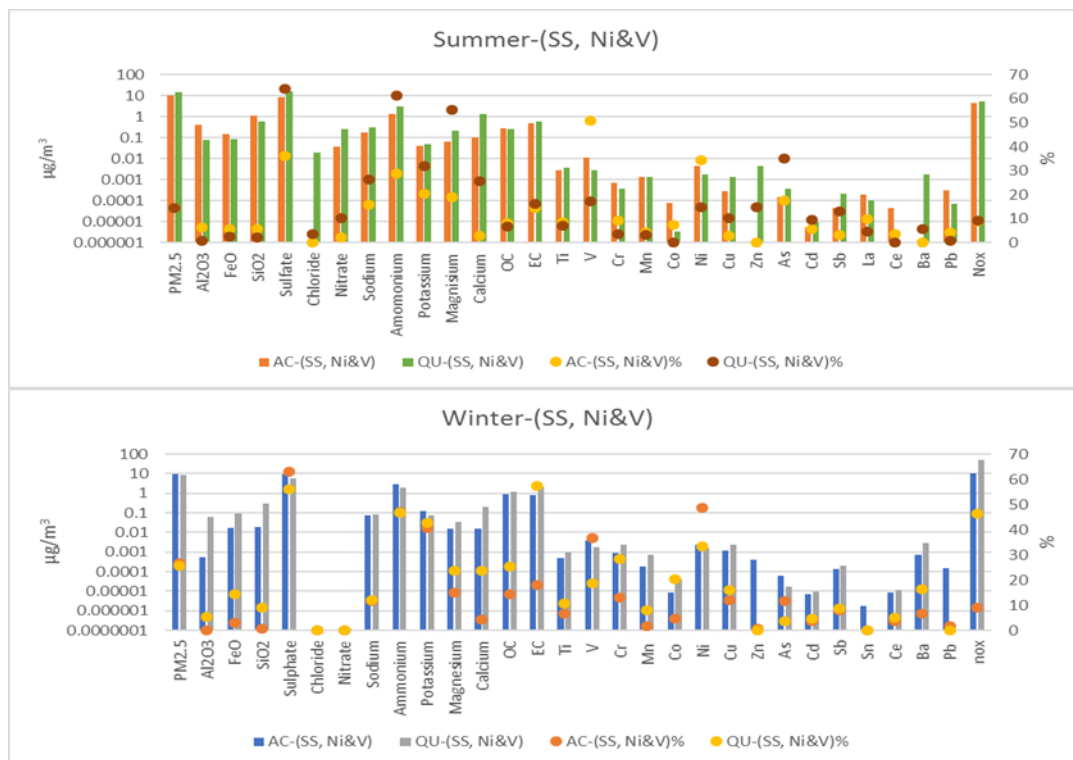


Figure 5.22 Source profile of (SS, Ni&V) factor in the summer and the winter seasons.

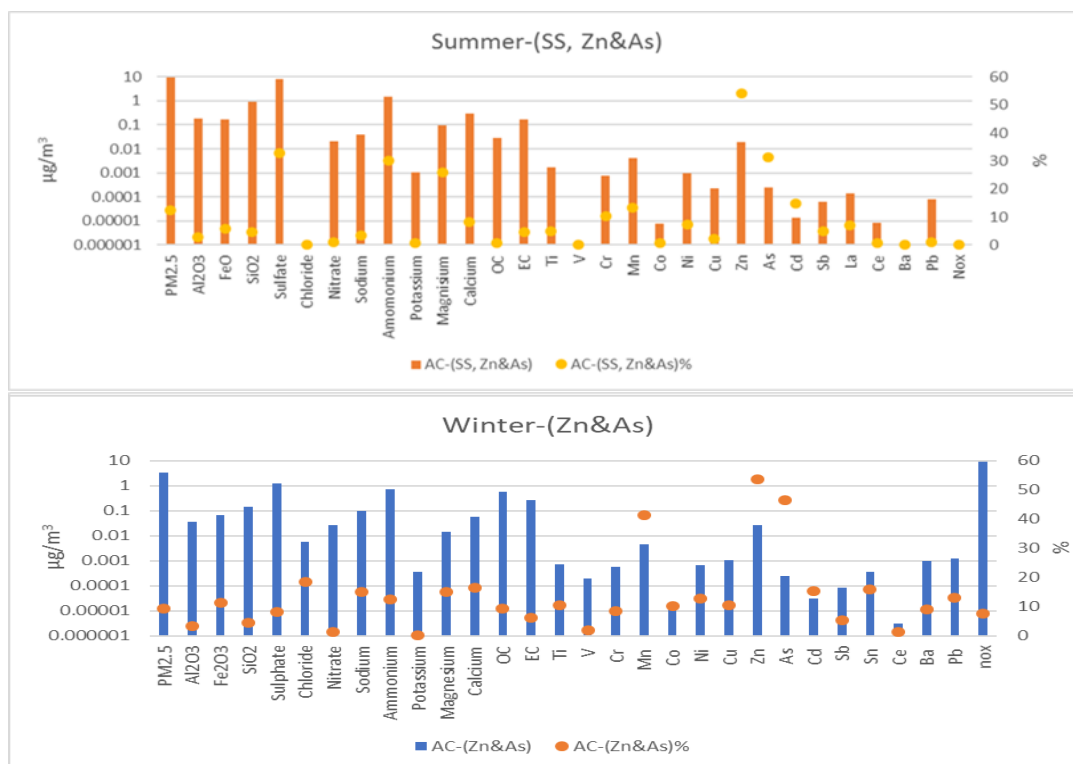


Figure 5.23 Source profile of (SS, Zn&As) factor in the summer and (Zn&As) in the winter seasons at the AC site.

At the QU site, on the other hand, only one secondary sulfate (SS, Ni & V) factor coming from the north-east direction (Figure 5.25) was identified. The factor is characterised by high contributions of Ni, V, As and Mg^{2+} (Figure 5.22). Although (SS, Ni & V) factor at the QU and (SS, Ni & V) at the AC sites arrived from north-east, and both contain high V and Ni elements, they were weakly correlated ($R^2 = 0.25$, $p < 0.01$). However, the (SS, Ni & V) factor at the QU showed a stronger correlation with (SS, Zn & As) factor at the AC site ($R^2 = 0.55$, $p < 0.01$).

In the winter season, a secondary sulfate factor (SS, Ni & V), with a notable amount of Ni and V was found at the QU and AC sites. The factors were significantly correlated ($R^2 = 0.49$, $p < 0.01$). The CPF 90th percentile rose analysis showed that the highest contribution is from the east at the AC site and from the north-east at the QU site (Figures 5.24 & 5.25). Another factor

(Zn & As) was characterised by high Zn, As and Mn was found at AC site coming mostly from the east direction (Figure 5.26). In contrast to the summer season results, the (Zn & As) factor in the winter season shows no correlation with the (SS, Ni & V) factor at the QU site.

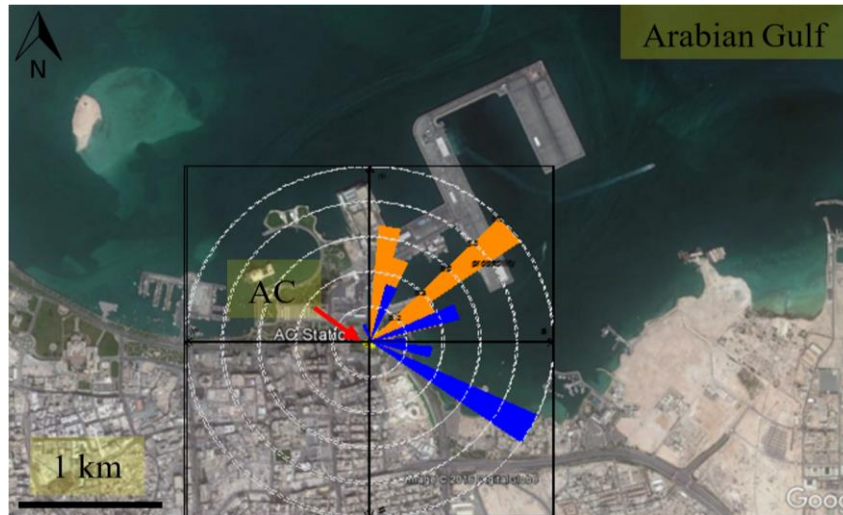


Figure 5.24 CPF 90th percentile rose at the AC site in summer (orange) and in winter (blue) showing the direction of (SS, Ni&V) source

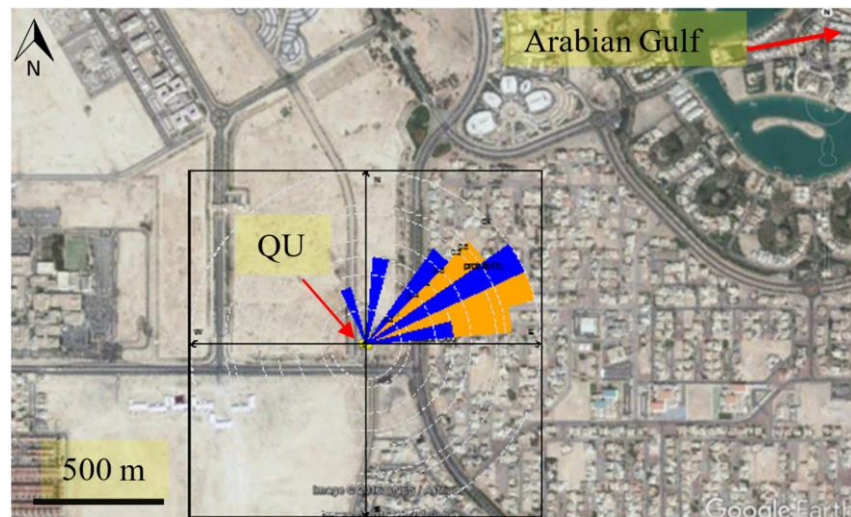


Figure 5.25 CPF 90th percentile rose at the QU site in summer (orange) and in winter (blue) showing the direction of (SS, Ni&V) source



Figure 5.26 CPF 90th percentile rose at the AC site showing the direction of (SS, Zn&As) factor in orange and (Zn & As) factor in blue. Red arch shows Doha port territory

High loadings of SO_4^{2-} , NH_4^+ , Ni, and V are established tracers for oil combustion and are related to shipping and harbor activity (Moreno et al., 2012), resulting in the long-range transport of secondary sulfate particles originating from offshore flaring activities for the petroleum industry, and from seagoing vessel emissions. The suspected source of the (SS, Ni & V) factor based on tracer markers and factor directions (Figures 5.24 and 5.25) are long-range transport of secondary sulfate aerosols from the Arabian Gulf.

On the other hand, the (Zn & As) factor was found only at the AC site indicating that the factor is likely downwind the QU site and closer to the AC site. The CPF 90th percentile rose and pollution rose analysis results at the AC site reveal that most of (SS, Zn & As) factor's high values come from north-east to east direction (Figure 5.26) at low wind speed (0.1 to 1.2 m/s) indicating a local source (Figures 5.27 & 5.28).

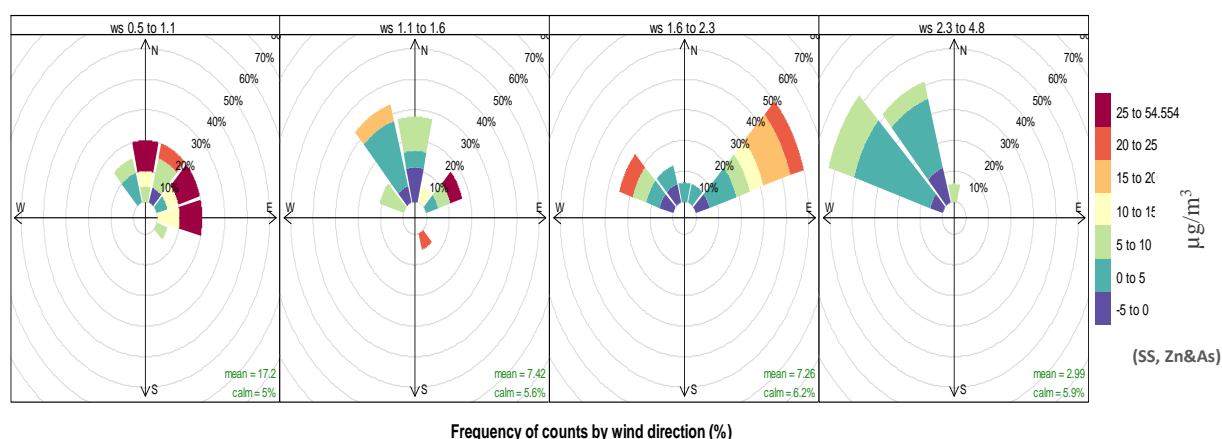


Figure 5.27 Pollution rose at the AC site showing the direction of (SS, Zn&As) factor as a function of wind speed in the summer season.

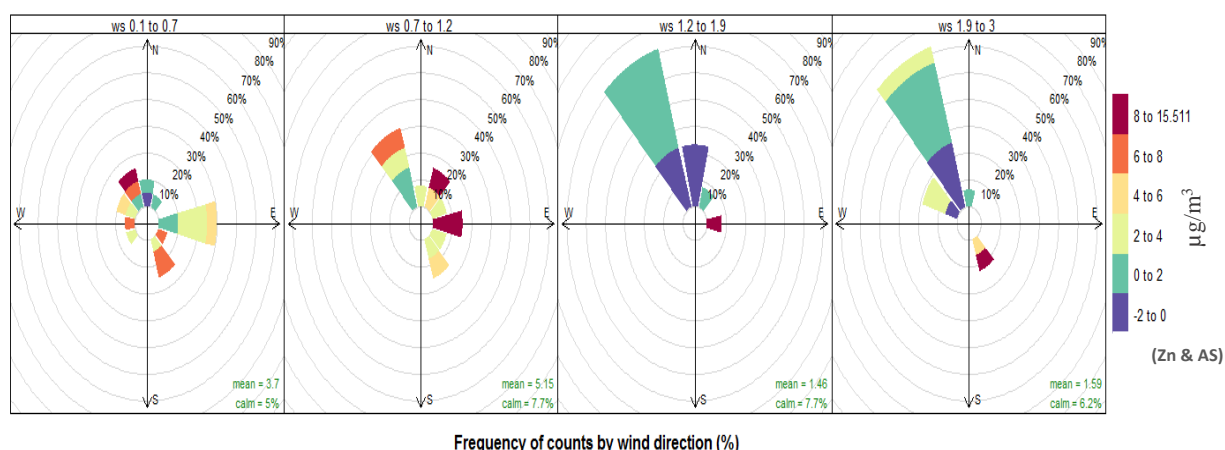




Figure 5.28 Pollution rose at the AC site showing the direction of (Zn&As) factor as a function of wind speed in the winter season

The (Zn & As) factor showed different mass contributions, and different correlations with QU-(SS, Ni & V) in both seasons. In the summer, the AC-(SS, Zn & As) factor showed a high percentage of sulfate contribution (63%), hence the “SS” in the factor name. This factor contributed $8.5 \mu\text{g}/\text{m}^3$ to $\text{PM}_{2.5}$ mass and was correlated with the QU-(SS, Ni & V) factor. In the winter season, AC-(Zn & As) factor showed a smaller percentage of sulfate (38%). The factor contributed $3.2 \mu\text{g}/\text{m}^3$ to $\text{PM}_{2.5}$ mass and did not correlate with the QU-(SS, Ni & V) factor. Table 5.3 provides a summary of the factors correlations between sites and the mass contribution in the winter and summer seasons.

Table 5.3 Summary of SS factors mass contributions and correlations between sites

Winter			Summer		
QU site	AC Site		QU site	AC Site	
QU-(SS, Ni&V)	AC-(SS, Ni&V)	AC-(Zn&As)	QU-(SS, Ni&V)	AC-(SS, Ni&V)	AC-(SS, Zn&As)
Correlations between factors			Correlations between factors		
<ul style="list-style-type: none"> - The correlation between QU-(SS, Ni&V) and AC-(SS, Ni&V) = ($R^2 = 0.49$, $p < 0.01$) - The correlation between QU-(SS, Ni&V) and AC-(Zn&As) = ($R^2 = 0.0004$, insignificant) 			<ul style="list-style-type: none"> - The correlation between QU-(SS, Ni&V) and AC-(SS, Ni&V) = ($R^2 = 0.25$, $p < 0.01$) - The correlation between QU-(SS, Ni&V) and AC-(SS, Zn&As) = ($R^2 = 0.55$, $p < 0.01$) 		
Mass contribution and percentage differences			Mass contribution and percentage differences		
 QU-(SS, Ni&V) mass contribution = $8.48 \mu\text{g}/\text{m}^3$ AC-(SS, Ni&V) mass contribution = $9.3 \mu\text{g}/\text{m}^3$ → Percentage difference in contribution = 9.78% AC-(Zn&As) mass contribution = $3.19 \mu\text{g}/\text{m}^3$			 QU-(SS, Ni&V) mass contribution = $14.39 \mu\text{g}/\text{m}^3$ AC-(SS, Ni&V) mass contribution = $11.02 \mu\text{g}/\text{m}^3$ → Percentage difference in contribution = -23.55% AC-(SS, Zn&As) mass contribution = $8.5 \mu\text{g}/\text{m}^3$		

In order to understand the changes in the correlations behavior of the SS factors through seasons, as well as the seasonal differences in mass contribution, two aspects were investigated:

- Number of factors. The numbers factors were reduced at the AC site in both seasons to ensure that the (SS, Zn&As)/(Zn&As) factors are real factors and not a split-up of the (SS, Ni & V) factor.
- Multicollinearity impact. Multicollinearity is caused by meteorological factors such as wind direction affecting two factors located in the same alignment from the receptor, wherein one factor's emissions are frequently "smeared" into another factor's emissions from a major source located in the same direction (Gordon, 1988); or due to two factors with the same profile signature which can result in incorrect source contribution (Pant and Harrison, 2012; Pant, 2014). The multicollinearity was investigated by 1) examining the correlation between secondary sulfate factors at AC and QU sites during different times of sampling in the

summer season to check the impact of wind direction changes on factors' correlations; and
2) calculating the difference in factors' mass contribution, which is likely to be caused by multicollinearity.

To investigate the number of factors, the model was re-run for the AC site for the summer season to ensure that the solution is unique and that both secondary sulfate factors are two different factors and not a splitting of one factor. Factor numbers were reduced to six and five factors, and rerun again. The results showed that both secondary sulfate factors exist for the final solution where other factors disappeared, such as the sea salt/nitrate factor at 6 factors and the Lusail factor at 5 factors. Therefore, they are considered as two factors and not a splitting of a secondary sulfate factor.

To investigate multicollinearity impact, first, the correlation between the QU-(SS, Ni & V) factor with the AC-(SS, Ni & V) and the AC-(SS, Zn & As) factors in the summer season was investigated, and it showed different correlation with time.

- At the beginning of sampling until late July, the QU-(SS, Ni & V) factor showed more correlation with the AC-(SS, Ni & V) factor ($R^2 = 0.59$, $p < 0.01$) than with the (SS, Zn & As) factor ($R^2 = 0.31$, $p < 0.01$).
- After the wind direction changed its course from north-west to north-east east direction in late July, sulfate concentration started to increase (Figure 5.29) and the correlation between the QU-(SS, Ni & V) factor with the AC-(SS, Ni & V) changed to ($R^2 = 0.51$, $p < 0.05$), and with the AC- (SS, Zn & As) factor to a weak, insignificant correlation ($R^2 = 0.089$).

In correlation analysis, high values at X and Y axes are likely to have a big impact on the regression line. Therefore, when all data were used in the correlation test previously, the QU-(SS, Ni & V) factor showed a strong correlation with the AC-(SS, Zn&As) factor, because

both factors showed a higher proportion of mass contribution toward the end of the sampling campaign (Figure 5.29). In contrast the QU-(SS, Ni & V) factor showed a weaker correlation with the AC-(SS, Ni&V) factor when using all data points because of the low mass contribution at the end of the sampling period even though they have more similar pattern (Figure 5.30), which indicates that changes in the correlations' behaviour between the different factors were most likely caused by the incorrect contribution caused by multicollinearity. Accordingly, the QU-(SS, Ni & V) factor is always more similar to the AC-(SS, Ni&V) factor than with the AC-(SS, Zn & As) factor.

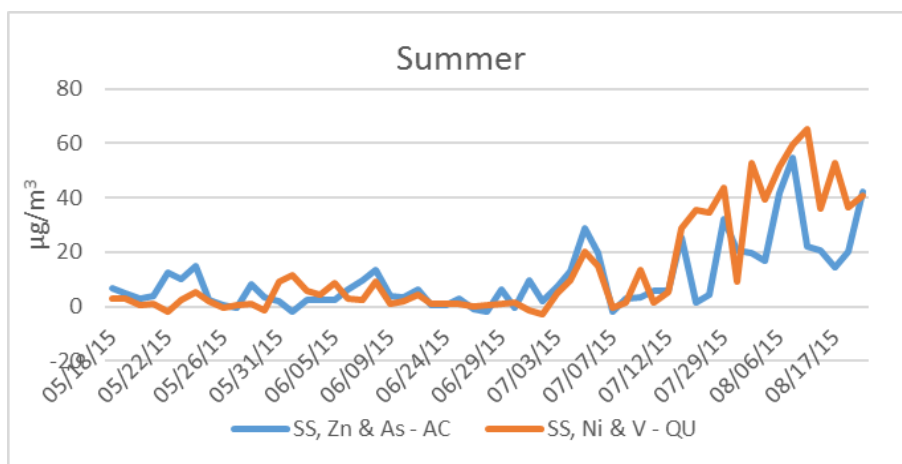


Figure 5.29 Time series of (SS, Zn & As) factor at the AC site and (SS, Ni & V) factor at the QU site in the summer season

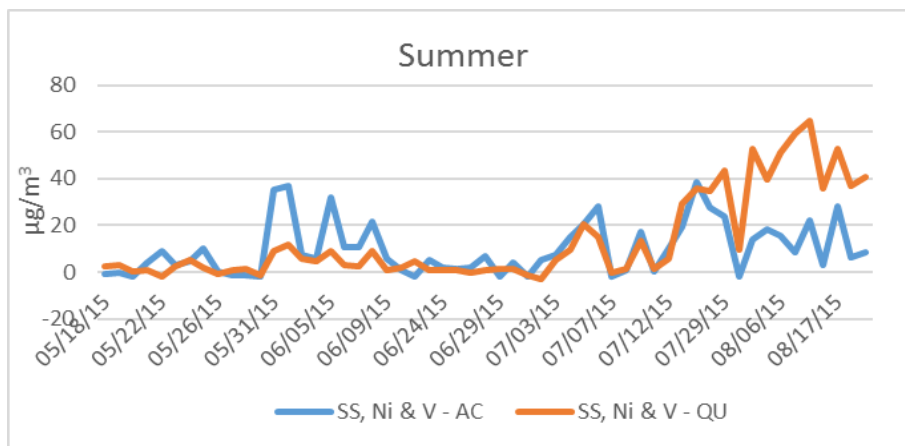


Figure 5.30 Time series of (SS, Ni & V) factor at the AC site and (SS, Ni & V) factor at the QU site in the summer season

The factors' mass and percentage contribution between (SS, Ni&V) and (SS, Zn&As) at the AC site were also investigated as well to calculate the incorrect mass contribution which is likely to be caused by multicollinearity. The incorrect mass contribution caused by multicollinearity was estimated as follow:

- The winter season result was assumed to be more accurate than the summer season result due to the strong correlation found between the (SS, Ni & V) factors at both sites and the similarity in the mass contribution. Hence, the 9.78% difference in the winter season (Table 5.3) was used as a reference to calculate the incorrect mass contribution for AC-(SS, Ni & V) in the summer season that was caused by multicollinearity.
- The new theoretical AC-(SS, Ni&V) factor mass contribution in the summer season was calculated from the QU-(SS, Ni&V) factor mass contribution of $14.39 \mu\text{g}/\text{m}^3$ using the 9.78% difference as follows:

$$\text{AC-(SS, Ni \& V) theoretical mass} = ((9.78\% + 100) * (14.39 \mu\text{g}/\text{m}^3))/100 = 15.8 \mu\text{g}/\text{m}^3$$

The new theoretical AC-(SS, Ni & V) mass of $15.8 \mu\text{g}/\text{m}^3$ is $4.8 \mu\text{g}/\text{m}^3$ higher than the modeled mass of $11 \mu\text{g}/\text{m}^3$. Therefore, to compensate for the AC-(SS, Ni & V), the factor's extra mass of $4.8 \mu\text{g}/\text{m}^3$ was subtracted from the AC-(SS, Zn & As) factor's mass of $8.5 \mu\text{g}/\text{m}^3$.

$$\text{The new AC-(SS, Zn\&As) factor mass} = (8.5 \mu\text{g}/\text{m}^3 - 4.8 \mu\text{g}/\text{m}^3) = 3.7 \mu\text{g}/\text{m}^3$$

These calculations demonstrate that when the percentage difference remained the same (9.78%) for the (SS, Ni & V) factor mass contribution at both sites through both seasons, then the AC-(SS, Zn & As) factor mass contribution was also comparable through both seasons ($3.2 \mu\text{g}/\text{m}^3$ and $3.7 \mu\text{g}/\text{m}^3$ in the winter and summer seasons, respectively).

The variation in the (Zn & As) source contribution between seasons affected both the (SS, Ni & V) and the (Zn & As) factors' mass contribution at the AC site and their correlation with the (SS, Ni & V) factor at the QU site. It is most likely that during the summer season when the wind changes direction from the north to the north-east in late July; the (Zn & As) factor interacted and homogenized well with secondary sulfate air masses coming from the Arabian Gulf. As a result, the model could not distinguish the (Zn & As) factor from the secondary sulfate background.

It is difficult to draw a defined conclusion on the source type of (Zn & As) factor. The (Zn & As) factor contribution to PM_{2.5} mass ranged between 3.19 and 3.7 µg/m³. The main chemical constituents in (Zn & As) factor are Zn, As, Mn, and Cd. However, the typical PM emitted from marine engines includes SO₄²⁻, OC, EC, and heavy metals such as Ni, V, Zn, Ca²⁺, Mg²⁺, Na⁺, K⁺, Fe, P and As (Sippula et al., 2014), which didn't appear strongly in the (Zn & As) factor. The Zn element is a metal marker for marine engines' lubrication oil (Sippula et al., 2014), and also a marker for tyre wear (Pant, 2014), which could be released from the heavy presence of cargo trucks used in transporting goods from and to Doha harbor. On the other hand, the As element is mainly emitted from combustion sources (EPA, 1989, 2002), while Mn is used as a diesel and gasoline additive to reduce emissions and enhance the octane number (EBA, 2017; Roos et al., 2008). Hence, based on the source profile of the (Zn & As) factor and the wind direction and speed that indicates a local source (Figures 5.27 and 5.28), it is highly likely that the source is related to operations at the Doha Harbour. However, a factor with high Zn, As, Cd and Mn has been repeatedly found in Spain, in a harbor vicinity (Perez et al., 2016; Pey et al., 2013), and it always been attributed to industrial emissions related to smelters and cement kilns. Due to the similarity in the source profile, it could be that the

factor is caused by industrial source, and it reached Doha harbor by sea breeze at low wind speed.

5.7.5 Lusail Factor

In the summer season, a factor was identified at the AC and QU sites which accounted for a high proportion of K^+ , OC, EC, V, Ni, and Pb (Figure 5.31).

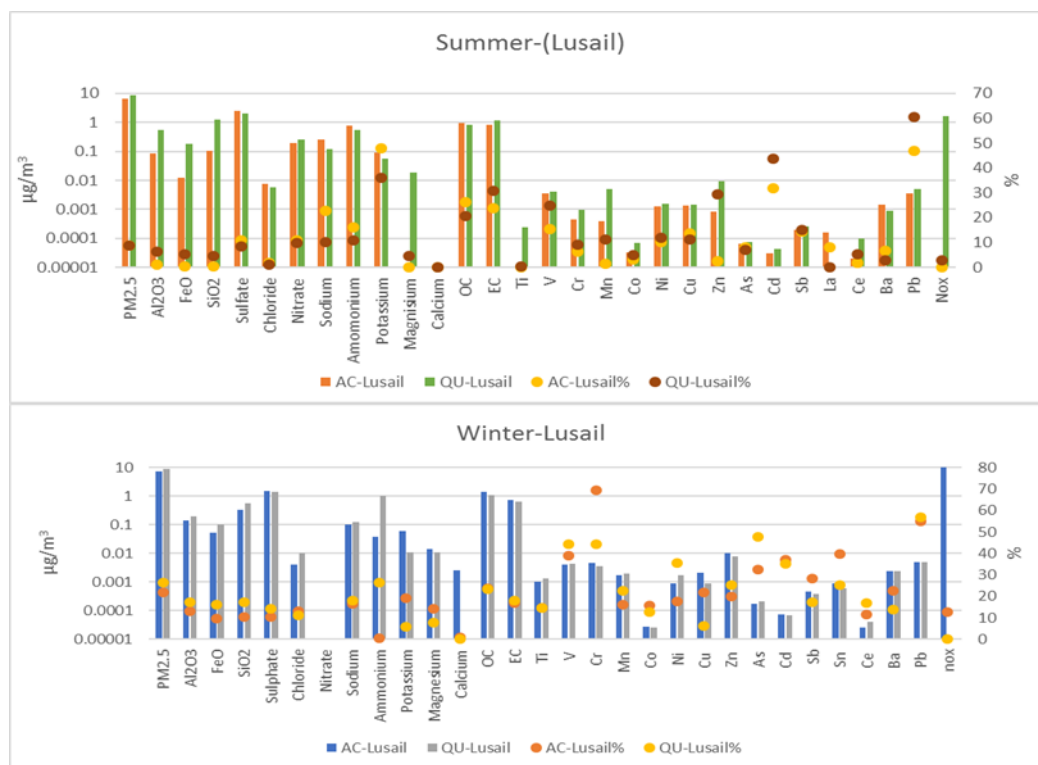


Figure 5.31 Source profile of Lusail factor in the summer and the winter seasons.

Factors at both sites have a similar profile, and they were correlated ($R^2 = 0.39$, $p < 0.01$). Figure 5.32 shows the time series of the Lusail factor at both sites. Although both factors had the same trend, there were two points showing high PM concentration at the QU site and causing the weak correlations between sites. After removing the points on 22nd of May and 12th of July; the correlation increased between factors to $R^2 = 0.53$ ($p < 0.01$)

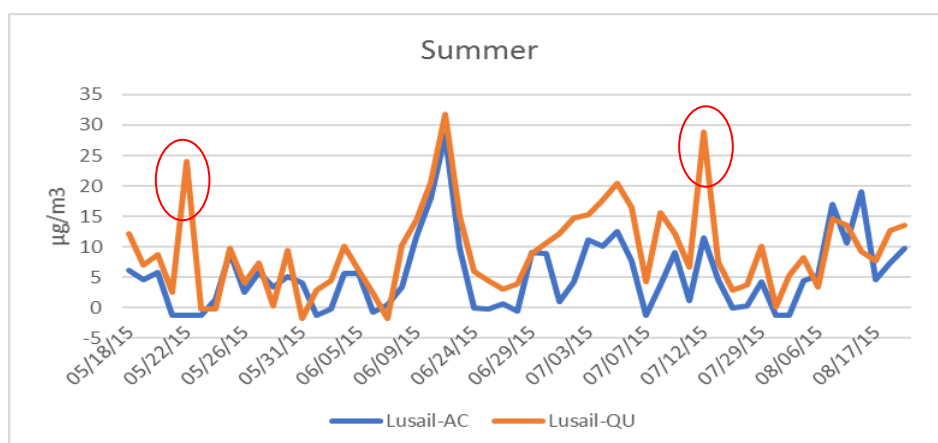


Figure 5.32 Time series of Lusail factor in the summer season at both sites. The two circles show high points found at the QU site causing the weak correlation between both sites

The CPF analysis showed that the highest source contribution of the Lusail factor came from north north-east at the QU site and from the north at the AC site. Both factors intersect at Lusail city (Figure 5.33). Therefore the name was chosen.

The elements Ni, V, OC, EC, Pb, Zn, and Cd are associated with vehicle exhaust emissions (Pant, 2014). High loading from K^+ can indicate tailpipe emissions of lubricant oils (Lin et al., 2015) or wood burning (Crimley et al., 2015). The wood burning source was excluded, since Qatar is not an agriculture country, and there are no biomass burning activities in Doha. Also, municipal waste including any sort of wood is treated and burned in Um-Saeed city, in the south of Doha, downwind of the sampling sites. High OC, EC, Ni, and V indicates fuel combustion. Also, the Zn/Pb ratio range of 0.24 to 1.8 indicates gasoline and diesel emissions (Matawle et al., 2015). Lusail city is a newly developing city, which is undergoing huge earthwork activities. As a result, there are a large number of non-road mobile machinery in the area in addition to power generators that work on diesel fuel. Hence the factor is likely related to emissions from heavy-duty construction equipment, powered by diesel fuel.

In the winter season, a factor coming from Lusail city direction appears on both sites characterized by OC, EC, V, Ni, Pb and moderate K^+ in addition to the relatively higher

percentage of the crustal components than in the summer season. The correlation between Lusail factor at both sites was ($R^2=0.36$, $p<0.01$). Figure 5.34 shows the time series of Lusail factor at both sites in the winter season.

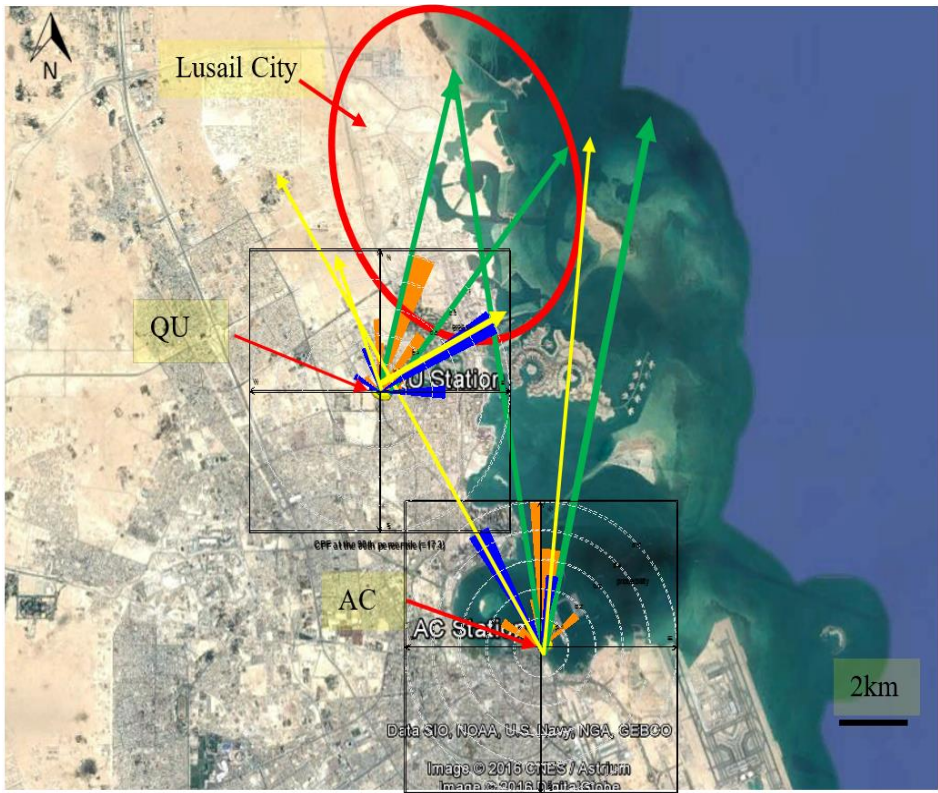


Figure 5.33 CPF 90th percentile roses for Lusail factor in summer (orange) and winter (blue) at the QU and AC sites intersecting at Lusail city . Yellow and green guide arrows to show the range of wind direction at both sites and their intersection at the Lusail city in the winter and summer seasons.

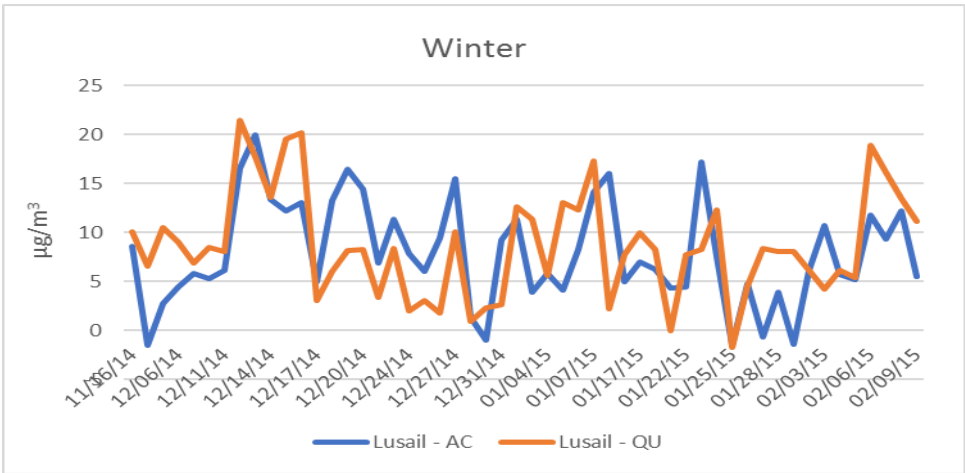


Figure 5.34 Time series of Lusail factor in the winter season at both sites

In comparison to summer season, the Lusail factor showed same source profile with high OC, EC, Ni, and V indicating fuel combustion coming from Lusail city hence the source is thought to be related to diesel machinery, and diesel generators for workforces' temporary housing facility, and engineers' offices at Lusail construction site.

5.7.6 (La & Co) factor

In the summer season, a factor characterized by a high percentage of La and Co was found at both sites (Figure 5.35). The La and Co factor follow the same trend as the abundance of the Lanthanum element (Figures 5.36 & 5.37). The correlation between the La and Co factor and Lanthanum element is ($R^2 = 0.784$, $p < 0.01$) at the QU site and ($R^2 = 0.923$, $p < 0.01$) at the AC site. Lanthanum elemental concentration at both sites (Figure 5.38) are correlated ($R^2 = 0.64$, $p < 0.01$). However, when high values on 30th May and 7th July are omitted from the data, the correlation weakened to ($R^2 = 0.2$, $p < 0.01$).

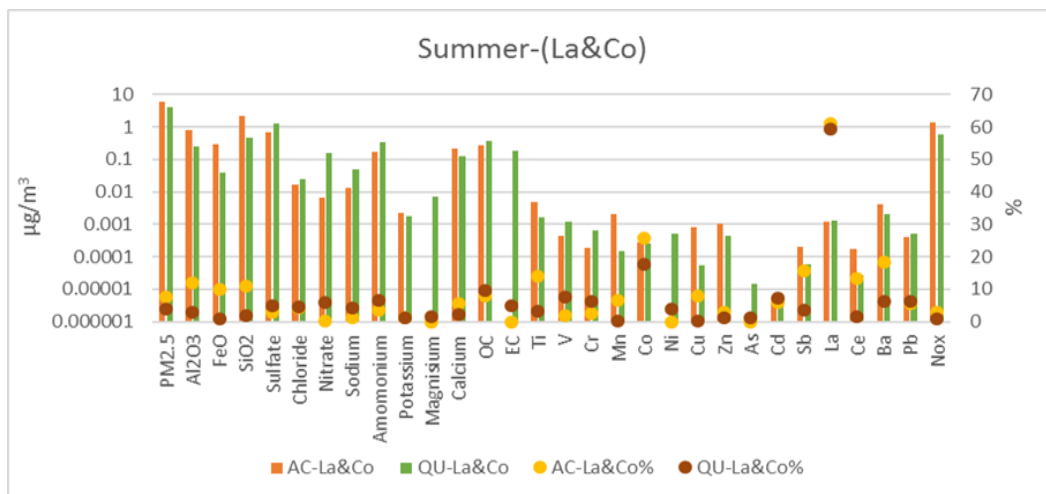


Figure 5.35 Source profile of (La&Co) factor in the summer season

Two sources were suspected at first; La and Co catalyst in vehicle engine exhaust (Sorenson et al., 1975) and La and Co catalysts for the Fischer Tropsch process in the gas to liquid (GTL) industry. The factor contribution profile shows a highly variable period with a high concentration of La and Co (Figure 5.36 and 37) at both sites indicating irregular emissions, which is contraries to the continuous emission nature of traffic sources, hence emissions from vehicle catalyst was excluded. As for the GTL plants, after investigating with Shell and Oryx GTL, it emerged that, both companies do not use La in their operations.

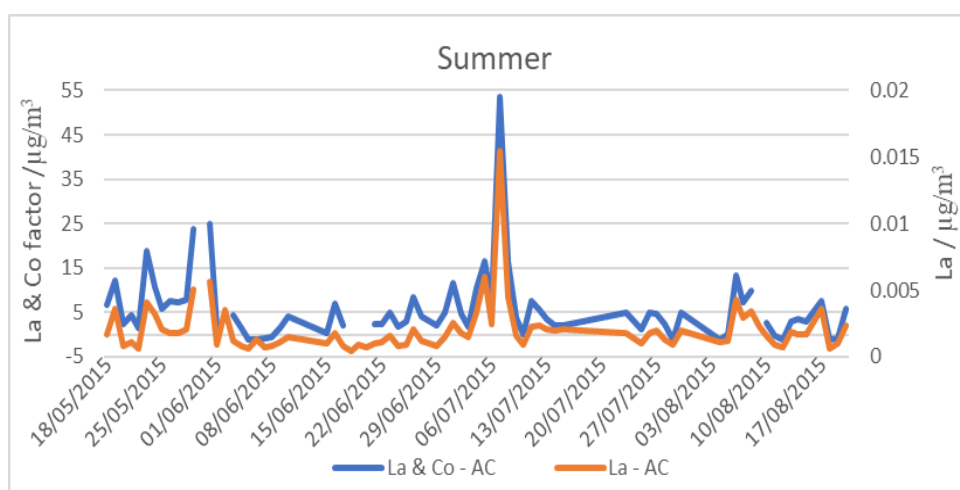


Figure 5.36 Time series of (La & Co) factor and La element at the AC site in summer. The high value on the May 30th was considered as an outlier and was omitted from PMF-5 analysis.

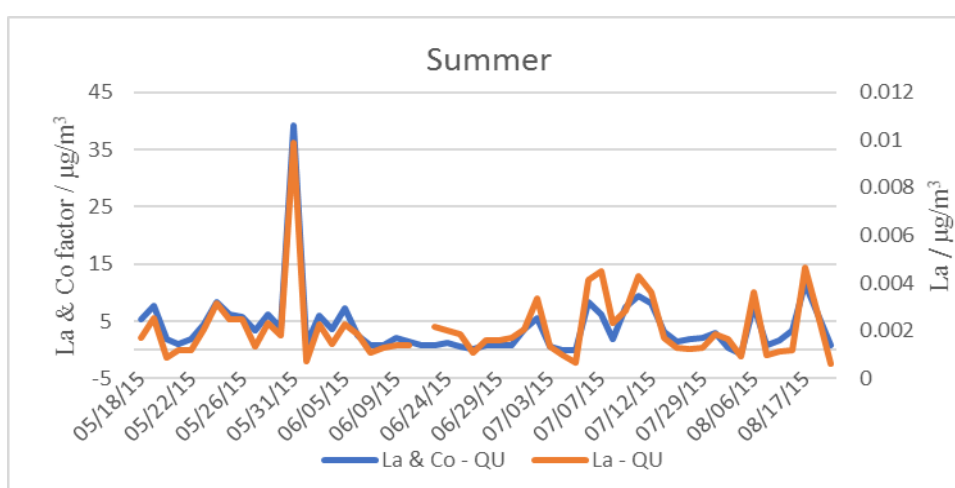


Figure 5.37 Time series of (La & Co) factor and La element at the QU site in summer

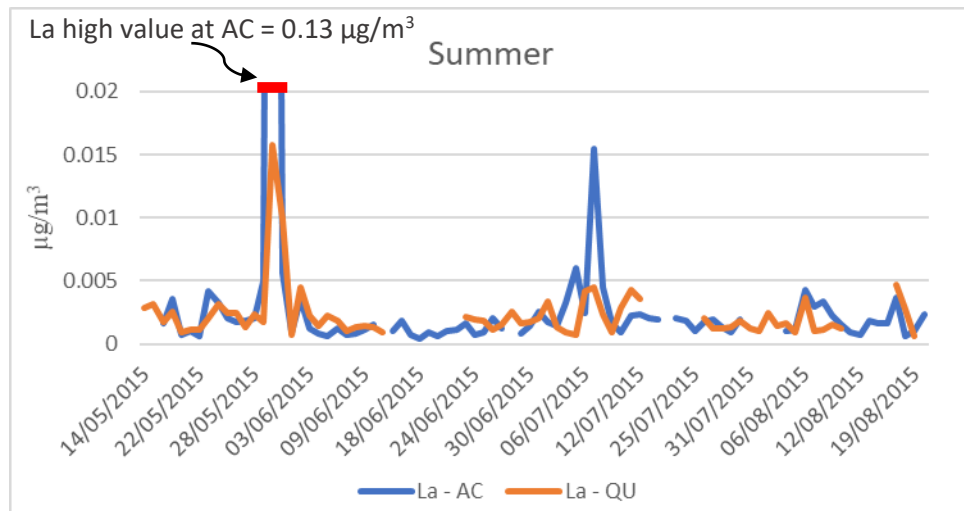


Figure 5.38 Time series of La element in summer at both sites

The concentration of La occurred in episodic events indicating industrial sources; the concentration, however, showed a decline for the two high episodes while wind direction moves from east to west direction (Figure 5.39). When two sites are affected by emissions from the same specific point source, the emission trajectory at both sites are likely to intersect at the source unless the air masses reaching the receptors are affected by different wind turbulence and land topography. Both episodes are affecting both sites however in different concentration, and the wind direction doesn't intersect inside Qatar border which maybe indicates a source located in the Arabian Gulf.



Figure 5.39 Two high episodic concentrations of La element measured at the AC and QU sites. La concentration is showing a declining behavior while the wind moves from east to west direction. In the small frame, two potential sources located in the Arabian Gulf namely Halul island and the Al-Shamal north field at 80 Km and 140 km from Doha city respectively. Both sources deal with oil and gas exploration and extraction, and oil storages tanks. Number (1) Represent the episode occurred in the May 30th 2015, while (2) represent episode on the July 7th 2015

The pollution rose analysis shown in Figures 5.40 and 5.41 for the QU and AC sites respectively shows that high values come at different wind speed. With low wind speed; high values came from the north-east sector, whereas at high wind speed; high values came from the north-west direction. This factor could be a local or regional industrial source; most likely located north the sampling sites in the Arabian Gulf. Hence the source was designated to industrial sources in the Arabian Gulf.

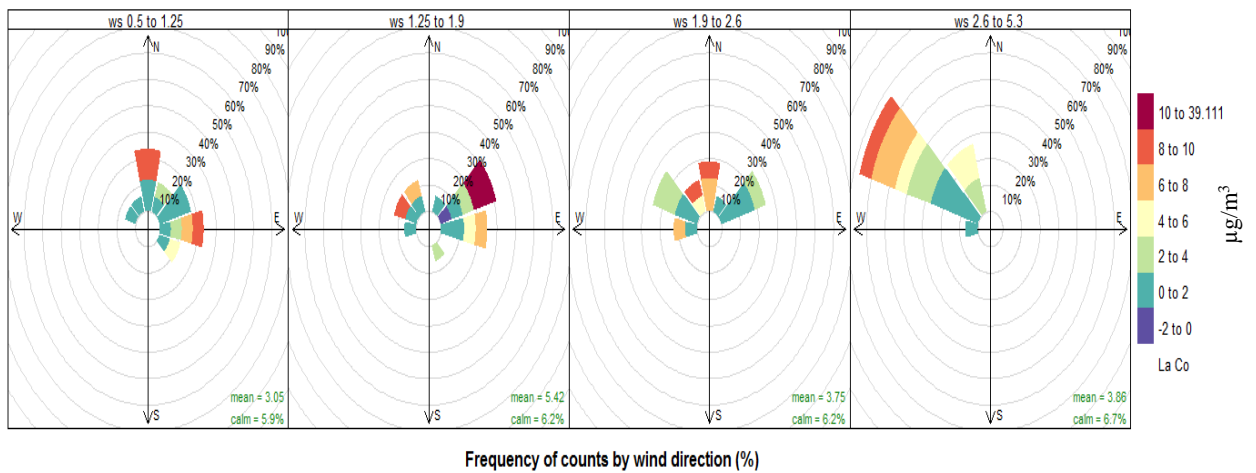


Figure 5.40 Pollution rose at the QU site showing the direction of (La & Co) factor as a function of wind speed

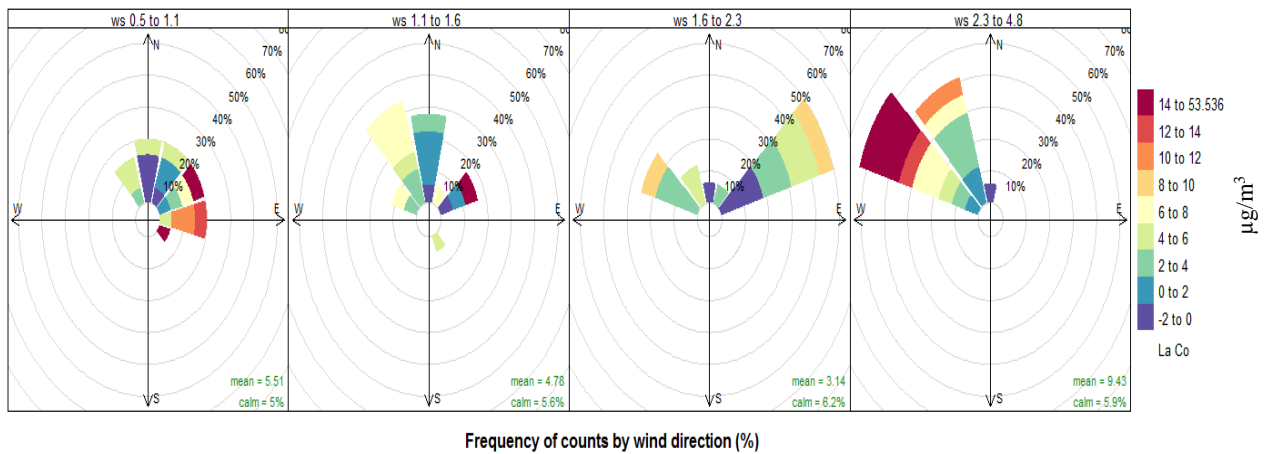


Figure 5.41 Pollution rose at the AC site showing the direction of (La & Co) factor as a function of wind speed

5.8 Quantitative Variations between Seasons and Locations

The factor pie chart demonstrates the distribution of mass concentration among the factors resolved by the PMF. Four charts are presented below showing the changes in sources proportion contributions to $\text{PM}_{2.5}$ mass concentration due to the influence of seasonal variations at the AC and QU sites (Figures 5.42, 5.43, 5.44, and 5.45). The percentiles contribution to $\text{PM}_{2.5}$ mass changed between the summer and winter seasons. In the summer,

crustal fraction had the largest percentile contribution followed by secondary sulfate and traffic factors, whereas in the winter, without dust events effect (exclusion of four dust events days), the largest contribution was from secondary sulfate and Lusail city (construction site).

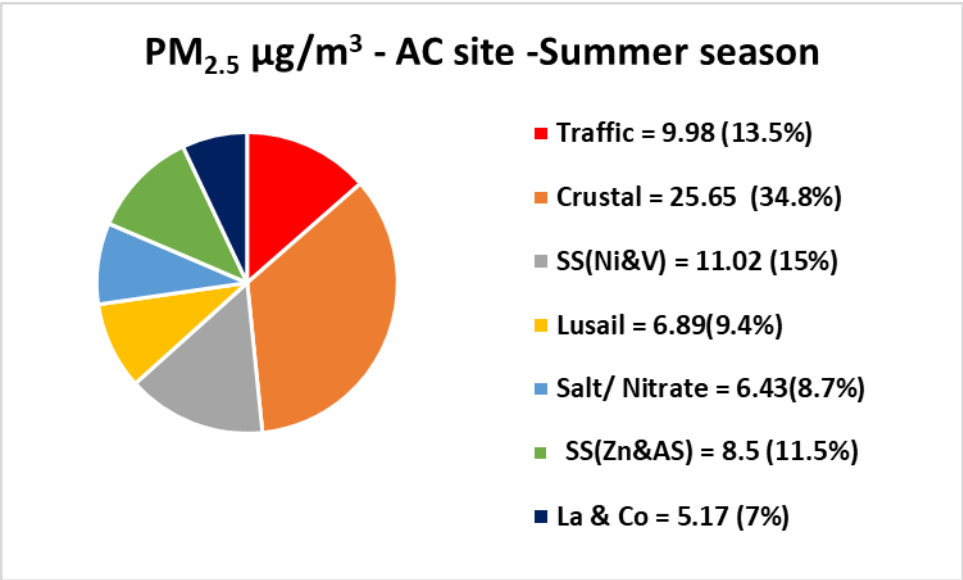


Figure 5.42 Factor pie chart for mass concentration distribution among the factors resolved by the PMF-5, at the AC site in the summer season

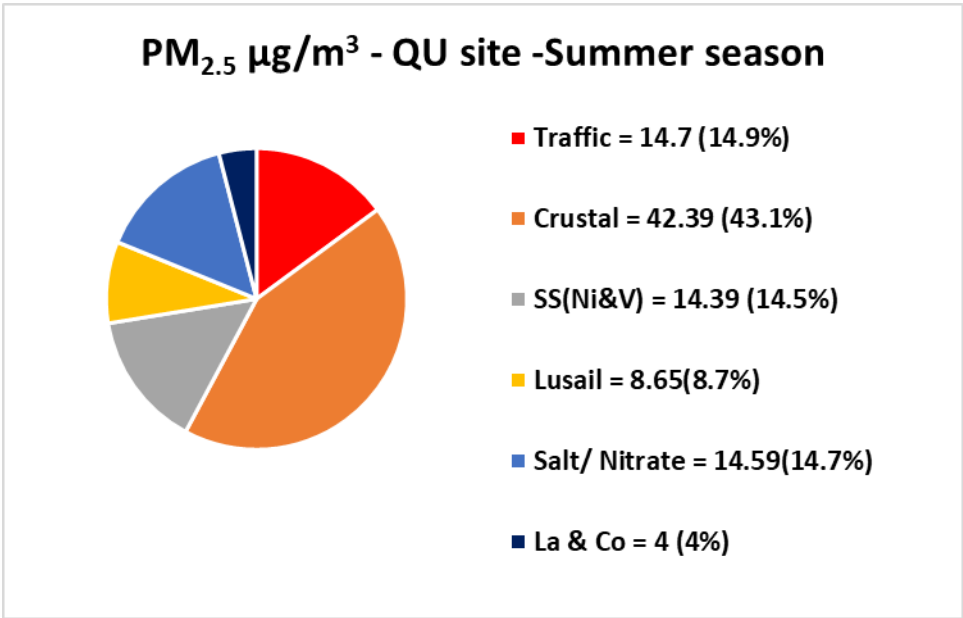


Figure 5.43 Factor pie chart for mass concentration distribution among the factors resolved by the PMF-5, at the QU site in the summer season (no correction for multicollinearity was done here)

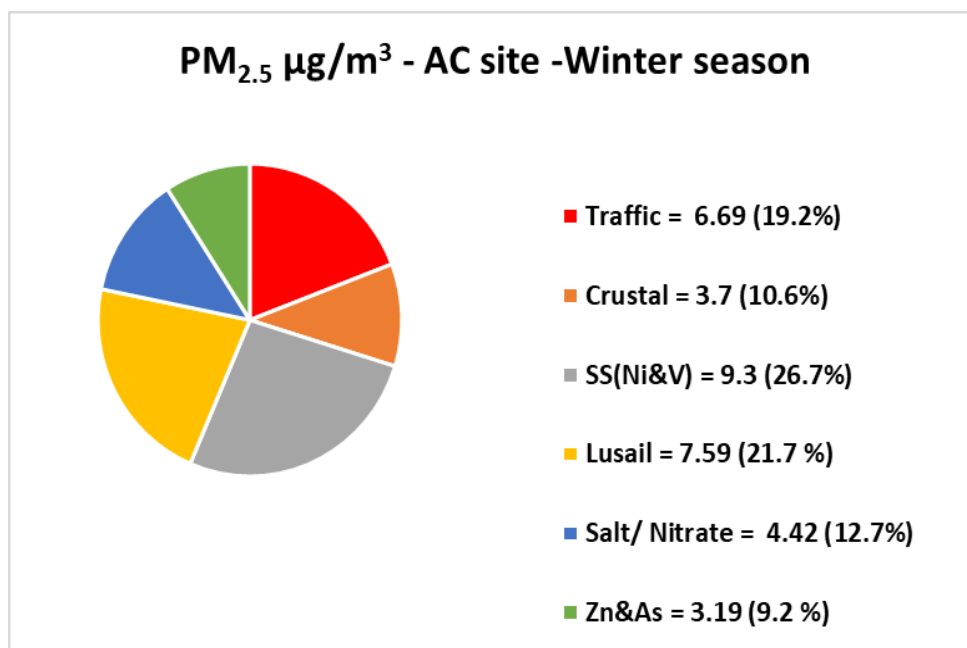


Figure 5.44 Factor pie chart for mass concentration distribution among the factors resolved by the PMF-5, at the AC site in the winter season

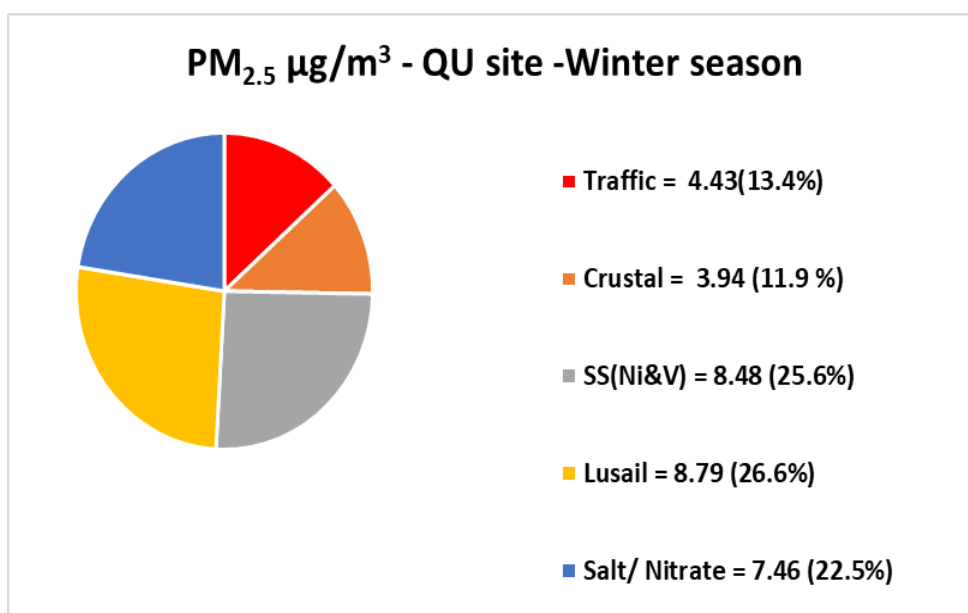


Figure 5.45 Factor pie chart for mass concentration distribution among the factors resolved by the PMF-5, at the QU site in the winter season

Following are a summary of factors contributions distributed based on sources types to natural, anthropogenic, and intermittently sources.

5.8.1 Natural Sources Contribution

Crustal and sea salt/nitrate factors are the two natural sources found in Doha. In the summer season, dust contributes $25.6 \mu\text{g}/\text{m}^3$ (34.8%) and $42.6 \mu\text{g}/\text{m}^3$ (43.1%) to $\text{PM}_{2.5}$ mass at the AC and QU sites respectively. Dust events are a regional phenomenon, and their effect should equally impact both locations, but Figure 5.14 shows that crustal components have a higher influence on the QU site. In the winter, the crustal contribution was $3.7 \mu\text{g}/\text{m}^3$ (10.6%) and $3.9 \mu\text{g}/\text{m}^3$ (11.9%) at the AC and QU sites respectively. The crustal contribution was much lower in the winter season, and there were no big differences between the sites. The effect of precipitation on fixing the crust by increasing its moisture had an influence reducing particles suspension from crust by wind force.

Although, the salt/nitrate factor is classified here as a natural source; it showed a high nitrate concentration due to reaction with anthropogenic emissions. Salt particles mass was higher in the summer season than in the winter season. Salt/nitrate contributed $6.42 \mu\text{g}/\text{m}^3$ (8.7%) and $14.59 \mu\text{g}/\text{m}^3$ (14%) to the AC and QU sites, in the summer season and $4.42 \mu\text{g}/\text{m}^3$ (12.7%) and $7.46 \mu\text{g}/\text{m}^3$ (22.5%) to AC and QU in the winter season. The high salt mass in the summer season likely caused by the monsoon effect in increasing sea salt particles in the Arabian Sea in addition to salt coming from the remote west coast driven by the north-westerly wind which is likely contributed to salt mass by high-level dust background. In both seasons, the QU site showed a higher salt contribution than AC site. Both sites should be closely affected by salt particles produced by seawater since they are not far from each other and from the coastline. In winter, the high salt contribution was found at the QU site caused by the high

nitrate mass concentration. In the summer, however, the high salt contribution was caused by higher crustal and salt elements which caused most likely by the contribution of high background dust level at the QU site.

5.8.2 Anthropogenic Sources Contribution

The main anthropogenic sources are secondary sulfate aerosols, traffic, in addition to (Zn & AS) and (La & Co) sources. Traffic source contributed $6.69 \mu\text{g}/\text{m}^3$ (19.2%) and $4.43 \mu\text{g}/\text{m}^3$ (14.3%) to the AC and QU sites respectively in the winter season. Traffic mass is higher at the AC site since its closer to Al-Corniche busy road. In summer, however, traffic contributed a higher mass $14.7 \mu\text{g}/\text{m}^3$ (14.9%) to the QU site, comparing to the AC site mass of $9.98 \mu\text{g}/\text{m}^3$ (13.5%). Generally, traffic mass contribution is higher in the summer season due to the resuspension of road dust by vehicles turbulence. In the summer season, road dust increases due to the accumulation of dust from dust events and the subsequent suspension by vehicles turbulence. Since the crustal contribution from vacant surroundings is greater at the QU site, it showed higher traffic contribution.

The model identified a secondary sulfate aerosols source at both sites. The (SS, Ni&V) factor contributed 9.3 and $8.48 \mu\text{g}/\text{m}^3$ at AC and QU sites in the winter season and 15.8 and $14.39 \mu\text{g}/\text{m}^3$ at the AC and QU sites in the summer season. The factor was coming from the Arabian Gulf, based on wind direction, and was most likely related to seagoing vessels and flaring emissions.

The (Zn & As) factor was only found at the AC site. In the winter season, the factor contributed a $3.12 \mu\text{g}/\text{m}^3$ to $\text{PM}_{2.5}$ mass. However, in the summer season, the model incorrectly apportioned (Zn & As) and (SS, Ni & V) factors due to multicollinearity effect. This caused a different behavior correlation with (SS, Ni & V) factor at the QU site and an

incorrect mass contribution proportion between (Zn & As) and (SS, Ni & V) factors at the AC site. The calculations in point 5.7.4 showed that (Zn & As) factor in the summer season contributed a similar mass $3.7 \mu\text{g}/\text{m}^3$ as in the winter season. The (Zn & As) factor was accredited to emissions from Doha port activity based on pollution rose results (Figures 5.27 & 5.28).

La and Co factor contributed 5.17 and $4 \mu\text{g}/\text{m}^3$ at the AC and QU sites respectively. La and Co metals are enriched in catalyst materials that used in petrochemical industries, and the factor showed episodic events hence it is most likely contributed by an industrial source located in the Arabian Gulf.

5.8.3 Intermittently Sources Contribution

Lusail factor is related to construction activity which supposedly their influence should end with the end of the project. Lusail contributed by an average of $7.64 \mu\text{g}/\text{m}^3$ in all seasons and locations.

5.9 Conclusion

A PMF model was applied for the source apportionment of the particle mass at both sites and seasons with similar sources being identified, which included crustal components, salt, traffic emissions, secondary inorganic aerosols, and emissions from Lusail city. In addition, a distinct (Zn & As) factor was identified at the AC site at both seasons related to Doha harbor. Another distinct factor namely (La & Co) was identified in the summer season at both sites, with two high episodic concentrations arriving from two different directions north-east and north-west, which were likely contributed by a source located north the sampling sites; probably outside Qatar borders. The main factors in Doha city were crustal components in the summer season and secondary sulfate aerosol in the summer and winter seasons. Overall,

anthropogenic sources contributed $41.54 \mu\text{g}/\text{m}^3$ (56.3%) at the AC site and $41.74 \mu\text{g}/\text{m}^3$ (42.15%) at the QU site in the summer season; and $26.77 \mu\text{g}/\text{m}^3$ (76.6%) at the AC site and $21.7 \mu\text{g}/\text{m}^3$ (65.5%) at QU site in the winter season. On the other hand, natural sources contributed $32 \mu\text{g}/\text{m}^3$ (43.4%) at the AC site and $57 \mu\text{g}/\text{m}^3$ (57.6%) at the QU site in the summer season; and $8 \mu\text{g}/\text{m}^3$ (22.9%) at the AC site and $11.4 \mu\text{g}/\text{m}^3$ (34.4%) at the QU site in the winter season. Dust events contributed directly to natural sources (e.g., crustal factor) but also indirectly to anthropogenic sources (e.g., Traffic factor) by increasing road dust. These results highlight the big impact dust events can have on increasing PM mass concentrations and degrading air quality in Doha.

CHAPTER 6: POLICY IMPLICATIONS

6.1 Introduction

The main objective of this study was to obtain general knowledge about the sources of PM pollution in Doha city and the contribution of natural and anthropogenic sources to PM_{2.5} ambient concentrations, particularly to estimate the contribution of dust events to PM_{2.5} increments. Identifying these sources will help to focus on the emission sources that needs immediate mitigation, develop an effective air quality management action plan, and more importantly to develop a suitable air quality standard for particulate matter which takes into account a margin for PM introduced by natural sources (e.g., dust events/ sea salt).

In order to provide a basis for protecting public health from the adverse effects of air pollutants and to support action plans to improve air quality, the WHO (2005) developed Air Quality Guidelines (AQGs) and interim targets for worldwide use. The AQGs are pollutant concentrations that are considered to be acceptable in the light of what is known about their effect on human health (Harrop, 2002), whereas the interim targets aim to lower air pollutant concentrations in incremental steps towards the guideline values and are intended for use in highly polluted areas. According to WHO (2005) before adopting the air quality standards (AQSs) directly as legally based standards, governments should consider their local circumstances carefully when formulating national standards, because the AQSs will vary according to pollution levels, national capability in air quality management, methods used for balancing health risks, and economic, political and social considerations.

The Qatar Executive Regulation of The Environmental Protection Law (30), Legislative Decree No. 2 of the year 2002 (MOE, 2005), established national air quality standards for daily and annual PM₁₀. These standards were set before the establishment of air quality

monitoring networks in Doha and without consideration for the natural and anthropogenic air pollutants levels and to the country's abatement capabilities. As a result, PM₁₀ annual mass concentrations exceeded Qatar's annual AQS of 50 µg/m³ since the establishment of the air quality monitoring network in 2007, and PM_{2.5} annual mass concentrations exceeded the WHO Interim target-2 value of 25 µg/m³ since 2012. Table 6.1 presents Qatar's current air quality standards for PM₁₀ with no allowance for a permitted number of exceedances, the corresponding WHO air quality interim-targets for PM₁₀ and PM_{2.5}; and the WHO air quality guideline for PM₁₀ and PM_{2.5}.

Table 6.1 Qatar air quality standard for particulate matter with corresponding WHO air quality interim-targets for PM₁₀ and PM_{2.5}, and WHO air quality guidelines for PM₁₀ and PM_{2.5}

	Pollutant	limit	Averaging period	unit	The basis for the selected level
Qatar	PM ₁₀	150	24-h	µg/m ³	
		50	1-year		
WHO Air quality guideline (AQG)	PM ₁₀	150	24-h	µg/m ³	Interim target-1 (IT-1), Based on published risk coefficients from multicenter studies and meta-analyses (about 5% increase in short-term mortality over the AQG value).
	PM _{2.5}	75			
	PM ₁₀	50	1-year		Interim target-2 (IT-2), In addition to other health benefits, these levels lower the risk of premature mortality by approximately 6% [2–11%] relative to the IT-1 level, which is associated with about a 15% higher long-term mortality risk
	PM _{2.5}	25			
WHO Air quality guideline (AQG)	PM ₁₀	50	24-h	µg/m ³	These are the lowest levels at which total, cardiopulmonary and lung cancer mortality have been shown to increase with more than 95% confidence in response to long-term exposure to PM _{2.5}
	PM _{2.5}	25			
	PM ₁₀	20	1-year		Based on the relationship between 24-hour and annual PM levels.
	PM _{2.5}	10			

Table 6.2 Shows PM_{10} annual mass concentrations exceeds Qatar's annual AQS of $50 \mu\text{g}/\text{m}^3$ since the establishment of the air quality monitoring network in 2007, and $PM_{2.5}$ annual mass concentration exceeding the WHO interim target-2 value of $25 \mu\text{g}/\text{m}^3$ since 2012.

Table 6.2 PM_{10} and $PM_{2.5}$ annual concentrations in $\mu\text{g}/\text{m}^3$ from 2007 to 2013 at Doha monitoring stations. Qatar's PM_{10} annual AQS is $50 \mu\text{g}/\text{m}^3$ (MDPS, 2007 & 2013).

PM Size	Stationes	2007	2008	2009	2010	2011	2012	2013
PM_{10}	Al-Corniche (AC)	129	201	261	155	120	130	147
	Qatar University (QU)	197	340	338	269	186	219	122
$PM_{2.5}$	Al-Corniche (AC)						78	75
	Qatar University (QU)						119	64

6.2 Accounting for The Exceedances of PM Limit Values from Natural Sources

Based on the results in this study, there were no exceedances of the $PM_{2.5}$ daily interim-target (IT-1) of $75 \mu\text{g}/\text{m}^3$ in the winter season except for the 4 days of dust events, whereas in the summer season, many exceedances occurred during dust events in June and July, and during the sulfate increase period from late July onward. The PMF model results found that the average crustal component concentrations in summer were 25.65 and $42.39 \mu\text{g}/\text{m}^3$ at AC and QU sites respectively. These results prove that it is difficult to meet the daily WHO guideline of $25 \mu\text{g}/\text{m}^3$ in Doha city when the crustal concentration alone in the summer seasons exceeds the limit. Moreover, the results of this study showed that $PM_{2.5}$ concentrations in Doha have a seasonal dependence on natural and anthropogenic sources. In winter, $PM_{2.5}$ concentration depended primarily upon sulfate concentration (Figure 6.1) while in summer, $PM_{2.5}$ showed a

dependence on natural sources by following the SiO_2 trend (Figure 6.2). The seasonal dependency of $\text{PM}_{2.5}$ reveals that a single fixed standard for $\text{PM}_{2.5}$ is not suitable to be applied throughout the year and that changing to a different more representative PM metric for anthropogenic sources (e.g., $\text{PM}_{1.0}$) could provide a better solution for Qatar.

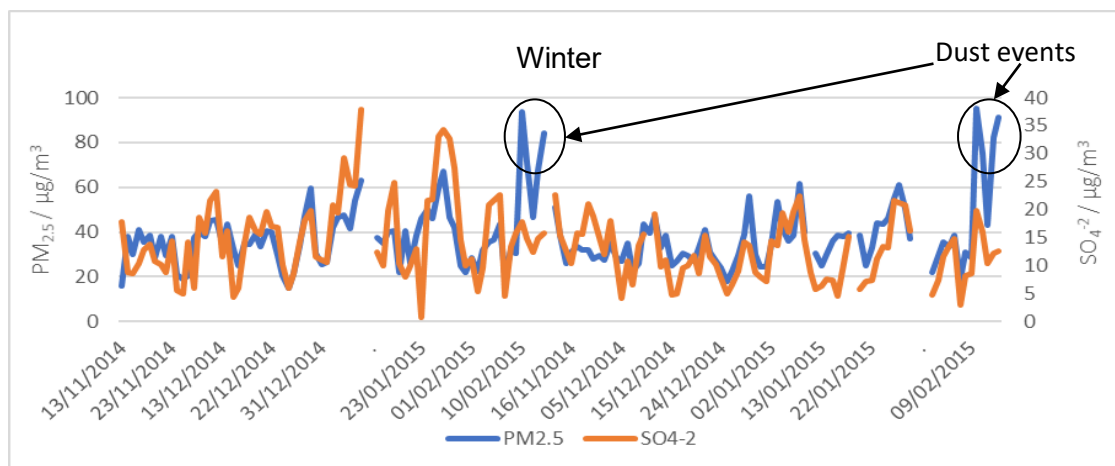


Figure 6.1 Time series of $\text{PM}_{2.5}$ concentration along with sulfate concentration in the winter season for the whole study period, at both sites.

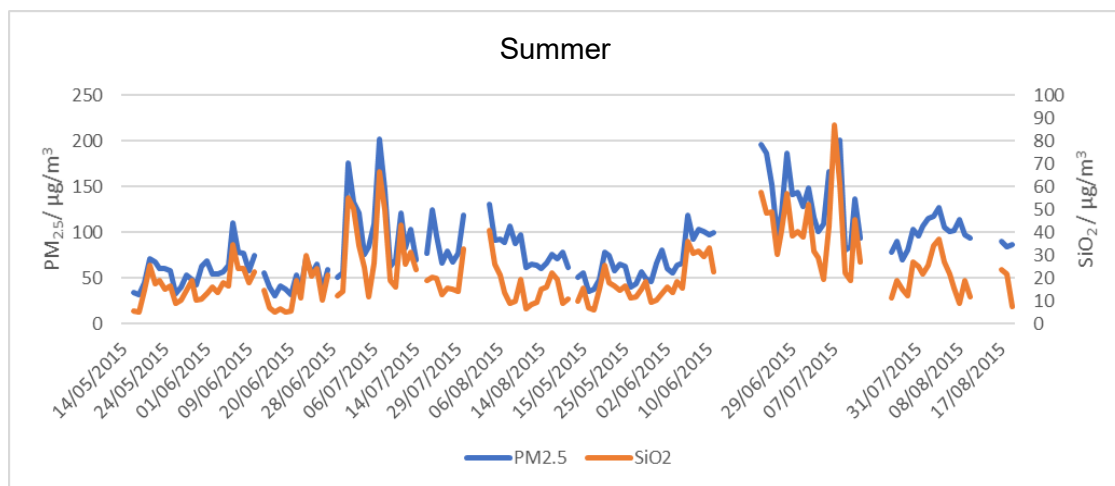


Figure 6.2 Time series of $\text{PM}_{2.5}$ concentration along with silicon oxide concentration in the summer season for the whole study period, at both sites.

Natural PM sources can contribute significantly to $\text{PM}_{2.5}$. Hence either derogation for exceedances of PM limit values should be included in air quality standards to allow for natural sources, or a more representative PM metric for anthropogenic sources should be

selected (e.g., $PM_{1.0}$). A number of aspects are impacting both options and should be considered when implementing either of these solutions.

Choosing an appropriate marginal value or derogation for the PM limit will be impacted by dust event variability in occurrences between years, their intensity, and the residence time of particles in the atmosphere, which could take days to a week to settle down by dry deposition following a dust event. Setting a marginal value or derogations without a thorough study of these variables could result in making a small margin or derogation that will still show exceedances for the limit value by natural sources. Otherwise, it will result in making derogations for PM limit values throughout the whole summer season which will not protect against potential pollution episodes such as the high sulfate concentration detected in this study during late July and August when the wind blew from Arabian Gulf direction.

Also, adopting a number of allowed exceedances for air quality standard will not likely fit Qatar as in other countries. In the EU, the margin allowance for the daily PM_{10} limit value of $50 \mu g/m^3$ is 35 days exceedances at $75 \mu g/m^3$. The $75 \mu g/m^3$ limit value is equal to the lowest interim target-3 set by the WHO (2005) and is responsible for a 1.2% increase in short-term mortality. However, in Doha, the daily limit value of $150 \mu g/m^3$ is already equal to the highest interim target -1 value set by the WHO (2005) which is responsible for a 5% increase in short-term mortality. Making allowance for air quality standards which are established in the first place to protect public health will compromise the purpose of these standards and will expose people to the damaging effects of particulate matter. Hence these standards should be kept without changes as a public informative index.

On the other hand, using a different PM metric which more closely reflects anthropogenic sources, i.e., $PM_{1.0}$, could be a suitable solution for Qatar to drive control of anthropogenic

emissions. According to Yin and Harrison (2008) most particles with a diameter below 1.0 μm , arise from anthropogenic sources hence they could in principle be controlled by regulatory action. The coarse fraction particles ($>1.0 \mu\text{m}$) arise largely from mechanical attrition sources, many of which are natural (e.g., sea spray, wind-blown dust), therefore are not readily amenable to control.

The $\text{PM}_{1.0}$ metric was considered by the Clean Air for Europe study group (CAFE, 2004) however; they judged that it is too early to consider regulation of $\text{PM}_{1.0}$ and that the Member States should carry out research to establish valid information on concentration levels and adverse health effects avoided for the potential $\text{PM}_{1.0}$ metric. Using a $\text{PM}_{1.0}$ metric in Doha will likely be the best solution to tackle anthropogenic sources and reduce the error arising from natural source contributions. However other uncertainties will arise due to the scarcity of data based on health studies, the scarcity of information available on current $\text{PM}_{1.0}$ concentration levels, uncertainties related to the measurement methods, and the cost of monitoring all three metrics (PM_{10} , $\text{PM}_{2.5}$, and $\text{PM}_{1.0}$).

There is a crucial need to incorporate a $\text{PM}_{1.0}$ metric in Doha air quality standards to measure anthropogenic contributions and to evaluate the improvement in the air quality after applying control measures. One practical way to start using a $\text{PM}_{1.0}$ metric in the interim is to estimate a $\text{PM}_{1.0}$ limit value using its ratio to $\text{PM}_{2.5}$ as applied by the WHO when estimating PM_{10} limit values based on their ratios with $\text{PM}_{2.5}$. According to the WHO (2005), PM AQGs are based on studies that use $\text{PM}_{2.5}$ as a health indicator. The WHO (2005) approach to estimate the corresponding PM_{10} guideline values from $\text{PM}_{2.5}$ applied a $\text{PM}_{2.5}/\text{PM}_{10}$ ratio of 0.5, which is a typical ratio of developing country urban environments and is at the lower end of the range found in developed urban areas (0.5–0.8). The WHO (2005) stated that when setting local standards, a different ratio that better reflects local conditions could be employed. This

statement supports both the alteration of the PM₁₀ limit value and the estimation of a PM_{1.0} limit value for Qatar's national air quality standards. Including a PM_{1.0} metric into the pollutant list of the air quality standards requires several changes including:

- The current PM_{1.0} and PM_{2.5} monitors at Doha air quality stations are based on optical method for real-time optical counting. This monitoring method needs to be compared with a reference method to investigate its compatibility with Qatar's environmental conditions such as relative humidity, temperature and dust storm. Start monitoring PM_{1.0}, PM_{2.5}, and PM₁₀ concentration and build a database on these metrics.
- Collect information on PM_{1.0}, and PM_{2.5} ratios and related health issues from literature, and try to estimate a more representative guideline limit for Qatar from WHO(2005) air quality guidelines and more recent work.
- Add a PM_{1.0} limit to Qatar air quality standards along with PM_{2.5} and PM₁₀ as a trial and informative measure until more health studies are available for the health risk exposure to PM_{1.0} of the composition found in Qatar, and then set legally binding standard limits.

6.3 An Action Plan for Improving Air Quality in Doha

Actions at local, national, and regional levels need to be set out to improve Qatar's air quality and reduce exposure to PM. A first step in the air quality management plan is understanding PM sources. This study identified the major air pollutants in Doha city as crustal material from dust events and secondary sulfate. Crustal materials in the summer season contributed a 25.65 µg/m³ at AC site and 42.66 µg/m³ at QU site; while secondary sulfate aerosols

contributed an average of $8.9 \mu\text{g}/\text{m}^3$ in the winter season and $15 \mu\text{g}/\text{m}^3$ in summer at both sites.

The crustal components mostly arise from natural sources in Qatar (e.g., dust events and wind-blown dust from unpaved areas and road/sidewalks). Dust storms and haze are a natural phenomenon of countries with arid climates, yet these natural sources also have a big impact on health. Dust storms are related to diseases such as silicosis which is reported among the inhabitants of desert regions which cause damage to the lung by scarring the alveolar wall (fibrosis) and distension of the alveoles (emphysema) (Pye, 1987). So-called “haboob lung syndrome” has also been observed in the USA in the 1930s after exposure to intensive dust storms causing hypoxemia and multilobar infiltrates (Panikkath et al., 2012). Besides, the WHO (2005) found that the health risks associated with short-term exposure to PM_{10} are likely to be similar in cities in developed and developing countries despite different pollution mixes. The vast majority of health studies into exposure to PM_{10} from different multi-city studies has been conducted in western Europe, North America, and Asian cities found similar results; a mortality increase of 0.5% per $10 \mu\text{g}/\text{m}^3$ of PM_{10} (WHO, 2005)

Dust storms cannot be controlled. Rather, residents of arid climate regions should adapt to dust events and reduce personal exposure by:

1. Improving indoor air quality and prevent dust infiltration to indoors to protect people against PM exposure by requiring the use of dustproof windows and doors in construction regulations Improve indoor.
2. Staying indoors during dust storms, and reducing outside exposure shortly after dust storms end

3. Road cleaning regimes after dust storms and haze to remove particle deposits from roads are needed to prevent resuspension caused by wind and vehicle-induced turbulence
4. Consolidate the crust surrounding vital areas by pavement or plants and cover sand stockpiles in construction areas to minimize particles generation by wind and vehicles turbulence.
5. Inform, educate and involve the public. Information about particulate matter levels, related health issues, and measures to reduce exposure and control indoor particulate levels should be promoted and made widely available to the public.

PM_{2.5} at the QU site showed on average 16.95 µg/m³ higher crustal components than that found at the AC site. This difference shows the big impact fugitive emissions from unpaved surroundings have on degrading air quality. Hence, fugitive dust which arises from unpaved areas should be controlled to reduce its impact, particularly when close to sensitive receptors such as Qatar university campus, where students at the campus are exposed to the outdoor environment while moving between classes. Fugitive dust arising from construction and demolition activities, and from cement, lime, and sand stockpiles must be controlled by promoting knowledge of best working practices. Fugitive dust emissions at construction sites arise from a variety of areas and through a different process which makes them difficult to quantify and control. Hence it is important to develop a policy for construction and demolition best practice. This policy should explain in detail all aspects of relevant control measures, i.e., wet suppression, and coverage of materials to reduce particle emissions from construction activities including fugitive dust during different processes, transport of materials and storage stockpiles.

The other major component of Doha's PM_{2.5} is sulfate aerosols. Anthropogenic sulfate is mainly formed from the combustion of fossil fuel containing sulfur (Wallace and Hobbs, 2006). In Qatar, anthropogenic sulfate sources are mainly from gas flaring activities. Gas flaring is associated with petroleum refineries, natural gas processing plants as well as onshore and offshore oil and gas extraction activities. Apart from gas flaring, SO₂ emissions are also released from seagoing vessels in the Arabian Gulf which make secondary sulfate a regional rather than national matter. The increment in anthropogenic sulfate aerosols should be tackled regionally by:

- Agreement on legally enforceable emission limitations for industrial activities with a schedule and timetable for compliance with these limits.
- Monitoring of sulfate aerosols and SO₂ concentrations in the Arabian Gulf region, to develop a register of air pollution sources along with their emissions and control strategy.
- All neighboring countries affected by sulfate aerosols should seek a regional agreement under the umbrella of the International Convention for the Prevention of Pollution from Ships (MARPOL) to designate the Arabian Gulf as an Emission Control Area (ECA). The Annex VI - Prevention of Air Pollution from Ships (2005) set limits on sulfur dioxide emissions from ship exhausts. In 2012 a sulfur content limit in the fuel of 3.5 m/m% by mass was set for non-ECA areas, whereas in ECA areas the limit set on 2015 was 0.1 m/m% by mass. The Arabian Gulf is a narrow area that is burdened with sulfur dioxide emissions from the increased volume of vessels which directly affect eight countries. Hence there is an urgent need to designate it as an ECA and reduce sulfur emissions.

Reducing sulfur emissions from vessels could be manageable by using a lower sulfur content fuel when vessels are entering the regional water of the Arabian Gulf. However, reducing sulfur from industrial processes and flaring activities in regions that mainly depend economically on the oil and gas industry is a hard task to implement and likely needs more time, and investment to look for new abatement techniques and strategies.

Minimizing the impact of crustal components on health, amenity, and the environment is needed in Doha. Efforts must be directed to find ways to adapt to this phenomenon by continually improving indoor air quality. Also, to invest in scientific research to find solutions to accelerate particle settling and reduce resuspension, and to test alternative self-cleaning building materials or superhydrophobic self-cleaning coating substances to reduce the effort, time and amount of water used in cleaning buildings, prevent soiling and improve towers and buildings' appearances.

Using $PM_{2.5}$ and PM_{10} current standards is beneficial to inform the public when particle concentrations are above the acceptable levels to protect health yet using a $PM_{1.0}$ metric which more closely reflects anthropogenic emissions should be considered in order to monitor anthropogenic contributions and the effectiveness of abatement measures.

CHAPTER 7 – CONCLUSION AND FUTURE WORK

This thesis presents results from characterization and source estimation of PM_{2.5} in Doha city. The study aimed to identify and quantify key pollution sources and to assess the burden of PM from natural sources in Qatar by comparing the abundance and chemical composition of dust storm and non-dust storm seasons. The study outcomes will provide policymakers with information on key pollution sources to focus on the sources that need immediate control and will allow them to evaluate the current air quality standards taking in account the contribution of natural sources.

Two sampling campaigns were carried out in the winter of 2014/2015 and the summer of 2015 to enable comparison between dust storm season (summer) and non-dust storm season (winter).

The results showed that PM_{2.5} mass concentrations increased from 34.93 and 33.12 µg/m³ in winter to 73.74 and 99.02 µg/m³ in summer at the AC and QU sites respectively.

During the winter season, the air quality index (AQI) for the daily PM_{2.5} in Doha were in the moderate and unhealthy for sensitive groups, however, in the summer season, daily PM_{2.5} levels were mostly in the unhealthy range.

The mass closure results showed a mass discrepancy between the gravimetric mass and the reconstructed mass which ranged between -5.3% and +12%. The mass discrepancy was likely to have been caused by two reasons; 1) the assumptions made regarding conversion factors used for unmeasured species (oxygen and hydrogen) associated with assumed compounds. 2) the laboratory determination of chemical constituents in two different types of materials (Teflon and Quartz), with contradictory behavior in retaining and releasing organic carbon

and ammonium nitrate, ahead of comparing the sum of these constituents with the mass collected on Teflon filters. The percentage and mass concentration of the major chemical species found by the mass closure solution is shown in table 7.1

Table 7.1 Major chemical species percentage and mass concentration found by the mass closure solution

	AC-Winter	QU-Winter	AC-summer	QU-Summer
<i>Mineral</i>	15% (5.2 $\mu\text{g}/\text{m}^3$)	25% (8.3 $\mu\text{g}/\text{m}^3$)	38% (28 $\mu\text{g}/\text{m}^3$)	43% (42.6 $\mu\text{g}/\text{m}^3$)
<i>Ammonium sulfate</i>	47% (16.4 $\mu\text{g}/\text{m}^3$)	42% (13.9 $\mu\text{g}/\text{m}^3$)	41% (30.2 $\mu\text{g}/\text{m}^3$)	38% (37.6 $\mu\text{g}/\text{m}^3$)
<i>OC/EC</i>	26% 9.1 $\mu\text{g}/\text{m}^3$	23% (7.6 $\mu\text{g}/\text{m}^3$)	13% (9.6 $\mu\text{g}/\text{m}^3$)	8% (7.9 $\mu\text{g}/\text{m}^3$)
<i>Salt</i>	2% 0.7 $\mu\text{g}/\text{m}^3$	3% (1 $\mu\text{g}/\text{m}^3$)	2% (1.5 $\mu\text{g}/\text{m}^3$)	2% (2 $\mu\text{g}/\text{m}^3$)
<i>Ammonium nitrate</i>	5% (1.7 $\mu\text{g}/\text{m}^3$)	7% (2.3 $\mu\text{g}/\text{m}^3$)	3% (2.2 $\mu\text{g}/\text{m}^3$)	3% (3 $\mu\text{g}/\text{m}^3$)

The PMF-5 solution found, among others, five main / similar sources for both sites and seasons which included crustal components, aged sea salt, traffic emissions, secondary inorganic aerosols, and emissions from Lusail city. The PMF-5 solution showed that the contribution of natural sources, namely crustal components and sea salt nitrate increased in abundance from 8.12 $\mu\text{g}/\text{m}^3$ (23.24 %) and 11.36 $\mu\text{g}/\text{m}^3$ (34.29 %) in the winter season to 32.07 $\mu\text{g}/\text{m}^3$ (43.49 %) and 57.25 $\mu\text{g}/\text{m}^3$ (57.81 %) in the summer season at the AC and QU sites respectively. The anthropogenic sources increased from 26.77 $\mu\text{g}/\text{m}^3$ (76.63 %) and 21.7 $\mu\text{g}/\text{m}^3$ (65.51 %) in the winter season to 41.51 $\mu\text{g}/\text{m}^3$ (56.29 %) and 41.74 $\mu\text{g}/\text{m}^3$ (42.15 %) in the summer season at the AC and QU sites respectively.

The increase in PM mass in the summer was caused mainly by dust storms and a sulfate aerosol increase from late July onwards. Natural sources increased significantly in the

summer season by $23.95 \mu\text{g}/\text{m}^3$ at the AC site and $45.89 \mu\text{g}/\text{m}^3$ at the QU site mostly from the influence of dust events. However, the QU site showed a greater PM mass than at the AC site, which shows the effect of dust storms on the re-suspension of loose surface crusts from local unpaved areas in the dry, warm weather.

The anthropogenic sources also showed seasonal variations. $\text{PM}_{2.5}$ mass increased by $14.97 \mu\text{g}/\text{m}^3$ at the AC site and $20.04 \mu\text{g}/\text{m}^3$ at the QU site from winter to summer. The increase in anthropogenic sources was mainly due to sulfate, for which the absolute mass of sulfate increased by about $10 \mu\text{g}/\text{m}^3$ in the summer season as wind direction changed in late June to east east-north, transporting sulfate from the Arabian Gulf, alongside the effect of dust events in increasing the amount of road dust which was allocated to the traffic factor through resuspension by vehicle turbulence.

This detailed chemical characterization and sources apportionment study of $\text{PM}_{2.5}$ in Doha has highlighted the influence of regional sources (e.g., dust storms and secondary sulfate) in addition to the local (often undocumented) sources. Dust storms have an important impact in increasing PM levels by the burden of particles they deliver directly, their weathering action on the crust surface, and the amount of dust they leave on roads to be resuspended by traffic movements and winds. The dust storms influence on $\text{PM}_{2.5}$ concentrations, in addition to their persistence due to their fine size and the scarcity of rainfall, make this phenomenon the main driver of the highest PM levels in Qatar, in the dust storm seasons. Moreover, the study showed that sulfate emitted from seagoing vessels in the Arabian Gulf is contributing to high PM levels in Doha.

Specific recommendations and potential future studies include:

- 1) To reach agreement between all the countries bordering the Arabian Gulf to designate it as an Emission Control Area (ECA) to reduce the sulfur content in fuel used by vessels, and to invest in controlling sulfate emissions from flaring activities.
- 2) To review the Air Quality Law and allow for a number of exceedances to account for natural sources, evaluated using a different PM metric that closely reflects anthropogenic emissions.
- 3) There is a lack of monitoring and reporting air pollutants in other cities in Qatar namely Al-Wakrah and Al-Khor. Both cities are highly populated and in the vicinity of industrial areas. It is therefore vital to monitor and identify the main source contributions and to assess the influence of nearby industrial activities on those areas.
- 4) In Doha, several organizations including the Ministry of Municipality and Environment (MME), Ministry of public health (MOPH), Qatar Environment and Energy Research Institute (QEERI), Hamad Airport Doha (DOH), and several other universities and agencies currently conduct online measurements in Doha at different sites. However, access to data is often restricted. Standardisation of the monitoring and sampling equipment is needed, as well as establishing a common quality assurance, quality control, data validation method, and founding a central data sharing facility. This will contribute to a better understanding of the air quality in Doha and facilitate researchers' access to data.
- 5) To prepare an emission inventory for PM and its constituents and precursor gases from industrial cities and the traffic fleets in Qatar
- 6) To continue monitoring, sampling and chemically speciating PM to determine seasonal and annual trends in Qatar.

- 7) To assess relevant metal and organic source markers and metals ratios for local sources.
- 8) To study the organic matter composition in PM in Qatar to determine a more suitable conversion factor for organic carbon.
- 9) To study the seasonality impact on diseases burden in Qatar.
- 10) To apply and assess mitigation measures for fugitive dust and non-exhaust emission control (e.g., wet suppression, coverage of materials, and washing of roads).
- 11) To study the air quality in indoor environments and invest in finding solutions to reduce infiltration of PM to indoor locations, reducing personal exposure.
- 12) To invest in self-cleaning building materials to minimize the amount of dust settling on surfaces and improve buildings appearance.

REFERENCES

- Abal, A.T, Ayed, A., and Nair, P.C. et al. (2010) Factors responsible for asthma and rhinitis among Kuwaiti schoolchildren. *Med Princ Pract* 19:295-298
- Abdeen, Z. Qasrawi, R. and Jongbe, H. et al. (2014) Spatial and temporal variation in fine particulate matter mass and chemical composition: The Middle East consortium for aerosol research study. *The Scientific World Journals*. Articles ID 878704
- Abrahamowicz, m., Schpflocher, T., and Leffondre, K. et al. (2003) Flexible modling of exposure-response relationship between long-term average levels of particulate air pollution and mortality in the American cancer society study. *Toxicology Environ Health*. 66:1625-1654
- Abdul-Wahab. S.A (2005) Impact of fugitive dust emissions from cement plants on nearby communities. *Ecological Modelling*. V. 195, Issues 3–4, P 338-348
- Abu Sukar, H.K., Almerri, F.H. and Almurekki, A.A. et al. (2007) Agro-hydro-meteorological data book for the State of Qatar. DAWR
- Adachi, K., and Tainosho, Y. (2004) Characterization of heavy metal particles embedded in tire dust. *Environment International*, 30(8): 1009-1017
- Agranovski, I. E. (1995) Filtration of ultra-small particles on fibrous filters. Thèse Griffith University, Faculty of Environmental Sciences.
- Agrawal, H., Malloy, Q.G., and Welch, W.A. et al. (2008) In-use gaseous and particulate matter emissions from a modern ocean-going container vessel. *Atmospheric environment*, 42: 5504-5510
- Agrawal, H., Sawanta, A.A. and Jansen, K. et al. (2008) Characterization of chemical and particulate emissions from aircraft engines. *Atmospheric environment*, 42: 4380-4392
- Ahrenes, C.D. (2000) *Meteorology Today. An Introduction to weather climate, and the environment*. 6th. USA.
- Al-Awadhi, J. M. (2005) Dust fallout characteristics in Kuwait: a case study, *Kuwait J. Sci. Eng.*, 32, 135–151.
- Allen, A.G., Nemitz, E. and Shi, J.P. et al. (2001) Size distributions of trace metals in atmospheric aerosols in the United Kingdom. *Atmospheric Environment*, 35(27): 4581-4591.
- Alastuey, A., Moreno, N., and Querol, X. et al. (2007) Contribution of harbour activities to levels of particulate matter in a harbour area: Hada Project-Tarragona Spain. *Atmospheric Environment*, 41 (2007), pp. 6366-6378
- Al-Dabbous, A.N. and Kumar, P. (2015) Source apportionment of airborne nanoparticles in a middle eastern city using positive matrix factorization. *Environl Sci.: Process and Impact*. 17:802-812
- Al-Dawood K (2000) Epidemiology of bronchial asthma among school boys in Al-Khobar city. Saudi Arabia: cross-sectional study. *Croat Med J* 41:437-441
- Alolayan, M.A, Brown, K.W, and Evans, J.S (2013) Source apportionment of fine particles in Kuwait City. *Sci Total Environ* 448: 14-25
- Amato, F., Pandolfi, M. and Viana, M. et al. (2009a) Spatial and chemical patterns of PM₁₀ in road dust deposited in an urban environment. *Atmospheric Environment*, 43(9): 1650-165
- Amato, F., Pandolfi, M. and Moreno, T., et al. (2011b) Source and Variability of Inhalable Road Dust Particles in Three European Cites. *Atmospheric Environment*, 45(37): 6777-6787

- Amato, F., Viana, M. and Richard, A., et al. (2011b) Size and time-resolved roadside enrichment of atmospheric particulate pollutants. *Atmospheric Chemistry and Physics*, 11(6): 2917-2931.
- Andrews, E., Saxena, P. and Musarra, S. et al. (2000) Concentration and composition of atmospheric aerosols from the 1995 SEAVS Experiment and a review of the closure between chemical and gravimetric measurements. *Journal of the Air Waste Manage Assoc.* 50:648–664
- Ashour, M..M. (2013) Sabkhas in Qatar Peninsula. *Landscape and Geodiversity*, p. 10-35
- Catnaps (2014) Geography [online]. <http://catnaps.org/islamic/geography.html>. [Accessed Feb 21st, 2014].
- AQICN (2017) Revised PM_{2.5} AQI breakpoints. [Online] <http://aqicn.org/faq/2013-09-09/revised-pm25-aqi-breakpoints/> [Accessed on June 9th 2017]
- Aydin, F., Aydin, I. and Erdogan, S. et al. (2011) Chemical Characteristics of Settled Particles during a Dust-Storm. *Pol. J. Environ. Stud*, 21(3):533-537
- Ayres, J., Maynard, R. and Richards, R. et al. (2006) Air pollution and Health. *Air Pollution Review*. 3^{ed}. London. Imperial college Press
- Belis, C., Larsen, B., and Amato, F. et al. (2013) European guide on air pollution source apportionment with receptor models. *Environment and climate change* [online]
<http://publications.jrc.ec.europa.eu/repository/bitstream/JRC83309/lb-na-26-080-en-n.pdf>
[Accessed June 5th 2015]
- Brimblecombe, P.: 1986, *Air Composition and Chemistry*, Cambridge University Press, Cambridge, U.K.
- Brook, J.R., Graham, L and Charland, J.P. et al. (2007) Investigation of the motor vehicle exhaust contribution to primary fine particle organic carbon in urban air. *Atmospheric Environment*, 41(1): 119-135.
- Brown, K.W, Bouhamra, W, and Lamoureux, D.P., et al. (2008) Characterization of particulate matter for three sites in Kuwait. *J Air waste management Assoc* 58: 994-1003
- Cabal, A., Legrand, S., and Janssens, K. et al. (2017) Study of the uniformity of aerosol filters by scanning MA-XRF. *X-Ray Spectrom.*, 46: 461–466. doi: 10.1002/xrs.2767
- CAFE Working Group on Particulate Matter (2004) Second Position Paper on Particulate Matter [Online] http://ec.europa.eu/environment/archives/cafe/pdf/working_groups/2nd_position_paper_pm.pdf [accessed 13th August 2016]
- Callén, M.S., López, J.M. and Mastral, A.M. et al. (2013) Influence of organic and inorganic markers in the source apportionment of airborne PM₁₀ in Zaragoza (Spain) by two receptor models. *Environ Sci Pollut Res Int*, 20(5):3240-51
- Cao, J.J., Chow, J.C. and Lee, S.C. (2013) Evolution of PM_{2.5} measurements and Standards in the US and Future perspectives for China. *Aerosol and Air Quality Research*. 10.4209/aaqr.2012.11.0302
- Carlsaw, D.C. (2013) *The openair manual—open-source tools for analysing air pollution data*. Manual for version 0.6-0, King's College London
- Cavalli, F., Viana, M., Yttri, K.E., Genberg, J. and Putaud, J.-P. (2010) Towards a standardized thermal-optical protocol for measuring atmospheric organic and elemental carbon: the EUSAAR protocol. *Atmospheric Measurement Techniques*, 3: 79-89.
- Celis, J.E., Morales, J.R. and Zaror, C.A. (2004) A study of the particulate matter PM₁₀ composition in the atmosphere of Chillan, Chile. *Chemosphere*, 54, 541-550
- Cesari, D., Donato, A., and Cone, M. et al. (2016) An inter-comparison of PM_{2.5} at urban and urban background sites: Chemical characterization and source apportionment. *Atmospheric research*. 171-175, 106-119
- CENR (2006) *Atmospheric Ammonia: Sources and Fate A Review of Ongoing Federal Research and Future Needs*. [online] <https://www.esrl.noaa.gov/csd/AQRS/reports/ammonia.pdf> [Accessed 14th March 2016]

- Chang, M.B., Huang, C.K. and Wu, H.T. et al. (2000) Characteristics of heavy metals on particles with different sizes from municipal solid waste incineration. *Journal of Hazardous Materials*. 79(3):229-239.
- Charron, A., Harrison, R.M. and Quincey, P. et al. (2007) What are the source and conditions responsible for exceedances of the 24 h PM₁₀ limit Value (50 µgm-3) at a heavily trafficked London site? *Atmos Environ*, 41: 1960-75.
- Cheng, Y., Hel, K.B. and Zheng, M. et al. (2011) Optical properties of elemental carbon and water-soluble organic carbon in Beijing, China. *Atmos. Chem. Phys. Discuss.*, 11, 6221–6258.
- Chester, R., Nimmo, M. and Preston, M.R. et al. (1999) The trace metal chemistry of atmospheric dry deposition samples collected at Cap Ferrat: a coastal site in the Western Mediterranean. *Marine Chemistry* 68, 15–30
- Choi, J.K., Heo, J.B. and Ban, S.J. et al. (2013) Source apportionment of PM_{2.5} at the coastal area in Korea. *Science of The Total Environment*. 447, pp. 370-380
- Chow, J.C. and Watson, J.G (1998) Ion chromatography in Elemental Analysis of Airborne Particles. Pp. 97-137 In *Elemental Analysis of Airborne Particles*, Vol. 1, edited by S. Landsberger and M. Creatchman. Amsterdam: Gordon and Breach Science.
- Chow, J.C. and Watson, J.G. (1998) Guideline of Speciated Particulate Monitoring, US EPA, 3–2, p. 15–21.
- Chow, J.C., Watson, J.G. and Lowenthal, D.H. et al. (1994b) PM₁₀ and PM_{2.5} chemical characteristics and source apportionment in the San Joaquin Valley. In. Solomon, P.A. (ED), *Planning and Managing Regional Air Quality, Modeling and Measurement studies*. CRC Press Inc., Boca Ration, FL., pp. 687-698
- Chow, J.C., Douglas, H. and Lowenthal, L.W. et al. (2015) Mass reconstruction methods for PM_{2.5}: a review. *Air Quality Atmos Health*. 8(3): 243–263.
- Chow, J., Frazier, C.A., and Solomon, P.A., et al. (1996) Descriptive analysis of PM_{2.5} and PM₁₀ at regionally representative locations during SJVAQS/AUSPEX. *Atmos Environ*. 1996; 30:2079–2112
- Chow, J., Watson, J.G, and Tropp, R. et al. (2016) Testing Assumptions of Mass Reconstruction Methods to Evaluate and Interpret PM Chemical Speciation Measurements. Desert Research Institute, Reno. [Online] https://www.epa.gov/sites/production/files/2016-10/documents/mass_reconstruction.pdf [Accessed July 1st 2016]
- ChunXiang, Y.E., HongJun, L.I. and Tong, Z.H.U. et al. (2010) Heterogeneous reaction of NO₂ with sea salt particles. *Chemistry*. 53, pp. 2652-2656
- CIA world fact book (2014) Qatar Geography [online]. <https://www.cia.gov/library/publications/the-world-factbook/geos/qa.html> [Accessed Feb 17th 2014].
- Colville, R.N., Hutchinson, E.J., and Mindell, J.S., et al. (2001) the transport sector as a source of air pollution. *Atmospheric Environment*. 35:1537-1565.
- Committee On The Medical Effects Of Air Pollutants (COMEAP) (2010) [Online] https://www.gov.uk/government/uploads/system/uploads/attachment_data/file/304641/COMEAP_mortality_effects_of_long_term_exposure.pdf [Accessed March 12th 2017]
- Countess, R.J., Wolff, G., and Cadle, S.H. et al. (1980) The Denver winter aerosol: A comprehensive chemical characterization. *J. Air Poll. Control Assoc*. 30:1194-1200
- Corbett, J.J. Winebrake, J.J. and. Green, E.H et al. (2007) Mortality from ship emissions: a global assessment. *Environmental Science and Technology*, 41, pp. 8512-8518
- Crilly, L., Bloss, W.J. and Yin, J et al. (2015) Sources and contributions of wood smoke during winter in London: assessing local and regional influences. *Atmos. Chem. Phys.*, 15, 3149-3171.

- Crilley, L.R., Lucarelli, F. and Bloss, W.J. (2017) Source apportionment of fine and coarse particles at a roadside and urban background site in London during the 2012 summer ClearfLo campaign. *Environmental Pollution*, 220, 766-778
- Dall'Osto, M., Querol, X. and Alastuey, A. et al. (2013) On the spatial distribution and evolution of ultrafine particles in Barcelona. *Atmos. Chem. Phys.*, 13, 741-759.
- Davidson, C.I., Phalen, R.F., and Solomon, P.A. (2005) Airborne Particulate Matter and Human Health: A Review. *Aerosol Science and Technology*, 39:737-749.
- DeBell, L.J., Gebhart K.A., and Hand, J.L. et al. (2006) Spatial and seasonal patterns and temporal variability of haze and its constituents in the United States: Report IV. Fort Collins, CO: National Parks Service
- Dirgo, J. and Leith, D. (1985) Cyclone Collection Efficiency: Comparison of Experimental Results with Theoretical Predictions, *Aerosol Science and Technology*, 4:4, 401-415, DOI: 10.1080/02786828508959066
- Donaldson, K., Mills, N., and MacNee, W. et al. (2005) Role of inflammation in cardiopulmonary health effects of PM. *Toxicology and Applied Pharmacology*, 207: 483-488.
- Dorevitch, S., Demirtas, H., and Perksy, V.W. et al. (2006) Demolition of high-rise public housing increases particulate pollution matter in communities of high risk asthmatic. *Air Waste Manag Assoc.* 56(7) 1022-1032
- Downs H.S, Schindler, c., Liu L.J. et al., (2007) reduce exposure to PM₁₀ and attenuated age related decline in lung function. *New England Journal of Medicine*. 357(23):2338-2347.
- EC (2011a) Commission Staff Working Paper 6771/11 establishing guidelines for demonstration and subtraction of exceedances attributable to natural sources under the Directive 2008/50/EC on ambient air quality and cleaner air for Europe, European Commission [Online]
<http://register.consilium.europa.eu/doc/srv?l=EN&f=ST%206771%202011%20INIT> [Accessed 21st December 2016]
- Eldred, R., (2001) Sulfur-Sulfate Trends for IMPROVE University of California [Online]
http://vista.cira.colostate.edu/improve/publications/graylit/005_Sulfur-Sulfate_Trends/005_sulfur-sulfate_trends.htm [Accessed July 10th 2017]
- Engelbrecht, J., Moosmüller, H. and Pincock, S. et al. 2016) Technical note: Mineralogical, chemical, morphological, and optical inter relationships of mineral dust resuspensions. *Atmos. Chem. Phys.*, 16, 10809–10830
- Environment S.A (2012) MP101M with CPM – Automatic & Real-Time Particulate Monitor[Online]
<http://www.environnement-sa.com/products-page/en/air-quality-monitoring-en/particulates-samplers-and-analyzers-en/particulate-monitor-mp101m-with-cpm-option/?cat=88> [Accessed on May 1st, 2016]
- Environment S.A (2011) PM 162 M Particulate Matter. Technical Manual.
- Embabi, N.S. and Ashour, M.M. (1993) Barchans dunes in Qatar. *Arid Environments*. 25: 49-69
- Endresen, E., Sørsgård, J.K. and Sundet, S.B. et al. (2003) Emission from international sea transportation and environmental impact. *Journal of Geophysical Research: Atmospheres*, 108, pp.1984–2012
- Engelbrecht, J.P., McDonald, E.V., and Gillies, J. et al. (2009) Characterizing mineral dusts and other aerosols from the Middle East – Part 1: ambient sampling, *Inhal. Toxicol.*, 21, 297–326.
- Engelbrecht, J.P., McDonald, E.V., and Gillies, J. et al. (2009b) Characterizing mineral dusts and other aerosols from the Middle East – Part 2: Grab samples and re-suspension, *Inhal. Toxicol.*, 21, 327–336.
- Engelbrecht, J.P., Moosmüller, H., and Pincock, S. et al. (2016) Technical note: Mineralogical, chemical, morphological, and optical interrelationships of mineral dust suspensions. *Atmos. Chem. Phys.*, 16, 10809–10830.

- EPA (1989) Locating and estimating air emissions from sources of arsenic and arsenic compounds. [online] <https://www3.epa.gov/ttnchie1/le/arsenic.pdf>. [Accessed May 5th, 2016].
- EPA (2002) Diesel exhaust, air quality and health. [online] <http://www.epa.vic.gov.au/~media/Publications/849%20%20IB.pdf> [Accessed May 5th, 2016].
- EPA (2008) EPA Positive Matrix Factorization (PMF) 3.0 Fundamental and User Guide. Office Research and Development. Washington.
- EPA (2014) A Guide to Positive Matrix Factorization [online] <http://www.epa.gov/ttnamti1/files/ambient/pm25/workshop/laymen.pdf> [Accessed on May 10th, 2014]
- EPA (2014) PMF 5 User Guide [online] <https://www.epa.gov/air-research/epa-positive-matrix-factorization-50-fundamentals-and-user-guide> [Accessed on October 10th, 2014]
- EPA (2017) EPA Comments on the Gasoline Additive MMT [online] <https://www.epa.gov/gasoline-standards/epa-comments-gasoline-additive-mmt> [Accessed on October 29th, 2017]
- EEA (2012) Particulate matter from natural sources and related reporting under the EU Air Quality Directive in 2008 and 2009. Luxembourg: Publications Office of the European Union.
- Etyemezian, V. (2014) Particulate Matter Pollution in Desert Cities: Ambient Measurements, Source Identification, And Management Options. Division of Atmospheric Sciences Desert Research Institute, Las Vegas, Nevada, USA (Presentation)
- Fan, T. and Toon, O. B. (2011) Modeling sea-salt aerosol in a coupled climate and sectional microphysical model: mass, optical depth and number concentration. *Atmospheric Chemistry and Physics*. Atmos. Chem. Phys., 11, 4587–4610
- Farfel, M.R., Orlova, A.O. and Lees, P.S. et al. (2003) A Study of Urban Housing Demolitions as Sources of Lead in Ambient Dust: Demolition Practices and Exterior Dust Fall. *Environmental Health Perspectives*, 111(9).
- Fernandes, M.B., Skjemstad, J.O. and Johnson, B.B. et al. (2000) Characterization of carbonaceous combustion residues. I. Morphological, elemental and spectroscopic features. *Chemosphere*, 51: 785-795.
- Figuerola, D.A., Rodri'guez-Sierra, C.J. and Jime'nez-Velez, B.D. et al. (2006) Concentrations of Ni and V, other heavy metals, arsenic, elemental and organic carbon in atmospheric fine particles (PM_{2.5}) from Puerto Rico. *Toxicology and Industrial Health*, 22, pp. 87-99
- Friend, A.J., Ayoko, G.A. and Elbagir, S.G. et al. (2011a) Source apportionment of fine particles at a suburban site in Queensland, Australia. *Environ Chem*. 8 (2):163-173
- Furuta, N., Iijima, A. and Kambe, A. et al. (2005) Concentrations, enrichment and predominant sources of Sb and other trace elements in size classified airborne particulate matter collected in Tokyo from 1995 to 2000. *Journal of Environmental Monitoring*, 7, pp. 1155-1161
- Guerreiro, C.B., Fltescu, V., and Leeuw, F. et al. (2014) Air quality status and trends in Europe. *Atmospheric Environment*. 98: 376-384
- Gillies, J., Gertler, A. and Sagebiel, J. et al. (2001) On-road particulate matter (PM_{2.5} and PM₁₀) emissions in the Sepulveda Tunnel, Los Angeles, California. *Environ Sci Technol* 35:1054-1063.
- Giusti, C., Carlsen, J., and Watson, K. et al. (2014) The control of dust and emissions during construction and demolition. Supplementary Planning Guidance Greater London Authority
- Gordon, G.E. (1988) Receptor Models. *Environmental Science and Technology*, 22: 1132-1142.

- Green, M.C., Chow, J.C., Oliver Chang, M.-C., Chen, L.W.A., Kuhns, H.D., Etyemezian, V.R. and Watson, J.G. (2013) Source apportionment of atmospheric particulate carbon in Las Vegas, Nevada, USA. *Particuology*, 11: 110-118.
- Grewal, D. and Haugstetter, H. (2007) Capturing and sharing knowledge in supply chains in the maritime transport sector: critical issues. *Maritime Policy & Management*, pp. 169-183
- Griffin, D.W. (2007) atmospheric movement of microorganism in cloud of desert dust and implications for human health. *Clinical Microbiology Review*. 20, 459-477.
- Guieu, C., Loye-Pilot, and Thomas, C. et al. (2002) Chemical Characterization of Saharan dust end-member; Some biogeochemical implications for the western Mediterranean sea, *J. Geophys. Res.*, 107, doi: 10.1029/2001JD000582.
- Gurjar, B.R., Butler, T.M. and Lawrence, M.G. (2008) Evaluation of emissions and air quality in megacities. *Atmospheric Environment*. 42, 1593-1606
- Harmel, R., Otto, U., and Haupt, O. et al. (1999) Reduction of the Sample Size in the Analysis of Rock by EDXRF. University of Hamburg, Institute of Inorganic and Applied Chemistry, Martin-Luther-King-Platz 6, 20146 Hamburg, Germany [Online] http://www.icdd.com/resources/axa/vol41/V41_93.pdf [Accessed March 7th, 2017]
- Harrison, R.M., Deacon, A.R. and Jones, M.R. et al. (1997) Sources and processes affecting concentrations of PM₁₀ and PM_{2.5} particulate matter in Birmingham (U.K.). *Atmos. Environ.* 31, 24, 4103-4117.
- Harrison, R.M., Yin, J. and Mark, D. et al. (2001) Studies of the coarse particle (2.5-10 µm) component in UK urban atmospheres. *Atmos. Environ.* 35, 3667-3679.
- Harrop, D.O. (2002) Air quality assessment and management (A practical guide). SPON PRESS. London and New York
- Harrison, R.M., Deacon, A.R. and Jones, M.R. (1997) Sources and process affecting concentration of PM₁₀ and PM_{2.5} particulate matter in Birmingham UK. *Atmospheric Environment*, 34:4103-4117.
- Harrison, R.M. and Grieken, R.E. (1998) *Atmospheric Particles*. Volume 5. England. John Wiley & Sons Ltd.
- Harrison, R.M., Giorio, C., and Beddow, D., et al. (2010) Size distribution of airborne particles controls outcome of epidemiological studies. *Science of the Total Environment* 409, 289-293.
- Harrison, R.M., Jones, A.M. and Lawrence, R.G. et al. (2003) A pragmatic mass closure model for airborne particulate matter at urban background and roadside site. *Atmospheric Environment*, 37: 4927-4933.
- Harrison, R.M. and Yin, J. (2000) Particulate matter in the atmosphere: which particle properties are important for its effects on health? *Science of the total Environment*, 249(1-3):85-101.
- Harrison, R.M. and Yin, J. (2004) Characterisation of particulate matter in the United Kingdom. University of Birmingham.
- Harrison, R.M., Giorio, C., Beddows, D.C.S. and Dall'Osto, M., (2010) Size distribution of airborne particles controls outcome of epidemiological studies. *Science of the Total Environment*, 409: 289-293
- Ho, K.F., Lee, S.C., and Cao, J.J. et al. (2006) Seasonal variations and mass closure analysis of particulate matter in Hong Kong. *Sci Total Environ.* 355:276-287.
- Hopke, P.K. (1990) An Introduction to receptor model. *Chemometric and Intelligent Laboratory System*, 10: 21-43
- Hopke, P.K. (2016) Review of receptor modeling methods for source apportionment. *Journal of the Air & Waste Management Association*. 66, pp. 237-259

- Hsiao, T. (2009) Aerosol Filtration and Separation. Washington University. St. Louis Washington[Online] <http://openscholarship.wustl.edu/cgi/viewcontent.cgi?article=1158&context=etd> [Accessed March 4th, 2017]
- Hsu, S.C., Liu, S.C., and Huang, Y.T. et al. (2008) A criterion for identifying Asian dust events based on Al concentration data collected from northern Taiwan between 2002 and early 2007. *J Geophys Res-Atmos* 113. doi:10.1029/2007JD009574
- Huang, S., Rahn, K.A., Arimoto, R. et al. (1999) Testing and Optimizing Two Factor-Analysis Techniques on Aerosol at Narragansett, Rhode Island; *Atmos. Environ.* 33, 2169–2185.
- Huggins, E.F., Shah, N. and Huffman, G.P. et al. (2000) XAFS spectroscopic characterization of elements in combustion ash and fine particulate matter. *Fuel Process Technol*, pp. 203-218
- ILO (2011) Environmental and Public Health Issues [online]. <http://www.ilo.org/oshenc/part-xi/iron-and-steel/item/593-environmental-and-public-health-issues> [Accessed March 21st, 2014]
- IMO(2017)[online][http://www.imo.org/en/OurWork/Environment/PollutionPrevention/AirPollution/Pages/Sulfur-oxides-\(SOx\)-%E2%80%93Regulation-14.aspx](http://www.imo.org/en/OurWork/Environment/PollutionPrevention/AirPollution/Pages/Sulfur-oxides-(SOx)-%E2%80%93Regulation-14.aspx) [Accessed on July 7th, 2017]
- Institute of Air Quality Management (2014) Guidance on the assessment of dust from demolition and construction[Online] <http://www.iaqm.co.uk/text/guidance/construction-dust-2014.pdf> [Accessed on November 5th, 2016]
- IPCC (2001) climate change 2001: The scientific basis. Contribution of working Group 1 to the third assessment report of the intergovernmental panel on climate change. Cambridge University press. Cambridge, UK.
- Jaafar, M., Baalbaki, R., and Mrad, R. et al. (2014) Dust episodes in Beirut and their effect on the chemical composition of coarse and fine particulate matter, *Sci. Total Environ.*, 496, 75–83.
- Joseph, A.E., Unnikrishnan, S. and Kumar, R. et al. (2012) Chemical Characterization of fine aerosol for different land use pattern in Mumbai city. *Aerosol and air quality research*, 12: 61-72.
- JRC (2009) Positive Matrix Factorization (PMF) [online]. http://ies.jrc.ec.europa.eu/uploads/fileadmin/Documentation/Reports/RWER/EUR_23946_EN.pdf [Accessed on May 10th, 2014]
- Kapposa, A.D., Bruckmannb, P., and Eikmannc, T. et al. (2004) Health effect of particles in ambient air. *Hyg. Environ. Health*, 207:399-407.
- Kasumba, J., Hopke, P.K. and Chalupa, D.C. et al. (2009) Comparison of sources of submicron particle number concentrations measured at two sites in Rochester, NY. *Sci Total Environ* 407 (18):5071-5084.
- Kelly, F.J. and Fussell, J.C., (2015) air pollution and public health: emerging hazards and improved understanding of risk. *Environ Geochem Health*. 37(4): 631-649.
- Khillare, P.S., Pandey, R. and Balachandran, S. et al. (2004) Characterization of indoor PM10 in residential areas of Delhi. *Indoor and Built Environment*, 13:139-147
- Khodeir, M. Shamy, M. and Alghamdi, M. et al. (2012) Source apportionment and elemental composition of PM2.5 and PM10 in Jeddah City, Saudi Arabia. *Atmospheric Pollution Research*. 3:331-340.
- Kim, E., Larson, T.V. and Hopke, P.K. (2003a) Source apportionment of PM2.5 in an arid northwest U.S. city by positive matrix factorization. *Atmo. Res.* 66, 291-305 .
- Krewski, D., Burnett, R.T., and Goldberg, M.S. et al. (2003) Overview of the analysis of the Harvard six cities study and the American cancer society study of particulate pollution and mortality. *Journal of Toxicology and Environmental health*. 66: 1507-1551

- Kroll, J.H. and Seinfeld, J.H. (2008) Chemistry of secondary organic aerosol: Formation and evolution of low-volatility organics in the atmosphere. *Atmospheric Environment*. 42, 3593-3624.
- Kulkarni, P. Chellam, S. and Fraser, M.P. et al. (2005) Lanthanum and Lanthanides in atmospheric fine particles and their apportionment to refinery and petrochemical operations in Houston, TX. *Atmospheric Environment* 40: 508-520.
- Kwon, H.J., Cho, S.H., and Chun, Y., et al. (2002) Effect of Asian dust events on daily mortality in Seoul, Korea. *Environmental research*. 90(1),1-5.
- Laden, F., Neas, L.M., and Dockery, D.W. et al. (2000) Association of fine particulate matter from different sources with daily mortality in six U.S. cities. *Environ Health Perspect*.10: 941-947.
- Landsberg, H.E., Arakawa, H., and Bonn, H.F. et al. (1981) *Climates of Southern and Western Asia* . 9. Amsterdam: Elsevier Scientific.
- Lai, A., Zhao, Y., and Ding, A. (2016) et al. Characterization of PM_{2.5} and the major chemical components during a 1-year campaign in rural Guangzhou, Southern China. *Atmospheric Research*. Volume 167. Pages 208-215
- Laumbach, R., Meng, Q. and Kipen, H. (2014) What can individuals do to reduce personal health risks from air pollution? *Journal of Thoracic Disease*. 7:96-107
- Lewis, E.R. and Schwartz, S.E. (2004) *Sea Salt Aerosol Production: Mechanisms, Methods, Measurements, and Models. A Critical Review*. Geophysical Monograph Series.
- Li, N., Hopke, P.K. and Kumar, P. et al. (2013) Source Apportionment of time and size-resolved ambient particulate matter. *Chemometric and Intelligent Laboratory Systems*. 129, p.p 15-20
- Lighty, J.S., Veranth, J.M. and Sarofim, A.F. (2000) Combustion aerosols: Factors governing their size and composition and implications to human health. *Journal of Air and Waste Management Association*, 50(9): 1565-1618
- Lin, C., and Jeng, Y. (1996) Influences of Charge Air Humidity and Temperature on the Performance and Emission Characteristics of Diesel Engines. *Journal of Ship Research*, Vol. 40, No. 2, pp. 172-177
- Lin, Y., Chuang, H.C., and Liu, I.J. et al. (2013) Reducing indoor air pollution by air conditioning is associated with improvement in cardiovascular health among the general population. *Sci Total Environ*. 463-464: 176-181
- Lin, Y.C., Tsai, C.J. and Wu, Y.C. et al. (2015) Characteristics of trace metals in traffic-derived particles in Hsuehshan Tunnel, Taiwan: size distribution, fingerprinting metal ratio, and emission factor. *Atmospheric Chemistry and Physics Discussions*, 14: 13963-14004
- Lindsley, W.G. (2016) *Filter Pore Size and Aerosol Sample Collection*. NIOSH Manual of Analytical Methods. 5th Edition.
- Lough, G.C., Schauer, J.J., and Park, J.S. et al. (2005) Emissions of metals associated with motor vehicle roadways. *Environmental Science and Technology*, 39 (3): 826-836.
- Lodge, J.P. (1988) *Method of air sampling and analysis*. 3^{ed} ed. CRC Press.
- Lloyd, A.C. and Cackette, T.A. (2001) Diesel engines: Environmental impact and control. *Journal of Air and Waste Management Association*, 51 (6): 809-847.
- Malm, W.C. (2003) "Fundamentals of Visibility", In Potter, T.D. and Colman, B.R. (eds) *Handbook of Weather, Climate, and Water: Atmospheric Chemistry, Hydrology, and Societal Impacts*. New York: John Wiley & Sons. pp. 285-329.
- Malm, W.C., Sisler, J.F., and Huffman, D. et al. (1994) Spatial and seasonal trends in particle concentration and optical extinction in the United States. *J Geophys Res*. 99:1347–1370.

- Marcazzan, G.M., Vaccaro S., and Valli, G. (2001) Characterisation of PM₁₀ and PM_{2.5} particulate matter in the ambient air of Milan (Italy). *Atmospheric Environment*, 35, pp. 4639-4650
- Marine vessel traffic (2013) [Online] <http://www.marinevesseltraffic.com/2013/06/persian-gulf-marine-traffic.html> [Accessed on June 1st 2017]
- Masiol, M. and Harrison, R. (2014) Aircraft engine exhaust emissions and other airport-related contributions to ambient air pollution: A review. *Atmospheric Environment*. 95409e455.
- Mason, B. (1966) *Principles of Geochemistry*. (3rd), Wiley, New York.
- Matawle, J.L., Pervez, S. and Dewangan, S. et al. (2015) Characterization of PM_{2.5} source profiles for traffic and Dust source in Raipur, India. *Aerosol and Air Quality Research*, 15: 2537-2548
- Metoffice (2015) Annual rainfall [Online] <https://www.metoffice.gov.uk/public/weather> [Accessed on August 5th, 2017]
- Metoffice (2017) Atmospheric pressure [Online] <https://www.metoffice.gov.uk/learning/learn-about-the-weather/how-weather-works/highs-and-lows/pressure> [Accessed on March 11th, 2018]
- McKenna, A. M., Williams, J.T. and Putman, J.C et al. (2014) Unprecedented Ultrahigh Resolution FT-ICR Mass Spectrometry and Parts-Per-Billion Mass Accuracy Enable Direct Characterization of Nickel and Vanadyl Porphyrins in Petroleum from Natural Seeps. *Energy Fuels*, 28 (4): 2454–2464
- MDPS (2007) Environment Statics [Online] https://www.mdps.gov.qa/en/statistics/Statistical%20Releases/Environmental/EnvironmentalStatistics/Environment_QSA_AE_2007.pdf [Accessed on January 2014]
- MDPS (2013) Environment Statics Annual Report [Online] https://www.mdps.gov.qa/en/statistics/Statistical%20Releases/Environmental/EnvironmentalStatistics/Environment_Statistics_Annual_Report_2013_En.pdf [Accessed on January 2014]
- MDPS (2013) Environmental Statistics (2013) [Online] https://www.mdps.gov.qa/en/statistics/Statistical%20Releases/Environmental/EnvironmentalStatistics/Environment_MDPS_AE_2013.pdf [Accessed on January 2014]
- MDPS (2014) Transport and communication statistics chapter 9-2014 [Online] <https://www.mdps.gov.qa/en/statistics1/pages/topicslisting.aspx?parent=Economic&child=TransportCommunications> [Accessed on January 2014]
- MDPS (2014) Bulletin of industry and energy statistics [Online] <https://www.mdps.gov.qa/en/statistics1/pages/topicslisting.aspx?parent=Economic&child=EnergyandIndustry> [Accessed on January 2014]
- MDPS (2015) Transport and communication statistics chapter 9-2015 [Online] <https://www.mdps.gov.qa/en/statistics1/pages/topicslisting.aspx?parent=Economic&child=TransportCommunications> [Accessed on January 2014]
- MDPS (2016) Transport and communication statistics chapter 10-2016 [Online] <https://www.mdps.gov.qa/en/statistics1/pages/topicslisting.aspx?parent=Economic&child=TransportCommunications> [Accessed on January 2014]
- Miller, S.D., Kuciauskas, A.P. and Liu, M. et al. (2008) Haboob dust storms of the southern Arabian Peninsula. *Geophysical research*, 113, D01202
- Middleton, N.J. (1985) A Geography of Dust Storms in South-West Asia. *Climatology* 6: 183-196

- Minguillon, M.C., Arhami, M., and Schauer, J.J. et al. (2008) Seasonal and spatial variations of sources of fine and quasi-ultrafine particulate matter in neighbourhoods near the Los Angeles–Long Beach harbour. *Atmospheric Environment*. 42,32, p 7317-7328
- Ministry of Environment (MOE) (2013) Air Quality Annual Report. Doha: MOE.
- Ministry of Environment (MOE) (2005) Environmental Protection Law. Doha: MOE
- MME (2016). mashamari@mme.gov.qa. Meteorological Data. 24/9/2016
- Molinelli, A.R., Madden, M.C., and McGee, J.K. et al. (2002) Effect of metal removal on the toxicity of airborne particulate matter from Utah Valley. *Inhal toxicol*. 14(10) 1069-1086
- Monod, A., and Liu, Y. (2011) Aerosol formation and heterogeneous chemistry in the atmosphere. EPJ Web of Conferences 18, 04002 (2011) DOI: 10.1051/epjconf/20111804002 C Owned by the authors, published by EDP Sciences [Online] https://www.epj-conferences.org/articles/epjconf/pdf/2011/08/epjconf_cma2011_04002.pdf [Accessed on 26th, March 2018]
- Mooibroek, D., Schaap, M., and Weijers, E.P. et al. (2011) Source apportionment and spatial variability of PM_{2.5} using measurements at five sites in the Netherland. *Atmospheric Science*, 45: 4180-4191
- Morsilli, L., Zappoli, S. and Militreno, S. et al. (1993) The presence and distribution of the heavy metals in municipal solid waste incineration. *Toxicol. Environ. Chem*. 37, 139-145
- Moreno-Gutiérrez¹, J., Durán-Grados¹, and Z. Uriondo, Z. (2012) Emission-factor uncertainties in maritime transport in the Strait of Gibraltar, Spain. *Atmospheric measurements techniques. Discuss.*, <https://doi.org/10.5194/amtd-5-5953-2012>.
- NARSTO (2004) particulate matter science for policy markers: A NARSTO Assessment. Cambridge University Press, Cambridge, England. ISBN 0 52184287 5
- NASA Earth Observatory (2009) Dust Storm over Arabian Peninsula [online]. <http://earthobservatory.nasa.gov/NaturalHazards/view.php?id=37459> [Accessed August 21st 2015] .
- Najafi, M.S., Khoshakhllagh, F., and Zamanzadeh, S.M. et al. (2014) Characteristics of TSP loads during the Middle East springtime dust storm (MESDS) in Western Iran, *Arabian Journal of Geosciences*, 7, 5367–5381.
- NCMS (2011) Dust Sources Affecting the United Arab Emirates [Online] file:///C:/Users/27763401653/Downloads/ncms-dust-en-2011.pdf [Accessed on the 11th March 2018]
- Nigam, A., W. Welch, W. and Wayne Miller, J. (2006) Effect of fuel sulfur content and control technology on PM emission from ship's auxiliary engine. *Proceedings of the International Aerosol Conference*, St. Paul, USA, pp. 1531-1532
- O'Donoghue, R. (2010) Cuase and effect course. Univesity of Birmingham.
- Ohta, S. and Okita, T. (1994) Measurements of particulate carbon in urban and marine air in Japanese areas. *Atmos Environ* 18:2439–2445
- Okada, K., Ishizaka, Y., and Masuzawa, T. et al. (1978) Chlorine deficiency in costal Aerosols. Water research Institute, Nagoya University.
- Ogulei, D., Hopke, P.K. and Zhou, L. et al. (2006) Source apportionment of Baltimore aerosol from combined size distribution and chemical composition data. *Atmos. Environ*. 40(S2):396–410
- Paatero, P. (1997) Least squares formulation of robust non-negative factor analysis. *Chemometric and Intelligent Laboratory System*. 37, 23-35
- Paatero, P. Hopke, P.K. (2003) Discarding or Downweighing High-Noise Variables in Factor Analytic Models; *Anal. Chem. Acta*. 490, 277–289.

- Paatero, P., Hopke, P.K., and Song, X.H. et al. (2002) Understanding and controlling rotations in factor analytic models. *Chemometric and Intelligent Laboratory System*, 60, pp. 253-264.
- Paatero, P., Hopke, P.K., and Begum, B.A. et al. (2005) Graphical Diagnostic Method for Assessing the Rotation in Factor Analytical Models of Atmospheric Pollution; *Atmos. Environ.* 39, 193–201.
- Paatero, P., and Tapper, U. (1994) Positive Matrix Factorization. A Non-Negative Factor Model with Optimal Utilization of Error Estimates of Data Values; *Envirometrics*, 5, 111–126.
- Pandolfi, M.Y., Castanedo, G.A., Alastuey, J.D et al. (2011) Source apportionment of PM₁₀ and PM_{2.5} at multiple sites in the strait of Gibraltar by PMF: impact of shipping emissions. *Environ. Sci. Pollut. Res.*, 18, pp. 260-269
- Pant, P. and Harrison, R.M. (2012) Critical review of receptor modeling for particulate matter: A case study of India. *Atmospheric Environment*, 49: 1-12
- Pant, P. and Harrison, R.M. (2013) Estimation of the contribution of road traffic emissions to particulate matter concentrations from field measurements: A review. *Atmospheric Environment*, 77: 78-97
- Pant, P. (2014) Receptor modelling studies of airborne particulate matter in the United Kingdom and India. PhD thesis University of Birmingham
- Panikkath, R., Jumper, C.A, and Mulkey, Z. et al. (2012) Multilobar lung infiltrates after exposure to dust storm: the Haboob Lung Syndrome. *The American journal of medicine* 126(2):e5-e7
- Paterson, K.G., Sagady, J.L. and Hooper, D.L. et al. (1999) Analysis of air quality data using positive matrix factorization. *Environ. Sci. Technol.* 33, 635-641
- Pacyna, J., Semb, A. and Hanssen, J. et al. (1984) Emission and long-range transport of trace elements in Europe. *Tellus B*, 36B: 163–178. doi:10.1111/j.1600-0889.1984.tb00238
- Pérez, N., Pey, J., and Reche, C. et al. (2016) Impact of harbour emissions on ambient PM₁₀ and PM_{2.5} in Barcelona (Spain): Evidences of secondary aerosol formation within the urban area. *Science of the Total Environment*. 571, 237-250
- Perrino, C., Canepari, S., and Catrambone, M. (2013) Comparing the performance of Teflon and quartz membrane filters collecting atmospheric PM: influence of atmospheric water. *Aerosol and air quality research*. 13: 137 – 147.
- Perrone, M.G., Larsen, B.R. and Ferrero, L., et al. (2012) Sources of high PM_{2.5} concentrations in Milan, Northern Italy: Molecular marker data and CMB modelling. *Science of the Total Environment*, 414: 343-355.
- Peters, S., and Ewing, G. (1996) Reaction of NO₂(g) with NaCl(100). Department of Chemistry, Indiana University, Bloomington, Indiana 47405. *J. Phys. Chem.*100 (33), pp 14093–14102
- Polissar, A.V., Hopke, P.K., and Paatero, P. et al. (1998) Atmospheric Aerosol over Alaska 2. Elemental Composition and Sources; *J. Geophys. Res.* 103, 19045–19057.
- Polissar, A.V., Hopke, P.K. and Poirot, R.L. (2001) Atmospheric Aerosol over Vermont: Chemical Composition and Sources; *Environ. Sci. Technol.* 35, 4604–4621
- Pope, C.A., Ezzati, M., and Dockery D.W., (2009) fine particulate air pollution and life expectancy in the United States. *New England Journal of Medicine*. 360(4) 376-386
- Prijith, S.S., Aloyaius, M. and Mohan, M. et al. (2014) Relationship between wind speed and sea salt aerosol production: A new approach. *Atmospheric and Solar-Terrestrial Physics* 108: 34–40

- Pye, K. (1987) Aeolian dust and dust deposits. London. Academic Press Inc. London (Ltd).
- QCAA (2014) Metrological data. Qatar Civil Aviation Authority. Department of Meteorology. Qatar
- Qatar Petroleum (2014) Raslaffan [online].
http://www.raslaffan.qp.qa/irj/portal/anonymous?guest_user=erlcinternet [Accessed March 1st, 2014]
- QNCC (2014) Product Information [online]. <http://www.qatarcement.com/eng/product.html> [Accessed February 23rd, 2014]
- QSC (2014) Product Specifications [online] <http://www.qatarsteel.com.qa/Products/SitePages/Products.aspx> [Accessed March 22nd, 2014]
- Querol, A., Alastuey, A., and Rodriguez, F. et al. (2001) PM₁₀ and PM_{2.5} source apportionment in the Barcelona Metropolitan area, Catalonia, Spain. *Atmos Environ*, 35, pp. 6407-6419
- Querol, X., Alastuey, A. and Ruiz, C.R. et al. (2004) Speciation and Origin of PM₁₀ and PM_{2.5} in selected European Cities. *Atmospheric Environment*, 38: 6547-6555.
- Querol, X., Viana, M. and Alastuey, A. (2007b) Source origin of trace elements in PM from regional background, urban and industrial sites of Spain. *Atmos Environ* 24
- QUARG (1996) Airborne Particulate Matter in the United Kingdom. Quality of Urban Air Review Group. 3ed [online] https://uk-air.defra.gov.uk/assets/documents/reports/empire/quarg/quarg_11.pdf [Accessed on May 16th, 2014]
- Rees, S.L., Robinson, A.L., and Khlystov, A. et al. (2004) Mass balance closure and the Federal Reference Method for PM_{2.5} in Pittsburgh, Pennsylvania. *Atmospheric Environment*, 38: 3305-3318
- Reff, A., Eberly, S.I. and Bhave, P.V. (2007) Receptor modeling of ambient particulate matter data using positive matrix factorization Review of existing models. *J. Air waste manage. Assoc.* 57, 146-154.
- Remoundaki, E., Kassomenos, P., and Mantas, E. et al. (2013) Mihalopoulos N, Tsezos M. Composition and mass closure of PM_{2.5} in urban environment (Athens, Greece) AAQR. 13:72-82.
- Rogula-Kozłowska, W., Klejnowski, K., and Rogula-Kopiec, P. et al. (2012) A study on the seasonal mass closure of ambient fine and coarse dusts in Zabrze, Poland. *Bull Environ Contam Toxicol*. 88:722-729.
- Roos, J.W., Richardson, D. and Claydon, D.G. et al. (2008) Diesel fuel additives containing cerium or manganese and detergents. [Online] <http://www.google.com/patents/EP1905813A2?cl=en> [Accessed on October 29th 2017]
- Saarikoski, S., Timonen, K. and Saarnio, M. (2008) Source of organic carbon in fine particulate matter in northern European urban air. *Atmos. Chem. Phys.*, 8, pp. 6281-6295
- Sciare, J., Oikonomou, K. and Cachier, H. et al. (2005) Aerosol mass closure and reconstruction of the light scattering coefficient over the Eastern Mediterranean Sea during the MINOS campaign. *Atmos. Chem. Phys.*, 5, 2253-2265
- Shafer, M.M., Perkins, D.A., Antkiewicz, D.S., Stone, E.A., Quraishi, T.A. and Schauer, J.J. (2010) Reactive oxygen species activity and chemical speciation of size-fractionated atmospheric particulate matter from Lahore, Pakistan: an important role for transition metals. *Journal of Environmental Monitoring*, 12: 704-715.
- Shen, Z., Cao, J., and Arimoto, R. (2009) Ionic composition of TSP and PM_{2.5} during dust storms and air pollution episodes at Xi'an, China. *Atmospheric Environment*, 43: 2911-2918
- Smith, L., Means, J., and Chen, A., et al. (1995) Remedial operation for metals contaminated sites. RC Press, Inc. USA.

- Sillanpää, M., Hillamo, R., and Saarikoski, S. et al. (2006) Chemical composition and mass closure of particulate matter at six urban sites in Europe. *Atmospheric Environment*, 40: S212-S223.
- Simon, H., Bhawe, P.V., and Swall, J.L. et al. (2011) Determining the spatial and seasonal variability in OM/OC ratios across the US using multiple regression. *Atmos Chem Phys*. 11:2933–2949.
- Sippula, O., Stengel, B., and Sklorz, M. et al. (2014) Particle Emissions from a Marine Engine: Chemical Composition and Aromatic Emission Profiles under Various Operating Conditions[online]
<https://www.theguardian.com/sustainable-business/2017/apr/20/air-pollution-construction-industry-cities-diesel-emissions-london> [Accessed February 2^{ed}, 2017]
- Solomon, P.A., Fall, T., and Salmon, L.G. et al. (1989) Chemical characteristics of PM₁₀ aerosols collected in the Los Angeles area. *J Air Pollut Control Assoc*. 39:154–163.
- Song, X.H., Polissar, A.V., and Hopke, P.K. et al. (2001) Sources of fine particle composition in the northeastern US. *Atmospheric Environment*, 35: pp. 5277–5286.
- Sowlat, M.H., Naddafi, K. and Yuncesian, M. et al. (2012) Source apportionment of total suspended particulates in an arid area in southwestern Iran using positive matrix factorization. *B Environ Contam Tox* 88: 735-740.
- Sternbeck, J., Sjödin, Å. and Andréasson, K. et al. (2002) Metal emissions from road traffic and the influence of resuspension results from two tunnel studies. *Atmospheric Environment*, 36 (30): 4735-4744.
- Stieb, D.M., Doiron, M.S. and Blagden, P. et al. (2005) Estimating the public health burden attributable to air pollution: an illustration using the development of an alternative air quality index. *Journal of Toxicology and Environmental Health*, 68 (13) pp. 1275-1288
- Strauss, W. and Mainwaring, S.J. (1984) *Air Pollution*. Hodder Arnold
- Szidat, S., Ruff, M., and Perron, N., et al. (2009) Fossil and non-fossil sources of organic carbon (OC) and elemental carbon (EC) in Göteborg, Sweden. *Atmos. Chem. Phys.*, 9, pp. 1521-1535
- Taiwo, A.M. (2013) *Receptor Modelling of Industrial Air Pollutants*. PhD thesis University of Birmingham.
- Taylor, S.R. and McLennan, S.M. (1995) The geochemical evolution of the continental crust. *Reviews of Geophysics*, 33: 241-265.
- Terzi, E., Argyropoulos, G., and Bougatioti, A. et al. (2010) Chemical composition and mass closure of ambient PM₁₀ at urban sites. *Atmos Environ*. 44:2231–2239.
- Tesseraux, I. (2004) Risk factors of jet fuel combustion products. *Toxicology Letters* 149: 295–300
- Thatcher, T.L. and Layton, D.W. (1994) Deposition, Resuspension, and Penetration of particles within a residence. *Atmospheric Environment*. 29, No. 13, pp. 1487-1497
- The World Bank (2014) Population Total [online]. <http://data.worldbank.org/indicator/SP.POP.TOTL>. [Accessed Feb 21st, 2014].
- Thorpe, A. and Harrison, R.M. (2008) Source and properties of non-exhaust particulate matter from road traffic: a review. *The science of the total Environment* 400, 270-282.:
- Thurston, G.D. and Liou, P.J. (1987) Receptor modeling and aerosol transport. *Atmospheric Environment* (1967), Volume 21, Issue 3, p. 687-698.
- Tindale, N.W. and Pease, P.P. (1998) Aerosols over the Arabian Sea: Atmospheric transport pathways and concentrations of dust and sea salt. *Deep-Sea Research* 2 (46):1577-1595
- Tuncel, G., Güllü, G. and Tuncel, S.G., et al. (1997) Atmospheric transport of pollutants to the Eastern Mediterranean Basin, IAETECDOC, IAE, Vienna

- Turpin, B.J. and Lim, H. (2001) Species Contribution to PM_{2.5} Mass concentrations: Revisiting Common Assumptions for Estimating Organic Mass. *Aerosol Science and Technology*, 35: 602-610
- Tsiouri, V. and Kakosimos, K.E., Kumar, P. et al. (2015) Concentrations, sources and exposure risks associated with particulate matter in the middle east area – a review. *Air Qual Atmos Health*. 8: 67-80
- Valavadinis, A., Fiotakis, K. and Vlachogianni, T. (2008) Airborne particulate matter and human health: toxicological assessment and important of size and composition of particles for oxidative damage and carcinogenic mechanism. *Journal of Environmental Science and Health Part C*, 26: 339-362.
- Vecchi, R., Chiari, M. and Alssandro, A.D. et al. (2008) A mass closure and PMF source apportionment study on the sub-micron sized aerosol fraction at urban sites in Italy. *Atmospheric Environment* 42, 2240-2253.
- Vecchi, R., Valli, G., and Fermo, P. et al. (2009) Organic and Inorganic Sampling Artefacts Assessment. *Atmos. Environ.* 43: 1713–1720.
- Viana, M., Amato, F. and Alastuey, A. et al. (2009) Chemical Tracers of Particulate Emissions from Commercial Shipping. *Environ. Sci. Technol*, 43: 7472-7477.
- Viana, M., Maenhaut, W. and Chib, X. et al. (2007) Comparative chemical mass closure of fine and coarse aerosols at two sites in south and west Europe: Implications for EU air pollution policies. *Atmospheric Environment*, 41:315–326
- Viana, a., Hammingh, P., and Colette, A. et al. (2014) Impact of maritime transport emissions on coastal air quality in Europe. *Atmospheric Environment*, 90: 96-105
- Vinoj, V. and Satheesh, S.K. (2004) Direct and indirect radiative effects of sea-salt aerosols over Arabian Sea. Centre for Atmospheric and Oceanic Sciences, Indian Institute of Science, Bangalore 560 012, India
- Wallace, J.M. and Hobbs, P.V. (2006) *Atmospheric Science: An Introduction Survey*. 2nd ed. Elsevier Inc.
- Wang, B. and Laskin, A. (2014) Reactions between water-soluble organic acids and nitrates in atmospheric aerosols: Recycling of nitric acid and formation of organic salts, *J. Geophys. Res.-Atmos.*, 119, 2013JD021169, doi:10.1002/2013jd021169, 2014
- Watson, J.G., Chow, J.C. and Chen, L. et al. (2011) Measurement System Evaluation for Upwind/Downwind Sampling of Fugitive Dust Emissions. *Aerosol and Air Quality Research*. 11:331-350
- Watson, J.G., Zhu, T. and Chow, J.C. et al. (2002) Receptor modeling application framework for particle source apportionment, *Chemosphere*, 49: 1093-1136
- Weather online (2017)[Online]
<http://www.weatheronline.co.uk/weather/maps/city?FMM=1&FYY=2000&LMM=12&LYY=2016&WMO=41170&CONT=asie®ION=0023&LAND=QT&ART=WDR&R=0&NOREGION=0&LEVEL=162&LANG=en&MOD=tab> [Accessed July 27th 2017]
- Weckwerth, G. (2001) Verification of traffic emitted aerosol components in the ambient air of Cologne(Germany). *Atmos Environ*, 35(32): 5525-36.
- White, W.H., and Roberts, P.T. (1977) On the nature and origins of visibility-reducing aerosols in the Los Angeles air basin. *Atmos. Environ.* 11:803–812.
- WHO (1976) Manual in air quality management. Regional office for Europe Copenhagen .WHO Regional Publications. Europe Series No1.Copenhagen
- WHO (2005) Air quality guidelines - global update [Online]
http://www.who.int/phe/health_topics/outdoorair/outdoorair_aqg/en/ [Accessed March 2^{ed} 2017].
- WHO (2006) health risks of particulate matter from long-range transboundary air pollution. Convention task force on the health aspects of air pollution. European centre for environment and health

- WHO (2013) Health effects of particulate matter [online].
http://www.euro.who.int/__data/assets/pdf_file/0006/189051/Health-effects-of-particulate-matter-final-Eng.pdf
 [Accessed on 29th May 2014]
- WHO (2016) Ambient Air Pollution: A Global Assessment of Exposure and Burden of Disease [online]
<http://apps.who.int/iris/bitstream/10665/250141/1/9789241511353-eng.pdf?ua=1> [Accessed on 17th November 2017]
- Whickham, H. (2017) ggplot2 – Elegant Graphics for Data Analysis. Journal of Statistical Software. doi:10.18637/jss.v077.b02[online]
file:///C:/Users/lubna/AppData/Local/Packages/Microsoft.MicrosoftEdge_8wekyb3d8bbwe/TempState/Downloads/v77b02.pdf [Accessed on 17th March 2018]
- WMO (2012) WMO Sand and Dust Storm Warning Advisory and Assessment System (SDS-WAS) [online]
http://www.wmo.int/pages/prog/arep/wwrp/new/documents/SDS_WAS_implementation_plan_01052012.pdf
 [Accessed March 1st 2014]
- Yan, P., Zhang, R.J. and Huan, N. et al. (2012) Characteristics of aerosols and mass closure study at two WMO GAW regional background stations in eastern China. Atmos Environ. 60:121–131.
- Yin, J. and Harrison, R. (2008) Pragmatic mass closure study for PM_{1.0}, PM_{2.5} and PM₁₀ at roadside, urban background and rural sites. Atmospheric Environment. Volume 42, Issue 5, Pages 980-988.
- Ying, W., Zhuang, G. and Tang, A. et al. (2005) The ion chemistry and the source of PM_{2.5} aerosol in Beijing. Atmospheric Environment, 39: 3771–3784
- Zdziennicka, A., Szymczyk, K. and Janczuk, B. et al. (2009) Correlation between Surface Free Energy of Quartz and Its Wettability by Aqueous Solutions of Non-ionic, Anionic and Cationic Surfactants. J. Colloid Interface Sci. 340: 243–248.
- Zhang, X.Y., Cao, J.J. and Li, L.M. et al. (2002) Characterization of atmospheric aerosol over Xi'an in the south margin of the Loess Plateau, China. Atmospheric Environment, 36 (26), pp. 4189-4199
- Zhou, L., Hopke, P.K. and Karl, T. et al. (2004) Source identification of volatile organic compounds in Houston. Environ. Sci. Technol 38, 1338-1347.